Cranfield University

College of Aeronautics

PhD THESIS

Mustapha GOURMA

Towards Better Understanding of the Smooth Particle Hydrodynamic Method

Cranfield University

College of Aeronautics

PhD THESIS

Academic Year 2002-2003

Mustapha GOURMA

Towards Better Understanding of the Smoothed Particle Hydrodynamic Method

Supervisor: Professor. Rade Vignjevic

September 2003

This thesis is submitted in partial fulfilment of the requirements for the Degree of Doctor of Philosophy

ABSTRACT

Numerous approaches have been proposed for solving partial differential equations; all these methods have their own advantages and disadvantages depending on the problems being treated. In recent years there has been much development of particle methods for mechanical problems. Among these are the Smoothed Particle Hydrodynamics (SPH), Reproducing Kernel Particle Method (RKPM), Element Free Galerkin (EFG) and Moving Least Squares (MLS) methods. This development is motivated by the extension of their applications to mechanical and engineering problems.

Since numerical experiments are one of the basic tools used in computational mechanics, in physics, in biology etc, a robust spatial discretization would be a significant contribution towards solutions of a number of problems. Even a well-defined stable and convergent formulation of a continuous model does not guarantee a perfect numerical solution to the problem under investigation.

Particle methods especially SPH and RKPM have advantages over meshed methods for problems, in which large distortions and high discontinuities occur, such as high velocity impact, fragmentation, hydrodynamic ram. These methods are also convenient for open problems. Recently, SPH and its family have grown into a successful simulation tools and the extension of these methods to initial boundary value problems requires further research in numerical fields.

In this thesis, several problem areas of the SPH formulation were examined. Firstly, a new approach based on *'Hamilton's variational principle'* is used to derive the equations of motion in the SPH form. Secondly, the application of a complex Von Neumann analysis to SPH method reveals the existence of a number of physical mechanisms accountable for the stability of the method. Finally, the notion of the amplification matrix is used to detect how numerical errors propagate permits the identification of the mechanisms responsible for the delimitation of the domain of numerical stability.

By doing so, we were able to erect a link between the physics and the numerics that govern the SPH formulation.

ACKNOWLEDGEMENTS

The work presented in this thesis would not have been possible without the help of several individuals.

I would like to thank in particular my supervisor Professor Rade Vignjevic for his insight, recommendation and cooperation. I am also indebted to Dr. James Campbell for his availability and suggestions concerning this work.

Thanks to Cranfield University who supported me financially during the course of my candidature.

Special thanks to my friend and fellow colleague Dr. Laurent Dala, without whom, this thesis would not have taken place.

I would like to thank all my fellow research students of Crashworthiness Impacts and Structural Dynamic Group.

To my Children *Ayoub* and *Layla*

Contraria non contrdictora

Sed complementa sunt.

Niels Bohr

TABLE OF CONTENTS

LIST OF FIGURES

LIST OF SYMBOLS

V = Volume of the system

B = Boundary of the volume of the system

$\Re$ = real Euclidean space

nd = Spatial dimension

t_0 = Initial time

t, t' = Time variables

T = Period of time

dt = Time step

$\frac{d(\cdot)}{dt}$, $\frac{\partial(\cdot)}{\partial t}$ = Total and partial time derivative operator

W, W_N = Spatial Kernel and Normalized Kernel

h = Scalar smoothing length

$\overline{\overline{H}}$, h_{ij} = Smoothing length Tensor

τ = Scalar smoothing time

$D_W = Supp(W)$ = Support of the Kernel

$\Gamma(t-t')$ = Temporal Kernel

$\vec{r}$, $\vec{r}'$, x, s = Spatial positions

ρ = Density

ψ = Physical field

$\vec{v}$, u_i = Vector and scalar velocity

$\delta(\cdot)$, δ_{ij} = Dirac distribution and delta Kronecker

E, e = Total energy and internal specific energy

m_i = mass of particle i

$\nabla_\eta(\cdot)$ = Gradient operator with respect of η

$S(\cdot)$ = Source term in Eulerian equations

$\langle \cdot \rangle_S$ = Smoothing operator

$\overline{\overline{\sigma}}$, σ_{ij} = Stress Tensor

$\overline{\overline{S}}$, S_{ij} = Deviatoric Tensor

$ds(\cdot)$ = Element of surface

$\hat{n}(\cdot)$ = Unit normal to surface element

Q_i = Artificial Viscosity of particle I C_S=Speed of Sound

$\overline{\overline{\varepsilon}}$, ε_{ij} = Spin Tensor

$\overline{\overline{\varepsilon^e}}$, $\overline{\overline{\varepsilon^P}}$, ε^P = Elastic, Plastic strain Tensor and Effective Plastic strain

$\overline{\overline{\Omega}}$, Ω_{ij} = Rotation Tensor

$V(\cdot)$, V_n = Internal Energy by unit mass (Potential Energy)

T_n , S_n = Temperature and Entropy of particle n

H , L = Hamiltonian and Lagrangian of the system

Ξ = Strain Energy Function

$G_{Gh}(\cdot)$ = Ensemble of fictitious particles.

$\gamma(\cdot)$ = Mie-Grüneisen parameter

$\omega(\cdot)$ = Complex Frequency

$\mathrm{Re}[\omega(\cdot)]=\omega_r(\cdot)$, $\mathrm{Im}[\omega(\cdot)]=\omega_i(\cdot)$ = Real part and Imaginary part of the frequency

$M(\cdot)$, $N(\cdot)$ = First and Second coefficients of Normalisations.

$\overline{\overline{\overline{F_i^n(\cdot)}}}$ = Source term in Lagrangian form. $\overline{\overline{I_d}}$ =Identity Matrix

$\overline{\overline{\overline{G_i^n(\cdot)}}}$, $\overline{\overline{\overline{H_i^n(\cdot)}}}$ = Jacobeans in Particles approximations

λ_1 , λ_2 , λ_3 = Eigenvalues

dt_1 , dt_2 , dt_3 = Eigenvalues

D_S = Domain of stability

$\Phi(\cdot)$, $\Omega(\cdot)$, $\Gamma(\cdot)$ = Time-step dependant functions

$\Phi_N(\cdot)$, $\Omega_N(\cdot)$, $\xi(\cdot)$ = Time-step dependant functions

$S^\beta(\cdot,\ \cdot)$ = Shape of parameterized surface.

1. FORMALISM OF SMOOTHED PARTICLE HYDRODYNAMICS SPH

1.1 Introduction

The fundamental difference between Lagrangian and Eulerian formalisms lies in the choice of the coordinates. In the Eulerian formalism spatial coordinates are used in the Lagrangian formalism material coordinates are used.

The essential advantage of the Lagrangian formalism is that the convection terms are not present in the equations making the system much easier to integrate. Numerically, the errors resulting from these terms disappear too.

The main short coming of the Lagrangian formalism is that the mesh becomes severely distorted and the process of numerical integration deteriorates and breaks down, especially if shear motion and in-homogeneities are present.

To keep accurate histories of the evolution associated with each continuum element requires re-meshing procedures, however these are expensive operations and accompanied by significant diffusion of all physical quantities.

The common point of the Lagrangian and Eulerian formalism is the use of mesh for spatial discretization. In computational continuum dynamics meshing operations are for a wide variety of problems fastidious and require special attention when one wants to have acceptable and accurate results.

It has been now about three decades since the first paper by Lucy [1] using the SPH method to test the fission hypothesis. The extension of the SPH method to gas dynamic and to hydrodynamic problems can be attributed largely to the work of Gingold and Monaghan [2, 3] and Benz [4].

At the beginning of the 90's, W. Benz [5], L. Libersky et al [6] and Johnson et al [7] extended SPH method to simulate problems of solid mechanics including impacts, penetrations and large deformations.

The stability analysis of the SPH method was pioneered by Mas-Gallic and Raviart [8], Swegle et al [9], D. Balsara [10], Dilisio et al [11], D. Hicks and L. Liebrock [12] and Ben Moussa and Vila [13].

The main advantage of the SPH method over Eulerian methods is that it is a Lagrangian gridless one. The originality of this method lies in the manner the space derivatives are evaluated.

The objectives of this research project are multiple and can be regarded as theoretical and practical aim. The primary objective is to give the SPH method certain truthfulness. To accomplish this objective, the Hamilton's principle is used to derive the equations of motion in the SPH form.

Hamilton's variational principle is the most prominent one so far and processes the unifying nature throughout all physics. The author, by using Hamilton's principle intends to furnish firm mathematical and physical evidence to sustain the SPH method as complete and respected numerical tool such as other classical numerical methods (PIC, finite volume and finite element, etc…).

The second objective of this research concerns the boundary condition treatment in particle method and in SPH particularly. Boundary condition implementation is a very subtle yet difficult issue; many authors mentioned the 'Ghost particles' approach for boundary condition treatment. In our knowledge, there is no available or published complete description of the meaning of 'Ghost particles' notion. To remedy this situation, in this research as the first step, a best understanding of the concept of 'Ghost Particles' is derived theoretically from the equations of motion and in the second step a clear depiction of the algorithm is given.

The third goal of this research project is to inspect some of the problem areas of the SPH method. These aspects concern the identification of the mechanisms behind the development of the physical and numerical instabilities when SPH or its progeny method is used for solving engineering applications. In this field, for the first time a complex Von Neumann analysis is used to detect the physical mechanisms accountable of the development of the instabilities in the SPH method. Furthermore, the final objective is to provide a clear connection between the numerical stability of the scheme and the mechanisms outlined above.

These are the most important and significant objectives of the thesis presented here, some other specific objectives and applications of the SPH method were studied. The decomposition of this work is as follow.

The first part of the thesis addresses several derivations of SPH formalism. The first derivation is based on the Eulerian formalism and on the Eulerian kernel. The second derivation uses many-body interacting particles and the third derivation refers to the well known Hamilton's principle.

In the second part an overview concerning kernels commonly engaged in SPH methods is given. A criterion for choosing a kernel is established.

The third part addresses the comparison between the SPH method and the RKPM method for a certain number of numerical tests. The choice of RKPM was motivated by the fact it is similar to SPH.

The fourth part investigates both theoretical and practical sides of the mirroring or 'Ghost particles' algorithm commonly employed is SPH and in particle methods.

The fifth part examines Von Neumann stability analysis for both SPH and normalised SPH (NSPH). Also the error propagation and amplification matrix using Jacobeans in SPH and its progeny was studied.

The final chapter concerns the closure of the equations of dynamics with a specific material model and equation of state. Hydrodynamic ram problem was treated to give evidence on the ability of SPH method to handle a complex problem encountered in engineering applications.

1.2 SPH Formalism

The objective of this section is to introduce fundamental concepts governing the formalism of smoothed particle hydrodynamics SPH.

The first basic idea behind the SPH method is that any observable or measurable field is smoothed over the spatial domain by using appropriate smoothing kernels.

Let V be the space of all possible displacements in Euclidian space $\Re^{nd}$ $\left(V \subset \Re^{nd}\right)$ and B a regular hyper-plane representing the boundary of V $\left(B \subset \Re^{nd-1}\right)$ where nd is the space dimension that could be time dependant and let the time $t \in \mathrm{T}^* \subset \Re^{+}$.

The smoothed value of any conservative physical field $\rho(r,t).\psi(r,t)$ is given by.

$$\left\langle \rho \cdot \psi(r,t) \right\rangle_s = \int_{T^\bullet} \Gamma(t-t',\tau)\, dt' . \int_V W(r-r'(t'),h) \cdot \rho(r',t') \cdot \psi(r',t') \cdot d^3 r' \qquad (1.1)$$

Where ρ stands for the density, ψ represents a physical quantity, with r and r' are the three-dimensional space coordinates and given $T > 0$ $(t, t') \in [0,T]^2 \subset \Re^{+2}$ denote time variables. W represents an appropriate positive radial kernel with a single maximum at $r'(t') = r$ and compact support $D_W^h \equiv Supp(W)$. The parameter h is a geometrical parameter that measures the size of D_W^h. The smoothing kernel should fulfil the following properties.

A / Normalization condition $\qquad \int_V W(r-r',h) \cdot d^3 r' = 1$

B / Dirac limit condition $\qquad \lim_{h \to 0} W(r-r',h) = \delta(r-r')$

Where $\delta(r-r')$ is Dirac delta distribution.

$\Gamma(t)$ represents a temporal kernel having the same properties as W with h being replaced by τ and space positions V being replaced by temporal interval $T^\bullet$.

Since the focus of the consideration is on spatial discretization and the detection of signals instantaneously taking place this forces the temporal kernel to fulfil the Dirac limit condition, where $\tau \cong 0$ and then $\Gamma(t-t', \tau \cong 0) \equiv \delta(t-t')$, consequently relation (1.1) reduces to spatial convolution, then:

$$\left\langle \rho \cdot \psi(r,t) \right\rangle_s = \int_V W(r - r'(t), h) \cdot \rho(r', t) \cdot \psi(r', t) \cdot d^3 r' \qquad (1.2)$$

The second important assumption in SPH is that a continuum M is assimilated to identifiable set of discrete interacting entities named particles. These entities will be assimilated to N interacting points with masses $m_1, m_2, ...m_i .....m_N$.

Let the value of any non-conservative field for particle i located at discrete position $(r_i, t) \in V \times [0,T]$ be $\psi_i(t) = \psi(r_i, t)$, then for any continuous point $(r,t) \in V \times [0,T]$ the continuous form of the smoothed value is estimated by summation over all particles i, $i \in M$.

$$\left\langle \rho.\psi(r,t) \right\rangle_s = \sum_{i \in M} m_i \cdot \psi_i(t) \cdot W(r - r_i(t), h) \qquad (1.3)$$

In this summation particle mass m_i was defined by the introduction of the control volume (or Lumped volume) for each particle. It follows by comparing continuous form to its discretized counterpart that.

$$m_i = \rho(r_i, t) \cdot d^3 r_i(t) \qquad \forall t \in [0,T] \qquad (1.4)$$

1.3 Equations of dynamics in SPH

In this section semi-discretized equations of motion for continuum are derived. For the following we consider the general equation of conservation in Eulerian form, see Boillat et al [14], P. A. Raviart [15]. These equations must be combined with appropriate initial conditions, boundary conditions and the material model.

$$\frac{\partial \rho \cdot \vec{\psi}}{\partial t} + \nabla_r \vec{F}^T = -\nabla_r S\left(\overline{\overline{\sigma}}\right) \tag{1.5}$$

Where $\frac{\partial .}{\partial t}$ is the partial derivative with respect to time, $\nabla_r = \sum_{i=1}^{nd} \frac{\partial .}{\partial x_i}$ is the divergence operator, nd represents the spatial dimension, $\vec{\psi}$ is non-conservative vector field, $\vec{F}^T$ is vectors of nd rows of convective term and $S(\overline{\overline{\sigma}})$ contains viscous and source terms.

$$\vec{\psi} = \begin{pmatrix} \psi^1 \\ \psi^2 \\ \psi^3 \end{pmatrix} = \begin{pmatrix} 1 \\ \vec{v} \\ E \end{pmatrix}, \qquad \vec{F}^T = \left(\vec{f}_1, \ldots, \vec{f}_{nd}\right), \qquad \vec{f}_i = \begin{pmatrix} \rho \cdot v_i \\ \rho \cdot v_i \cdot \vec{v} \\ \rho \cdot v_i \cdot E \end{pmatrix} = \rho \cdot v_i \cdot \vec{\psi}$$

$$1 \le i \le nd \qquad \text{and} \quad S(\overline{\overline{\sigma}}) = \begin{pmatrix} S^1 \\ S^2 \\ S^3 \end{pmatrix} = \begin{pmatrix} 0 \\ \overline{\overline{\sigma}} \\ \overline{\overline{\sigma}} \cdot \vec{v} \end{pmatrix}$$

In the above system (1.5), $E = e + v^2/2$ denotes specific total energy, $\rho, \vec{v}$ and e are material density, velocity field and internal energy. Finally, $\overline{\overline{\sigma}}$ is the second order stress tensor.

Let us consider the left hand side of (.1.5) as a general time-space divergence:

$$D(\rho \cdot \vec{\psi}) = \frac{\partial \rho \cdot \vec{\psi}}{\partial t} + \vec{\nabla}_r (\rho \cdot \vec{v} \cdot \vec{\psi}) \tag{1.6}$$

The smoothed divergence of (1.6) results from spatial convolution over the volume $V \subset \Re^{nd}$ with an appropriate kernel W.

$$\left\langle D(\rho\cdot\vec{\psi}(r,t)\right\rangle_S = \int_V W(r-r')\cdot\frac{\partial\left[\rho\,.\vec{\psi}(r')\right]}{\partial t}.d^3r + \int_V W(r-r')\cdot\nabla_{r'}\left[\rho\cdot\vec{v}(r')\cdot\vec{\psi}(r')\right]\cdot d^3r' \tag{1.7}$$

For clarity, the smoothed length h is omitted from the expression (1.7). Integrating these integrals by parts and let $B\subset\Re^{nd-1}$ represents the boundary of the volume V, then:

$$\begin{aligned}\left\langle D(\rho\cdot\vec{\psi}(r,t)\right\rangle_s = &\int_V\frac{\partial\left[W(r-r')\cdot\rho(r')\cdot\vec{\psi}(r')\right]}{\partial t}\cdot d^3r' \\ &-\int_V\rho(r')\cdot\vec{\psi}(r')\cdot\frac{\partial W(r-r')}{\partial t}\cdot d^3r' \\ &-\int_V\rho(r')\cdot\vec{v}(r').\vec{\psi}(r')\cdot\nabla_{r'}W(r-r')\cdot d^3r' \\ &+\int_B W(r-r')\cdot\rho(r')\cdot\vec{v}(r')\cdot\vec{\psi}(r')\cdot\hat{n}(r')\cdot ds(r')\end{aligned} \tag{1.8}$$

In the above relation $\hat{n}(r')$ is the unit normal of the surface element $d\vec{s}(r')=\hat{n}(r')\cdot ds(r')$ bounding the element volume d^3r'.

Using the Leibniz theorem and letting $\vec{v}_B(r')$ be the velocity field of the surface element $d\vec{s}(r')$, then the first term of (1.8) becomes.

$$\begin{aligned}\int_V\partial_t\left[W(r-r')\cdot\rho(r')\cdot\vec{\psi}(r')\right]d^3r' = &\frac{d}{dt}\left[\int_V W(r-r')\cdot\rho(r')\cdot\vec{\psi}(r')\cdot d^3r'\right] \\ &-\int_B W(r-r').\rho(r')\cdot\vec{\psi}(r')\cdot\vec{v}_B(r')\cdot\hat{n}(r')\cdot ds(r')\end{aligned} \tag{1.9}$$

The expression (1.9) allows us to rewrite the relation (1.8) in useful way by collecting volume terms and surface terms separately and rearranging terms to contain the term $\rho(r')\cdot d^3r'$.

$$\begin{aligned}\left\langle D(\rho\cdot\vec{\psi}(r,t)\right\rangle_s = \frac{d}{dt}\left[\int_V W(r-r').\vec{\psi}(r').\rho(r')\cdot d^3r'\right] \\ -\int_V \frac{\partial W(r-r')}{\partial t}\cdot\vec{\psi}(r')\cdot\rho(r')\cdot d^3r' \\ -\int_V \vec{\psi}(r')\cdot\vec{v}(r')\cdot\nabla_{r'}W(r-r')\cdot\rho(r')\cdot d^3r' \\ +\int_B W(r-r')\cdot\vec{\psi}(r')\cdot\left[\vec{v}_B(r')-\vec{v}(r')\right]\cdot\hat{n}(r')\cdot\rho(r')\cdot ds(r')\end{aligned} \tag{1.10}$$

The last term on the right hand side contains the relative flux across the surface element $\hat{n}(r')\cdot ds(r')$. There are some situations where this term vanishes. This is the case for systems evolving within open domains or when $W(r-r')\big|_{r'\in B}=0$. This term will be zero also when boundaries move at the same velocities as the material. The general case occurs when materials penetrate boundaries with an arbitrary relative velocity field $\left[\vec{v}_B(r')-\vec{v}(r')\right]\hat{n}(r')\neq 0$.

Here, let us consider cases where there are no fluxes across boundaries, then the boundary integral vanishes and numerical approximation for integrals in (1.10) gives.

$$\begin{aligned}\left\langle D(\rho.\vec{\psi}(r,t)\right\rangle_s \approx \sum_{i=1}^{N} m_i\left[\frac{d\vec{\psi}_i(t)}{dt}\cdot W(r-r_i')+\vec{\psi}_i(t)\cdot\frac{dW(r-r_i')}{dt}\right] \\ -\sum_{i=1}^{N} m_i\cdot\left[\vec{\psi}_i(t)\cdot\frac{\partial W(r-r_i')}{\partial t}\right] \\ -\sum_{i=1}^{N} m_i.\vec{v}(r_i')\cdot\vec{\psi}_i(t)\cdot\nabla_{r_i'}W(r-r_i')\end{aligned} \tag{1.11}$$

In the previous expression, the relation (1.3) expressing the constancy of masses was used.

Since $W = W(r - r')$ is symmetric and has Eulerian character depending on time t implicitly through $r' = r'(t)$, the second term in the first sum contains the material derivative that relates the partial derivative by:

$$\frac{dW(r - r'_i)}{dt} = \frac{\partial W(r - r_i')}{\partial t} + \frac{d\vec{r}_i'(t)}{dt} \cdot \nabla_{r_i'} W(r - r_i') \tag{1.12}$$

Terms containing partial derivatives of $W(r - r_i')$ compensate and the final expression of the smoothed left hand side of the conservation equation becomes.

.

$$\begin{aligned} \left\langle D(\rho \cdot \psi(r,t)) \right\rangle_s \approx & \sum_{i=1}^{N} m_i \cdot \left[\frac{d\vec{r}'_i(t)}{dt} - \vec{v}(r_i') \right] \cdot \nabla_{r_i'} W(r - r_i') \\ & + \sum_{i=1}^{N} m_i \cdot \frac{d\vec{\psi}_i(t)}{dt} \cdot W(r - r_i') \end{aligned} \tag{1.13}$$

By applying the same treatment to the right hand side of the conservation equation, the smoothed term gives:

$$\left\langle \nabla_r S(\overline{\overline{\sigma}}(r)) \right\rangle_s = \int_V \left[\frac{\nabla_{r'} S(\overline{\overline{\sigma}}(r'))}{\rho(r',t)} \right] \cdot W(r - r') \cdot \rho(r') \cdot d^3 r' \tag{1.14}$$

This supposes naturally that, depending on tolerance of problems and materials, there exists a lower bound limit for density, that is $\{\exists \rho_0 > 0 / \forall (r,t) \in V \times [0,T],\ \rho_0 \le \rho(r,t) < \infty\}$.

This constraint is inherent to the definition of the mass or 'measure' introduced in (1.4). For accuracy of the integrals, lumped volume has to be finite and 'small' in comparison to the measure of D_W. Numerical approximation of (1.14) is then given by:

$$\left\langle \nabla_r S(\overline{\overline{\sigma}}(r)) \right\rangle_s \approx \sum_{i=1}^{N} m_i \cdot \left(\frac{\nabla_{r'_i} S(r'_i)}{\rho(r'_i)} \right) W(r - r'_i(t)) \tag{1.15}$$

As pointed out by Monaghan and Gingold [16], there are several ways to write the above equation. Here, a classical form also known as sum form.

$$\left\langle \nabla_r S(\overline{\overline{\sigma}}) \right\rangle_s = \int_V \left\{ \nabla_{r'} \left[\frac{S(\overline{\overline{\sigma}})}{\rho(r')} \right] + \frac{S(\overline{\overline{\sigma}})}{\rho^2(r')} \cdot \nabla_{r'} \rho(r') \right\} \cdot Wr - r') \cdot \rho(r') \cdot d^3 r' \tag{1.16}$$

In the equation (1.15) the stress tensor $\overline{\overline{\sigma}}$ depends on the position r (respectively on r') and time t, so in the following, for simplicity one uses $S(r)$ (respectively $S(r')$). It follows that:

$$\left\langle \nabla_r S(r,t) \right\rangle_s = \left\langle \nabla_r \frac{S(r)}{\rho(r)} \right\rangle_s + \left\langle \frac{S(r)}{\rho^2(r)} \cdot \nabla_r \rho(r) \right\rangle_s \tag{1.17}$$

To estimate numerically (1.16), SPH formalism uses the following linearization

$$\left\langle \nabla_r S(r,t) \right\rangle_s \approx \left\langle \nabla_r \frac{S(r)}{\rho(r)} \right\rangle_s + \frac{S(r)}{\rho^2(r)} \cdot \left\langle \nabla_r \rho(r) \right\rangle_s \tag{1.18}$$

To outline the validity of this approximation, let us consider (1.18) and expand $\frac{S}{\rho^2}$ in a Taylor series around the position r, the resulting expression in first order gives.

$$\left\langle \nabla_r S(r,t) \right\rangle_s \approx \left\langle \nabla_r \frac{S(r)}{\rho(r)} \right\rangle_s + \frac{S(r)}{\rho^2(r)_s} \cdot \left\langle \nabla_r \rho \right\rangle_s + \rho(r) \cdot \nabla_r \left(\frac{S(r)}{\rho(r)^2} \right) \cdot \mu(r) \tag{1.19}$$

The extra term in (1.19) depends on the 'Compressibility coefficient' $\mu(r) = \frac{\langle \rho(r) \rangle_s}{\rho(r)} - 1$, in order to understand its role and to evaluate its predominance, dimensional analysis with symmetric kernels is used and then it follows:

$$\rho(r) \cdot \mu(r) \sim \left(\langle r \rangle_s - r \right)^2 \qquad \nabla_r \left(\frac{S(r)}{\rho^2(r)} \right) \sim \left(\frac{\delta S}{\delta \rho} \right) \cdot \frac{\left(\langle r \rangle_s - r \right)^2}{\rho(r)^2}$$

Finally

$$\rho(r) . \nabla_r \left(\frac{S(r)}{\rho(r)^2} \right) . \mu(r) \approx \frac{\delta S}{\delta \rho} \cdot \left(\langle r \rangle_S - r \right)^4 \tag{1.20}$$

The previous term is of fourth order except for particles under shocks; $\delta\rho = \langle \rho(r) \rangle_s - \rho(r) \to 0$ but $\frac{\delta S}{\delta \rho} \to Const < \infty$. The approximation in (1.18) is also valid for regions where $\frac{\delta S}{\delta \rho} \sim \frac{S}{\rho}$.

Integrating by parts the expression in (1.16) and using Gauss theorem, one obtains:

$$\begin{aligned} \langle \nabla_r S(r,t) \rangle_s \approx & -\int_V \left[\frac{S(r')}{\rho(r')^2} + \frac{S(r)}{\rho(r)^2} \right] \cdot \nabla_{r'} W(r - r'(t)) \cdot \rho(r') \cdot d^3 r' \\ & + \int_B \left[\frac{S(r')}{\rho(r')^2} + \frac{S(r)}{\rho(r)^2} \right] \cdot \nabla_{r'} W(r - r'(t)) \cdot \hat{n}(r') \cdot \rho(r') \cdot ds(r') \end{aligned} \tag{1.21}$$

Given boundary particles such that $m_i^B = \rho(r') \cdot ds(r')$ and assuming that all fields in boundaries are constant by surface elements, these are labelled with subscript B. The discretized approximation of the expression above becomes.

$$\left\langle \nabla_r S(r,t) \right\rangle_s \approx -\sum_{i=1}^{N} m_i \cdot \left[\frac{S(r'_i)}{\rho(r'_i)^2} + \frac{S(r)}{\rho(r)^2} \right] \cdot \nabla_{r_i'} W(r - r'_i(t)) + \sum_{i=1}^{N_B} m_i^B \cdot \left[\frac{S(r_i^B)}{\rho(r_i^B)^2} + \frac{S(r)}{\rho(r)^2} \right] \cdot \nabla_{r_i^B} W(r - r_i^B(t)) \cdot \hat{n}_i^B \tag{1.22}$$

The last term in the right hand side expresses the interaction of the boundaries with particles located at (r,t). In this expression, the boundaries are represented by a set of N_B particles located at (r_i^B, t). Several approaches exist to approximate the boundary term. The 'Ghost-Particles' method is amongst one of the approaches (See chapter 4).

1.4 Governing equations in SPH

The governing equations in the SPH approximation are obtained by equating expressions (1.13) and (1.22). The continuity equation is obtained by setting $\left(\psi^1 = 1, S^1 = 0\right)$. It states that along free paths the particles trajectories obey:

$$\left\langle D\rho(r,t) \right\rangle_s = \sum_{i=1}^{N} m_i \cdot \left[\frac{d\vec{r}_i'(t)}{dt} - \vec{v}(r'_i) \right] \cdot \nabla_{r_i'} W(r - r'_i(t)) = 0$$

Since kernels are arbitrary, one recovers a basis equation common to all particles methods:

$$\frac{d\vec{r}_i'(t)}{dt} = \vec{v}(r'_i(t)) \tag{1.23}$$

This means that velocities of interpolating points are equal to the fluid velocity, then the expression of generalized smoothed divergence reduces to

$$\left\langle D(\rho \cdot \vec{\psi}(r,t) \right\rangle_s \approx \sum_{i=1}^{N} m_i \cdot \frac{d\vec{\psi}_i(t)}{dt} \cdot W(r - r'_i(t)) \tag{1.24}$$

From (1.14) since the kernel is arbitrary one gets a Lagrangian form of the equation of motion.

$$\frac{d\vec{\psi}_i(t)}{dt} = -\left\langle \nabla_r S(r,t) \right\rangle_{r=r_i(t)} \tag{1.25}$$

In explicit form, one has the system below:

$$\begin{cases} \dfrac{d\vec{r}(t)}{dt} = \vec{v}(r,t) \\ \dfrac{d\vec{v}(r,t)}{dt} = \displaystyle\sum_{i=1}^{N} m_i \cdot \left[\frac{\overline{\overline{\sigma}}(r)}{\rho(r)^2} + \frac{\overline{\overline{\sigma}}(r'_i)}{\rho(r'_i)^2} \right] \nabla_{r_i} W(r - r_i) \\ \qquad - \displaystyle\sum_{i=1}^{N_B} m_i^B \cdot \left[\frac{\sigma(r)}{\rho(r)^2} + \frac{\sigma(r'^B_i)}{\rho(r_i^B)^2} \right] \cdot \nabla_{r_i^B} W(r - r'^B_i).\hat{n}_i^B \\ \dfrac{dE(r,t)}{dt} = \displaystyle\sum_{i=1}^{N} m_i \cdot \left[\frac{\overline{\overline{\sigma}} \cdot \vec{v}(r)}{\rho(r)^2} + \frac{\overline{\overline{\sigma}} \cdot \vec{v}(r'_i)}{\rho(r'_i)^2} \right] \cdot \nabla_{r_i} W(r - r_i) \\ \qquad - \displaystyle\sum_{i=1}^{N_B} m_i^B \cdot \left[\frac{\overline{\overline{\sigma}} \cdot \vec{v}(r)}{\rho(r)^2} + \frac{\overline{\overline{\sigma}} \cdot \vec{v}(r'^B_i)}{\rho(r_i^B)^2} \right] \cdot \nabla_{r_i^B} W(r - r'^B_i).\hat{n}_i^B \end{cases} \tag{1.26}$$

1.4.1 Further discussion of the conservation of energy equation

In Lagrangian approach, often the equations of continuum dynamics use an equation for internal specific energy instead of total specific energy.

To achieve that, let us first start from the relation $\delta e = \delta E - \vec{v}.\delta \vec{v}$ then the evolution of internal energy becomes.

$$\frac{de(r,t)}{dt} = \sum_{i=1}^{N} m_i \cdot \frac{\overline{\overline{\sigma}}(r'_i)}{\rho(r_i')^2} \cdot \left(\vec{v}(r_i') - \vec{v}(r)\right) \cdot \nabla_{r_i} W(r - r_i) - \sum_{i=1}^{N_B} m_i^B \cdot \frac{\overline{\overline{\sigma}}(r'^B_i)}{\rho(r'^B_i)^2} \cdot \left(\vec{v}(r'^B_i) - \vec{v}(r)\right) \cdot \nabla_{r_i} W(r - r'^B_i) \cdot \hat{n}_i^B \tag{1.27}$$

Conversely, starting from the conservative Eulerian approach, the system (1.5) will have its last component modified to a 'Difference Form'.

$$\begin{aligned} \frac{\partial(\rho \cdot e)}{\partial t} + \nabla_r(\rho \cdot e \cdot \vec{v}) &= -\overline{\overline{\sigma}} \cdot \vec{\nabla}_r \vec{v} \\ &= -\frac{\overline{\overline{\sigma}}}{\rho} \cdot \left(\nabla_r(\rho \cdot \vec{v}) - \vec{v} \cdot \nabla_r \rho\right) \\ &= -\frac{\overline{\overline{\sigma}}}{\rho} \cdot \nabla_r(\rho \cdot \vec{v}) + \frac{\overline{\overline{\sigma}} \cdot \vec{v}}{\rho} \cdot \nabla_r(\rho) \end{aligned} \tag{1.28}$$

Other form of (1.27) can be derived if one considers that only terms under derivative operators have to be smoothed. Multiplying equation (1.28) by a Kernel W and integrating by parts leads to.

$$\frac{de(r,t)}{dt} = \frac{\overline{\overline{\sigma}}(r)}{\rho(r)^2} \cdot \sum_{i=1}^{N} m_i \cdot \left(\vec{v}(r_i) - \vec{v}(r)\right) \cdot \nabla_{r_i} W(r - r_i) - \frac{\overline{\overline{\sigma}}(r)}{\rho(r)^2} \cdot \sum_{i=1}^{N_B} m_i^B \cdot \left(\vec{v}(r_i^B) - \vec{v}(r)\right) \cdot \nabla_{r_i} W(r - r_i^B) \cdot \hat{n}_i^B \tag{1.29}$$

The expression (1.29) is preferred to (1.27) for simulations using large number of particles. In the opposite, the principle of the conservation of the total energy suggests the use of (1.27).

1.4.2 Further discussion of the conservation of the density equation

There are two computational strategies for finding the material density $\rho(r,t)$. The first one uses spatial convolution named 'summation over neighbours'.

Let $N_i = \left\{ i \in \mathrm{Z} / \left| r - r_i(t) \right| \in D_W \right\}$ be a family of particles interacting with the particle in (r,t), then the discrete form of the equation (1.3) with $\psi_i(t) = 1$ leads to.

$$\rho(r,t) = \sum_{i=1}^{N_r} m_i \cdot W(r - r_i(t)) \tag{1.30}$$

The second method is based on the integration of the continuity equation.

$$\frac{d\rho(r,t)}{dt} = -\rho(r,t).\nabla_r \vec{v}(r,t) \tag{1.31}$$

As for internal specific energy, one uses conservative form to smooth the right hand side of the equation above.

$$\rho.\nabla_r \vec{v} = \nabla_r(\rho.\vec{v}) - \vec{v}.\nabla_r \rho \tag{1.32}$$

By smoothing terms under derivative operators, the particle approximation of the continuity equation becomes:

$$\frac{d\rho(r,t)}{dt} \approx \sum_{i=1}^{N_r} m_i \cdot \left(\vec{v}(r_i) - \vec{v}(r) \right) \cdot \nabla_{r_i} W(r - r_i(t)) \tag{1.33}$$

In practice, initial distribution of particles is known and (1.30) is used for initial density and (1.33) is integrated explicitly in time.

1.5 Artificial Viscosity and Wall Heating

Following Von Neumann and Richtmyer [17], the artificial viscosity was introduced to mimic dissipative mechanisms that occur in shocks. They added an extra-term Q to the pressure term.

Physically this leads the model to take into account the thermodynamic irreversibility due to the entropy by dissipating a part of kinetic energy into shocks.

For simplicity, consider an ideal gas. In the absence of a thermal source, from the energy equation, one has.

$$de = -(P+Q)\cdot dV \quad \Leftrightarrow \quad Q\cdot dV = de + P\cdot dV \tag{1.34}$$

Identifying the equation above with the first law of thermodynamics implies that the entropy Σ of the model is given by.

$$d\sum = -\frac{Q}{T}\cdot dV$$

Where e is the specific internal energy, P is the pressure, T is the temperature and $V = \frac{1}{\rho}$ is the specific volume.

Numerically, the effect of artificial viscosity is to dump spurious oscillations and to make numerical schemes able to handle shocks. Physically, artificial viscosity converts kinetic energy into internal energy.

Efforts were invested in adapting artificial viscosity to the SPH equations of motion. Nowadays, it is commonly agreed that in the SPH method, the artificial viscosity is expressed by a combination

of linear and quadratic terms. Here one considers the two commonly used forms of artificial viscosity, as described by Monaghan and Gingold [16].

The first form named 'Nodal viscosity' is similar to that used in finite volume and finite difference methods. Its version in smoothed particle hydrodynamics is expressed as follow.

$$\begin{cases} Q(r_i) = -\alpha \cdot \rho(r_i) \cdot C_s(r_i) \cdot h(r_i) \cdot \langle \nabla \vec{v} \rangle_s + \beta \cdot \rho(r_i) \cdot h^2(r_i) \cdot \langle \nabla \vec{v} \rangle_s^2 \quad for \quad \nabla \vec{v} < 0 \\ Q(r_i) = 0 \quad for \quad \nabla \vec{v} \geq 0 \end{cases} \tag{1.35}$$

The second form 'Monaghan's Viscosity' is pair interaction potential and can be written in the way below.

$$\begin{cases} Q(r_i, r_k) = \dfrac{-\alpha \cdot C_{i,k} \cdot \mu_{i,k} + \beta \cdot \mu_{i,k}^2}{\rho_{i,k}} \quad for \quad \mu_{i,k} < 0 \\ Q(r_i, r_k) = 0 \qquad\qquad for \quad \mu_{i,k} \geq 0 \\ Where \quad \mu_{i,k} = h_{i,k} \cdot \dfrac{(\vec{v}(r_i) - \vec{v}(r_k)) \cdot (\vec{r}_i - \vec{r}_k)}{(\vec{r}_i - \vec{r}_k)^2 + \varepsilon_0 \cdot h^2_{i,k}} \end{cases} \tag{1.36}$$

In the previous expressions α, β are constant close to unity while $\varepsilon_0 \sim 0.01$. $C_s(r_i)$ and $h(r_i)$ are the speed of sound carried by the particle i and its smoothing length. $C_{i,k}$, $h_{i,k}$ and $\rho_{i,k}$ represent the average quantities at particles i and k.

For higher dimensions a tensorial form of (1.35) was introduced by Randles and Libersky [18]. The authors in their work used an "Interior Hull" method of finding neighbours based on the matrix $\overline{\overline{H_i}} = \sum_i (\vec{r}_i - \vec{r}_k) \otimes (\vec{r}_i - \vec{r}_k)$.

The central initiative in the procedure detailed in [18] for building a viscosity tensor $Q_i^{\alpha\beta}$ is the use of eigenvalues of the covariance matrix $\overline{\overline{H_i}}$ in order to obtain length scales corresponding to the principal strain rate direction. Also it involves eigenvalues and eigenvectors of the strain rate deviator tensor. Only negative eigenvalues were considered (compressive deformations) and the eigenvectors establish the principal components of the viscosity tensor.

The wall heating term, Fulk [19] is an artificial heat conduction term that is added to the energy equation.

$$\begin{cases} H(r_i) = \sum_{k=1}^{N_r} m_k \cdot \dfrac{Q_{i,k} \cdot \left(e(r_k) - e(r_i)\right) \cdot (\vec{r}_k - \vec{r}_i)}{\rho_{i,k} \cdot \left((\vec{r}_k - \vec{r}_i)^2 + \varepsilon_0 \cdot h^2{}_{i,k}\right)} \cdot \nabla_{r_k} W(r_i - r_k) \\ \\ Q(r_i) = g_1 \cdot h(r_i) \cdot C_s(r_i) \cdot \left| \left\langle \nabla_{r_i} \vec{v} \right\rangle_s \right| + g_2 \cdot h^2(r_i) \cdot \left\langle \nabla_{r_i} \vec{v} \right\rangle_s^2 \end{cases} \tag{1.36}$$

Where $Q_{i,k} = (Q(r_i) + Q(r_k))/2.$, g_1 and g_2 e the wall heating coefficients and are in the range of $[0.25\,,1.5\,]$.

J. J. Monaghan [18] considered dissipative terms in SPH and those appearing in Riemann solvers

and built an interesting and appropriate artificial viscosity and wall heating terms for momentum and energy equations.

It is often difficult to determine an appropriate choice of parameters α, β, g_1, g_2 which would introduce just enough viscosity to suppress numerical noise of a method without causing unnecessary shrinking of a shock.

1.6 Smoothing Length

The smoothing length h is not a thermodynamic quantity. In the interpolation formalism, as in SPH, it plays the role of the 'Power of Resolution' which expresses the ability of Kernels to estimate locally and accurately the fields during the evolution of the system.

The accuracy of the method depends on how and where densely physical fields are estimated. In SPH, variable smoothing length is analog to an adaptative gridding in meshing based Eulerian codes.

To maintain an accurate estimation 'High Power of Resolution' of the physical fields during the evolution of the system it is necessary to increase the smoothing length where the system is subjected to decompressions and to decrease it where compression occurs, this translates to.

Let dt represents the time step between two successive iterations and nd the spatial dimension, then.

$$\rho(r_i,\ t)\cdot h^{nd}(r_i,t)=\rho(r_i,t-dt)\cdot h^{nd}(r_i,t-dt) \tag{1.37}$$

In practice, the explicit integrated form below is preferred to the expression (1.37).

$$\frac{dh(r_i,t)}{dt}=-\left(\frac{h(r_i,t)}{nd.\rho(r_i,t)}\right).\frac{d\rho(r_i,t)}{dt} \tag{1.38}$$

The equations (1.37) and (1.38) have an isotropic evolution of the smoothing length. In general, experiments involve materials under anisotropic stresses and consequently the deformations and the distributions of particles become also anisotropic.

The example below represents the impact of two plates; it shows two configurations where the resolution becomes poor. In the flyer plate $(red\ particles)$, specific particles lose neighbours in the direction perpendicular to the impact while in the target plate $(blue\ particles)$ some impacted particles lose neighbours in the direction of the impact.

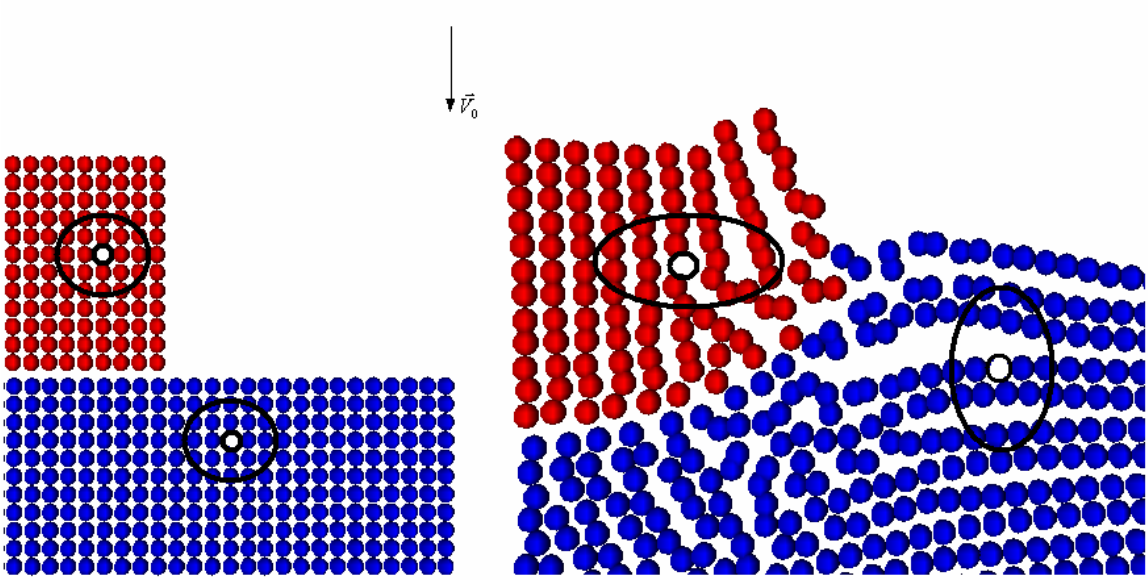

Figure1.1: Undeformed support for h (Left), and deformed support (Right)

To incorporate anisotropy effects in the numerical tests and to maintain acceptable accuracy in the derivative estimate in different directions, Benz first suggested that $h(r,t)$ should be treated as tensor $\overline{\overline{H}}$ that have to be diagonalized, J. P. Vila [20]

$$\overline{\overline{H}} = \begin{pmatrix} h_{11} & h_{12} & h_{13} \\ h_{21} & h_{22} & h_{23} \\ h_{31} & h_{32} & h_{33} \end{pmatrix} \rightarrow \overline{\overline{H}} = \begin{pmatrix} h_x & 0 & 0 \\ 0 & h_y & 0 \\ 0 & 0 & h_z \end{pmatrix} \tag{1.39}$$

Then the equation of evolution for each eigenvalue is obtained via an objective rate, i.e Jaumann rate:

$$\frac{d\overline{\overline{H}}}{dt} = \overline{\overline{H}} \cdot \overline{\varepsilon} + \overline{\overline{H}} \cdot \overline{\Omega} + \overline{\Omega} \cdot \overline{\overline{H}} \tag{1.40}$$

The deformation tensor $\overline{\overline{\varepsilon}}$ and the rotation tensor $\overline{\overline{\Omega}}$ are expressed by $\varepsilon_{\alpha\beta} = \frac{1}{2}\left(\frac{\partial v_\alpha}{\partial x_\beta} + \frac{\partial v_\beta}{\partial x_\alpha}\right)$ and by $\Omega_{\alpha\beta} = \frac{1}{2}\left(\frac{\partial v_\alpha}{\partial x_\beta} - \frac{\partial v_\beta}{\partial x_\alpha}\right)$ respectively.

The idea above takes into account the deformation and the rotation of the particles, but despite of its elegancy it was discarded because of its expensive computation cost for the calculation of the egeinvalue and eigenvectors for each particle especially in $3D$ tests.

As mentioned in section 1.5, to overcome the loss of neighbours due to anisotropy Randles and Libersky [17] performed an "Interior Hull" method based on convex hull algorithm for selecting neighbours. This approach has the advantage over the previous methods in sense that it is geometrical and autonomous from physical considerations.

1.7 Conclusion

An approach based on Eulerian formalism was used to derive a SPH based approximation of the continuum dynamic. Eulerian formalism is considered here as a reference approach because it is well established concerning its mathematical developments and analyses (Riemann Problem). The method attracted early interest from scientists and Engineers and was successfully validated for a large variety of problems in Computational Fluid Dynamics, Hydrodynamic, Aerodynamic, Combustions, Multi-phase flows and Multiple condensed phases etc….

It is important to stress that during derivation of the SPH formalism in this chapter, Kernels and convolutions (integrals) were Eulerian in nature.

The introduction of the 'mass' and of the 'variable smoothing length' attached to each particle (point) is central to SPH. Both of these entities are intimately associated with density and very important in point wise integration.

However, the need for the smoothing length equation calls for observations. First, one notes that the equation of smoothing length can be derived by using energy conservation or momentum instead of density conservation. A second observation to be made concerns the redundancy introduced when the equation (1.38) is added to the laws of conservation of mass, momentum and energy.

1.8 References

[1] L. Lucy. (1977): "A Numerical Approach to the Testing of the Fission Hypothesis", The Astronomical J., 82, 1013-1024.

[2] R. A. Gingold and J. J. Monaghan (1977): Mon. Not. R. Astr. Soc., 181, 375-389.

[3] J. J. Monaghan (1982): "On the Problem of Penetration in Particle Methods", J. of Comp. Phys., 82, 1-15.

[4] W. Benz. (1992): "Smooth Particle Hydrodynamics" Ann. Rev. Astro. Astrophy., 30, 543-74.

[5] W. Benz.(1995): "Simulation of Brittle Solids using Smoothed Particle Hydrodynamics", Comput. Phys. Comm., Vol. 87, 253-265.

[6] L. Libersky L., A. Petchek, T. Carney, J. Hipp, F. Allahdadi. (1993): "High Strain Lagrangian Hydrodynamics", J. Comput. Phys., 109, 67-75.

[7] S. Johnson, R. Stryck, S. Beissel. (1996): "SPH for High Velocity Impact Computations", Comp. Meth. Appl. Mech. Engrg., Vol 139, 347-373.

[8] S. Mas-Gallic, P. A. Raviart . Num Math.51, 323-352 (1987).

[9] J. Swegle, D.Hicks, S. Attaway (1994): "An Analysis of Smoothed Particle Hydrodynamics", SAND93-2513, Sandia National Laboratories, Albuquerque.

[10] D. S. Balsara (1995): "Von Neumann stability analysis of Smooth Particle Hydrodynamics suggestions for optimal algorithms". J. Comp. Phys, 121, 357-372.

[11] R. Dilisio, E. Grenier, M. Pulvirenti: 'The Convergence of the SPH method'. Comput. Math. Applic .Vol 35, No 1 / 2, pp.95-102 (1998).

[12] D. L. Hicks and L. M. Liebrock.'SPH Hydrocodes can be stabilized with shape-shifting'. Inter. J. Comput and Math, Appl. 38 (1999) 1-16.

[13] Ben Moussa and J. P. Vila:'Convergence of SPH for scalar non-linear conservation laws'. SIAM J. Numer. Anal. Vol 37, No 3,pp. 863-887.(2000).

[14] G. Boillat, C. M. Dafermos, P.D. Lax, T. P. Liu: 'Recent Mathematical Methods in Nonlinear Wave Propagation', 1640 Lectures Notes in Mathematics. Editor: T.Ruggeri. Montecatini 1994. Springer.

[15] P. A. Raviart:' Methodes Numeriques en Transport de Particules Chargees'. GdR. SPARCH, Models Mathematique et Simulation en Physique. Oleron , Sep 1993.

[16] J. J. Monaghan, R. A. Gingold (1983): Shock Simulation by the Particle SPH. J. Compu. Phys. 52, 374-389.

[17] J. Von Neumann and R. D. Richtmeyer:'A Method for The Numerical Calculation of Hydrdynamic Shocks'. J. Appl. Phys 1949.

[18] P. Randles and L. Libersky,"Normalised SPH with stress points", *Int. j. Num. Meth. Engng* 2000; 48:1445-1462.

[19] D. A. Fulk, A Numerical Analysis of Smoothed Particle Hydrodynamics, PhD Thesis, Air Force Institut of Technology, Wright-Patterson AFB OH (1994).

[20] J. P. Vila. Private Comminucations.

2. CONNECTION BETWEEN HAMILTONIAN MANY-PARTICLES SYSTEM AND THE SMOOTHED PARTICLE HYDRODYNAMICS (SPH) FORMALISM

2.1 Introduction

The Newtonian mechanics elegantly reformulated by Lagrange (1736-1813) and Hamilton (1805-1865) did very well for predicting the evolutions and behaviours of classical mechanical systems.

It turns out that the Hamiltonian formulation based on the principle of least action rather than the Lagrangian formulation is the formalism that most readily develops after physicists discover the existence of non-Newtonian particles (statistical and quantum mechanics), then the concept of energy became central in many complex physical systems.

Historically, the transition from classical mechanics to statistical mechanics and to quantum mechanics Tolman [1], Prigogine [2], Ruelle [3] was much easier to make within the framework of the Hamiltonian formalism.

In the other hand, at practical level, the ‘’generalized coordinates’’ in Lagrangian formalism result in non-symmetrical set of equations. In general, it is convenient to have a symmetric set of equations. The Hamiltonian approach is easily adapted and allows having a symmetric set of equations of motions, which is of great importance in general research. These are some sources of the motivations to focus on the Hamiltonian formalism in this work rather than on the Lagrangian one.

The object of this work is to derive the equations of motion for SPH formalism by using the concept of energy and the properties of the Hamiltonian function of a given system of N point masses interacting through a pair-wise potential whose range is in the same width as the smoothing length associated with each particle. The approach adopted in section two of this chapter follows the idea of Luehr *et al* [4].

In the second part, the *Hamilton' principle* is considered as starting point to obtains particles approximation of transport equations in a bounded domain.

2.2 Energy and the Hamiltonian Function

One considers a system of N non-deformable particles evolving with time t within a domain $D \subset \Re^{nd}$, whose constant masses, positions and velocities are respectively designated by $m_n, \vec{x}_n(t)$ and $\vec{v}_n(t) = \dfrac{\vec{P}_n(t)}{m_n}$, where $n = 1,2,....N$ labels the n^{th} particles and $\vec{P}_n(t)$ represents its momentum or generalized momentum. The Hamiltonian of such system is given by:

$$H(\vec{p}_1(t), \vec{p}_2(t),..., \vec{p}_N(t), \vec{x}_1(t), \vec{x}_2(t),..., \vec{x}_N(t)) = \sum_{n=1}^{N} \frac{\vec{p}_n^{\,2}}{2.m_n} + \sum_{n=1}^{N} m_n \cdot V_n \qquad (2.1)$$

The first term is the kinetic energy of the system and the second term defines its potential energy; this later is to be regarded as the work necessary to bring the system of particles from some standard state to its actual state at time considered, V_n is also called internal energy per particle. The potential (or internal) energy depends explicitly on the particles positions.

To derive the equations of motion in SPH forms, one needs to assume that particle sets or interpolating points can be considered at some limit as a continuum. This assumption should be made, because the range of the interactions in SPH defined by the smoothing length which is much biger than the intra-atomic interaction range. Thus allows for the thermodynamics principles of continuum to be mapped on to the masses points.

Classical thermodynamics of a continuum deals with systems, which, from a phenomeno-logical point of view, are submitted, to infinitely slow transformations, then, at each stage, the system is in an equilibrium state; the consequence is that every sufficiently slow process is claimed to be reversible. This assumption does not hold in general.

In thermo-dynamic field theory, the assumption of slow transformations is avoided by considering elements of masses and elements of continuum (Volume element).

Conservation principles hold for the mass element while the element of continuum changes geometrically depending on the strain tensor ε^{ij}. Also its thermal energy may change with the

presence of gradient of temperatures T and in general, other internal fields and characteristics can evolve following certain internal parameters that are denoted here by α^{ij}. For detailed and complete developments in thermodynamic and thermo mechanic of continuum media, see Malvern [5], Ziegler [6].

In SPH formalism, the particles are the centre of mass of the elements, while volumes elements are delimited by the centres of mass of the neighbouring particles.

From here on, only conservative systems are considered, then, the Hamiltonian is not a function of time and therefore:

$$\begin{aligned}\frac{dH}{dt} &= \sum_n \left[\frac{d\vec{p}_n}{dt} \cdot \vec{v}_n + m_n \cdot \frac{dV_n}{dt} \right] \\ &= 0\end{aligned} \tag{2.2}$$

In the light of the assumptions concerning the internal energy by unit mass $V_n(\varepsilon, \alpha, T)$, its material derivative gives:

$$\begin{aligned}\frac{dV_n}{dt} = &\left(\frac{\partial V_n}{\partial \varepsilon_n^{ij}} \right)_{\alpha, T} \cdot \frac{d\varepsilon_n^{ij}}{dt} + \left(\frac{\partial V_n}{\partial \alpha_n^{ij}} \right)_{\varepsilon, T} \cdot \frac{d\alpha_{ij}^{n}}{dt} \\ &+ \left(\frac{\partial V_n}{\partial T_n} \right)_{\alpha, \varepsilon} \cdot \frac{dT_n}{dt}\end{aligned} \tag{2.3}$$

If the transformation consists only on heating process, then $\frac{d\varepsilon_n^{ij}}{dt} = \frac{d\alpha_n^{ij}}{dt} = 0$ and, (2.3) reduces to $dV_n = \left(\frac{\partial V_n}{\partial T_n} \right)_{\varepsilon, \alpha} \cdot dT_n$, where $\left(\frac{dV_n}{dT_n} \right)_{\varepsilon, \alpha}$ and T_n are the specific heat capacity and temperature carried by the particle n. In the following, for simplicity, one is concerned only with adiabatic processes

The first term in the RHS of (2.3) is the rate of mechanical work (power) due to the interactions between particles and their surroundings. From, the principle of virtual power in continuum mechanics, one obtains:

$$\rho_n \cdot \frac{dV_n}{dt} = \rho_n \cdot \left(\frac{\partial V_n}{\partial \varepsilon_n^{ij}} \right)_{\alpha, T} \cdot \frac{d\varepsilon_n^{ij}}{dt} = \sigma_n^{ij} \cdot D_n^{ij} \qquad (2.4)$$

In (2.4), the small displacements theory is used, and then $D_n^{ij} = \frac{d\varepsilon_n^{ij}}{dt} = \frac{\partial v_n^i}{\partial x_n^j}$. Where σ_{ij}^n is the stress tensor exerted on the volume surrounding the particle n.

In the theory of elasticity, a function Ξ called the *Strain energy function* is often defined, with the property that:

$$\frac{\partial \Xi}{\partial \varepsilon^{ij}} = \sigma^{ij} \qquad \text{with} \qquad (i, j = 1,2,3).$$

The *Strain energy function* Ξ is identified with internal energy in an isentropic process and the free energy in an isothermal process.

2.2.1 Energy Equation in SPH

In SPH formalism, the density and flux are defined as the continuum density and continuum flux per unit volume from corpuscular masses and velocities by convolution operation with a given interpolating kernel W :

$$\langle \rho_n(t) \rangle = \sum_k m_k \cdot W(x_n - x_k(t)) \qquad (2.5)$$

and $$\left\langle \rho_n \cdot \vec{v}_n(t) \right\rangle = \sum_k m_k \cdot \vec{v}_k(t) \cdot W(x_n - x_k(t)) \tag{2.6}$$

The gradient of the quantities above are given by:

$$\nabla_{x_n} \left\langle \rho_n(t) \right\rangle = \sum_k m_k \cdot \nabla_{x_n} W(x_n - x_k) \tag{2.7}$$

A symmetric kernel was used in (2.7); with the same reasoning, one has for the flux:

$$\nabla_{x_n} \left\langle \rho_n \cdot \vec{v}_n(t) \right\rangle = \sum_k m_k . \vec{v}_k(t) \cdot \nabla_{x_n} W(x_n - x_k) \tag{2.8}$$

In order to derive the equation of energy for SPH, one needs to express, the strain rate tensor D_n^{ij} in a conservative form:

$$D_n^{ij} = \frac{\partial v_n^i}{\partial x_n^j} = \frac{1}{\rho_n} \cdot \left[\frac{\partial \left(\rho_n \cdot v_n^i \right)}{\partial x_n^j} - v_n^i \cdot \frac{\partial \rho_n}{\partial x_n^j} \right] \tag{2.9}$$

Combining, (2.7), (2.8) and (2.9) in the equation of energy (2.4), one obtains:

$$\frac{dV_n(t)}{dt} = \frac{\sigma_n^{ij}}{\rho_n^2} \cdot \sum_k m_k \cdot \left\{ \vec{v}_k(t) - \vec{v}_n \right\} \cdot \nabla_{x_n} W(x_n - x_k) \tag{2.10}$$

The equation (2.10) is identical to the equation for energy (1.29) derived in the chapter 1

2.2.2 Momentum Equation in SPH

The conservation of the total energy expressed in (2.2) becomes with the help of (2.8)

$$\begin{aligned}
\sum_n \frac{d\vec{p}_n(t)}{dt}\cdot\vec{v}_n(t) &= -\sum_n m_n \cdot \frac{\overline{\overline{\sigma_n}}}{\rho_n^2}\cdot\sum_k m_k\cdot\{\vec{v}_k(t)-\vec{v}_n(t)\}\cdot\nabla_n W(x_n-x_k)\\
&= -\sum_n m_n\cdot\frac{\overline{\overline{\sigma_n}}}{\rho_n^2}\cdot\sum_k m_k\cdot\vec{v}_k(t)\cdot\nabla_n W+\sum_n m_n\cdot\frac{\overline{\overline{\sigma_n}}}{\rho_n^2}\cdot\sum_k m_k\cdot\vec{v}_n(t)\cdot\nabla_n W\\
&= -\sum_k m_k\cdot\frac{\overline{\overline{\sigma_k}}}{\rho_k^2}\cdot\sum_n m_n\cdot\vec{v}_n(t)\cdot\nabla_k W+\sum_n m_n\cdot\frac{\overline{\overline{\sigma_n}}}{\rho_n^2}\cdot\sum_k m_k\cdot\vec{v}_n(t)\cdot\nabla_n W \qquad (2.12)\\
&= -\sum_k m_k\cdot\frac{\overline{\overline{\sigma_k}}}{\rho_k^2}\cdot\sum_n m_n\cdot\vec{v}_n(t)\cdot\nabla_k W-\sum_n m_n\cdot\frac{\overline{\overline{\sigma_n}}}{\rho_n^2}\cdot\sum_k m_k\cdot\vec{v}_n(t)\cdot\nabla_k W\\
&= -\sum_n m_n\cdot\vec{v}_n(t)\cdot\left[\sum_n m_k\cdot\left\{\frac{\overline{\overline{\sigma_k}}}{\rho_k^2}+\frac{\overline{\overline{\sigma_n}}}{\rho_n^2}\right\}\cdot\nabla_k W(x_n-x_k)\right]
\end{aligned}$$

In the relation above, for sake of visibility, $\nabla_{x_k} W$ was replaced by $\nabla_k W$. Rearranging the expression above differently, one obtains:

$$\sum_n \vec{v}_n(t)\cdot\left[\frac{d\vec{p}_n(t)}{dt}+m_n\cdot\sum_k m_k\cdot\left\{\frac{\overline{\overline{\sigma_k}}}{\rho_k^2}+\frac{\overline{\overline{\sigma_n}}}{\rho_n^2}\right\}\cdot\nabla_{x_k} W(x_n-x_k)\right]=0 \qquad (2.13)$$

Since velocities of particles $\vec{v}_n(t)$ are arbitrary, the relation (2.13) is satisfied if the term under brackets vanishes, that is:

$$\frac{d\,\vec{p}_n(t)}{dt}=-m_n\cdot\sum_k m_k\cdot\left\{\frac{\overline{\overline{\sigma_k}}}{\rho_k^2}+\frac{\overline{\overline{\sigma_n}}}{\rho_n^2}\right\}\cdot\nabla_k W \qquad (2.14)$$

Or

$$\frac{d\vec{v}_n(t)}{dt} = -\sum_k m_k \cdot \left\{ \frac{\overline{\overline{\sigma_k}}}{\rho_k^2} + \frac{\overline{\overline{\sigma_n}}}{\rho_n^2} \right\} \cdot \nabla_k W \tag{2.15}$$

The expressions (2.5), (2.11) and (2.15) constitute a system that describes the dynamics of particles in SPH formalism.

2.2.3 Continuity Equation in SPH

It is natural to derive the conservation of matter from the equation of smoothed density (2.1). Then for particles with constant masses it follows by derivation with respect to time, that:

$$\begin{aligned} \frac{\partial \langle \rho_n(t) \rangle}{\partial t} &= \sum_k m_k \cdot \frac{\partial W(x_n - x_k(t))}{\partial t} \\ &= \sum_k m_k \cdot \frac{dx_k(t)}{dt} \cdot \frac{\partial W(x_n - x_k(t))}{\partial x_k} \end{aligned}$$

With the help of symmetric kernel, one gets:

$$\begin{aligned} \frac{\partial \langle \rho_n(t) \rangle}{\partial t} &= -\sum_k m_k \cdot \vec{v}_k \cdot \nabla_{x_n} W \\ &= -\langle \nabla_x \rho \cdot \vec{v} \rangle_{x_n} \\ &= -\langle \vec{v}(x) \cdot \nabla_x \rho(x,t) \rangle_{x_n} - \langle \rho(x,t) \cdot \nabla_x \vec{v}(x,) \rangle_{x_n} \end{aligned}$$

Using material derivative $\left(\frac{d(\bullet)}{dt} = \frac{\partial(\bullet)}{\partial t} + \vec{v} \cdot \vec{\nabla}(\bullet) \right)$, then, it follows the expression of the smoothed continuity equation:

$$\frac{d\langle \rho_n(t)\rangle}{dt} = -\langle \rho_n(t)\cdot \nabla_x \vec{v}(t)\rangle_{x_n} = -\left[\langle \nabla_x (\rho\cdot\vec{v})\rangle_{x_n} - \langle \vec{v}\cdot\nabla_x \rho\rangle_{x_n}\right] \tag{2.15}$$

Since symmetric kernel is used and boundary contributions are neglected, it is clear that $\langle \nabla\psi\rangle = \nabla\langle\psi\rangle$ for any field. Then by using again the expressions (2.8) and (2.9) in the expression (1.3.1), one has finally:

$$\frac{d\langle \rho_n(t)\rangle}{dt} = \sum_k m_k \cdot \{\vec{v}_n - \vec{v}_k(t)\}\cdot \nabla_{x_n} W(x_n - x_k) \tag{2.16}$$

2.3 Hamilton's principle

Let L be the Lagrangian of the continuum which occupies a domain $D \subset \Re^{nd}$ and bounded by a surface B, let K and U be its kinetic and potential energies parts respectively, then,

$$\begin{aligned} L &= K - U \\ &= \int_D \rho(r,t)\cdot\frac{v^2(r,t)}{2}\cdot d^3r - \int_D \rho(r,t)\cdot V(r)\cdot d^3r \end{aligned}$$

The ensemble of events E is determined by the centre of masses of the volumes elements and time t, $E = \{(\vec{r}_1, \vec{r}_2, ...\vec{r}_n .., t)/\, r_i \in D\}$, where the indices n and i refer to the volumes elements. Let Γ be any curve in E given by an equation $\vec{r}_i = \vec{r}_i(t)$ and a direction $\delta.\vec{v}_i = \frac{\partial(\delta.\vec{r}_i)}{\partial t}$.

The *Hamilton's principle or the principle of least action* is concerned with the minimization of Δ (action). The variation $\delta\Delta$ of the Lagrangian L over a set of processes along any oriented curve Γ drawn from point $A(t=0)$ to a point $A(t=\tau>0)$ that assume a given displacement at an initial time $t=0$ as well as at final time $t=\tau$, then:

$$\begin{aligned}\delta\Delta &= \delta\int_0^\tau L\cdot dt \\ &= \int_0^\tau \delta L\cdot dt \\ &= \int_0^\tau L(\vec{r}+\delta\vec{r},\vec{v}+\delta\vec{v},t)\cdot dt - \int_0^\tau L(\vec{r},\vec{v},t)\cdot dt \\ &= \int_0^\tau \left\{\frac{\partial L}{\partial v}\cdot\delta\vec{v}+\frac{\partial L}{\partial r}\cdot\delta\vec{r}\right\}\cdot dt\end{aligned}$$

Recall that $\delta\vec{v}=\dfrac{d(\delta\vec{r})}{dt}$, then

$$\delta\Delta = \int_0^\tau \left\{\frac{\partial L}{\partial v}\cdot\frac{d(\delta\vec{r})}{dt}+\frac{\partial L}{\partial r}\cdot\delta\vec{r}\right\}\cdot dt$$

The integration by parts of the first term in the right hand side gives:

$$\int_0^\tau \delta L\cdot dt = \int_0^\tau \left\{-\frac{d}{dt}\left(\frac{\partial L}{\partial v}\right)+\frac{\partial L}{\partial r}\right\}\cdot\delta\vec{r}\cdot dt + \left[\frac{\partial L}{\partial v}\cdot\delta\vec{r}\right]_0^\tau$$

The last term in the equation vanishes because initial and final displacements are prescribed, $\delta \vec{r}(t=0) = \delta \vec{r}(t=\tau) = 0$ in any point within the continuum.

From the expression of the Lagrangian, the first and the second term above give:

$$\int_0^\tau \delta\, L \cdot dt = -\int_0^\tau dt \cdot \left\{ \frac{d}{dt}\left(\frac{\partial K}{\partial v} \right) + \frac{\partial U}{\partial r} \right\} \cdot \delta . \vec{r}$$

$$= -\int_0^\tau dt \cdot \int_D \left(\rho \cdot \frac{d\vec{v}}{dt} \cdot \delta \vec{r} \right) \cdot d^3 r - \int_0^\tau \delta U \cdot dt$$

In the integral above, the density $\rho(r,t)$ and the volume element $d^3 r$ are varied in such a way that $\delta(\rho \cdot d^3 r) = 0$.

$$\int_0^\tau \delta\, L \cdot dt = -\int_0^\tau dt \cdot \int_D \left(\rho \cdot \frac{d\vec{v}}{dt} \cdot \delta \vec{r} \right) \cdot d^3 r - \int_0^\tau dt \cdot \int_D \rho \cdot \delta V \cdot d^3 r$$

$$= -\int_0^\tau dt \cdot \int_D \left(\frac{d\vec{v}}{dt} \cdot \delta \vec{r} + \delta V \right) \cdot \rho \cdot d^3 r \qquad (2.17)$$

The integral above vanishes and following the assumption used in the previous part in equation (2.4), $\rho \cdot \delta V = \rho \cdot \frac{\partial V}{\partial \varepsilon^{ij}} \cdot \delta \varepsilon^{ij} = \rho \cdot \frac{\partial V}{\partial \varepsilon^{ji}} \cdot \delta \varepsilon^{ji} = \sigma^{ij} \cdot \delta \varepsilon^{ij}$ with $\delta \varepsilon^{ij} = \frac{\partial(\delta r_i)}{\partial r_j}$ it follows then:

$$\int_D \delta V \cdot \rho \cdot d^3 r = \int_D \left(\rho \cdot \frac{\partial V}{\partial \varepsilon^{ij}} \right) \cdot \frac{\partial(\delta r_i)}{\partial r_j} \cdot d^3 r \qquad (2.18)$$

The integration by part the expression above gives,

$$\int_D \delta V \cdot \rho \cdot d^3 r = \int_B \left(\rho \cdot \frac{\partial V}{\partial \varepsilon^{ij}} \right) \cdot \delta r_i(t) \cdot ds_j - \int_D \frac{\partial}{\partial r_j} \left(\rho \cdot \frac{\partial V}{\partial \varepsilon^{ij}} \right) \cdot \delta . r_i(t) \cdot d^3 r \qquad (2.19)$$

In the equality (2.18), ds_j is the j^{th} component of the surface element of the volume element $d^3 r$. Incorporating the expression (2.18) in (2.17), the variational equation gives:

$$\int_D \rho \cdot \frac{d\vec{v}}{dt} \cdot \delta \vec{r} \cdot d^3 r - \int_D \frac{\partial}{\partial r_j} \left(\rho \cdot \frac{\partial V}{\partial \varepsilon^{ij}} \right) \cdot \delta r_i \cdot d^3 r + \int_B \left(\rho \cdot \frac{\partial V}{\partial \varepsilon^{ij}} \cdot \delta r_i \right) \cdot \hat{n}_j \cdot ds = 0$$

And its compact counter-part form becomes:

$$\int_D \rho \cdot \frac{d\vec{v}}{dt} \cdot \delta \vec{r}(t) \cdot d^3 r = \int_D \nabla_r \left(\rho \cdot \frac{\partial V}{\partial \varepsilon} \right) \cdot \delta \vec{r}(t) \cdot d^3 r - \int_B \left(\rho \cdot \frac{\partial V}{\partial \varepsilon} \right) \cdot \hat{n} \cdot \delta \vec{r}(t) \cdot ds \quad (2.20)$$

Where $\hat{n}$ is the outward unit normal to the surface element ds and $\left(\rho \cdot \frac{\partial V}{\partial \varepsilon^{ij}} \right) = \sigma^{ij} = \overline{\overline{\sigma}}$.

The integral (2.20) has to be satisfied for all volumes and surfaces elements lying in $D \cup B$, then.

$$\begin{cases} \delta \vec{r}(t) = \vec{0} \quad for \quad r \in B_R \quad \forall t, 0 < t < \tau & 2.21-a \\ \overline{\overline{\sigma}} \cdot \hat{n} = \vec{0} \quad for \quad r \in B_F & 2.21-b \\ \int_D \left(\frac{d\vec{v}(r,t)}{dt} - \frac{\nabla_r \overline{\overline{\sigma}}}{\rho(r,t)} \right) \cdot \rho(r,t) \cdot d^3 r = 0 \quad for \quad r \in D & 2.21-c \end{cases}$$

In the system above B_R and B_F are rigid and free boundaries respectively.

2.3.1 Hamilton's principle and Momentum Equation in SPH

One began with the relation (2.21-c) that is reformulated differently by dropping $\rho(r,t)$ since the density is strictly positive and bounded quantity.

$$\int_V \left(\frac{d\vec{v}(r,t)}{dt} - \frac{\nabla_r \overline{\overline{\sigma(r)}}}{\rho(r,t)} \right) \cdot \rho(r,t) \cdot d^3 r = 0 \Leftrightarrow \int_V \left(\frac{d\vec{v}(r,t)}{dt} - \frac{\nabla_r \overline{\overline{\sigma(r)}}}{\rho(r,t)} \right) \cdot d^3 r = 0 \quad (2.22)$$

Secondly, one uses *Dirac* $\delta(r_n - r')$ distribution and the properties of the kernel distribution $W(r_n - r', H)$, then:

$$\begin{aligned} \int_V \delta(r_n - r') \cdot \frac{d\vec{v}(r',t)}{dt} \cdot d^3 r' &= \lim_{H \to 0^+} \int_D \left(\frac{\nabla_{r'} \overline{\overline{\sigma(r')}}}{\rho(r',t)} \right) \cdot W(r_n - r', H) \cdot d^3 r' \\ &= \int_D \left(\frac{\nabla_{r'} \overline{\overline{\sigma(r')}}}{\rho(r',t)} \right) \cdot \lim_{H \to 0^+} W(r_n - r', H) \cdot d^3 r' \end{aligned} \quad (2.23)$$

Or

$$\frac{d\vec{v}(r_n,t)}{dt} = \int_{D_W} \left(\frac{\nabla_{r'} \overline{\overline{\sigma(r')}}}{\rho(r',t)} \right) \cdot W(r_n - r', h) \cdot d^3 r' \quad (2.24)$$

Where D_W is a compact domain of the kernel W, $\lim_{H \to 0^+} W(z, H) = W(z,h)$ and h denote the limit of the smoothing length H, in practice h is strictly positive. In the following, for clarity, one uses W for $W(r_n - r', h)$, $\vec{v}_n$ for $\vec{v}(r_n,t)$ and so on. Re-writing the equation (2.24) differently;

$$\frac{d\vec{v}_n}{dt} = \int_{D_W} \left(\nabla_{r'} \left(\frac{\overline{\overline{\sigma(r')}}}{\rho^2(r')} \right) + \left(\frac{\overline{\overline{\sigma_n}}}{\rho_n^2} \right) \cdot \rho(r') \right) \cdot \nabla_{r'} W \cdot d^3 r'$$

$$= -\int_{D_W} \left(\frac{\overline{\overline{\sigma(r')}}}{\rho^2(r')} + \frac{\overline{\overline{\sigma_n}}}{\rho_n^2} \right) \rho(r') \cdot \nabla_{r'} W \cdot d^3 r' \qquad (2.25)$$

$$+ \int_{D_W} \nabla_{r'} \left[\left(\frac{\overline{\overline{\sigma(r')}}}{\rho^2(r')} + \frac{\overline{\overline{\sigma_n}}}{\rho_n^2} \right) \rho(r') \cdot W \right] \cdot d^3 r'$$

Using Gauss theorem for the second term on the right hand side above, it follows:

$$\frac{d\vec{v}_n}{dt} = -\int_{D_W} \left(\frac{\overline{\overline{\sigma(r')}}}{\rho^2(r')} + \frac{\overline{\overline{\sigma_n}}}{\rho_n^2} \right) \cdot \rho(r') \cdot \nabla_{r'} W \cdot d^3 r'$$

$$+ \int_{D_W \cap B} \left(\frac{\overline{\overline{\sigma(r')}}}{\rho^2(r')} + \frac{\overline{\overline{\sigma_n}}}{\rho_n^2} \right) \cdot \rho(r') \cdot W \cdot \hat{n}(r') \cdot ds(r') \qquad (2.26)$$

Those particles having their distribution $W(r_n - r', h)$ interacting with surfaces in r', ($D_W \cap B(r') \neq \varnothing$) will be submitted to a boundary forces given by the second term above which is the SPH version of the boundary term in the equation (2.20).

2.4 Hamilton' principle and Energy Equation in SPH

One now wants to express the equation of balance of energy, with forms derived from different parts of Hamilton's principle equation. To achieve this, one assumes that the system is isolated and considering the Hamiltonian $H = K + U$.

Following the expressions of kinetic and internal energies, one gets:

$$\delta K = \int_D \rho \cdot \vec{v} \cdot \delta \vec{v}(t) \cdot d^3 r \qquad (2.27)$$

and $$\delta U = \int_D \rho \cdot \delta V \cdot d^3 r \tag{2.28}$$

Let $\delta \vec{r}(t) = \vec{v}(r,t) \cdot \delta t$, then variational form of the Hamiltonian becomes,

$$\frac{\delta H}{\delta t} = \int_D \rho \cdot \frac{\delta \vec{v}}{\delta t} \cdot \vec{v}(t) \cdot .d^3 r + \int_D \rho \cdot \frac{\delta V(r)}{\delta t} \cdot d^3 r$$

$$\frac{dH}{dt} = \lim_{\delta t \to 0} \frac{\delta H}{\delta t}$$

$$= \int_D \rho \cdot \frac{d\vec{v}}{dt} \cdot \vec{v} \cdot d^3 r + \int_D \rho \cdot \frac{d V(r)}{d t} \cdot d^3 r$$

The principle of the conservation of energy, one obtains:

$$\int_D \rho \cdot \frac{d\vec{v}}{dt} \cdot \frac{\delta \vec{r}(t)}{\delta t} \cdot d^3 r + \int_D \rho \cdot \frac{dV(r)}{dt} .d^3 r = 0$$

Using the equation (2.20), the expression above becomes

$$\int_D \nabla_r \left(\rho \cdot \frac{\partial V}{\partial \varepsilon} \right) \cdot \frac{\delta \vec{r}(t)}{\delta t} \cdot d^3 r - \int_B \left(\rho \cdot \frac{\partial V}{\partial \varepsilon} \right) \cdot \hat{n} \cdot \frac{\delta \vec{r}(t)}{\delta t} \cdot ds + \int_D \rho \cdot \frac{dV(r)}{dt} \cdot d^3 r = 0$$

Finally, the equation of balance of internal energy gives:

$$\int_D \rho \cdot \frac{dV}{dt} \cdot d^3 r = -\int_V \left(\nabla_r \cdot \overline{\overline{\sigma(r)}} \right) \cdot \vec{v} \cdot d^3 r + \int_B \overline{\overline{\sigma(r)}} \cdot \vec{v} \cdot \hat{n} \cdot ds \qquad (2.29)$$

Integration by parts allows us to re-write (2.29).

$$\int_D \rho(r,t) \cdot \left(\frac{dV(r)}{dt} - \frac{\overline{\overline{\sigma(r)}}}{\rho(r)} \cdot \nabla_r \vec{v} \right) \cdot d^3 r = 0 \qquad (2.30)$$

In order to extend the relation (2.30) above to points located in (r_n, t), one proceeds again in the same way as for the momentum equation, then.

$$\int_D \delta(r_n - r') \cdot \frac{dV(r')}{dt} \cdot d^3 r' = \underset{H \mapsto 0^+}{Lim} \int_{D_W} \frac{\overline{\overline{\sigma(r')}}}{\rho(r')} : \nabla_{r'} \vec{v}(r') \cdot W(r_n - r', H) \cdot d^3 r'$$

Performing the limit above and smoothing only terms under the gradient operator, it follows.

$$\frac{dV_n}{dt} = \int_{D_W} \frac{\overline{\overline{\sigma(r')}}}{\rho(r')} \cdot \nabla_{r'} \vec{v}(r') \cdot W(r_n - r', h) \cdot d^3 r'$$

$$\approx \frac{\overline{\overline{\sigma(r_n)}}}{\rho(r_n)} \cdot \int_{D_W} \nabla_{r'} \vec{v}(r') \cdot W(r_n - r', h) \cdot d^3 r'$$

$$\approx \frac{\overline{\overline{\sigma(r_n)}}}{\rho(r_n)} \cdot \int_{D_W} \{\nabla_{r'} (\rho \cdot \vec{v}) - \vec{v}_n \cdot \nabla_{r'} \rho\} \cdot W(r_n - r', h) \cdot d^3 r'$$

$$\approx \frac{\overline{\overline{\sigma_n}}}{\rho_n} \cdot \int_{D_W} \{\nabla_{r'} (\rho \cdot (\vec{v}(r') - \vec{v}_n) \cdot W) - \rho \cdot (\vec{v}(r') - \vec{v}_n) \cdot \nabla_{r'} W\} \cdot d^3 r'$$

By using Gauss theorem for the first term, one obtains finally.

$$\begin{aligned} \frac{dV_n}{dt} &= -\frac{\overline{\overline{\sigma_n}}}{\rho_n^2} \cdot \int_{D_W} (\vec{v}(r') - \vec{v}_n) \cdot \nabla_{r'} W \cdot \rho \cdot d^3 r' \\ &+ \frac{\overline{\overline{\sigma_n}}}{\rho_n^2} \cdot \int_{D_W \cap B} \rho(r') \cdot (\vec{v}(r') - \vec{v}_n) \cdot \hat{n}(r') \cdot W \cdot ds \end{aligned} \tag{2.31}$$

By using the symmetry of $W(r_n - r', h)$, one obtains:

$$\begin{aligned} \frac{dV_n}{dt} &= \frac{\overline{\overline{\sigma_n}}}{\rho_n^2} \cdot \int_{D_W} (\vec{v}(r') - \vec{v}_n) \cdot \nabla_{r_n} W \cdot \rho \cdot d^3 r' \\ &+ \frac{\overline{\overline{\sigma_n}}}{\rho_n^2} \cdot \int_{D_W \cap B} \rho(r') \cdot (\vec{v}(r') - \vec{v}_n) \cdot \hat{n}(r') \cdot W \cdot ds \end{aligned} \tag{2.32}$$

Where $\overline{\overline{\sigma_n}} = \overline{\overline{\sigma(r_n)}}$, $\rho_n = \rho(r_n, t)$ and $\vec{v}_n = \vec{v}(r_n, t)$. The second term above expresses the rate power done by the stress on the bounding surface $D_W \cap B(r')$.

2.4.1 Hamilton's principle and Continuity Equation in SPH

In the previous sections, the analysis and the derivation of SPH equations are based on the assumption that $\delta(\rho \cdot d^3 r) = 0$ which is an expression of the equation of continuity, as we will show.

$$\begin{aligned} \delta(\rho \cdot d^3 r) = 0 \quad &\Leftrightarrow \quad \delta \int_D \rho(r,t) \cdot d^3 r(t) = 0 \\ &\Leftrightarrow \quad \int_D \rho(r,t) \cdot d^3 r(t) = \mathrm{M} \end{aligned} \tag{2.33}$$

Where M is an invariant called the mass of the system or measure. M is a constant of motion in classical dynamics. It follows from (2.33) that.

$$\begin{aligned} \frac{d}{dt}\mathrm{M} &= \frac{d}{dt}\int_D \rho(r,t) \cdot d^3 r(t) \\ &= \int_D \left(\frac{\partial \rho(r,t)}{\partial t} \cdot d^3 r(t) + \rho(r,t) \cdot \frac{d}{dt}\left(dx(t) \cdot dy(t) \cdot dz(t)\right) \right) \\ &= \int_D \left(\frac{d\rho(r,t)}{dt} - \vec{v} \cdot \nabla_r \rho(r,t) \right) \cdot d^3 r(t) + \int_B \rho(r,t) \vec{v}(t) \cdot \hat{n}\, ds \\ &= \int_D \left(\frac{d\rho(r,t)}{dt} + \rho(r,t) \cdot \nabla_r \vec{v} - \nabla_r (\rho \vec{v}) \right) \cdot d^3 r(t) + \int_B \rho(r,t) \vec{v}(t) \cdot \hat{n}\, ds \\ &= \int_D \left(\frac{d\rho(r,t)}{dt} + \rho(r,t) \cdot \nabla_r \vec{v} \right) \cdot d^3 r(t) \end{aligned} \tag{2.34}$$

In the above reasoning Gauss theorem and material derivative $\frac{d\rho}{dt}$ were used.

The generalization of the continuity equation to corpuscular points $(r_n,t)\in V\times[0,\tau]$, the use of the kernel and its property is needed; one proceeds in the same manner as in the two sections above, then:

$$\int_D \delta(r_n-r')\cdot\frac{d\rho(r',t)}{dt}\cdot d^3r' = -\lim_{H\to 0^+}\int_{D_W}\rho(r',t)\cdot\nabla_{r'}\vec{v}(r')\cdot W(r_n-r',H)\cdot d^3r'$$

$$= -\int_{D_W}\rho(r',t)\cdot\nabla_{r'}\vec{v}(r')\cdot W(r_n-r',h)\cdot d^3r'$$

$$= -\int_{D_W}\{\nabla_{r'}(\rho(r')\cdot\vec{v}(r'))-\vec{v}(r_n)\cdot\nabla_{r'}\rho(r')\}\cdot W(r_n-r',h)\cdot d^3r'$$

$$= -\int_{D_W}\{\nabla_{r'}(\rho(r')\cdot(\vec{v}(r')-\vec{v}(r_n)))\}\cdot W(r_n-r',h)\cdot d^3r'$$

$$= -\int_{D_W}\{\nabla_{r'}(\rho(r')\cdot(\vec{v}(r')-\vec{v}_n)\cdot W)-\rho(r')\cdot(\vec{v}(r')-\vec{v}_n)\nabla_{r'}W\}\cdot d^3r'$$

Using Gauss theorem for the first term in the right hand side above, one gets:

$$\frac{d\rho_n(t)}{dt} = -\int_D\rho(r')\cdot(\vec{v}(r')-\vec{v}_n)\cdot\nabla_{r'}W\cdot d^3r' - \int_B\rho(r')\cdot(\vec{v}(r')-\vec{v}_n)\cdot\hat{n}\cdot W\cdot ds$$

Or by using the symmetry of $W(r_n-r',h)$, one has

$$\frac{d\rho_n(t)}{dt} = \int_D\rho(r')\cdot(\vec{v}(r')-\vec{v}_n)\cdot\nabla_{r}W\cdot d^3r' - \int_B\rho(r')\cdot(\vec{v}(r')-\vec{v}_n)\cdot\hat{n}\cdot W\cdot ds \qquad (2.35)$$

The boundary term appearing in (2.35) expresses the smoothed flux across the surface $d\vec{s}(r') = \hat{n}(r') \cdot ds$, this additional flux has to be added for those particles such that: $D_W \cap B(r') \neq \emptyset$ and $(\vec{v}(r') - \vec{v}_n) \cdot \hat{n}(r') \neq 0$.

The figure 2.1 below depicts a schematic 2D picture with different components appearing in the boundary term of the equation (2.35).

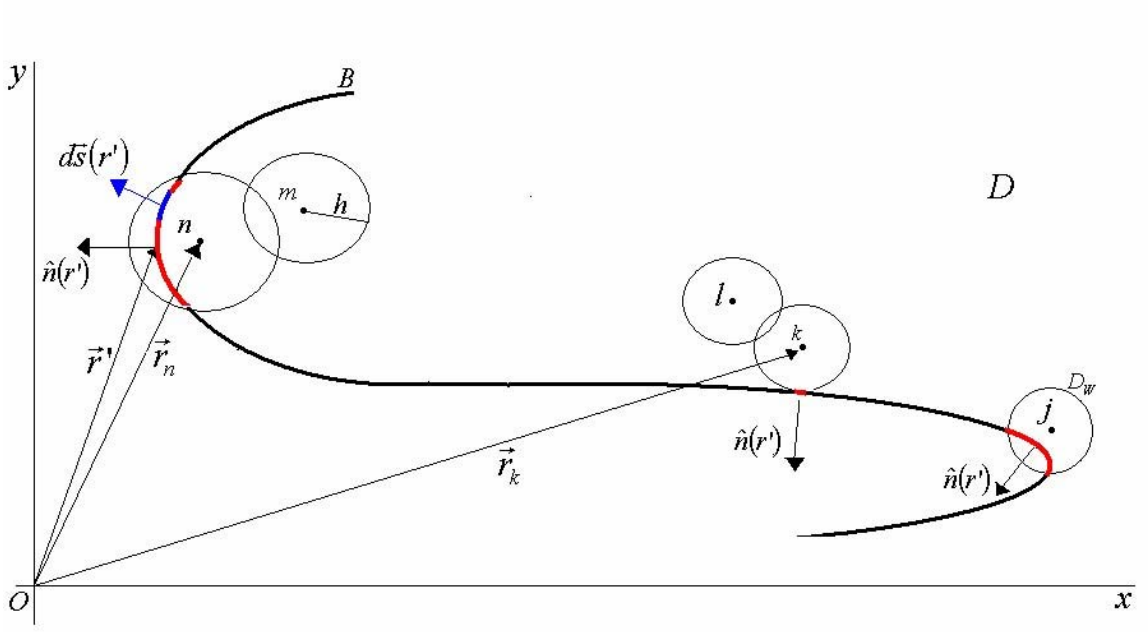

Figure 2.1: 2D projection of particles distribution in the domain V and near a regular Boundary B,

2.5 Conclusion

The first approach based on energy conservation (conservative systems) of a set of N particles is presented and used to derive the equations of motion for continuum in the SPH formalism.

Some assumptions were made to reach this objective, among of them, the ability that particles can be considered as a continuum, the need of symmetrical kernels assumption is crucial to satisfy Newton's law as one can see from the equation (2.8).This approach is convenient for open systems and for external flows.

The second approach starts from variational formulation applied to continuum m and consequently is satisfies treatment of boundary conditions. The only assumption concerning the kernel $W(r-r',h)$ is that it must fulfil the Dirac limit condition. The variational method results in derivation of the equation of continuity that one could not obtain by the method of discrete Hamiltonian.

Remark:

Hamilton's principle supposes the knowledge of displacements at later time, $\delta\vec{r}(\tau)=\vec{0}$ which is physical information that is not available in advance. This prescription allows us to skip the term $\left[\frac{\partial L}{\partial v}\cdot\delta\vec{r}\right]_0^\tau$ when integrating by parts.

2.6 References

[1] R. C. Tolman, *the Principles of Statitical Mechanics*. Oxford University Press 1938.

[2] I. Prigogine, *Non-Equilibrium Statistical Mechanics*. Monograph in Statistical Physics. Vol I Interscience Publishers 1962.

[3] D. Ruelle, *Statistical Mechanics, Rigorous Results*. Mathematical Physics Monograph Series W. A Benjamin, Inc 1969.

[4] C. Luehr and F. Allahdadi, Fundamentals of Smoothed Particle Hydrodynamics (SPH). AIAA 94-0066. 32nd Aerospace Sciemces. Meeting & Exhibit. January 10-13, 1994/ Reno, NV.

[5] L. E. Malvern, *Introduction to the Mechanics of Continuous Medium*, Prentic-Hall, Englwood Cliffs, N. J.1969.

[6] H. Ziegler, *An Introduction To Thermomechanics*. North-Holland Series In Applied Mathematics and Mechanics. North-Holland Publishing Company 1977.

3. CHOICE OF KERNEL W WITH VARYING SMOOTHING LENGTH h AND PROPERTY OF THE EULERIAN KERNELS

3.1 Introduction

In the previous chapters, the SPH formalism was discussed without any explicit form of the kernel W. However, from theoretical point of view, a number of constraints that kernels should satisfy were specified.

Originally, SPH used Normalized exponential and Gaussian kernels. Because these kernels are non-compact support, there is no clear limit of the number of contributing neighbours. To remedy to this problem, an artificial cut-off in the distance between particles has to be introduced to avoid a large computational cost.

Since in meshless methods the form of the kernel is not unique, the choice of kernels is still an open subject for many researchers. The objectives are either to improve the spatial interpolation of the physical fields characterizing the medium as well as their gradient or to handle boundary conditions correctly Liu *et al* [1].

The ability of SPH method and its progeny to vary the smoothing lengths of particles (characteristic size of the kernel support) is to be used to its advantage.

However, there are points to consider. First, in the simulations where the smoothing lengths are allowed to vary with position, meshless methods are no longer momentum and energy conservative. It is shown in Nelson and Papaloizou [2] that the inclusion of the gradient of the smoothing lengths terms in the equations of dynamic improves energy conservation in SPH simulations.

In the other hand, errors are implicitly introduced in the approximation of the spatial derivatives. These errors are of second order with respect to the smoothing length order Benz [3].

In the second section of this chapter, one addresses expressions of some common kernels that are most frequently used in practice, cubic spline, quartic spline or quantic spline and Gaussian kernels. For extended analysis of wide variety of kernels, readers are referred to work in Fulk [4].

Vinay & Jhon [5] present a novel B-K kernel, which is of exponential form and recently M.B. Liu *& al* [6] construct kernels based on Taylor series.

In the third section, a criterion for the selection of the kernel is introduced. This criterion is based on the minimization of the error terms due to the variable lengths. These interpolation terms arising from variable h should be present in the particles equations of motion.

The fourth section focuses on the consistency of two convolutions approaches Belytschko *et al* [7]. In the second part of this section a numerical example is presented to show the influence of the smoothing length on the stability.

Finally, in the fifth section one considers normalized kernels to illustrate some similarities between the time-evolutions of kernels and the evolution of scalar equation of conservation.

3.2 Choice of Kernel

Initially, kernels commonly used by SPH communities have been selected by the criteria of the minimization of the error between physical fields and their smoothed or spatially interpolated counter-part.

These kernels present a property of being of the general form:

$$W(z,h) \propto \frac{1}{h^{nd}} \cdot \eta\left(\frac{|z|}{h}\right) \tag{3.1}$$

Where $nd = 1, 2, 3$ is the space dimension, h is the smoothing length, $z = (x_1, \ldots, x_{nd})$ represents the position vector in $\Re^{nd}$ and $\eta\left(\frac{|z|}{h}\right)$ is even scalar function of real variable and possessing one maximum in their domains. Herein after some of most popular kernels are presented, where $u = \frac{|z|}{h}$.

Cubic spline:

$$W_3(u,h) = \frac{N_{nd}}{h^{nd}} \cdot \begin{cases} 1 - \frac{3}{2}u^2 + \frac{3}{4}u^3 & if, \quad 0 \le u \le 1 \\ \frac{(2-u)^3}{4} & if, \quad 1 \le u \le 2 \\ 0 & if, \quad u \ge 2 \end{cases} \tag{3.2}$$

Where, N_{nd} represents the normalization constant, $N_1 = \frac{2}{3}, N_2 = \frac{10}{7 \cdot \pi}$ and $N_3 = \frac{1}{\pi}$.

Quartic spline:

$$W_4(u,h) = \frac{N_{nd}}{h^{nd}} \cdot \begin{cases} \left(u + \frac{5}{2}\right)^4 + 10 \cdot \left(u + \frac{1}{2}\right)^4 - 5 \cdot \left(u + \frac{3}{2}\right)^4 & if, \quad 0 \le u \le 0.5 \\ \left(u - \frac{5}{2}\right)^4 - 5 \cdot \left(u - \frac{3}{2}\right)^4 & if, \quad 0.5 \le u \le 1.5 \\ \left(u - \frac{5}{2}\right)^4 & if, \quad 1.5 \le u \le 2.5 \\ 0 & if, \quad u \ge 2.5 \end{cases} \tag{3.3}$$

Where $N_1 = \frac{1}{24}, N_2 = \frac{48}{1199 \cdot \pi}$ and $N_3 = \frac{1}{40 \cdot \pi}$.

Quintic spline:

$$W_5(u,h) = \frac{N_{nd}}{h^{nd}} \cdot \begin{cases} (3-u)^5 + 15\cdot(1-u)^5 - 6\cdot(2-u)^5 & if, \quad 0 \le u \le 1 \\ (3-u)^5 - 6\cdot(2-u)^5 & if, \quad 1 \le u \le 2 \\ (3-u)^5 & if, \quad 2 \le u \le 3 \\ 0 & if, \quad u \ge 3 \end{cases} \tag{3.4}$$

Where $N_1 = \frac{1}{120}, N_2 = \frac{7}{956\cdot\pi}$ and $N_3 = \frac{1}{240\cdot\pi}$.

By their symmetry, these kernels interpolate to second order in h. However, it is known that W_3 is of class C^1 and it is preferable to use kernels which are of class C^2 at least since second derivatives of kernels are involved in the development of instability.

J. J. Monaghan [8] built super-Gaussian kernel by considering an even kernel that interpolates to fourth order in h.

$$W_{SG}(u,h) = \frac{N_{nd}}{h^{nd}} \cdot \left(a + b\cdot u^2\right)\cdot e^{-u^2} \tag{3.5}$$

Let D_W be the compact support of W_{SG} and let $\langle\psi(r)\rangle$ be any smoothed field that can be approximated by Taylor series around a position r as follow:

$$\begin{aligned} \langle\psi(r)\rangle &\approx \psi(x) + h\cdot\left(\frac{r-x}{h}\right)\cdot\langle\nabla_r\psi(x)\rangle \ldots + \frac{h^k}{k!}\cdot\left(\frac{r-x}{h}\right)^k \cdot\langle\nabla_r^k\psi(x)\rangle + \ldots \\ &\approx \psi(x) \ldots + \frac{N_{nd}\cdot h^k}{h^{nd}\cdot k!}\cdot\nabla_r^k\psi(x)\cdot\int_{D_W}\left(a + b\cdot\left(\frac{r-x}{h}\right)^2\right)\cdot\left(\frac{r-x}{h}\right)^k \cdot e^{-\left(\frac{r-x}{h}\right)^2}\cdot d^{nd}r \\ &\approx \psi(x) + V_{nd}\cdot\frac{N_{nd}}{h^{nd}}\cdot\sum_{n=1}\frac{h^{n+nd}}{n!}\cdot\nabla^n\psi(x)\cdot\int_{D_W}\left(a + b\cdot z^2\right)\cdot z^{n+nd-1}\cdot e^{-z^2}\cdot dz \end{aligned}$$

In the relation above, $z = \frac{r-x}{h}$, $d^{nd}r = V_{nd} \cdot z^{nd-1} \cdot h^{nd} \cdot dz$ and $V_{nd} = 2^{nd-1} \cdot \pi^{\min[1,\, nd-1]}$

The term with $n = 2$ has to vanish in order to obtain a fourth order accuracy, it follows then.

$$a \cdot \int_{D_W} z^{nd+1} \cdot e^{-z^2} \cdot dz + b \cdot \int_{D_W} z^{nd+3} \cdot e^{-z^2} \cdot dz = 0 \quad \Leftrightarrow \quad a \cdot \Gamma\left(\frac{nd}{2}+1\right) + b \cdot \Gamma\left(\frac{nd+2}{2}+1\right) = 0$$

$$\Leftrightarrow \quad \frac{nd}{2} \cdot \Gamma\left(\frac{nd}{2}\right) \cdot \left(a + \frac{nd+2}{2} \cdot b\right) = 0$$

In the relations above, the Gamma function $\Gamma(x)$ and the property, $\Gamma(x+1) = x \cdot \Gamma(x)$, were used. A general expression of the kernel in (3.3) is obtained:

$$W_{SG}(z,h) = \frac{1}{\left(\sqrt{\pi} \cdot h\right)^{nd}} \cdot \left(\frac{nd+2}{2} - z^2\right) \cdot e^{-z^2} \tag{3.6}$$

Despite of their highest order interpolation accuracy, these kernels exhibit negative values for $z^2 > \frac{nd+2}{2}$. This can lead to negative densities for critical distributions of particles.

3.3 A Criterion for Choice of Kernel

First, one considers even kernels of the form (3.1) with compact support $D_W \subset \Re^{nd}$. The smoothing lengths are position dependent and the smoothed physical fields are given by:

$$\langle \psi(r) \rangle = \int_{D_W} \psi(r') \cdot W(r - r', h(r)) \cdot d^{nd} r' \tag{3.7}$$

By applying the gradient operator to the relation (3.7) one calculates the gradient of the smoothed field:

$$\nabla_r \langle \psi(r) \rangle = \nabla_r \cdot \int_{D_W} \psi(r') \cdot W(r - r', h(r)) \cdot d^{nd} r' \tag{3.8}$$

On the other hand, let B_W be the boundary of the domain D_W and $\hat{n}$ its local outward unit normal, then the smoothed gradient of the field is obtained by:

$$\begin{aligned} \langle \nabla_r \psi(r) \rangle &= \int_{D_W} \nabla_{r'} \psi(r') \cdot W(r - r', h(r)) \cdot d^{nd} r' \\ &= \int_{B_W} \psi(r') \cdot W(r - r', h(r)) \cdot \hat{n} \cdot ds - \int_{D_W} \psi(r') \cdot \nabla_{r'} W(r - r', h(r)) \cdot d^{nd} r' \\ &= \int_{B_W} \psi(r') \cdot W(r - r', h(r)) \cdot \hat{n} \cdot ds + \int_{D_W} \psi(r') \cdot \frac{\partial W(r - r', h(r))}{\partial r} \cdot d^{nd} r' \end{aligned} \tag{3.9}$$

Where in the second identity Gauss theorem was applied to the first term in the right hand side and the property $\left(\frac{\partial W}{\partial r'} = -\frac{\partial W}{\partial r} \right)$ was used on the second term in the last equality.

With appropriate conditions, where the surface term can be omitted, the first term on the right hand side above vanishes. One then defines $\varepsilon(\psi(r), h(r)) = \nabla_r \langle \psi(r) \rangle - \langle \nabla_r \psi(r) \rangle$, an estimation of the difference between expressions (3.8) and (3.9) gives:

$$
\begin{aligned}
\varepsilon(\psi,h) &= \nabla_r \int_{D_W} \psi(r') \cdot W(r-r', h(r)) \cdot d^{nd} r' \\
&\quad - \int_{D_W} \psi(r') \cdot \frac{\partial W(r-r', h(r))}{\partial r} \cdot d^{nd} r' \\
&= \int_{D_W} \psi(r') \cdot \left\{ \frac{\partial W(r-r', h(r))}{\partial r} + \nabla_r h(r) \cdot \frac{\partial W(r-r', h(r))}{\partial h} \right\} \cdot d^{nd} r' \\
&\quad - \int_{D_W} \psi(r') \cdot \frac{\partial W(r-r', h(r))}{\partial r} \cdot d^{nd} r' \\
&= \nabla_r h(r) \cdot \int_{D_W} \psi(r') \cdot \frac{\partial W(r-r', h(r))}{\partial h} \cdot d^{nd} r'
\end{aligned}
\tag{3.10}
$$

Cases where $\nabla_r h(r) = 0$ are not of an interest, the equality $\varepsilon(\psi,h) = 0$ should hold for any constant physical quantities consequently.

$$
\int_{D_W} \frac{\partial W(r-r', h(r))}{\partial h} \cdot d^{nd} r' = 0 \tag{3.11}
$$

On the other hand, normalization condition leads to.

$$
\int_{D_W} W(r-r', h(r)) \cdot d^{nd} r' = M(r,h) = 1 \tag{3.12}
$$

From (3.12), it follows that:

$$\begin{aligned}\nabla_r M(r,h) &= \frac{\partial M(r,h)}{\partial r} + \nabla_r h(r) \cdot \frac{\partial M(r,h)}{\partial h} \\ &= \int_{D_W} \left\{ \frac{\partial W(r-r', h(r))}{\partial r} + \nabla_r h(r) \cdot \frac{\partial W(r-r', h(r))}{\partial h} \right\} \cdot d^{nd} r' \\ &= 0\end{aligned} \tag{3.13}$$

Using the relation (3.10) in (3.13) leads to.

$$\int_{D_W} \frac{\partial W(r-r', h(r))}{\partial r} \cdot d^{nd} r' = 0 \tag{3.14}$$

Introducing the form of kernels (1.1) in the expression (3.10), $\varepsilon(\psi, h)$ reads.

$$\varepsilon(\psi, h) = -\frac{\nabla_r h(r)}{h^4(r)} \cdot \int_{D_W} \psi(r') \cdot \left\{ nd \cdot \eta(z) + s \cdot \frac{\partial \eta(z)}{\partial z} \right\} \cdot d^{nd} r' \tag{3.15}$$

With the change variable $z = \frac{r-r'}{h(r)}$.

The minimization of (3.15) should hold independently from the interpolated field $\psi(r')$. This occurs for functions satisfying the differential equation below:

$$nd \cdot \eta(z) + z \cdot \frac{\partial \eta(z)}{\partial z} = 0 \tag{3.16}$$

The solutions of (3.16) are given by $\eta(z)=\frac{K}{z^{nd}}$, where K is the constant of integration. The problem with these functions is that they are unbounded and then could not be considered.

Let us assume that physical fields considered here are smooth and at least of class C^2, taking into account the symmetry of the kernels, then by Taylor expansion up to second order, one gets (3.17):

$$\begin{aligned}
\varepsilon(\psi,h) &= -\frac{\nabla_r h(r)}{h^4(r)}\cdot\int_{D_W}\left\{\psi(r)+(r-r')\cdot\nabla_r\psi(r)+\frac{(r-r')^2}{2}\cdot\nabla_r^2\psi(r)+..\right\} \\
&\qquad\cdot\left\{nd\cdot\eta(z)+z\cdot\frac{\partial\eta(z)}{\partial z}\right\}\cdot d^{nd}r' \\
&= -\frac{\nabla_r h(r)}{h^4(r)}\cdot\nabla_r^2\psi(r)\cdot\int_{D_W}\frac{(r-r')^2}{2}\cdot\left\{nd\cdot\eta(z)+z\cdot\frac{\partial\eta(z)}{\partial z}\right\}\cdot d^{nd}r' \\
&= -\frac{\nabla_r h(r)}{2}\cdot h(r)\cdot\nabla_r^2\psi(r)\cdot\int_{D_W} z^2\cdot\left\{nd\cdot\eta(z)+z\cdot\frac{\partial\eta(z)}{\partial z}\right\}\cdot d^{nd}z \\
&= -V_{nd}\cdot\nabla_r h(r)\cdot h(r)\cdot\nabla_r^2\psi(r)\cdot\int_0^{\infty} z^{nd+1}\cdot\left\{nd\cdot\eta(z)+z\cdot\frac{\partial\eta(z)}{\partial z}\right\}\cdot dz
\end{aligned} \tag{3.17}$$

Where $d^{nd}r'=h^{nd}(r)\cdot d^{nd}z$ and $d^{nd}z=V_{nd}\cdot z^{nd-1}\cdot dz$ with $V_{nd}=2^{nd-1}\cdot\pi^{\min[1,nd-1]}$ were used in the last two integrals.

Instead of (3.16), the criterion for the choice of the kernel becomes.

$$\int_0^{\infty} z^{nd+1}\cdot\left\{nd\cdot\eta(z)+z\cdot\frac{\partial\eta(z)}{\partial z}\right\}\cdot dz=0 \tag{3.18}$$

By using the normalization condition one obtains.

$$V_{nd} \cdot \int_0^{\infty} z^{nd-1} \cdot \eta(z) \cdot dz = 1 \tag{3.19}$$

3.3.1 Examples

It should be noted that super Gaussian kernel $W_{SG}(z,h)$ given in (3.6) fulfils the criterion (3.18) but not B-splines kernel family. To built a B-Splines satisfying the criterion one starts from a general expression below.

$$W(z,h) = \frac{N_{nd}}{h^{nd}} \cdot \begin{cases} a \cdot z^3 + b \cdot z^2 + c \cdot z + d & if \quad 0 \le z \le 1 \\ e \cdot z^3 + f \cdot z^2 + g \cdot z + k & if \quad 1 \le z \le 2 \\ 0 & if \quad z \ge 2 \end{cases} \tag{3.20}$$

Where (a, b, c, d, e, f, g, k) are constants that should be determined by the criterion (3.18) and by the following conditions of continuity and boundaries constraints.

Continuity of $\eta(z)$ *and* $\frac{\partial \eta(z)}{\partial z}$ *for* $z = 1$

Constraints $\frac{\partial \eta(0)}{\partial z} = \frac{\partial \eta(2)}{\partial z} = 0$ *and* $\eta(2) = 0$

Calculations of the new B-Spline kernels were performed under Derive 5.0 [9] which is a mathematical assistant solving symbolic and numeric problem. Hereinafter calculation for one dimensional space is given in (3.21) and graphical comparison with classical B-spline plotted in the figure1 and also their derivatives.

$$W(z,h)=\frac{21}{23\cdot h}\cdot\begin{cases} z^3-\frac{41}{21}z^2+1 & if \quad 0\le z\le 1 \\ (z-2)^2\cdot\left(\frac{6}{7}-\frac{17}{21}z\right) & if \quad 1\le z\le 2 \\ 0 & if \quad z\ge 2 \end{cases} \tag{3.21}$$

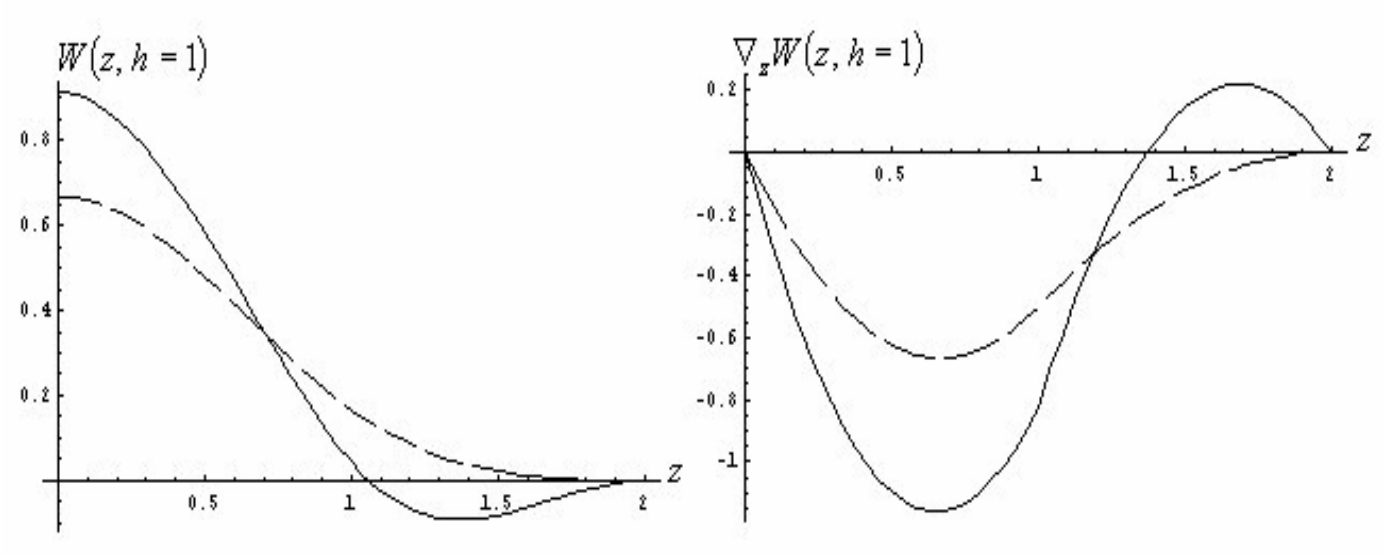

Figure 3.1: Representation of standard B-spline (Dashed curve)
and the selected kernel (Continuous curve).

Below, a $3D$ selected kernel and its representation are sketched in figure 2:

$$W(z,h)=\frac{15}{1152\cdot\pi\cdot h^3}\cdot\begin{cases} 171\cdot z^3-321\cdot z^2+172 & if \quad 0\le z\le 1 \\ (z-2)^2\cdot(107-85\cdot z) & if \quad 1\le z\le 2 \\ 0 & if \quad z\ge 2 \end{cases} \tag{3.22}$$

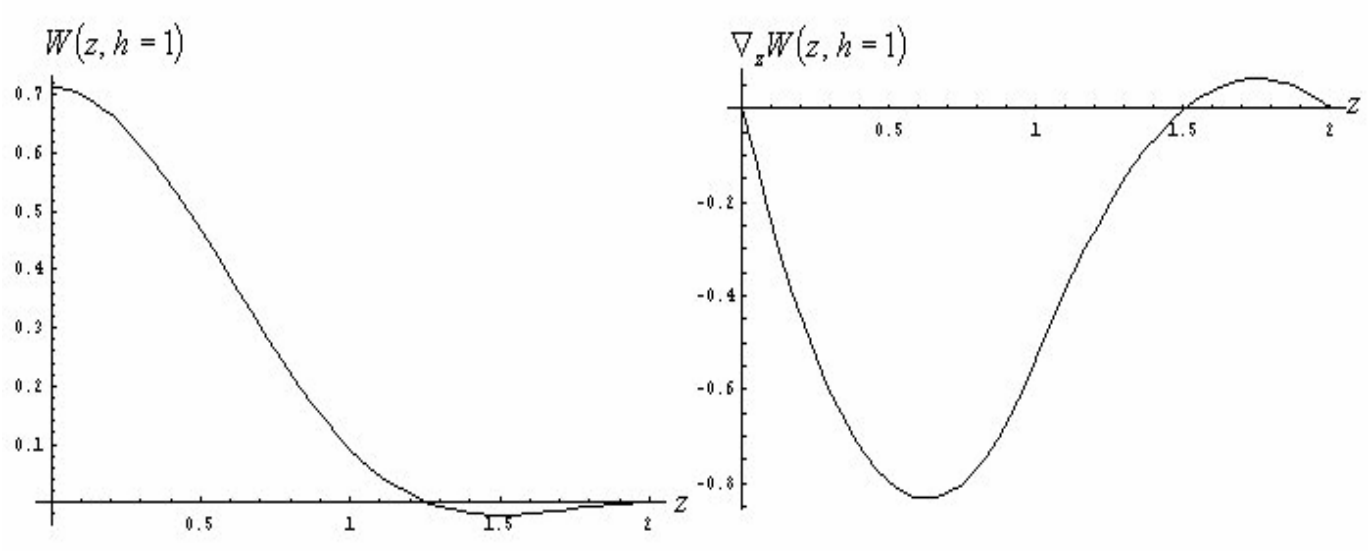

Figure 3-2: Graphs of selected B-Spline in 3D (Left graph) and its gradient (Right graph)

Like super-Gaussian kernels, these selected kernels exhibit negative values at certain interval, this is not in contradiction with the criterion, were the positivity of $\eta(s)$ was not required.

Below, a graph showing the comparison of the simulation with standard B-spline and with the kernel selected here.

At first, it was attempted to make use of the shock tube problem as reference to confirm the aptitude of selected kernels to reproduce strong shock but simulation diverges after a couple of cycles.

A second test problem applies to solid impact was chosen as substitute. The simulated problem is 1D impact of two elastic bars of aluminium with equal opposite velocities. The ratio of the smoothing length to the particle space is $\frac{h}{\delta_0} = 1\ (\delta_0 = 0.05\ Cm)$, the impact velocity $v_0 = 150\ m/s$, Young modulus $E = 200\ GPa$ and Poison's Coefficient $\nu = 0.3$.

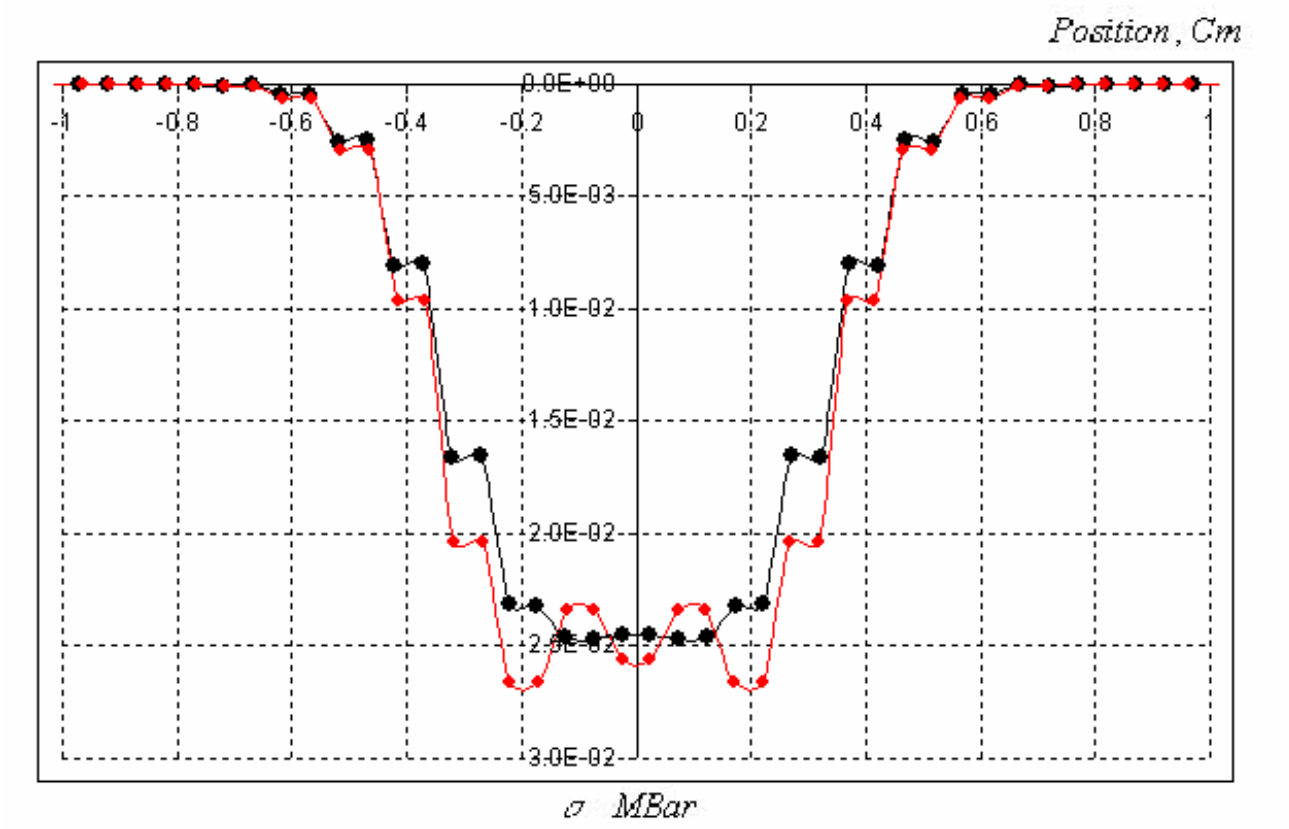

Figure 3-3: Profile of the stress at time $t = 0.3\ \mu s$, (Red curve) standard kernel,(Black curve) selected kernel

The previous figure shows that selected kernel produces regular values of the stress at the contact zone by reducing the amplitude of the oscillations. Also slightly lower amplitudes were generated.

3.4 Reproducing Kernel Particle Method RKPM

A succinct introduction to RKPM kernel is given here. Related numerical tests are presented in *chapter 6*. A recent type of corrected kernel was proposed by Liu *et al* [10, 11, 12, and 13], and takes the following form as a correction to the interpolation kernel itself:

$$W_{RKPM}(r, r-r', h) = \left\{ \sum_{k=0}^{M} C_k(r, h) \cdot \left(\frac{r'-r}{h} \right)^k \right\} \cdot W\left(\frac{|r-r'|}{h} \right) \qquad (3.23)$$

M represents the order of the correction function and $C_k(r,h)$ are coefficients that depend on the order M. These coefficients can be determined explicitly by imposing the condition that W_{CSPH} exactly interpolates polynomials of order up to M, ie.

$$\int_{DW_{RKPM}} r'^{\,k} \cdot W_{RKPM}(r,\, r-r',\, h) \cdot dr' = r^k \quad for \quad k = 1,\, 2,\, 3,\ldots M \quad (3.24)$$

Where DW_{RKPM} is the support of the $RKPM$ kernel. The corrected kernel of order $M = 1$ is given by.

$$W_{RKPM}(r,\, r-r',\, h) = \left\{ C_1(r,\, h) + C_2(r,\, h) \cdot \left(\frac{r'-r}{h} \right) \right\} \cdot W(r-r',\, h) \quad (3.25)$$

One can see that generally $W_{RKPM}(r,\, r-r',\, h) \neq W_{RKPM}(r',\, r'-r,\, h)$, i.e. the kernel function is no longer symmetric. Using the above fields can be approximated by:

$$\langle \psi(r) \rangle \approx \sum_j \frac{m_j}{\rho_j} \cdot \psi(r_j) \cdot \left\{ C_1(r,\, h) + C_2(r,\, h).(\frac{r_j - r}{h}) \right\} \cdot W \quad (3.26)$$

3.5 Consistency of the convolution in Particle method

Most meshless methods have their foundation based on the spatial convolution given in (3.7). With the expression of the kernel W in (3.1), one has:

$$\langle \psi(r) \rangle = \frac{N_{nd}}{h^{nd}(r)} \cdot \int_{D_W} \psi(r') \cdot \eta \left(\frac{r-r'}{h(r)} \right) \cdot d^{\,nd} r' \quad (3.27)$$

Here, one reproduces the result established by Benz [3].

Let $z = \frac{r - r'}{h(r)}$ where $z = (x_{1,} \ldots, x_{nd})$ and $r' = (r'_1, \ldots, r'_{nd})$ and nd the spatial dimension, the difference between the smoothed field $\langle \psi(r) \rangle$ and the local field $\psi(r)$ is given by.

$$\begin{aligned} \langle \psi(r) \rangle - \psi(r) &= \frac{N_{nd}}{h^{nd}(r)} \cdot \int_{D_W} (\psi(r') - \psi(r)) \cdot \eta\left(\frac{r - r'}{h(r)}\right) \cdot d^{nd} r' \\ &= N_{nd} \cdot \int_{D_W} (\psi(r - z \cdot h(r)) - \psi(r)) \cdot \eta(z) \cdot d^{nd} z \end{aligned} \tag{3.28}$$

Let $F(r, z) = N_{nd} \cdot \psi(r - z \cdot h(r))$, by Taylor expansion around $z = 0$ up to second order, one obtains.

$$F(r, z) - F(r, 0) = z \cdot \nabla_z F(r, 0) + \frac{z^2}{2!} \cdot \nabla_z^2 F(r, 0) \tag{3.29}$$

Where,

$$\nabla_z F(r, z) = -h(r) \cdot \nabla_r \psi(r - z \cdot h(r)) \qquad \text{and} \qquad \nabla_z^2 F(r, z) = h^2(r) \cdot \nabla_r^2 \psi(r - z \cdot h(r))$$

The substitution of the expression (3.29) into (3.28) gives.

$$\begin{aligned} \langle \psi(r) \rangle - \psi(r) = &-N_{nd} \cdot h(r) \cdot \nabla_z \psi(r) \cdot \int_D z \cdot \eta(z) \cdot d^{nd} z \\ &+ N_{nd} \cdot h^2(r) \cdot \nabla_r^2 \psi(r) \cdot \int_D z^2 \cdot \eta(z) \cdot d^{nd} z \end{aligned} \tag{3.30}$$

Knowing that $\eta(z)$ is an even function, the first integral above vanishes in the other hand the second integral is bounded, one gets an estimation of the difference above.

$$\left|\langle\psi(r)-\psi(r)\rangle\right| \le h^2(r)\cdot\left|N_{nd}\cdot\nabla^2\psi(r)\cdot\int_D z^2\cdot\eta(z)\cdot d^{nd}z\right| \tag{3.31}$$

The consistency of the field are then of second order.

The smoothing length can also be function of r' and then another variant of the convolution has to be considered, Belytschko *et al* [7], where (3.27) can be rewritten.

$$\langle\psi(r)\rangle = N_{nd}\cdot\int_{D_W}\psi(r')\cdot\frac{1}{h^{nd}(r')}\cdot\eta\left(\frac{r-r'}{h(r')}\right)\cdot d^{nd}r' \tag{3.32}$$

The intuitive difference between (3.27) and (3.32) is that in the first form the domain of interaction of the particle is always isotropic (Spherical) while in (3.32) it depends on the distribution of the neighbours as illustrated in Figure 3-4.

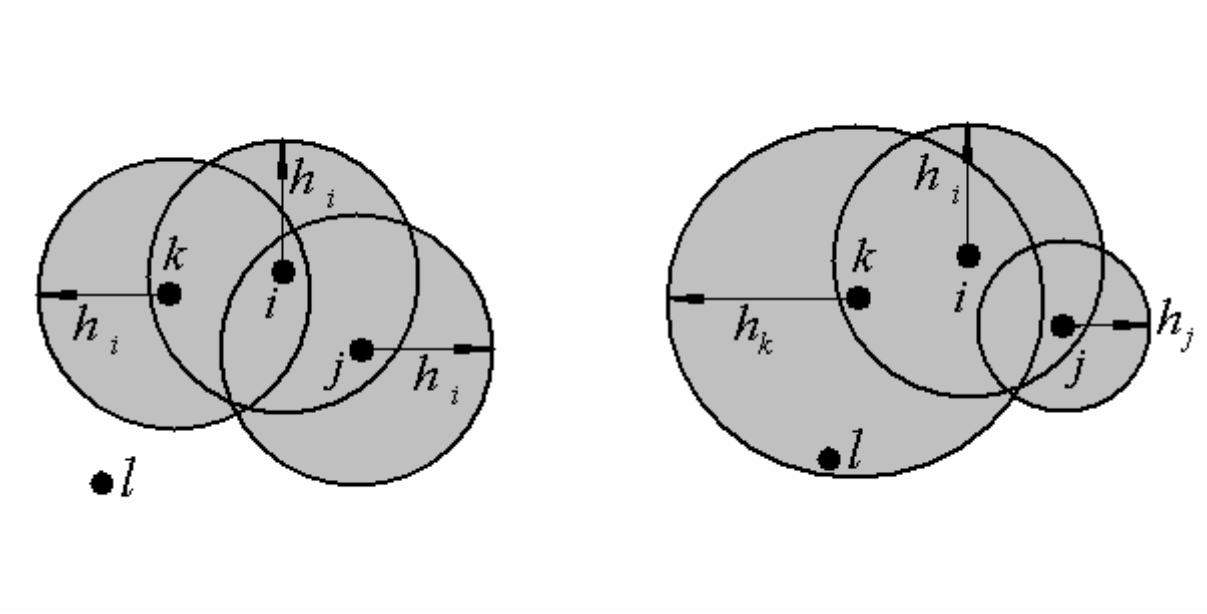

Figure 3-4: Domain of influence of the particle i (Grey area)

Recall that the change variable $z = \frac{r - r'}{h(r')}$ has to be continuously differentiable with $z = (x_1, \ldots, x_{nd}),\ r' = (r'_1, \ldots, r'_{nd})$ and considering that the compact support of the kernel is of the form $D_w \subseteq [-C \cdot h, +C \cdot h]$, where C is a positive constant. The change of variable or (mapping) is valid if the Jacobean $J = \det\left[\frac{\partial z_\alpha}{\partial r'_\beta}\right], 1 \le \alpha, \beta \le 3$ should not be singular.

$$J = \frac{1}{h(r')} \cdot \left(1 + \frac{r - r'}{h(r')} \cdot \nabla_{r'} h(r')\right) = \frac{1}{h(r')} \cdot \left(1 + z \cdot \nabla_{r'} h(r')\right) \tag{3.33}$$

Where $z \in D_W\ (z \le C)$, it comes that the gradient of the smoothing length has to verify:

$$\left| \nabla_{r'} h\,(r') \right| < \frac{1}{C}. \tag{3.34}$$

The equation (3.32) becomes then.

$$\begin{aligned} \langle \psi(r) \rangle &= N_{nd} \cdot \int_{D_W} \psi(r') \cdot \frac{1}{h^{nd}(r')} \cdot \eta\left(\frac{r - r'}{h\,(r)}\right) \cdot d^{nd} r' \\ &= N_{nd} \cdot \int_{D_W} \psi\left(r - z \cdot h\,(r')\right) \cdot \frac{\eta(z)}{h^{nd}(r')} \cdot \frac{h^{nd}(r')}{1 + z \cdot \nabla_{r'}\, h\,(r')} \cdot d^{nd} z \\ &= N_{nd} \cdot \int_{D_W} \psi\left(r - z \cdot h\,(r')\right) \cdot \frac{\eta(z)}{1 + z \cdot \nabla_{r'}\, h\,(r')} \cdot d^{nd} z \end{aligned} \tag{3.35}$$

And the counter part of the equation (3.28) becomes.

$$\langle \psi(r) \rangle - \psi(r) = N_{nd} \cdot \int_{D_W} \left(\frac{\psi\left(r - z \cdot h\left(r'\right)\right)}{1 + z \cdot \nabla_{r'} h\left(r'\right)} - \psi\left(r\right) \right) \cdot \eta\left(z\right) \cdot d^{nd} z \qquad (3.36)$$

Let $F(r,z) = N_{nd} \cdot \dfrac{\psi\left(r - z \cdot h\left(r'\right)\right)}{1 + z \cdot \nabla_{r'} h(r')}$, using Taylor expansion of $F(r, z)$ around $z = 0$, one obtains:

$$F(r, z) - F(r, 0) = z \cdot \nabla_z F(r, 0) + \frac{z^2}{2!} \cdot \nabla_z^2 F(r, 0)$$

For simplicity and clarity, one drops the normalization coefficient N_{nd} from the expressions below:

$$\begin{aligned} \nabla_z F(r, z) &= \frac{-\nabla_z \left(z \cdot \nabla_{r'} h(r')\right)}{\left(1 + z \cdot \nabla_{r'} h(r')\right)^2} \cdot \psi\left(r - z \cdot h\left(r'\right)\right) + \frac{\nabla_z \psi\left(r - z \cdot h\left(r'\right)\right)}{\left(1 + z \cdot \nabla_{r'} h(r')\right)} \\ &= \left(\frac{-\nabla_{r'} \left(z \cdot \nabla_{r'} h(r')\right)}{\left(1 + z \cdot \nabla_{r'} h(r')\right)^2} \cdot \psi\left(r - z \cdot h\left(r'\right)\right) + \frac{\nabla_{r'} \psi\left(r - z \cdot h\left(r'\right)\right)}{\left(1 + z \cdot \nabla_{r'} h(r')\right)} \right) \cdot \frac{\partial r'}{\partial z} \end{aligned} \qquad (3.37)$$

Keeping in mind that $\dfrac{\partial r'}{\partial z} = -h\left(r'\right)$ and then $\nabla_z h\left(r'\right) = -h\left(r'\right) \cdot \nabla_{r'} h\left(r'\right)$, the calculation of the expression above leads to:

$$\begin{aligned} \nabla_z F(r, z) = &\frac{h\left(r'\right) \cdot \nabla_{r'} z \cdot \nabla_{r'} h\left(r'\right) + z \cdot h\left(r'\right) \cdot \nabla_{r'}^2 h\left(r'\right)}{\left(1 + z \cdot \nabla_{r'} h(r')\right)^2} \cdot \psi\left(r - z \cdot h\left(r'\right)\right) \\ &- \frac{h\left(r'\right)}{\left(1 + z \cdot \nabla_{r'} h(r')\right)} \cdot \nabla_{r'} \psi\left(r - z \cdot h\left(r'\right)\right) \end{aligned} \qquad (3.38)$$

Taking into account the expression of the Jacobean $\nabla_{r'} z$, the expression (3.37) becomes:

$$\nabla_z F(r, z) = \frac{-(1 + z \cdot \nabla_{r'} h(r')) \cdot \nabla_{r'} h(r') + z \cdot h(r') \cdot \nabla_{r'}^2 h(r')}{(1 + z \cdot \nabla_{r'} h(r'))^2} \cdot \psi(r - z \cdot h(r')) \tag{3.39}$$
$$- \frac{h(r')}{(1 + z \cdot \nabla_{r'} h(r'))} \cdot \nabla_{r'} \psi(r - z \cdot h(r'))$$

This leads to.

$$\nabla_z F(r, z = 0) = -\nabla_{r'} h \cdot \psi(r) - h \cdot \nabla_{r'} \psi(r) \tag{3.40}$$

And to:

$$\nabla_z^2 F(r, z = 0) = h^2(r) \cdot \{\nabla_{r'}^2 \psi(r) - \nabla_{r'}^2 h \cdot \psi(r)\} + (\nabla_{r'} h)^2 \cdot \psi(r) \tag{3.41}$$
$$+ 3 \cdot h \cdot \nabla_{r'} h \cdot \nabla_{r'} \psi(r) + h \cdot \nabla_{r'}^2 h \cdot \psi(r)$$

The error becomes:

$$\langle \psi(r) \rangle - \psi(r) = -N_{nd} \cdot \{\nabla_{r'} h(r) \cdot \psi(r) + h(r) \cdot \nabla_{r'} \psi(r)\} \cdot \int_{D_W} z \cdot \eta(z) \cdot d^{nd} z \tag{3.42}$$
$$+ \frac{N_{nd}}{2} \cdot \nabla_z^2 F(r, 0) \cdot \int_{D_W} z^2 \cdot \eta(z) \cdot d^{nd} z$$

For $nd = 1$ or $nd = 3$ the first term on the right hand side above vanishes, using the expression (3.41), the estimation of the term $\nabla_z^2 F(r, 0)$ contains terms in $h^2(r)$, $(\nabla h(r))^2$ and $h(r) \cdot \nabla h(r)$.

For $nd = 2$, the second term in the right hand side of (3.42) vanishes but the first term is function of $h(r)$ and $\nabla h(r)$.

The consistency is obtained for $h(r) \to 0$, but one does not have the control of $\nabla_r h(r)$ nor $\nabla_r^2 h(r)$ when $h(r) \to 0$, the only information one has is expressed by the relation given in (3.34).

The second form of the convolution is consistent for $h(r) \to 0$ and for $\nabla_r h(r) \underset{h \to 0}{\to} 0$ and $\nabla_r^2 h(r) \underset{h \to 0}{\to} Cst < \infty$. One can express the error by:

$$\langle \psi(r) \rangle - \psi(r) = I_0 \cdot O(h) + I_1 \cdot O(\nabla h) \tag{3.43}$$

In the numerical experiments, generally, ∇h remains small except in regions with high discontinuities. And the initialization of the smoothing length has a great influence on the convergence of the numerical results. This initialization depends on the initial distance between particles δ_0.

In fact, to observe Newton's *law*, hydrocodes use a combination of the convolutions given in (3.27) and in (3.32). Several methods have been proposed to achieve this symmetry. This is achieved by replacing the smoothing length by combinations like $h(r,r') = \frac{h(r) + h(r')}{2}$ or $h(r, r') = \sqrt{h(r) \cdot h(r')}$.

Other method uses symmetry of the kernel rather than the smoothing length, $W(r - r, h(r,r')) = \frac{W(r - r', h(r)) + W(r - r', h(r'))}{2}$

In order to show the influence of the ratio the smoothing length to the distance between particles, $\frac{h}{\delta_0}$ on the numerical accuracy of RKPM, the shock tube simulation was performed with successive values of the smoothing length h; $h = h_{cr} = \delta_0$, $h = 2 \cdot h_{cr}$ *and* $h = 2^2 \cdot h_{cr}$. The figures 3.5, 3.6 and 3.7 show, the velocities profiles for response time $t = 0.2\,\mu s$.

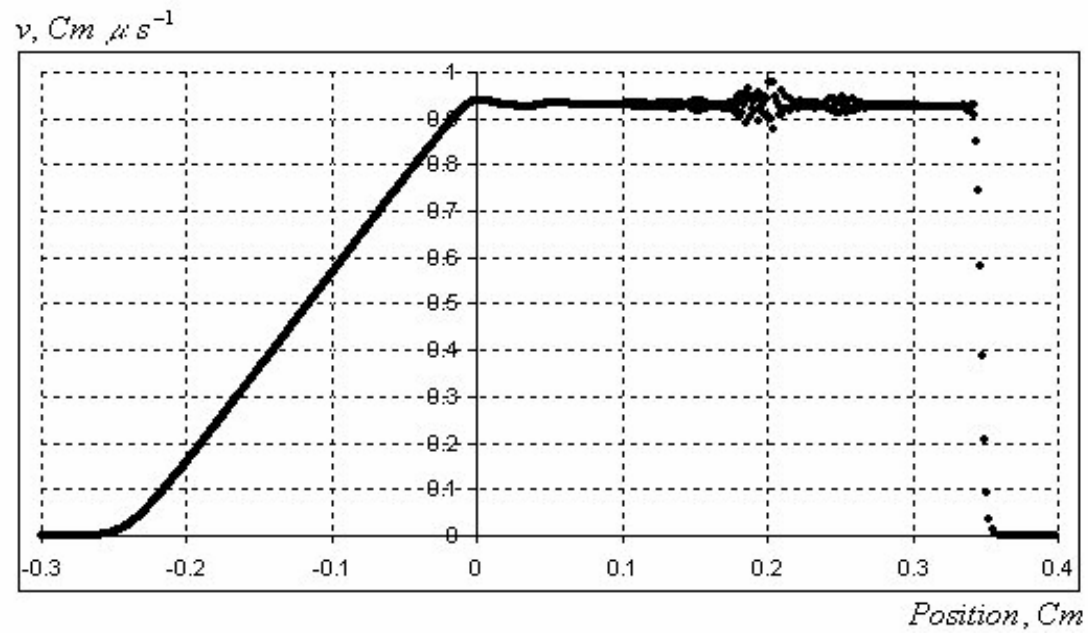

Figure 3-5: Profile of the velocity at time $t = 0.2\,\mu s$ with $h = h_{cr} = 2 \cdot 10^{-3}\ Cm$

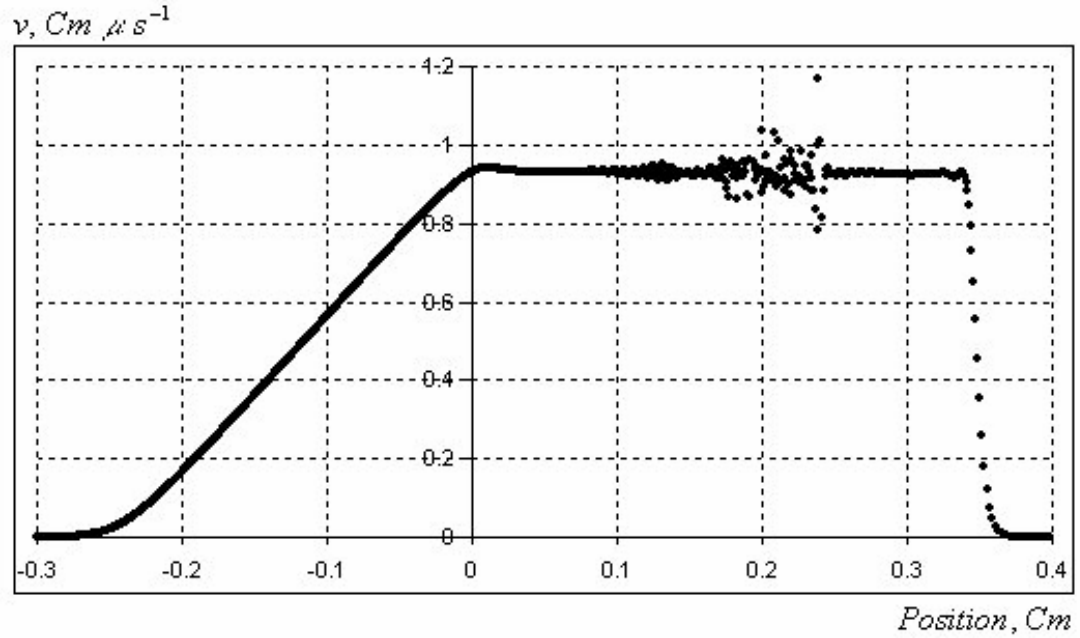

Figure 3-6: Profile of the velocity at time $t = 0.2\,\mu s$ with $h = 2 \cdot h_{cr} = 2 \cdot 10^{-3}\ Cm$

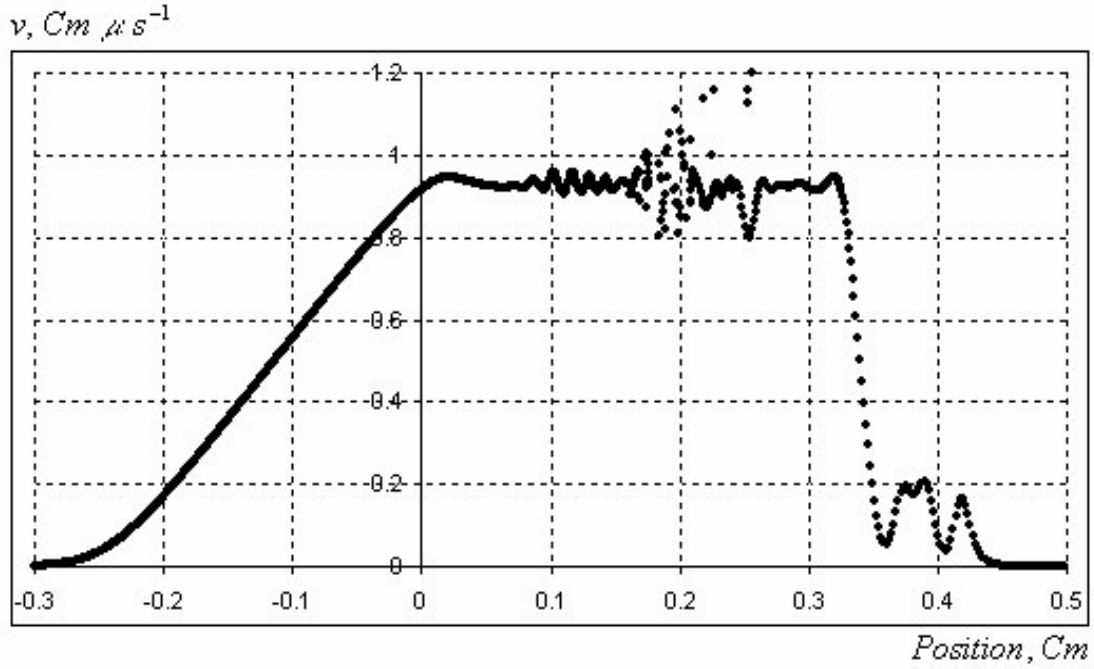

Figure 3-7: Profile of the velocity at time $t = 0.20\,\mu s$ with $h = 4 \cdot h_{ct}$

The plots above show not only that the interpolation deteriorates at the contact point but also at the front of the compressive wave. By increasing the ratio $\frac{h}{h_{cr}}$ the number of the neighbours becomes bigger for each particle, resulting as well as increase in CPU.

3.6 Conclusion

A criterion for the assessment and selection of kernels was given; it has the advantage to be simple and independent of the numerical scheme used. Examples of selected $1D$ and $3D$ kernels were compared with standard kernels and a numerical test shows promising results. Unfortunately with these kernels, one was not capable of obtaining results from shock tube test.

The consistency of the convolution was explored and one shows that it is controlled by smoothing length alone when the convolution form in (3.27) is adopted while the consistency is not assured when the convolution form in (3.32) is used. In this case, the gradient of the smoothing length has to be considered.

The influence of the ratio between the smoothing length and the particle spacing was highlighted with the shock tube example. As can be seen from figures 3.5, 3.6 and 3.7, caution should be taken for the initialization of the smoothing length.

3.7 References

[1] W. Liu, S. Yun, S. Li, J. Adee, T. Belytschko: "Reproducing Kernel Particle Methods for Structural Dynamics", *Int. J. Num. Meth. Engrg*., 38, 1655-1679 (1995).

[2] R. P. Nelson and J. C. B. Papaloizou:'Variable Smoothing Lengths and Energy Conservation in Smoothed Particle Hydrodynamic', *Mont. Not. Roy. Astronom. Soc.* 270(1990) 1.

[3] W. Benz:' An Introduction to Computational Methods in Hydrodynamics'. Late Stages of Stella Evolution, Computational Methods in Astrophysical Hydrodynamics. *Lectures Notes in Physics.*373. Astrophysics School II. Ponte de Lima, Portugal. 1989. Editor C. B. de Loore. Springer –Verlag.

[4] D. A. Fulk: A Numerical Analysis of Smoothed Particle Hydrodynamics, PhD Thesis, Air Force Institut of Technology, Wright-Patterson AFB OH (1994).

[5] S. J. Vinay III and M. S. Jhon:'A New Kernel for Smoothed Particle Hydrodynamic'. To be published.

[6] M. B. Liu, G. R.Liu and K. Y. Lam: "Constructing smoothing functions in smoothed particle hydrodynamics with application", *J. Comput. And Appl. Math.*., 155 (2003), 263 – 284.

[7] T. Belytschko, Y. Krongauz, J. Dolbow and C. Gerlach:'On the Completeness of Meshfree Particle Methods'. *Int. J. Num. Meth. Engng*. 43, 785-819 (1998).

[8] J. J. Monaghan: 'Smoothed Particle Hydrodynamics'. *Ann. Rev. Astron. Astrophys.*1992.30:543-74.

[9] B. Kutzler and V. Kokol-Voljc(2000), The Mathematical Assistant. *Derive*^{TM} 5.0 , version 5.07. Texas Instruments Incorporated Software, Dallas, Texas, USA.

4. BOUNDARY CONDITIONS AND SYMMETRY PLANS

4.1 Introduction

If one wants to describe physical behavior of a material (gas, fluid or solid, etc) using strong form the partial differential equations of continuum mechanics have to be completed by initial and by boundary conditions.

In order to apply the correct boundary conditions for the equations in the SPH formulation, the detection of boundary particles is needed to impose a correct boundary conditions on these particles.

Concerning bounded domain problems. There are several strategies and mathematical artifacts that allow for modeling the presence of boundaries with different degrees of accuracy. Monaghan initiated the use of ghost particles method for Cartesian type of boundary conditions; Takeda *et al* [1] applied this method to viscous flow. Randles and Libersky [2] extended this approach to general treatment of boundary conditions. An implementation of this approach in $2D$ was given in Cummins and Rudman [3].

The Ghost particle method uses mirroring of particles lying within some specified distance from a boundary. The effect of the fictitious 'Ghost' particles are explicitly included in the summations for the fields and for their gradients.

Since the smoothing length is the range of the interactions of the particles in SPH method, mirroring is limited to the smoothing length regardless of the distance of the particle to the boundary.

Another approach requires not only the knowledge of the topology of the geometry (Distribution of the particles) on the boundary but also a suitable force density that reflects physical and mechanical properties of the material at the boundaries.

This method named 'boundary force', initiated by Viecelli [4] applied a sufficient force along boundaries to ensure the non-penetration between fluid and flexible walls. Peskin [5] and Peskin and McQueen [6] used a finite impulse for the intensity of the boundary force to simulate elastic boundaries. Following the same idea, Sulsky and Brackbill [7] adopted the stress-strain constitutive relation to compute the boundary force.

In Monaghan *et al* [8, 9, 10] both an analytical expression and a pair-wise $12-6$ *Lennard – Jones* potential were selected to mimic the boundary forces. The pair-wise $12-6$ *Lennard – Jones* intermolecular potential is known to successfully reproduce the properties of interactions of many liquids. These choices ensure the normal component of the relative velocity to the boundary to vanish.

For open domain problems (external flows, free surfaces flows, free boundaries, etc), the challenge lies on the definition of robust and accurate criterion for the detection of boundary particles.

The intuitive approach to achieve this detection consists on the use the normalization condition or the gradient condition. This approach fails in its attempt to follow the boundary particles in the presence of strong perturbations.

The second approach is based on the construction of a function known as 'Color function' which was adapted to particle methods by Brackbill *et al* [12] and to SPH methods by Randles and Libersky [2]. The general version of this approach, known as the 'level set method' was first proposed by Osher and Sethian [11] and is used to represent the boundary or the interface by function where the zero level contour gives the current position of the front.

The third alternative is purely geometrical and requires the assimilation of the smoothing lengths to the sizes of particles. Recently Dilts and Hague [13] used this approach named 'exposure method' and performed 2D and 3D algorithms for moving least square method. Although this robust approach gives good results, the 'exposed particles 'filter is not clear and the computing time consuming can be non-negligible especially for 3D simulations.

Meshless numerical methods suffer difficulties concerning the theoretical investigation of boundaries conditions because of the presence of singularities in the normal on the boundary particles or nodes.

This chapter in its first part furnishes a theoretical derivation of the boundary condition on the basis of the 'Generalized Ghost particles' approach. The second part provides a detailed 'Standard Ghost particles' algorithm based on crystallographic representation of the materials which is the appropriate way of thinking to deal with symmetries and reflections. Finally numerical examples were performed to exemplify and to sustain the accuracy of the algorithm.

4.2 Governing Equations

One considers the system of equation (1.26) in the chapter one. The bounded domain $V \subset \Re^{nd}$ of the continuum is defined with suitable initial and boundary conditions on the boundary $B \subset \Re^{nd-1}$.

$$\left\{ \begin{array}{l} \left. \begin{array}{c} \dfrac{d\vec{r}(t)}{dt} = \vec{v}(r,t) \\ \dfrac{d\psi(r,t)}{dt} = -\left\langle \nabla_r S(\overline{\overline{\sigma}}) \right\rangle_s \end{array} \right\} \quad (r,t) \in V \; x \left[0,T\right] \\ \left. \begin{array}{c} \left(\vec{v}(r,t) - \vec{v}_B\right) \cdot \hat{n}_B = 0 \\ \rho\,(r,t) = \rho_B \\ S(r,t) = S_B \end{array} \right\} \quad (r,t) \in B \; x \left[0,T\right] \end{array} \right. \tag{4.1}$$

In the above system $\hat{n}_B$ is the outward unit normal on boundary.

The continuous form of the equations of conservation in the kernel approximation can be expressed as.

$$\begin{aligned} \frac{d\psi(r,t)}{dt} &= \int_V \left[\frac{S(r')}{\rho(r')^2} + \frac{S(r)}{\rho(r)^2} \right] \cdot \nabla_{r'} W(r-r') \cdot \rho(r') \cdot d^3 r' \\ &- \int_B \left[\frac{S(r')}{\rho(r')^2} + \frac{S(r)}{\rho(r)^2} \right] \cdot \nabla_{r'} W(r-r') \cdot \rho(r') \cdot \hat{n}(r') \cdot ds(r') \end{aligned} \tag{4.2}$$

4.3 Ghost Particles Approach

Let us defines $V^{[\alpha,\beta]} = \left\{ r \in \Re^{nd} \;/\; \alpha \le r \le \beta \right\}$ and let r_B be the location of the boundary.

For each particle located at (r_i,t) with the smoothing length $h(r_i)$ sufficiently close to the boundary, that is, $\left| r_i - r_B \right| \le 2 \cdot h(r_i)$ there exists a local coordinate over $B \times \left[0,\, 2.h(r_i)\right]$, which can be used to construct a local volume extension $\widetilde{V}_i = V \cup V^{[0,\, 2.h(r_i)]}$ around the boundary B of the volume V.

To a such particle $\vec{r}_i \in V$ corresponds a ghost(s) particle(s) located at position $\vec{r}_i^{\,Gh} \in \widetilde{V}_i$. There is an affine transformation of the type $\vec{r}_i^{\,Gh} = Tr(\vec{r}_i) = \overline{\overline{R}} \cdot \vec{r}_i + \vec{T}$ that is, a non-singular linear transformation followed by a translation which gives the position of ghost particles via a local rotation $\overline{\overline{R}}$ and translation $\vec{T}$ of the position of the parent particles, Hammer [14].

The boundary term in (4.2) can be extended to a volume $V^{[0,2.h(r)]}$ around a border B and then the boundary integral becomes.

$$\int_B \left[\frac{S(r)}{\rho(r)^2} + \frac{S(r')}{\rho(r')^2} \right] \nabla_{r'} W(r - r') \rho(r') d\vec{s}(r') \approx \int_{V^{[0,2.h(r)]}} \left[\frac{S(r)}{\rho(r)^2} + \frac{S(r')}{\rho(r')^2} \right] \nabla_{r'} W(r - r') \rho(r') d^3 r'$$

The particle approximation of the boundary integral at $r = r_i$ becomes (2.4):

$$\int_B \left[\frac{S(r_i)}{\rho(r_i)^2} + \frac{S(r')}{\rho(r')^2} \right] \nabla_{r'} W(r_i - r').\rho(r').d\vec{s}(r') \approx \sum_{j \in G_h(N_i)} m_j . \left[\frac{S(r_i)}{\rho(r_i)^2} + \frac{S(r_j)}{\rho(r_j)^2} \right] . \nabla_{r_j} W(r_i - r_j)$$

Where $G_h(N_i) = Gd(i) \cup Gi(i)$ contains Direct ghost particles and Indirect ghost particles of the particle i, thus.

$$G_h(N_i) = \left\{ r_i^{Gh} \right\} \cup \left\{ k \in Z,\ r_k \in Supp\left(W\left(r_i - r_k \right) \right) \text{ and } r_k^{Gh} \in Supp\left(W\left(r_i - r_k^{Gh} \right) \right) \right\}$$

4.3.1 Conservation of Momentum

Let us denotes by $G_h(N) = \bigcup_{i=1}^{i=N} G_h(N_i)$ all the ghost particles generated at a given instant and by $\widetilde{V} = \bigcup_{i=1}^{N} \widetilde{V}_i$ the global extended volume. The total momentum of the system is given by.

$$\vec{P} = \sum_{i=1}^{N} m_i . \vec{v}_i$$

Thus, in the SPH approximation, the rate of change of momentum due to the presence of ghost particles is given by:

$$\begin{aligned} \frac{d\vec{P}}{dt} &= -\sum_{i=1, j\in G_h(N)}^{N} m_i \cdot m_j \cdot \left[\frac{\overline{\overline{\sigma_i}}}{\rho_i^2} + \frac{\overline{\overline{\sigma_j}}}{\rho_j^2} \right] \cdot \nabla_{r_j} W(r_i - r_j) \\ &\approx -\int_B \overline{\overline{\sigma}}(r') \cdot \nabla_{r'} W(r - r') \cdot \hat{n} \cdot ds \end{aligned} \tag{4.3}$$

Which satisfies the momentum equation involving forces at the boundaries.

Since the Jacobean $J = Det\left[Tr(\vec{r}_i)\right] = Det\left[\overline{\overline{R}}\right] = 1$ (the transformation $Tr(\vec{r})$ is orientation-preserving) it follows that the lumped volume is conserved, and then for $j \in G_h(N_i)$ one possible solution is:

$$\begin{cases} m_j = m_i \\ \rho(r_j) = \rho_j = \rho_i \end{cases} \tag{4.4}$$

The second equation above allows us to write $h(r_j) = h_j = h_i$. Masses, densities and smoothing lengths of ghost particles are respectively are equal to their parent couterparts.

4.3.2 Conservation of the Total Specific Energy

The total energy of N Body particles is given by:

$$E = \sum_{i=1}^{N} \frac{m_i . v_i^2}{2} + m_i . e_i \tag{4.5}$$

The total energy is conserved for unbounded set of particles; this should be true with a specific choice of the velocities for ghost particles in any bounded domain.

If viscous part of the total energy is omitted, from the equation of total specific energy one gets:

$$\frac{dE}{dt} = -\sum_{i=1,\, j\in G_h(N)}^{i=N} m_i.m_j.\left[\frac{\overline{\overline{\sigma_i}}.\vec{v}_i}{\rho_i^2} + \frac{\overline{\overline{\sigma_j}}.\vec{v}_j}{\rho_j^2}\right].\nabla_j W(r_i - r_j) \tag{4.6}$$

In the following equations, one denotes by $G_h(i)$ the indices of the direct ghost particles of the particle i. The expression in (4.6) can be detailed and rearranged to.

$$\begin{aligned}
\frac{dE_T}{dt} &= -\sum_{i=1}^{N} m_i.\frac{\overline{\overline{\sigma_i}}.\vec{v}_i}{\rho_i^2}.\sum_{j\in G_h(N)} m_j.\nabla_{r_j} W(r_i - r_j) \\
&\quad -\sum_{i=1}^{N} m_i.\sum_{j\in G_h(N)} \frac{\overline{\overline{\sigma_j}}.\vec{v}_j}{\rho_j^2}.\nabla_{r_j} W(r_i - r_j) \\
&= -\sum_{i=1}^{N} m_i.\left[\frac{\overline{\overline{\sigma_i}}}{\rho_i^2}.\sum_{j=1}^{N} m_j.\nabla_{r_j^{Gh}} W(r_i - r_j^{Gh})\right].\vec{v}_i \\
&\quad -\sum_{i=1}^{N} m_i.\sum_{j=1}^{N} m_j.\frac{\overline{\overline{\sigma_{G_h(i)}}}}{\rho_j^2}.\vec{v}_{G_h(j)}.\nabla_{r_j^{Gh}} W(r_i - r_j^{Gh}) \\
&= -\sum_{i=1}^{N} m_i.\left[\frac{\overline{\overline{\sigma_i}}}{\rho_i^2}.\sum_{j=1}^{N} m_j.\nabla_{r_j^{Gh}} W(r_i - r_j^{Gh})\right].\vec{v}_i \\
&\quad -\sum_{j=1}^{N} m_j.\sum_{i=1}^{N} m_i.\frac{\overline{\overline{\sigma_{G_h(i)}}}}{\rho_i^2}.\vec{v}_{G_h(i)}.\nabla_{r_i^{Gh}} W(r_j - r_i^{Gh}) \\
&= -\sum_{i=1}^{N} \frac{m_i}{\rho_i^2}.\left\{\left[\sum_{j=1}^{N} m_j.\nabla_{r_j^{Gh}} W(r_i - r_j^{Gh})\right].\overline{\overline{\sigma_i}}.\vec{v}_i + \left[\sum_{j=1}^{N} m_j.\nabla_{r_i^{Gh}} W(r_j - r_i^{Gh})\right].\overline{\overline{\sigma_{G_h(i)}}}.\vec{v}_{G_h(i)}\right\}
\end{aligned}$$

A sufficient condition for the conservation of the total energy is that the stresses and the velocities of the particle and its ghost particles obey.

$$\left[\sum_{j=1}^{N} m_j . \nabla_{r_j^{Gh}} W(r_i - r_j^{Gh})\right] . \overline{\overline{\sigma}}_i . \vec{v}_i + \left[\sum_{j=1}^{N} m_j . \nabla_{r_i^{Gh}} W(r_j - r_i^{Gh})\right] . \overline{\overline{\sigma}}_{G_h(i)} . \vec{v}_{G_h(i)} = 0 \qquad (4.7)$$

In SPH generally radial kernels are used, thus:

$$\nabla_{r_k} W(r_i - r_k) = -\left.\frac{\partial W}{\partial r}\right|_{r_{ik}} \cdot \frac{\vec{r}_i - \vec{r}_k}{|\vec{r}_i - \vec{r}_k|} = -\nabla_r W\big|_{i,k} \cdot \hat{n}_{i,k} \qquad (4.8)$$

Then (4.7) simplifies to.

$$\left[\sum_{j=1}^{N} m_j . \nabla_r W\big|_{i,G_h(j)} \cdot \hat{n}_{i,G_h(j)}\right] \cdot \overline{\overline{\sigma}}_i . \vec{v}_i + \left[\sum_{j=1}^{N} m_j . \nabla_r W\big|_{j,G_h(i)} . \hat{n}_{j,G_h(i)}\right] \cdot \overline{\overline{\sigma}}_{G_h(i)} . \vec{v}_{G_h(i)} = 0 \qquad (4.9)$$

Let us define a local reference axis on the boundary by considering $(\hat{n}_B, \hat{t}_B)$ as outward unit normal and direct tangent to the boundary, one has then:

$$\hat{n}_{j,G_h(i)} = \alpha_{i,j} \cdot \hat{n}_B - \beta_{i,j} \cdot \hat{t}_B \qquad (4.10)$$

Where $\alpha_{i,j}$ and $\beta_{i,j}$ are function of coordinates of particles i and j. By incorporating (4.10) into (4.9) and using the property $\nabla_r W\big|_{i,G_h(j)} = \nabla_r W\big|_{j,G_h(i)}$, one obtains the relation below.

$$\sum_{j=1}^{N} m_j \cdot \nabla_r W\big|_{i,G_h(j)} \cdot \alpha_{i,j} \cdot \hat{n}_B \left[\overline{\overline{\sigma_i}} \cdot \vec{v}_i + \overline{\overline{\sigma_{G_h(i)}}} \cdot \vec{v}_{G_h(i)} \right] + \sum_{j=1}^{N} m_j \cdot \nabla_r W\big|_{i,G_h(j)} \cdot \beta_{i,j} . \hat{t}_B \cdot \left[\overline{\overline{\sigma_i}} \cdot \vec{v}_i - \overline{\overline{\sigma_{G_h(i)}}} \cdot \vec{v}_{G_h(i)} \right] = 0 \tag{4.11}$$

The equation above is linear in term of the unknown $\overline{\overline{\sigma_{G_h(i)}}} \cdot \vec{v}_{G_h(i)}$, and can be normalized and rearranged to:

$$\left[Cos\alpha_i \cdot \hat{n}_B + Sin\ \alpha_i \cdot \hat{t}_B \right] \cdot \left[\overline{\overline{\sigma_i}} \cdot \vec{v}_i + \overline{\overline{R_{(-2.\alpha_i)}}} \cdot \overline{\overline{\sigma_{G_h(i)}}} \cdot \vec{v}_{G_h(i)} \right] = 0 \tag{4.12}$$

In the previous equation, $Cos\alpha_i = \frac{A_i}{A_i^2 + B_i^2}$, $Sin\alpha_i = \frac{B_i}{A_i^2 + B_i^2}$ with $A_i = \sum_{j=1}^{N} m_j . \nabla_r W\big|_{i,G_h(j)} . \alpha_{i,j}$, $B_i = \sum_{j=1}^{N} m_j . \nabla_r W\big|_{i,G_h(j)} . \beta_{i,j}$ and $\overline{\overline{R_{(-2.\alpha_i)}}}$ is the rotation matrix of angle $(-2.\alpha_i)$. The solution of (4.12) is straightforward and is given by:

$$\overline{\overline{\sigma_{G_h(i)}}} \cdot \vec{v}_{G_h(i)} = -\overline{\overline{R_{(2.\alpha_i)}}} \cdot \overline{\overline{\sigma_i}} \cdot \vec{v}_i \tag{4.13}$$

Knowing that the velocities of ghost particles can be obtained by differentiating $\vec{r}_i^{\,Gh} = Tr(\vec{r}_i)$ with respect to time, it follows then that the extended fields are given by:

$$\begin{cases} \vec{v}_{G_h(i)} = \overline{\overline{R}} \cdot \vec{v}_i \\ \overline{\overline{\sigma_{G_h(i)}}} = -\overline{\overline{R_{(2.\alpha_i)}}} \cdot \overline{\overline{\sigma_i}} \cdot \left(\overline{\overline{R}}\right)^{-1} \end{cases} \tag{4.14}$$

The system of equations in (4.4) and (4.14) completed by the position $\vec{r}_i^{\,Gh}$ describe entirely the ghost particle.

In the analysis above viscous operators were omitted and the expression of energy $(1.27, \textit{Chapter}\,1)$ is used instead of the expression $(1.29, \textit{Chapter}\,1)$.

4.4 Algorithm for Ghost particles

One considers a system of particles distributed within the cubic P Bravais lattice see Figure 1. The system possesses a translational periodicity and three principal types of symmetry operators: Two-dimensional mirror planes, one-dimensional rotation axes and zero-dimensional inversion point that can be taken in conjunction with rotation axes.

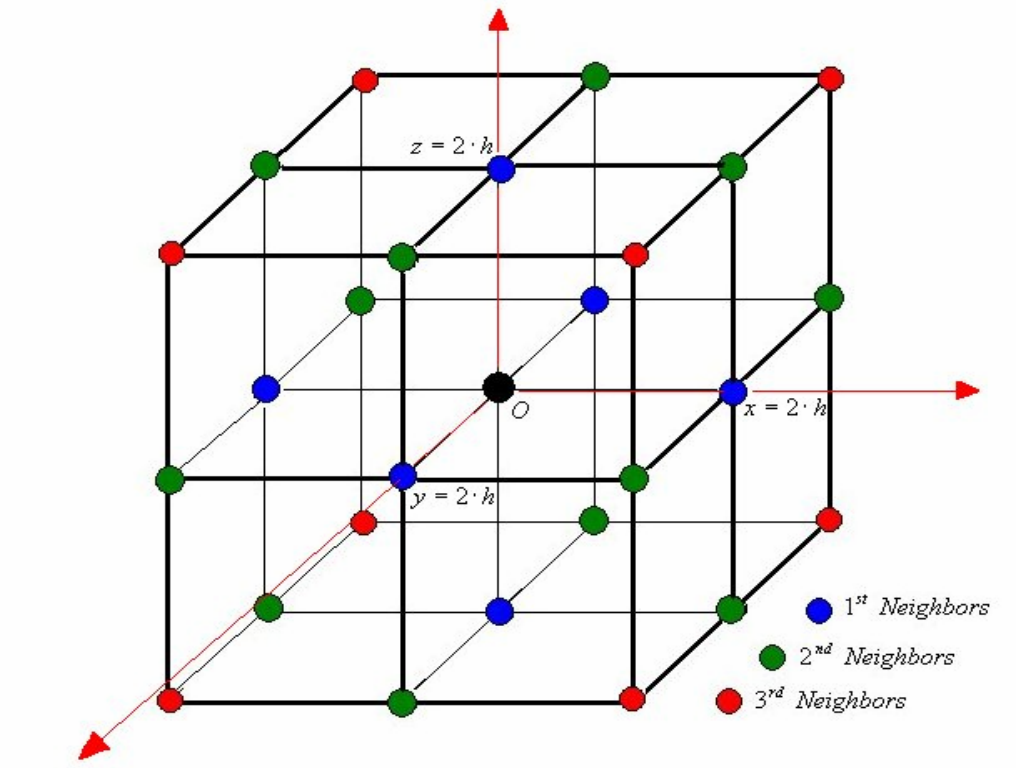

Figure 4-1: Bravais lattice Cubic P

Each particle within the infinite lattice has (6 first neighbors +12 Second neighbors +8 third neighbors= 26 neighbors), this means that there are 26 possible locations for the ghost particles.

In the other hand, one has:

A / One symmetry plane operation $\left(x = \pm h \; or \; y = \pm h \; or \; z = \pm h\right)$ mirrors each particle ones, produces one new particle *(First Neighbor).*

B / From two successive symmetries plane operations results three particles as follow:

For example, the first symmetry plane $\left(x = \pm h\right)$ produces one particle from each original particle *(First Neighbor).* The second symmetry plane operation $\left(y = \pm h\right)$ is applied to the previous two particles produces two new particles *(1First Neighbor and 1 Second Neighbor).*

C / From three successive symmetries planes operations $\left(x = \pm h \; and \; y = \pm h \; and \; z = \pm h\right)$ results seven new particles *(3First Neighbor, 3 Second Neighbor and 1 Third Neighbor).* .

The operations **A**, **B** and **C** above are the three cases to consider for particle that are close to the reflective boundaries or to symmetries planes, then:

A case: The particle is close to single symmetry plane, so, only 1 ghost particle is created.

B case: The particle is close to two perpendicular symmetries planes, also 3 ghost particles will be created.

C case: The particle is close to three perpendicular symmetries planes, and then 7 ghost particles are needed.

The position of i^{th} particle is $r_i = \left(x(1,i), x(2,i), x(3,i)\right)$ if it is within $C \cdot h_i$, $\left(C = 1 \; Or \; 2\right)$ of boundary or symmetry then it has to be mirrored and its integer flag is set to positive value $NFlag(i) > 0$.

The value associated to the address $Flag(i)$ gives one of the 26 positions that the i^{th} particle occupies in the lattice.

Consequently, the number of ghosts particles needed $Ngp(i) = \begin{cases} 1 \\ Or \; 3 \\ Or \; 7 \end{cases}$ is generated.

The spatial limits of the domain are known as well as the reflective boundaries of the system. $(Xb\min, Xb\max), (Yb\min, Yb\max)\ and\ (Zb\min, Zb\max)$. The positions of the parent particles are identified and the positions of the ghost particle are given by specular reflection, called also elastic reflexion.

The crosses in the table below indicate that the particle is close to a specified plane.

Xb min	Xb max	Yb min	Yb max	Zb min	Zb max	$NFlag(i)$	$Ngp(i)$
						0	
X						1	1
	X					2	1
		X				3	1
X		X				4	3
	X	X				5	3
			X			6	1
X			X			7	3
	X		X			8	3
				X		9	1
X				X		10	3
	X			X		11	3
		X		X		12	3
		X		X		13	7
	X	X		X		14	7
			X	X		15	3
X			X	X		16	7
	X		X	X		17	7
					X	18	1
X					X	19	3
	X				X	20	3
		X			X	21	3
X		X			X	22	7
	X	X			X	23	7
			X		X	24	3
X			X		X	25	7
	X		X		X	26	7

A useful way to implement, the computation of the ghost particles positions and their velocities is the introduction of the rotation $\overline{\overline{R}}$ and translation T mentioned in the section 2.1

$$\begin{cases} x(nd, ghost) = R[nd, NF, Ng] \cdot x(nd, i) + T[nd, NF, Ng] \\ v(nd, ghost) = R[nd, NF, Ng] \cdot v(nd, i) \end{cases}$$

with $\overline{\overline{R}} = R[nd, NFlag(i), Ngp(i)]$ and $\overline{\overline{Tr}} = Tr[nd, NFlag(i), Ngp(i)]$ with nd representing the space dimension.

$R[1, 26, 7]$	1	2	3	4	5	6	7	8	9	10	11	12	13	14	15	16	17	18	19	20	21	22	23	24	25	26
1	-1	-1	1	1	1	1	1	1	1	1	1	1	1	1	1	1	1	1	1	1	1	1	1	1	1	1
2	0	0	0	-1	-1	0	-1	-1	0	-1	-1	1	1	1	1	1	1	0	-1	-1	1	1	1	1	1	1
3	0	0	0	-1	-1	0	-1	-1	0	-1	-1	1	-1	-1	1	-1	-1	0	-1	-1	1	-1	-1	1	-1	-1
4	0	0	0	0	0	0	0	0	0	0	0	0	1	1	0	1	1	0	0	0	0	1	1	0	1	1
5	0	0	0	0	0	0	0	0	0	0	0	0	-1	-1	0	-1	-1	0	0	0	0	-1	-1	0	-1	-1
6	0	0	0	0	0	0	0	0	0	0	0	0	-1	-1	0	-1	-1	0	0	0	0	-1	-1	0	-1	-1
7	0	0	0	0	0	0	0	0	0	0	0	0	-1	-1	0	-1	-1	0	0	0	0	-1	-1	0	-1	-1

$\widetilde{T}[1, 26, 7]$	1	2	3	4	5	6	7	8	9	10	11	12	13	14	15	16	17	18	19	20	21	22	23	24	25	26
1	1	-1	0	0	0	0	0	0	0	0	0	0	0	0	0	0	0	0	0	0	0	0	0	0	0	0
2	0	0	0	1	-1	0	1	-1	0	1	-1	0	0	0	0	0	0	0	1	-1	0	0	0	0	0	0
3	0	0	0	1	-1	0	1	-1	0	1	-1	0	1	-1	0	1	-1	0	1	-1	0	1	-1	0	1	-1
4	0	0	0	0	0	0	0	0	0	0	0	0	0	0	0	0	0	0	0	0	0	0	0	0	0	0
5	0	0	0	0	0	0	0	0	0	0	0	0	1	-1	0	1	-1	0	0	0	0	1	-1	0	1	-1
6	0	0	0	0	0	0	0	0	0	0	0	0	1	-1	0	1	-1	0	0	0	0	1	-1	0	1	-1
7	0	0	0	0	0	0	0	0	0	0	0	0	1	-1	0	1	-1	0	0	0	0	1	-1	0	1	-1

$R[2,26,7]$	1	2	3	4	5	6	7	8	9	10	11	12	13	14	15	16	17	18	19	20	21	22	23	24	25	26
1	1	1	-1	-1	-1	-1	-1	-1	1	1	1	1	1	1	1	1	1	1	1	1	1	1	1	1	1	1
2	0	0	0	1	1	0	1	1	0	1	1	-1	-1	-1	-1	-1	-1	0	1	1	-1	-1	-1	-1	-1	-1
3	0	0	0	-1	-1	0	-1	-1	0	1	1	-1	1	1	-1	1	1	0	1	1	-1	1	1	-1	1	1
4	0	0	0	0	0	0	0	0	0	0	0	0	-1	-1	0	-1	-1	0	0	0	0	-1	-1	0	-1	-1
5	0	0	0	0	0	0	0	0	0	0	0	0	1	1	0	1	1	0	0	0	0	1	1	0	1	1
6	0	0	0	0	0	0	0	0	0	0	0	0	-1	-1	0	-1	-1	0	0	0	0	-1	-1	0	-1	-1
7	0	0	0	0	0	0	0	0	0	0	0	0	-1	-1	0	-1	-1	0	0	0	0	-1	-1	0	-1	-1

$\widetilde{T}[2,26,7]$	1	2	3	4	5	6	7	8	9	10	11	12	13	14	15	16	17	18	19	20	21	22	23	24	25	26
1	0	0	1	1	1	-1	-1	-1	0	0	0	0	0	0	0	0	0	0	0	0	0	0	0	0	0	0
2	0	0	0	0	0	0	0	0	0	0	0	1	1	1	-1	0	0	0	0	0	1	0	0	-1	0	0
3	0	0	0	1	1	0	-1	-1	0	0	0	1	0	0	-1	0	0	0	0	0	1	0	0	-1	0	0
4	0	0	0	0	0	0	0	0	0	0	0	0	1	1	0	-1	-1	0	0	0	0	1	1	0	-1	-1
5	0	0	0	0	0	0	0	0	0	0	0	0	0	0	0	0	0	0	0	0	0	0	0	0	0	0
6	0	0	0	0	0	0	0	0	0	0	0	0	1	1	0	-1	-1	0	0	0	0	1	1	0	-1	-1
7	0	0	0	0	0	0	0	0	0	0	0	0	1	1	0	-1	-1	0	0	0	0	1	1	0	-1	-1

$R[3,26,7]$	1	2	3	4	5	6	7	8	9	10	11	12	13	14	15	16	17	18	19	20	21	22	23	24	25	26
1	1	1	1	1	1	1	1	1	-1	-1	-1	-1	-1	-1	-1	-1	-1	-1	-1	-1	-1	-1	-1	-1	-1	-1
2	0	0	0	1	1	0	1	1	0	1	1	1	1	1	1	1	1	0	1	1	1	1	1	1	1	1
3	0	0	0	1	1	0	1	1	0	-1	-1	-1	1	1	-1	1	1	0	-1	-1	-1	1	1	-1	1	1
4	0	0	0	0	0	0	0	0	0	0	0	0	-1	-1	0	-1	-1	0	0	0	0	-1	-1	0	-1	-1
5	0	0	0	0	0	0	0	0	0	0	0	0	-1	-1	0	-1	-1	0	0	0	0	-1	-1	0	-1	-1
6	0	0	0	0	0	0	0	0	0	0	0	0	1	1	0	1	1	0	0	0	0	1	1	0	1	1
7	0	0	0	0	0	0	0	0	0	0	0	0	-1	-1	0	-1	-1	0	0	0	0	-1	-1	0	-1	-1

$\widetilde{T}[3,26,7]$	1	2	3	4	5	6	7	8	9	10	11	12	13	14	15	16	17	18	19	20	21	22	23	24	25	26
1	0	0	0	0	0	0	0	0	1	1	1	1	1	1	1	1	1	-1	-1	-1	-1	-1	-1	-1	-1	-1
2	0	0	0	0	0	0	0	0	0	0	0	0	0	0	0	0	0	0	0	0	0	0	0	0	0	0
3	0	0	0	0	0	0	0	0	0	1	1	1	0	0	1	0	0	0	-1	-1	-1	0	0	-1	0	0
4	0	0	0	0	0	0	0	0	0	0	0	0	1	1	0	1	1	0	0	0	0	-1	-1	0	-1	-1
5	0	0	0	0	0	0	0	0	0	0	0	0	1	1	0	1	1	0	0	0	0	-1	-1	0	-1	-1
6	0	0	0	0	0	0	0	0	0	0	0	0	0	0	0	0	0	0	0	0	0	0	0	0	0	0
7	0	0	0	0	0	0	0	0	0	0	0	0	1	1	0	1	1	0	0	0	0	-1	-1	0	-1	-1

The tables above are stored in the code once. Translations $\widetilde{T}[nd, NF, Ng]$ represent a local transformations that should be interpreted as follow:

$$\widetilde{T}[1, NF, Ng] = \begin{cases} 1 \Rightarrow T[1, NF, Ng] = 2 \cdot Xb\max \\ -1 \Rightarrow T[1, NF, Ng] = 2 \cdot Xb\min \end{cases}$$

$$\widetilde{T}[2, NF, Ng] = \begin{cases} 1 \Rightarrow T[2, NF, Ng] = 2 \cdot Yb\max \\ -1 \Rightarrow T[2, NF, Ng] = 2 \cdot Yb\min \end{cases}$$

$$\widetilde{T}[3, NF, Ng] = \begin{cases} 1 \Rightarrow T[3, NF, Ng] = 2 \cdot Zb\max \\ -1 \Rightarrow T[3, NF, Ng] = 2 \cdot Zb\min \end{cases}$$

The ‘Ghost particles’ creation algorithm can be summarized as follow:

Do Loop over all Particles i

$$NFlag(i) > 0 \Rightarrow \begin{cases} Create\ Ghost\ (s)\ particle\ (s)\ \_\ First\ \ Neighbor(s)\ ngi \\ Add\ The\ Contribution\ of\ \ ngi\ to\ the\ \ field\ \ of\ \ particle\ i \end{cases}$$

Do Loop Over Real particles k interacting with Particle i

$$NFlag(k) > 0 \Rightarrow \begin{cases} Create\ Ghost\ (s)\ particle\ (s)\ \_\ First\ \ Neighbor(s)\ ngk \\ ngk\ \text{int}\, eract\ with\ \ particle\ i \Rightarrow \begin{cases} Add\ The\ Contribution\ of\ \ ngk \\ to\ the\ \ field\ \ of\ \ particle\ i \end{cases} \end{cases}$$

Add the contribution of particles k to the field of particle I

Enddo Loop_k

Enddo Loop_i

The algorithm above uses a local list of ghost particles and avoid creating temporal connectivity between real and ghost particles.

4.5 Numerical experiments

The objective here is to test the robustness of the algorithm performed in the code. Two situations are involved; the first one deal with the impact of an aluminium sphere on a cylinder aluminium plate, both modeled materials as elastic-plastic, the impact velocity is $v_z = -0.668\ Cm\ \mu s^{-1}$. Two planes of symmetry were considered $(x = 0\ and\ \ y = 0)$.

In the figures (4.2), (4.3) and (4.4) particles distributions and effective plastic strain are shown at different response times.

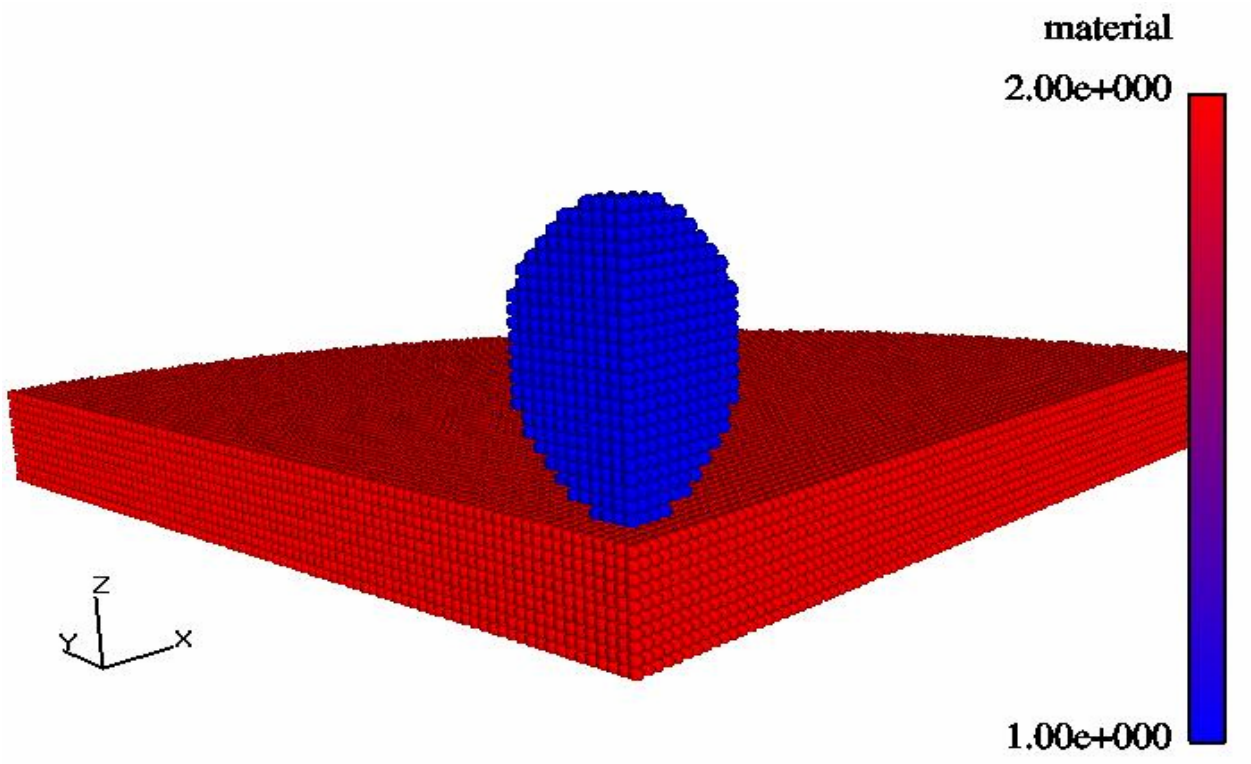

Figure 4-2: Initial distribution of 61192 particles (sphere 1612) particles

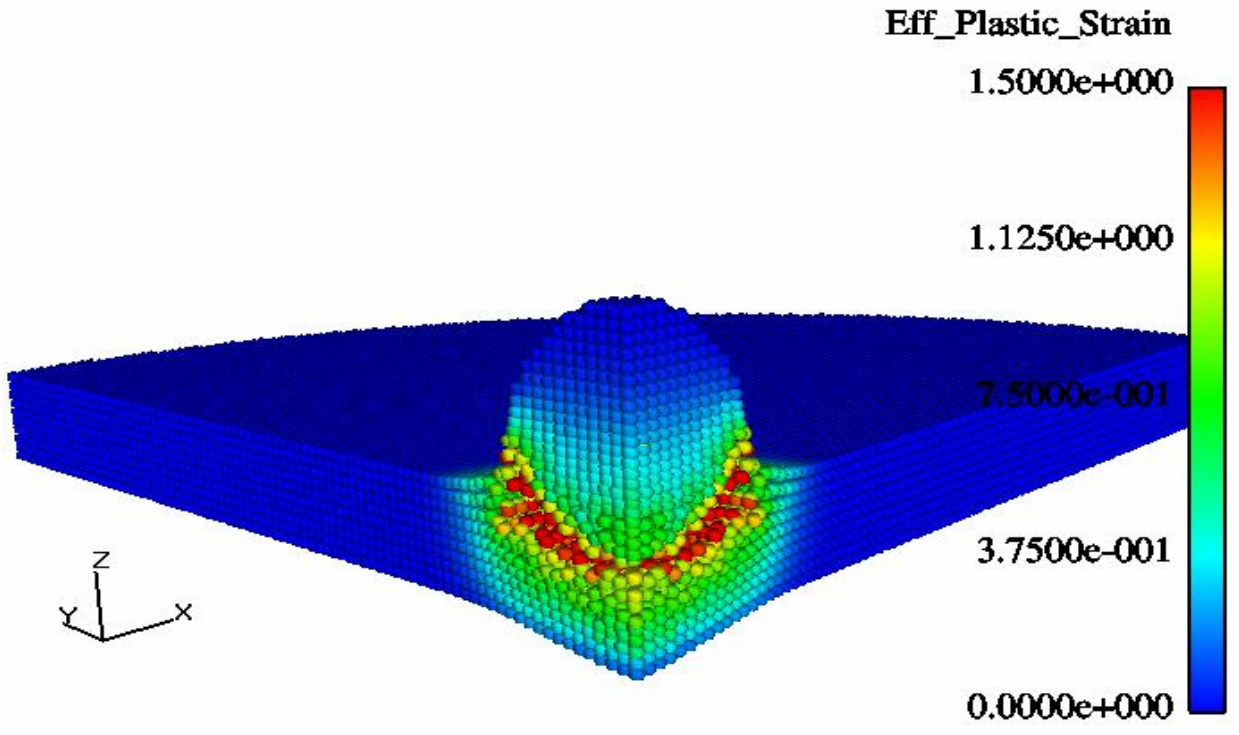

Figure 4-3: Effective plastic Strain at time $t = 1.009\,\mu s$ after impact

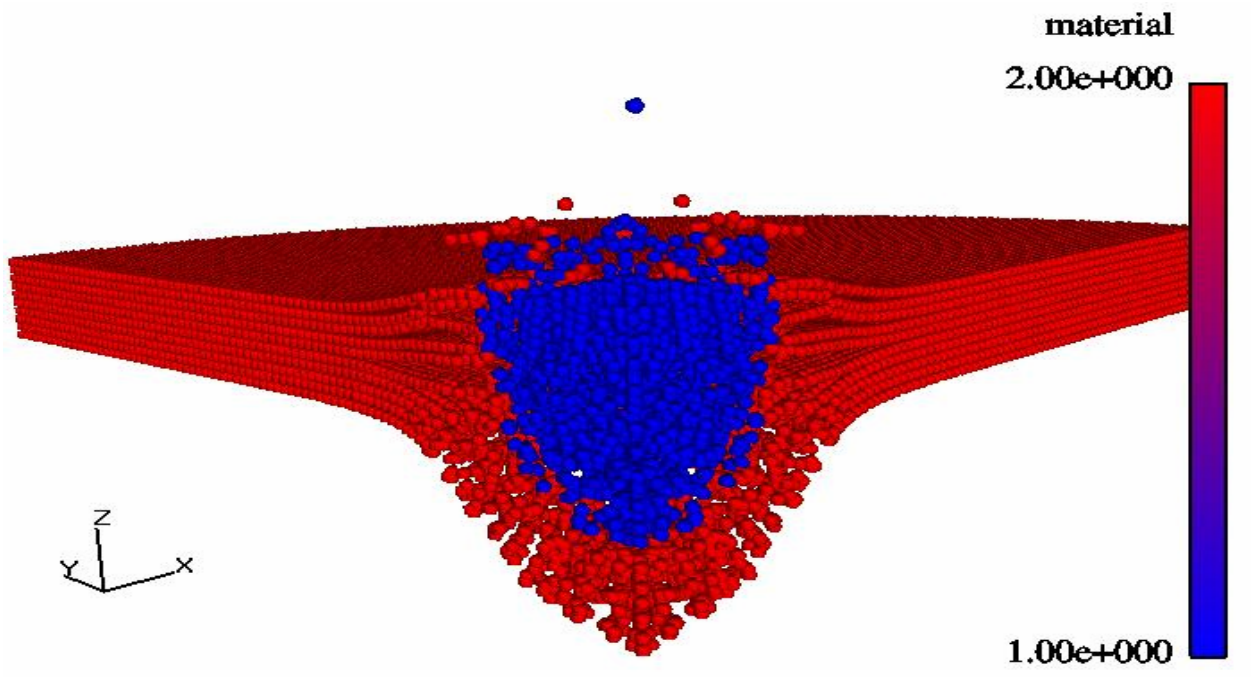

Figure 4-4: Distribution of particles time $t = 3.0084\,\mu s$ after impact

The second numerical test is the classical Taylor anvil impact with two symmetry planes $(x = 0\ and\ y = 0)$ and a reflective plane. An elastic-plastic copper cylinder represented by 20724 particles impacted a rigid wall at $z = 0$ with an initial velocity $v_z = -0.019\ Cm\ \mu s^{-1}$.

The distribution of particles and physical fields are shown in the figures (4.5) and (4.6) at two instants $t = 1.0\mu\ s$ and $t = 13.0\ \mu\ s$ after the initial contact.

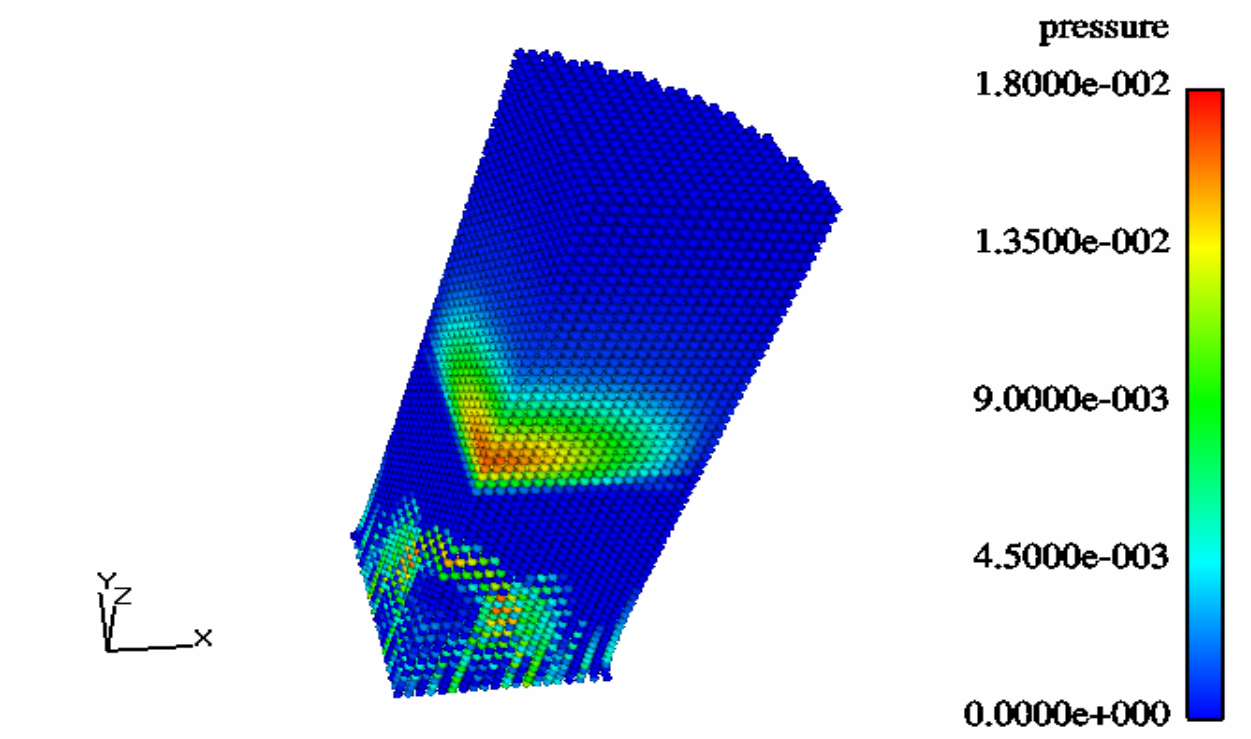

Figure 4-5: Pressure profile and the particles distribution at time $t = 1.000\,\mu s$ after impact

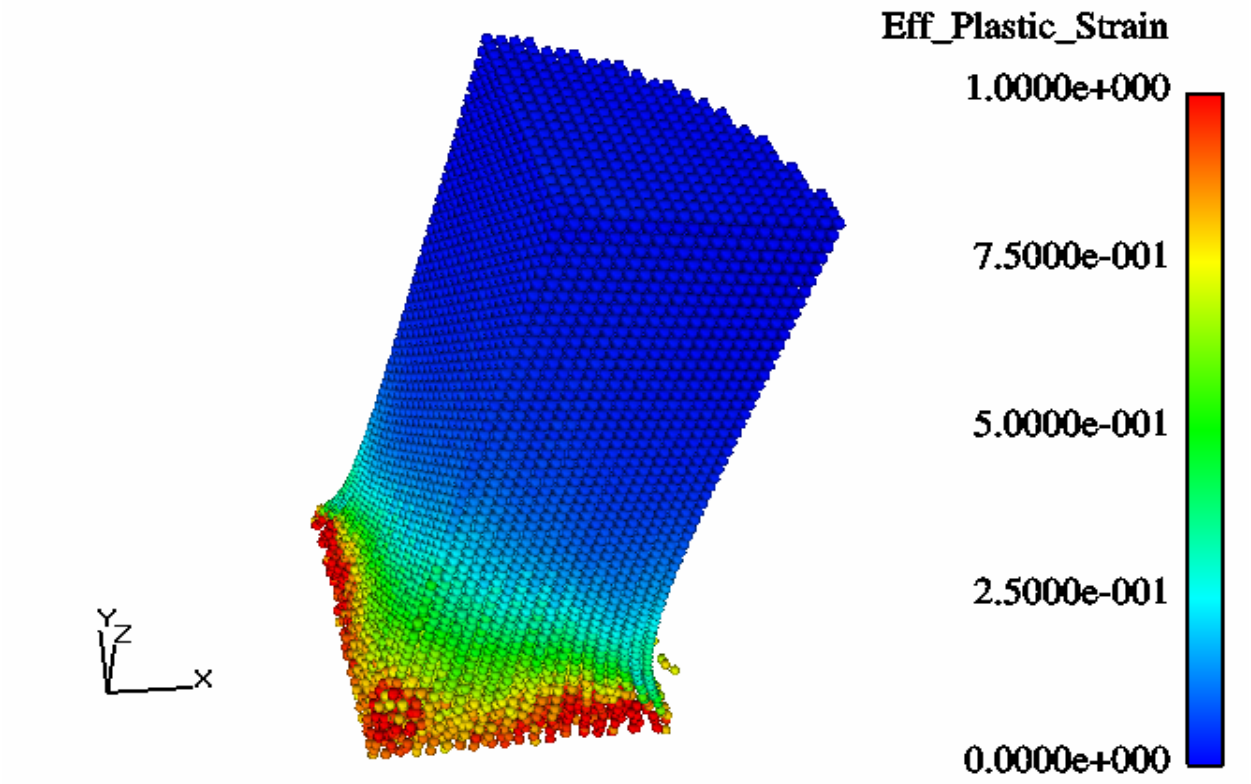

Figure 4-6: Effective Plastic Strain the particles distribution at time $t = 13.\mu\,s$ after impact

4.6 Conclusion

The proposed methodology based on the conservation of the total momentum and the total energy of the system provides a best understanding of the concept behind the creation and the introduction of fictitious particles in numerical codes. It shows also that the mirroring particle is an intuitive choice but it is not the only solution for treatment of boundary conditions.

It is interesting to note that the conservation of the total momentum leads to system (4.4) which does not enclose any information concerning the velocities of the particles.

Finally, numerical experiments performed showed a good behavior of materials near boundaries and symmetry plans.

'Ghost particle' method is of interest because especially for geometries possessing high degree of symmetry. Without a doubt, problems with inelastic boundary conditions where thermal and momentum transfers between particles and walls subsist could not treated by 'Ghost particles' methods.

4.7 References

[1] H. Takeda, S. Miyama and M. Sekiya:' Numerical Simulation of Viscous Flow by Smoothed Particle Hydrodynamics'. *Progress of Theoretical Physics*, Vol 92, No 5, November 1994.

[2] P. Randles and L. Libersky (1996):' Smoothed Particles Hydrodynamics: Some recent improvements and applications'.*Comput. Meth. Appl. Mech. Engng*. 139, 375-408.

[3] S. Cummins and M. Rudman (1999):'An SPH Projection Method'. *J. Comput. Phys*., 152, 584-607.

[4] J. Viecelli (1969):'A Method for Including Arbitrary External Boundaries in the MAC Incompressible Fluid Computing Technique'. *J. Comput. Phys*., 4, 543-551.

[5] C. Peskin (1972):' Flow Patterns Around Heart Valves:A Numerical Method'. *J. Comput. Phys*., 10, 252-271.

[6] C. Peskin and D. McQuinn (1989):' A Three-Dimensional Computational Method fo Blood Flow in the Hear I. Immersed Elastic Fibers in a Viscous Incompressible Fluid'. Method'. *J. Comput. Phys*., 82, 372-405.

[7] D. Sulsky and J. Brackbill (1991):'A Numerical Method for Suspension Flow'. *J. of Comp. Phys*., 96, 339-368.

[8] J. J. Monaghan (1995):'Lectures On SPH at Kaiserslautern University'.

[9] J. J.Monaghan (1994): "Simulating Free Surface Flows with SPH", *J. of Comp. Phys*., 110, 399-406

[10] J. J. Monaghan and A. Kos:'Solitary Waves on A Cretan Beach'. *J. Water. Port. Cost. Ocean. Engng*/May/June/1999.

[11] W. Mulder, S. Osher and J. Sethian (1992):"Fronts Propagating with Curvature-Dependant Speed: Algorithm Based on Hamilton-Jacobi Formulations". *J. of Comp. Phys*., 100, 209-228.

[12] J. Brackbill, D. Koth and C. Zemach.(1992):"A continuum method for modelling surface tension". *J. of Comp. Phys*., 100, 335-354.

[13] G. Dilts and A. Haque:'Three-Dimensional Boundary Detection for Smoothed Particle Methods'.LA-UR-00-4419. Los Alamos National Laboratory. September 23, 2000.

[14] J.Hammer:'Unsolved problems concerning lattice points'.1977.*Reseach Notes in Mathematics.*15 Pitman.

5. ON INTERPOLATION IN SPH

5.1 Introduction

The work presented in this chapter provides an overview of different types of kernel interpolation used in the SPH method: conventional SPH. Normalized SPH (NSPH), corrected kernel SPH (CSPH) and normalized corrected kernel SPH (NCSPH). These four methods are considered in a fully mesh-free form (using no background mesh). To illustrate the effect of using different interpolation methods a 1D shock-tube problem was simulated. An overview of the simulation results for the problem is given. Shortcomings for the interpolation schemes tested were identified and discussed. It is concluded that NCSPH provides the best results. To establish whether the better results obtained with the NCSPH method is sufficient, or further improvements are needed, it will be necessary to conduct tests in two and three dimensions.

There are two significant reasons for increased interest in the SPH method. The first reason is the method's flexibility due to its Lagrangian and meshless nature, the second reason is that it works reasonably well when applied to problems in an unbounded domain. In a bounded domain, the SPH method still shows poor accuracy near boundaries. The issue of treatment of boundary conditions (e.g. free boundaries or interface tracking) in the SPH method is still in the domain of research , especially for NSPH and CSPH, both in hydrodynamic and material strength problems.

Recently, to remedy some of the problems, a series of studies developed by Liu *et al* [1, 2, 3 and 4] introduced a polynomial correction function to the standard kernel function. This approach, called the 'Reproducing Kernel Particle Method' (RKPM) by the authors, seems to be able to handle material boundaries without losing consistency, and improving the accuracy of the solution.

In parallel to this a different type of correction was proposed by Johnson and Beissel [5] and Randles and Libersky [6]. They suggest a normalization of the kernel sum in order to ensure that the derivative of a linear function is calculated exactly.

5.2 Standard SPH

As stated before, the SPH method is based on the convolution principle or interpolant integral. The discrete estimation of any field is approximated by a point wise integration.

$$< \psi(r_i) > \approx \sum_{j \in N_i} \frac{m_j}{\rho\left(r_j\right)} \cdot \psi(x_j) \cdot W(r_i - r_j, h) \tag{5.1}$$

Where $W(r - r', h) = W(z, h)$ represents the kernel distribution with a compact support $D_h W$ and h is a geometric parameter or the smoothing length.

$$D_h W = \left\{ z / z \in \Re^+ , W\left(z, h\right) \in \Re^+ \right\} \equiv \left\{ -C \cdot h , +C \cdot h \right\} \tag{5.2}$$

Where C is a constant, the second equality is only valid for symmetric kernels. The kernel $\mathrm{W(z, h)}$ should possess properties exposed in the first chapter:

In the equation (5.1), m_j is the mass associated with particle j and N_i is the set of particles interacting with the i^{th} particle, thus:

$$N_i = \left\{ j \in N / -C.h \le r_i - r_j \le C.h \right\}$$

The spatial derivative of ψ can be calculated using:

$$< \nabla \psi(r_i) > \approx \sum_{j \in N_i} \frac{m_j}{\rho(r_j)} \cdot \psi(r_j) . \nabla W(r_i - r_j, h) \tag{5.3}$$

Conventional SPH approximations as well as their variations [5, 6] are inconsistent and unstable. As a consequence the accuracy of the approximations deteriorates near the boundaries (due to incomplete support) and with irregular particle distributions.

5.3 Normalised SPH

In order to correct for this problem the normalised SPH (NSPH) interpolation was introduced by Johnson and Biessel [5], Randles and Libersky [6] and Chen [7] and consists of correcting the interpolation to compensate for irregular particle distributions and incomplete supports.

If D is a bounded domain of the problem, the normalization condition becomes:

$$\int_{D \cap D_h W} W\left(r - r', h\right) \cdot dr' = 1 \tag{5.4}$$

The equality above is not satisfied if $D_h W \not\subset D$. In order to correct for this a correction factor C_0 is introduced in the normalization condition so that:

$$C_0 \cdot \int_{D_h W \cap D} W(r - r', h) \cdot dr' = 1 \tag{5.5}$$

Where $C_0(r,h)$ is constant function with respect to r and to h. It is determined by the equation (5.5). Using this approach the smoothed fields are given by:

$$\langle \psi(r) \rangle \approx \frac{\int_{DW \cap D} \psi(r') \cdot W_{sph}(r - r', h) \cdot dr'}{\int_{DW \cap D} W_{sph}(r - r', h) \cdot dr'} \tag{5.6}$$

To approximate the gradients one starts from a semi-local Taylor series expansion $\psi(r')$ about r:

$$\psi(r') \approx \psi(r) + (r'-r) \cdot \left\langle \nabla_r \psi(r) \right\rangle + \frac{(r'-r)^2}{2} \cdot \left\langle \nabla_r^2 \psi(r) \right\rangle + \ldots . \qquad (5.7)$$

Multiplying the above equation by $\nabla_{r'} W_{sph}(r-r')$ and integrating over $D_h W$ while ignoring second and higher order terms one gets:

$$\left\langle \nabla_r \psi(r) \right\rangle \approx \frac{\int_{DW} (\psi(r') - \psi(r)) \cdot \nabla_{r'} W_{sph}(r-r', h) \cdot dr'}{\int_{DW} (r'-r) \cdot \nabla_{r'} W_{sph}(r-r', h) \cdot dr'} \qquad (5.8)$$

The discrete forms of (5.6) and (5.8) are,

$$\left\langle \psi(r_i) \right\rangle \approx \frac{\sum_{j \in N_i} \frac{m_j}{\rho_j} \cdot \psi(r_j) \cdot W_{sph}(r_j - r_i, h)}{\sum_{j \in N_i} \frac{m_j}{\rho_j} \cdot W_{sph}(r_j - r_i, h)} \qquad (5.9)$$

$$\left\langle \nabla_r \psi(r_i) \right\rangle \approx \frac{\sum_{j \in N_i} \frac{m_j}{\rho_j} \cdot (\psi(r_j) - \psi(r_i)) \cdot \nabla_{rj} W_{sph}(r_j - r_i, h).}{\sum_{j \in N_i} \frac{m_j}{\rho_j} \cdot (r_j - r_i) \cdot \nabla_{rj} W_{sph}(r_j - r_i, h)} \qquad (5.10)$$

Two remarks can be made regarding normalised SPH. The first one is concerning the consistency of the approximation of the gradient. Due to the fact that higher order derivatives are neglected to obtain the equation (5.8), this equation cannot be integrated to obtain $\psi(r)$.

The second problem is that even the integral forms of the normalised SPH equations (5.6) and (5.8), unlike conventional SPH, does not satisfy the Gauss theorem.

5.4 Corrected SPH

The second type of correction was proposed by Liu *et al* [1, 2, 3 and 4], and takes the following form as a correction to the interpolation kernel itself:

$$W_{CSPH}(r, r-r', h) = \left\{ \sum_{k=0}^{M} C_k(r, h) \cdot \left(\frac{r'-r}{h} \right)^k \right\} \cdot W\left(\frac{|r-r'|}{h} \right) \qquad (5.11)$$

Where M is the order of the correction. $C_k(r,h)$ are coefficients that depend on the order M. These coefficients can be determined explicitly by imposing the condition that W_{CSPH} exactly interpolates polynomials of order up to M, ie.

$$\int_{DW_{RKPM}} r'^{\,k} \cdot W_{RKPM}(r, r-r', h) \cdot dr' = r^k \quad for \quad k = 1, 2, 3, ...M \qquad (5.12)$$

Where $D_h W_{CSPH}$ is the support of the CSPH kernel. In the results presented, a kernel correction of order $M = 1$ was used, hence:

$$W_{csph}(r, r-r', h) = \left\{ C_1(r, h) + C_2(r, h) \cdot \left(\frac{r'-r}{h} \right) \right\} \cdot W_{sph}(r-r', h) \quad (5.13)$$

One can see that generally $W_{CSPH}(r, r-r', h) \neq W_{CSPH}(r', r'-r, h)$, i.e. the kernel function is no longer symmetric. Using the above fields can be approximated by:

$$\langle \psi(r_i) \rangle \approx \sum_{j \in Di} \frac{m_j}{\rho_j} \cdot \psi(r_j) \cdot \left\{ C_1(r_i, h) + C_2(r_i, h).(\frac{r_j - r_i}{h}) \right\} \cdot W_{sph} \quad (5.14)$$

And consequently the gradient is approximated by (5.15):

$$\langle \nabla_r \psi(r_i) \rangle \approx \sum_{j \in Di} \frac{m_j}{\rho_j} \cdot \psi(r_j) \cdot \left\{ \left\{ C_1(r_i, h) + C_2(r_i, h).(\frac{r_j - r_i}{h}) \right\} \cdot \nabla_{rj} W_{sph} + \frac{C_2(r_i, h)}{h} \cdot W_{sph} \right\}$$

With the objective to preserve the Lagrangian and mesh free nature of the method, a background mesh combined with Gauss quadrature, as proposed by Liu, was not used. Instead, a simple point-wise integration was used.

5.5 Normalised Corrected Kernel SPH

Finally, a combination of normalization and kernel correction was considered. The idea behind this is that the kernel correction restores consistency, while the normalization enhances accuracy of the integration process. The kernel function can then be written as:

$$W_{ncsph}(r, r-r', h) = \left\{ \hat{C}_1(r, h) + \hat{C}_2(r, h) \cdot \left(\frac{r'-r}{h}\right) \right\} \cdot \frac{W_{sph}(r'-r, h)}{\int_{DW} W_{sph}(r'-r, h) \cdot dr'} \qquad (5.16)$$

Where $\hat{C}_1(r,h)$ and $\hat{C}_2(r,h)$ are calculated by using a normalized kernel interpolation. A similar interpolation was proposed by Bonet and Kulasegaram [8].

5.6 Velocity Smoothing

The velocity smoothing consists of applying a kernel interpolation to the velocity field. This process reduces or eliminates material inter-penetration and the fact that particles of the same material in a one-dimensional case can overtake each other. This type of procedure was published, in slight variations, by Randles and Libersky [9], Guenther [10] and Balsara [11] as a potential cure for tensile instability. The formulation proposed by Libersky [9] is as follows:

$$\tilde{\vec{v}}(r_i) = \vec{v}(r_i) + \alpha_{cs} \cdot \left\{ \frac{\sum_j \frac{m_j}{\rho_j} \cdot \vec{v}(r_j) \cdot W(r_i - r_j, h)}{\sum_j \frac{m_j}{\rho_j} \cdot W(r_i - r_j, h)} - \vec{v}(r_i) \right\} \qquad (5.17)$$

Where α_{CS} is a conservative smoothing coefficient and has a value between 0 and 1. The smoothing function for these tests is a variation of the above formula with $\alpha_{CS} = 1$, and including the i^{th} particle in the kernel sum:

$$\tilde{\vec{v}}(r_i) = \frac{\sum_j \frac{m_j}{\rho_j} \cdot \vec{v}(r_j) \cdot W(r_i - r_j, h)}{\sum_j \frac{m_j}{\rho_j} \cdot W(r_i - r_j, h)} \qquad (5.18)$$

One can see that this corresponds to a normalised SPH interpolation of a function. A second type of velocity smoothing that was considered is a Corrected Kernel SPH interpolation:

$$\tilde{\vec{v}}(r_i) = \sum_j \frac{m_j}{\rho_j} \cdot \vec{v}(r_j) \cdot \left\{ C_1(r_i, h) + C_2(r_i, h) \cdot \left(\frac{r_j - r_i}{h} \right) \right\} \cdot W(r_i - r_j, h) \qquad (5.19)$$

The use of velocity smoothing is an alternative to the use of artificial viscosity. An assessment of the performance of these two methods is given by Guenther [10].

5.7 Conservation Equations

As pointed out in earlier, there are several formulations of the equations of motion in the SPH method. This is in part due to the fact that the kernels used are symmetric. This allows, without great difficulty, handling of conservation of momentum and energy. In the CSPH approach, due to the fact that the kernel is no longer symmetric, the possibilities of deriving a CSPH version of the equations of motion are restricted.

In general let $\psi(r,t)$ be any physical quantity carried by particle $i, \rho(r',t)$ and $S(\sigma)$ be the density and a source term describing the state of the environment of that particle, its time derivative can then be expressed by:

$$\frac{d\psi(r_i, t)}{dt} = -\left\langle \frac{\vec{\nabla}_{r'} S(\overline{\overline{\sigma}})}{\rho(r', t)} \right\rangle_{r'=r_i(t)} \quad \text{with} \quad \psi = \begin{pmatrix} 1 \\ \vec{v} \\ e \end{pmatrix} \quad \text{and} \quad S(\sigma) = \begin{pmatrix} 0 \\ \overline{\overline{\sigma}} \\ \overline{\overline{\sigma}} : \vec{v} \end{pmatrix}$$

In this expression $\vec{v}$, e and $\overline{\overline{\sigma}}$ represent material velocity, internal energy and the stress tensor.

The system above is closed by an appropriate constitutive relation and compatibility equations.

For conventional SPH the conservation equations are:

$$\begin{cases} \dfrac{d\rho_i}{dt} = -\rho_i \cdot \sum_j \dfrac{m_j}{\rho_j} \cdot (v_j - v_i) \cdot \dfrac{\partial W_{ij}}{\partial x} & 5.20-a \\ \dfrac{dv_i^{\alpha}}{dt} = \sum_j m_j \cdot \left(\dfrac{\sigma_i^{\alpha\beta} - Q_i}{\rho_i^2} + \dfrac{\sigma_j^{\alpha\beta} - Q_j}{\rho_j^2} \right) \cdot \dfrac{\partial W_{ij}}{\partial x^{\beta}} & 5.20-b \\ \dfrac{de_i}{dt} = \dfrac{\sigma_i^{\alpha\beta}}{\rho_i^2} \cdot \sum_j m_j \cdot (v_j^{\alpha} - v_i^{\alpha}) \cdot \dfrac{\partial W_{ij}}{\partial x^{\beta}} & 5.20-c \end{cases}$$

Where Q_i defines the artificial viscosity generated by the particle i and is given by.

$$\begin{cases} Q_i = \alpha \cdot . \rho_i \cdot h \cdot C_{Si} \cdot \left| Trace(\sigma_i) \right| + \beta \cdot \rho_i \cdot (h_i \cdot Trace(\sigma_i))^2 & if \quad Trace(\sigma_i) < 0 \\ 0 & if \quad Trace(\sigma_i) \geq 0 \end{cases}$$

Where $Trace(\sigma_i) = \sum_{\alpha}^{nd} \sigma_i^{\alpha\alpha}$, where nd is the space dimension.

For the normalized SPH (NSPH) and corrected kernel SPH (CSPH) and normalized corrected kernel SPH (NCSPH) a different form of the momentum equation was used:

$$\frac{dv_i^{\alpha}}{dt} = -\frac{1}{\rho_i} \cdot \sum_{j \in N_i} m_j \cdot \left(\frac{\sigma_j^{\alpha\beta} - Q_j - \sigma_i^{\alpha\beta} + Q_i}{\rho_j} \right) \cdot \frac{\partial W_{CSPH}}{\partial x_j}(x_i - x_j, h) \qquad (5.21)$$

This provides greater stability, this was also observed by Randles and Libersky[9] and by Libersky *et al* [12]. The reason for the improved stability is that if there is zero stress and a density discontinuity, equation (5.20-b) produces acceleration, while equation (5.21) does not. It is

important to note that throughout this work only nodal integration has been performed, in order to preserve the mesh less character of the method.

5.8 Test Results

To get an initial idea of the influence of these different methods on the interpolation a simple reconstruction of a function and its derivative was performed. The function to be reconstructed is a simple sine function, its derivative a cosine function.

From Figure 5-1 it can be seen that for a regular particle distribution the sine wave is reasonably approximated by all four methods, the CSPH and NCSPH methods also shows good results at the boundaries, conventional SPH and NSPH show a clear deficiency at the boundaries. Looking at the estimate of the derivative, figure 6-2 identical conclusions can be drawn, except that NSPH now has similar accuracy compared to CSPH and NCSPH.

The effect of irregular particle distributions (Fig. 5-3 and 5-4) the superiority of normalized and corrected kernel interpolations over the conventional SPH approach is clear. The conventional SPH results have clearly deteriorated. The results of NSPH, CSPH and NCSPH are hardly affected by the irregular distribution of particles. This confirms the fact that, as intended, NSPH compensates for the irregular particle distribution. Even though the rationale behind CSPH is a restoration of consistency it leads to a similar improvement as NSPH. These effects are even more noticeable when looking at the results of the approximation of the derivative of the sine function. The SPH results show virtually no resemblance to a cosine function.

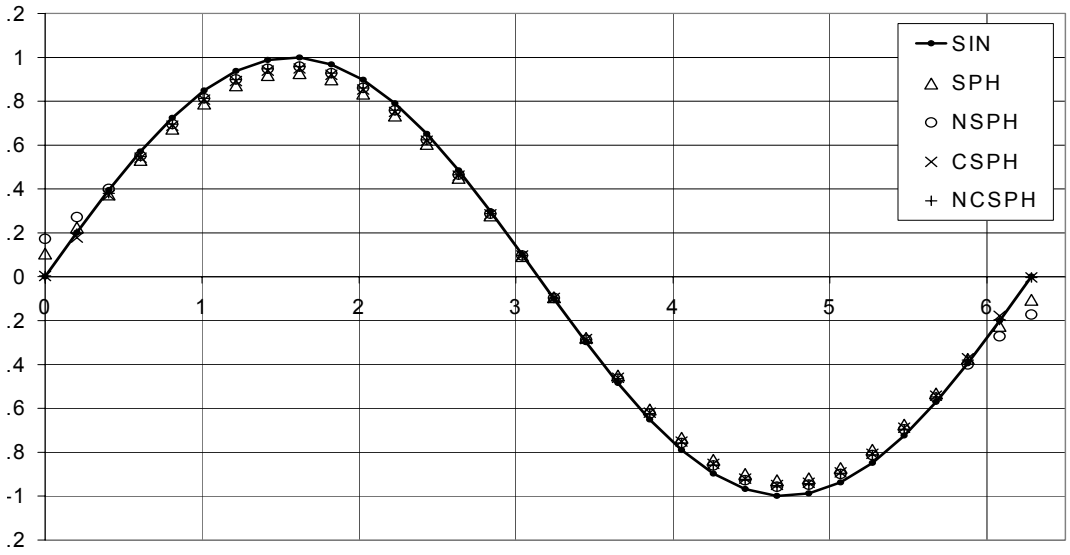

Figure 5-1

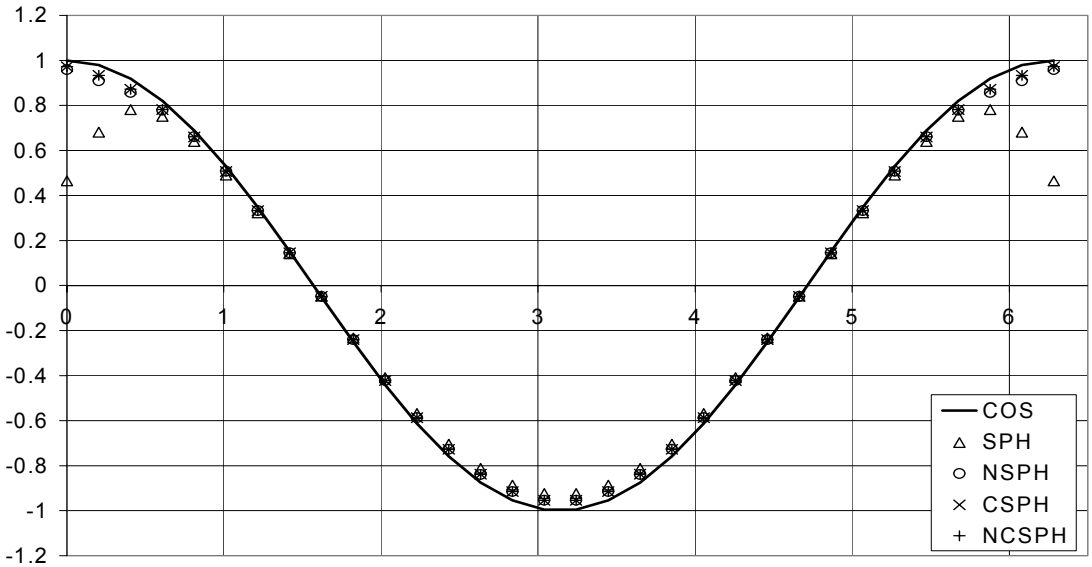

Figure 5-2

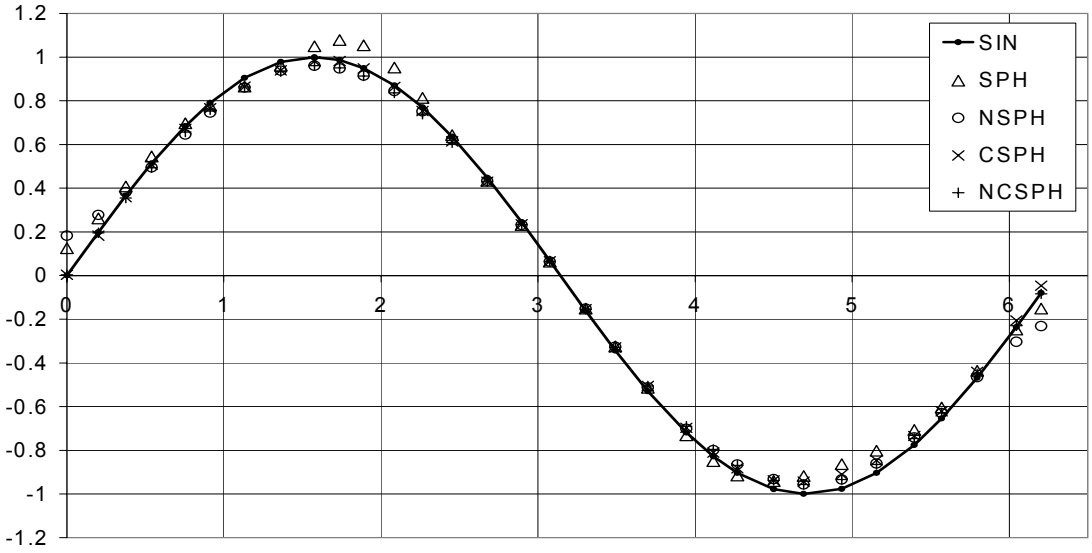

Figure 5-3

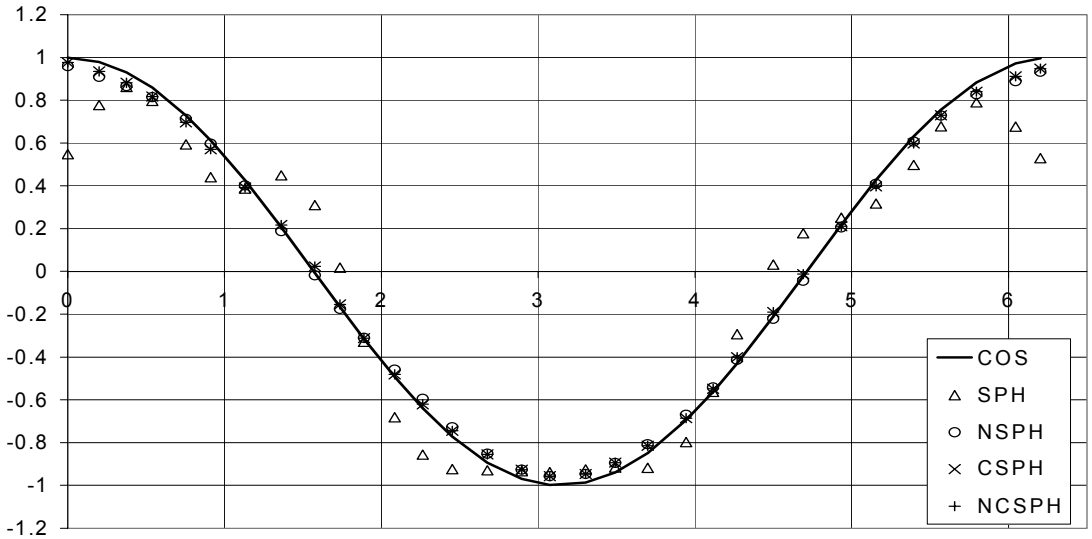

Figure 5-4

Due to the nature of the problems to be analysed, ie. Dynamics and wave propagation, a second function that was selected to be reconstructed is a step-function, and its derivative a Dirac function. The results for a regular particle distribution are displayed in Figures 5-5 and 5-6. Again one can observe the fact that NSPH, CSPH and NCSPH give better results at the boundaries. In the case of an irregular particle distribution (Fig. 5-7 and 5-8) it can be seen that the results for conventional SPH deteriorate, while the two other methods hardly are affected.

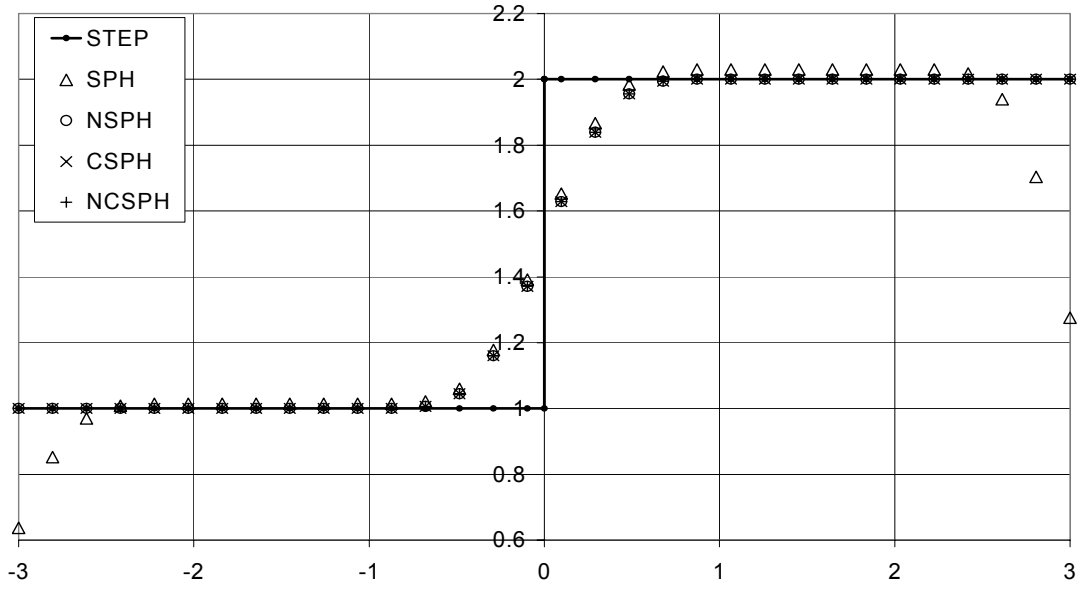

Figure 5-5

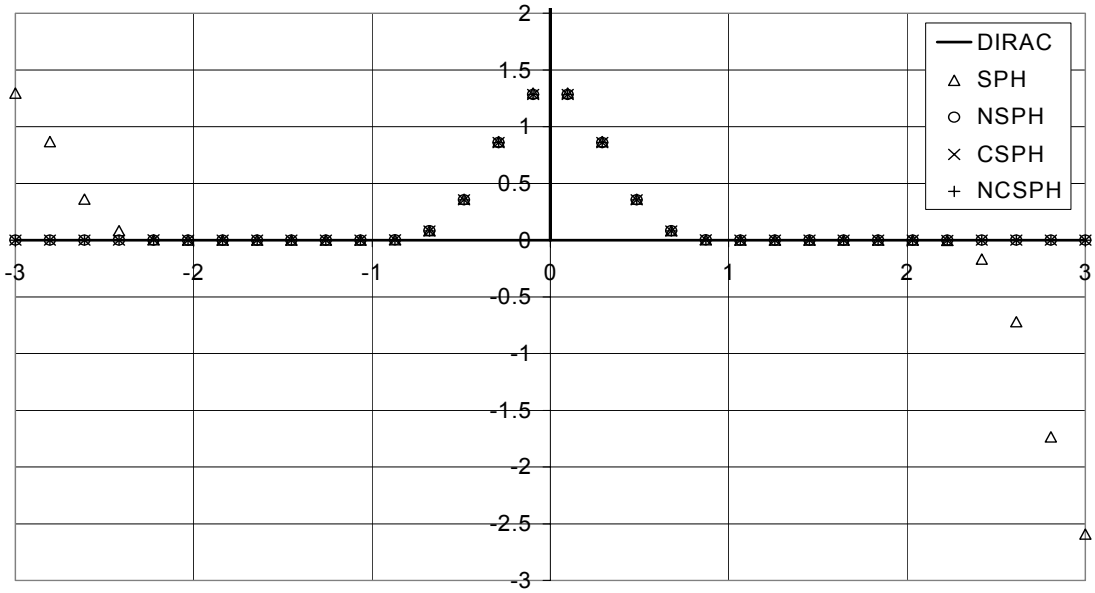

Figure 5-6

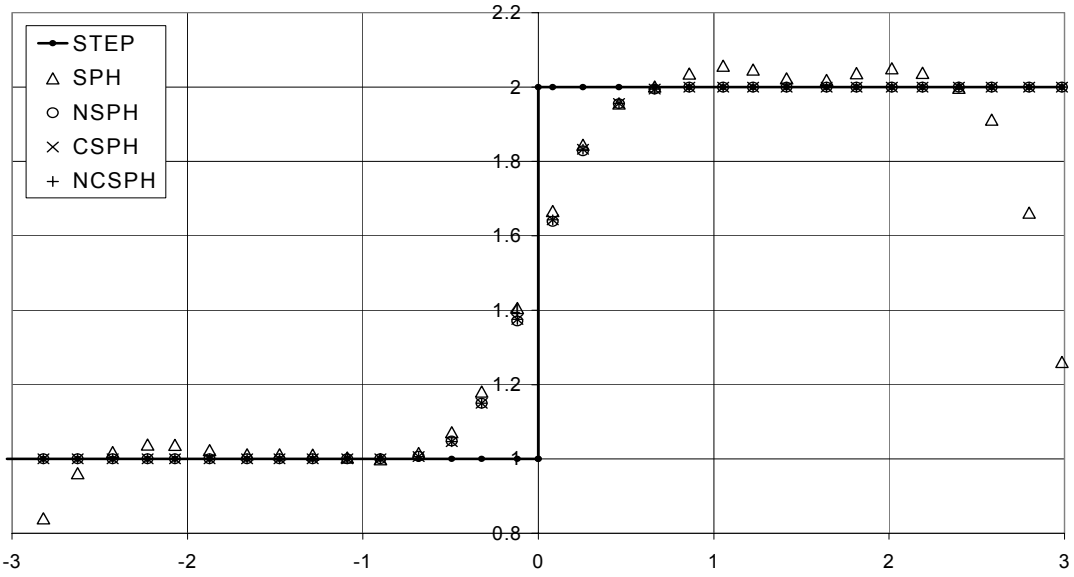

Figure 5-7

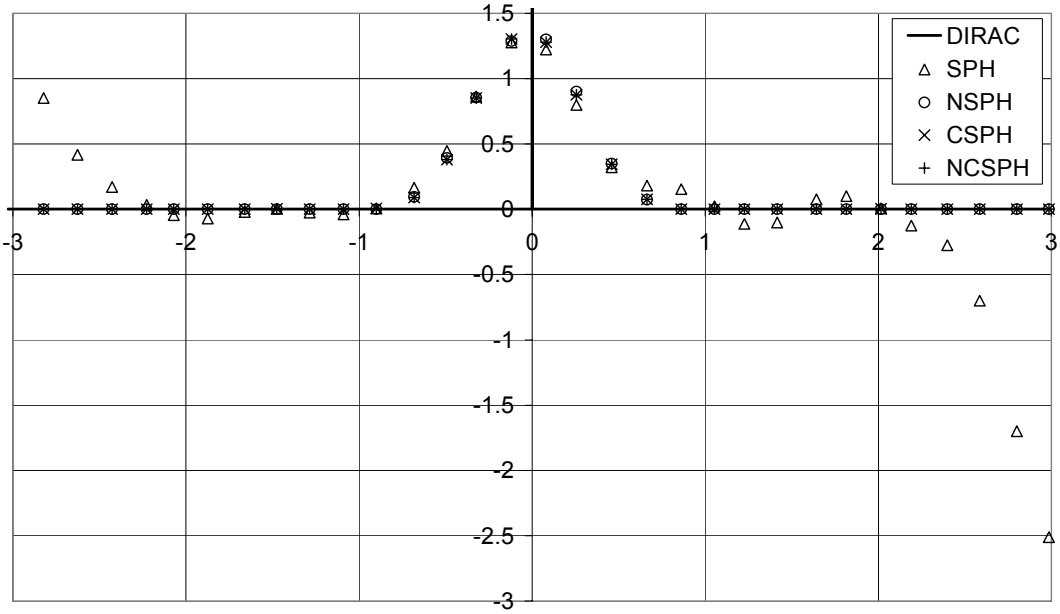

Figure 5-8

Finally, in the next four figures, the results of the reconstruction of a step function are presented using the particle distribution used to simulate the shock tube problem. The results of the shock tube problem will be discussed in a later paragraph. The main difference here is that to left of the origin the particle spacing is eight times denser than to the right. Consequently the volume of the particles also differs by a factor of eight. Conclusions drawn for the equal volume particle distribution case (Figures 5-5 to 5-8) also apply to non-equal volume case (Figures 5-9 to 5-10).

The same calculation was also performed after a few time steps, when the particles are no longer uniformly positioned; again the results are significantly worse for conventional SPH (Fig. 5-11 and 5-12).

To assess and compare the influence of the different interpolation methods on the discretization of conservation methods two tests were conducted. For this study we have restricted ourselves to one-dimensional problems.

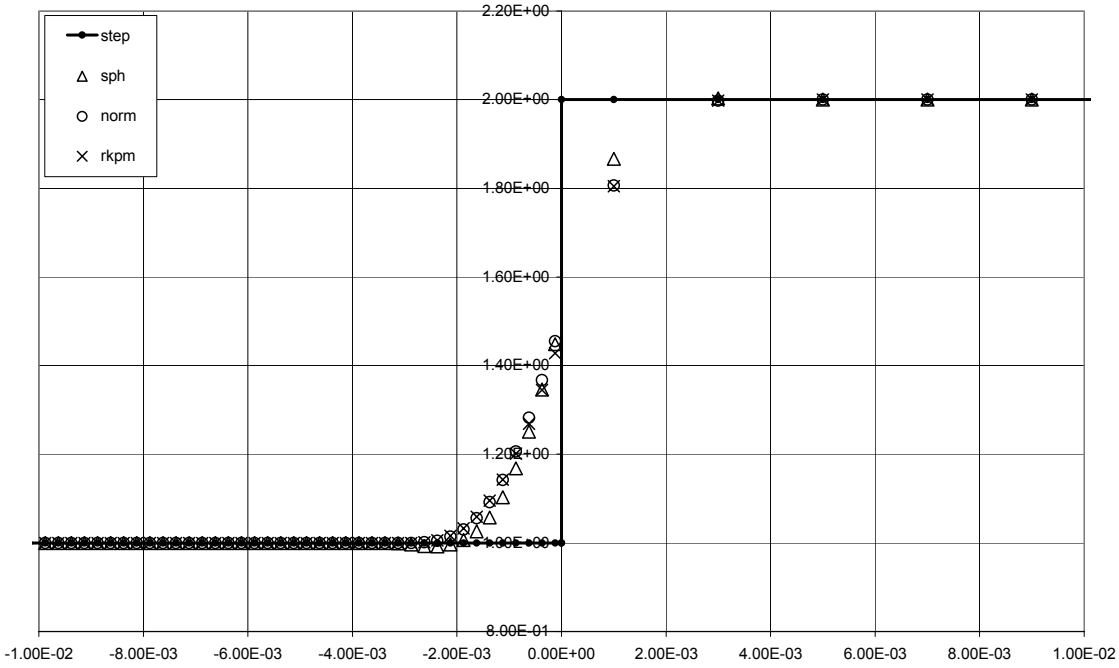

Figure 5-9

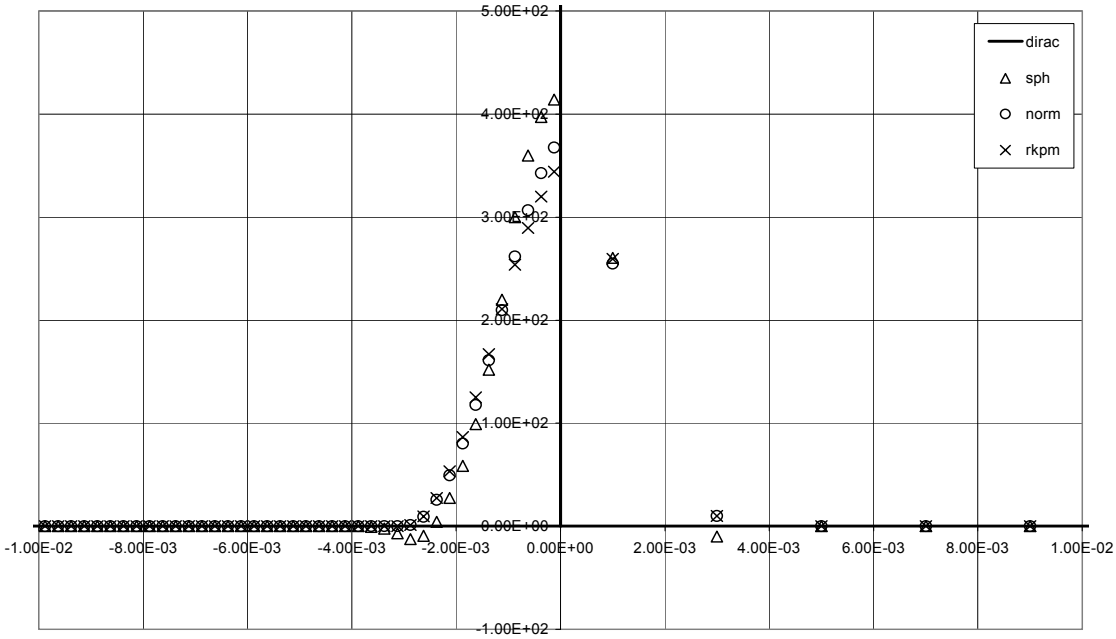

Figure 5-10

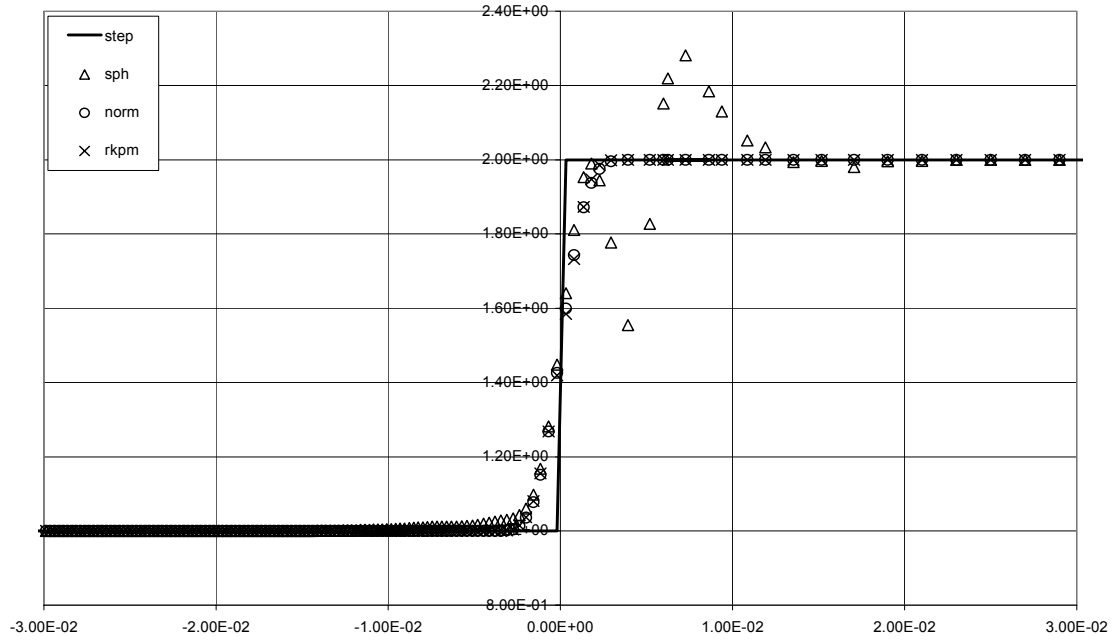

Figure 5-11

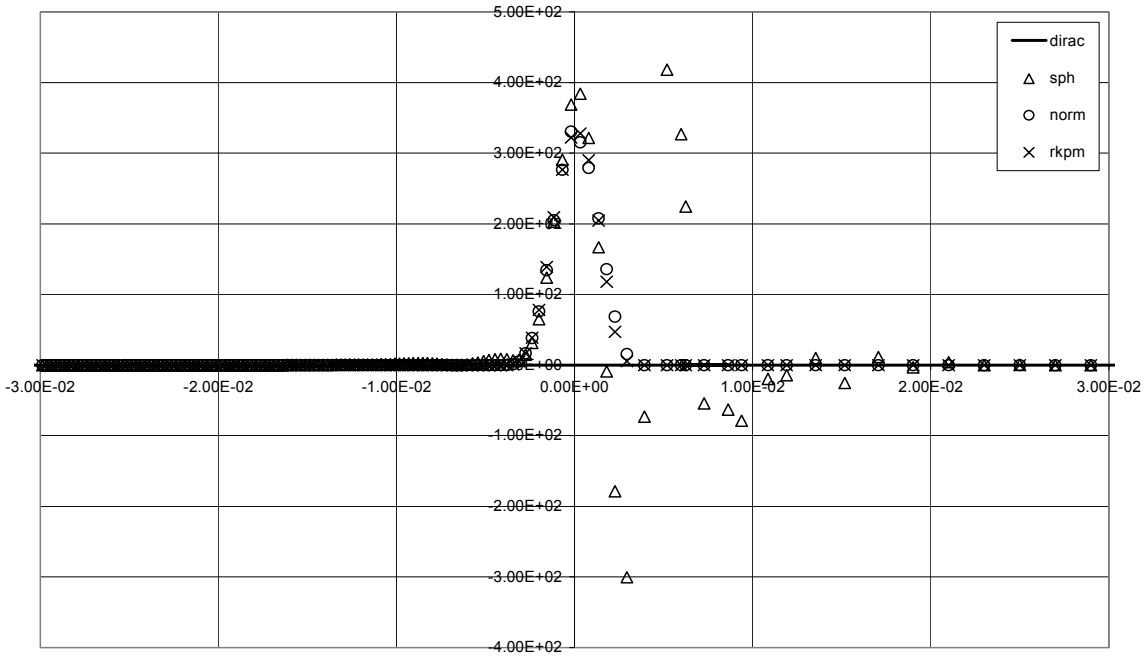

Figure 5-12

The problem that was selected for this test is a shock tube problem. The shock tube problem is a widely used test case to validate numerical algorithms for the simulation of hydrodynamic problems Sod [13]. The reason for its popularity is that the solution contains large density differences, and that several discontinuities, in the form of shock fronts, are present. For these reasons, and the inherent inability of SPH to deal with large density differences, the shock tube problem was selected as a test case.

The basic setup of the shock tube problem is two tubes of gas. One of the gasses has a high density, pressure and internal energy, while the other has low density, pressure and internal energy. The initial velocities of the both gasses are zero.

In experiment the gases are separated by a diaphragm. After the diaphragm is removed the low density gas is compressed resulting in a shockwave propagating into the low density gas and the high density gas expands resulting an expansion wave travelling in the opposite to the compression wave. The difficulty lies in accurately simulating the resulting compression and expansion waves, as well as obtaining accurate values for pressure, density, velocity and internal energy.

The problem that was used to test our SPH code has the characteristics summarized in Table 2:

Table 2: Initial Conditions of Shock tube Problem

Parameter	High Density Gas	Low Density Gas
Density ρ [g/cm^3]	1.0	0.125
Pressure p [mbar]	1.0	0.1
Velocity v [km/s]	0.0	0.0

The material model used was an ideal gas with the equation of state given below:

$$p(\rho, e) = (\gamma - 1) \cdot \rho \cdot e$$

In this case a value for γ of 1.4 was used for both gasses. The analytical solution was calculated using the method described in Toro [14]. The results are shown for a time of 0.25μs after breaking the diaphragm.

The particles were distributed over the domain such that the mass of each particle was the same. As a result of this the mesh density in the high-density gas was higher (ie. particles are closer together) than the low-density gas. This results from 4000 particles in the high-density part of the gas, and from 500 for the low-density gas.

The solution obtained with a conventional SPH procedure compares very well with the analytical solution, but exhibits a significant amount of oscillation through the solution domain. Furthermore one can observe a spike in all three plots at the point of contact between the two gasses (Figures 5-13, 5-14 and 5-15). These oscillations are caused by the fact that the particles of the two gasses mix around the contact area, and the particles of the same gas change order.

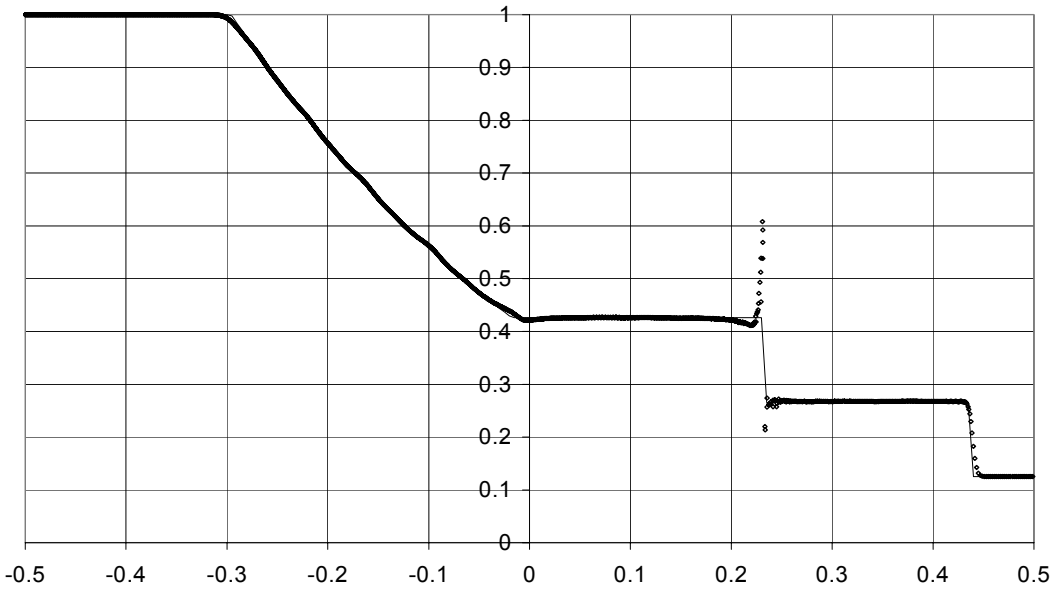

Figure 5-13: Density Profile after $0.25\,\mu s$ using Standard SPH

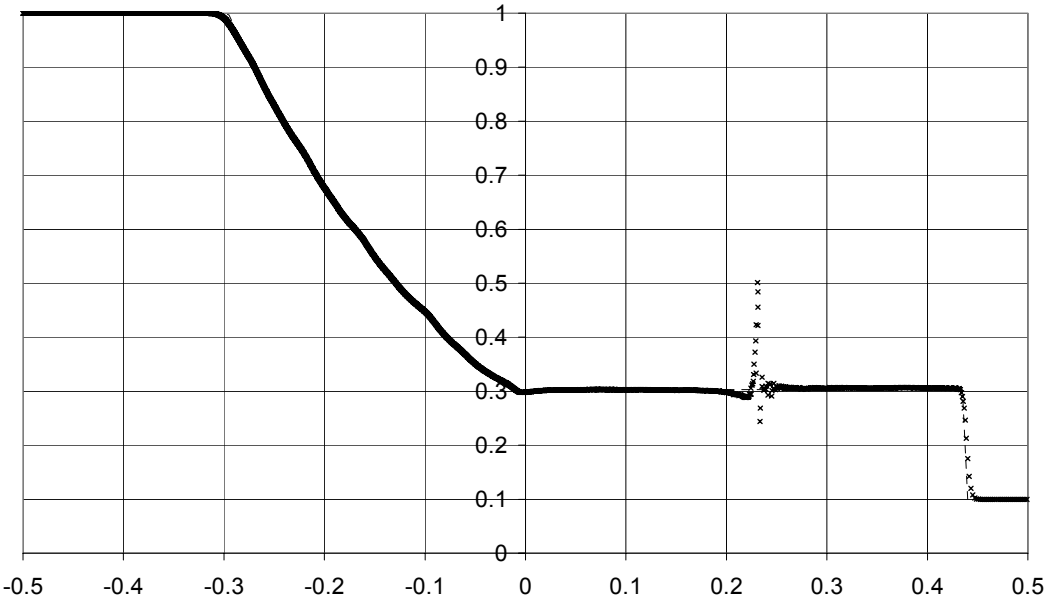

Figure 5-14: Pressure Profile after $0.25\,\mu s$ using Standard SPH

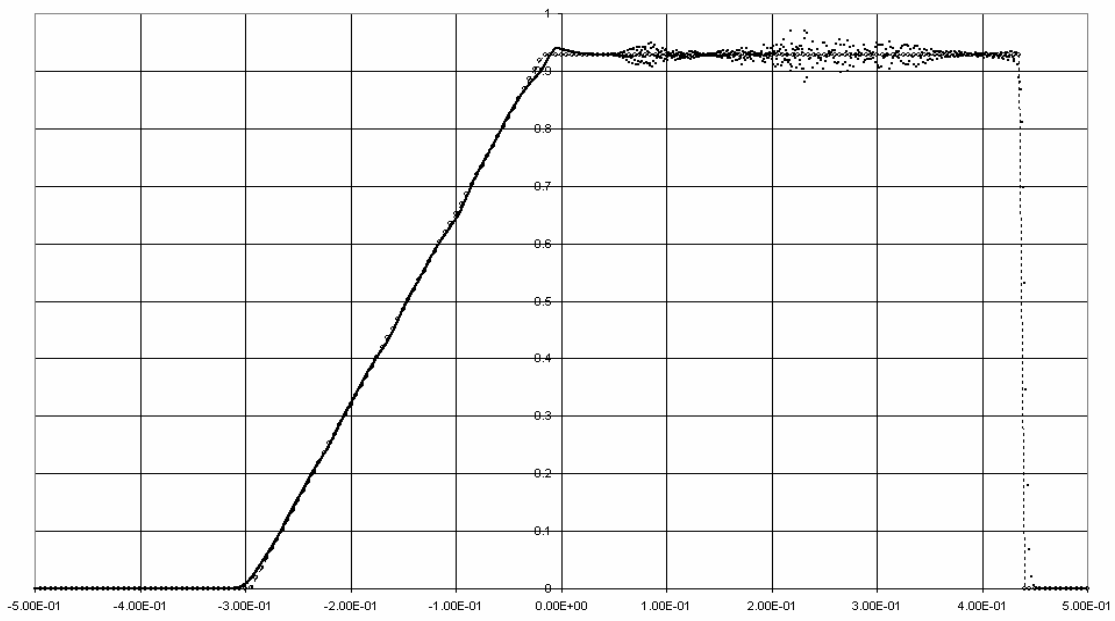

Figure 5.15: Velocity Profile after $0.25\mu s$ using Standard SPH

The normalized SPH test case crashes after about ten time steps, this is due to the fact that particles of the expanding gas overtake each other and that a large gap forms between the two gasses after one time step. Due to the latter effect a neighbour's deficiency develops for the particles at the point of contact of the two gasses. This causes the normalization factor of Equation 5-10: to become significant, and hence to result in a large correction to the calculation of gradients compared to conventional SPH. In this case this affects the calculation of the strain rate and accelerations.

Applying the velocity smoothing (VS) to the conventional SPH solution results in a solution without significant oscillation, especially the oscillations in the velocity field are much improved (Figure 5-18), apart from the obvious effect of slightly higher dispersion. There is however still a spike at the contact between the two gasses in the density and pressure field (Figures 5-16 and 5-17). This is despite the fact that the velocity smoothing prevents particle interpenetration, and the particles remain more or less evenly distributed, even around the contact point. This is probably due to the fact that if one smoothes the velocities then these values will no longer consistent with, for example, the density, pressure or specific internal energy fields. More work is required to investigate possible solutions for this problem. Of course an explicit modelling of the contact between the gasses, such as in Campbell *et al* [15], would solve interpenetration problems, but could in turn cause oscillations at the contact in the form of chatter between the contact nodes.

Furthermore, contrary to what was hoped the gradients of the velocity, density and pressure fields are not zero between the expansion and compression waves.

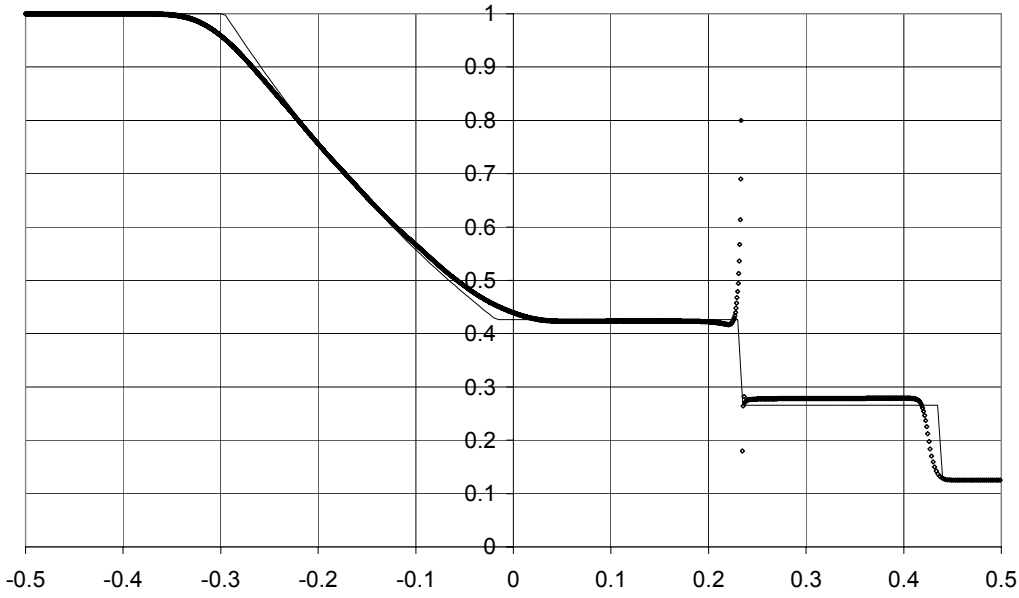

Figure 5-16: Density Profile using Standard SPH w NVS

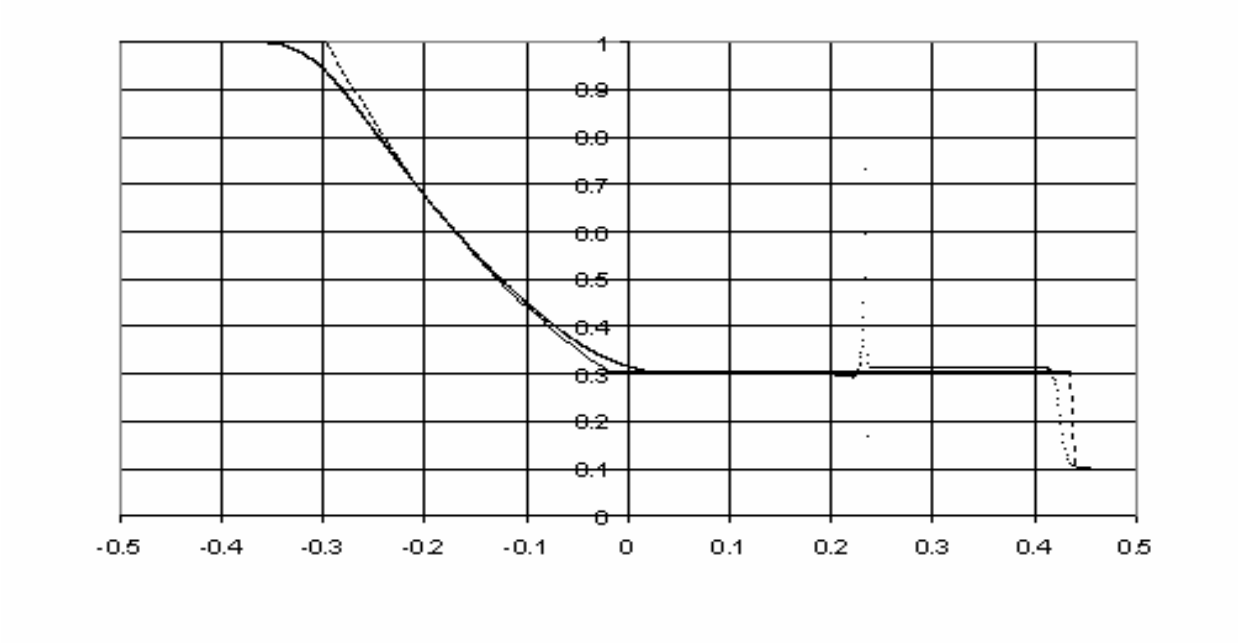

Figure 5-17: Pressure Profile using Standard SPH w. NVS

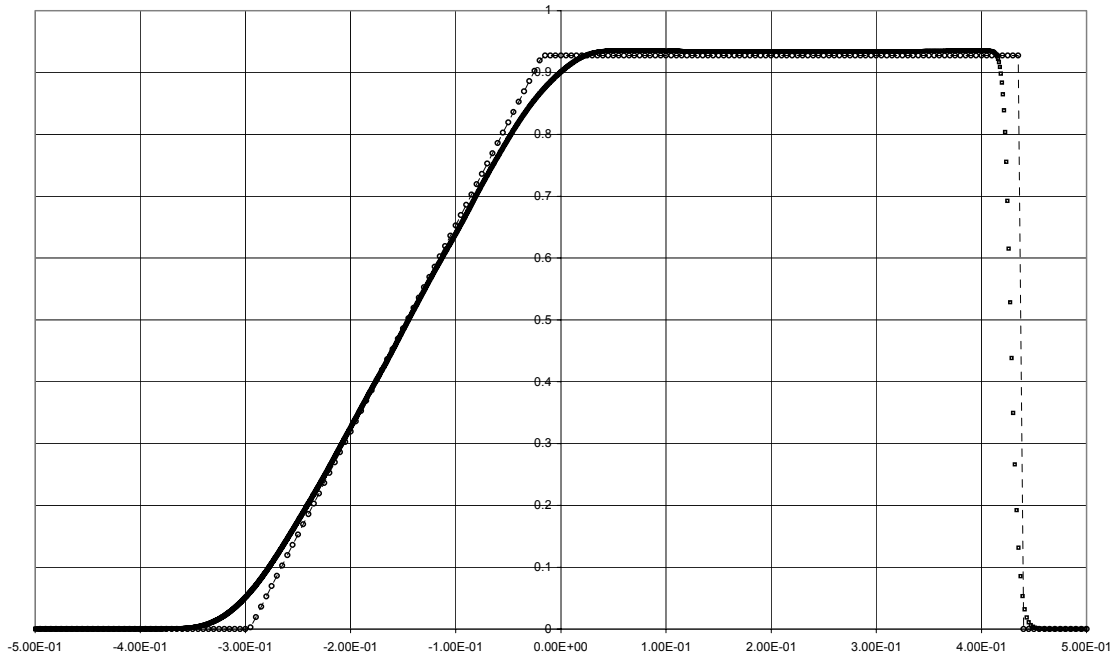

Figure 5-18: Velocity Profile using Standard SPH w. NVS

In the case of NSPH with normalized velocity smoothing the main observation is that the problem runs in a stable way. This confirms the fact that NSPH is unable to cope with such high density and pressure discontinuities because of particle interpenetration.

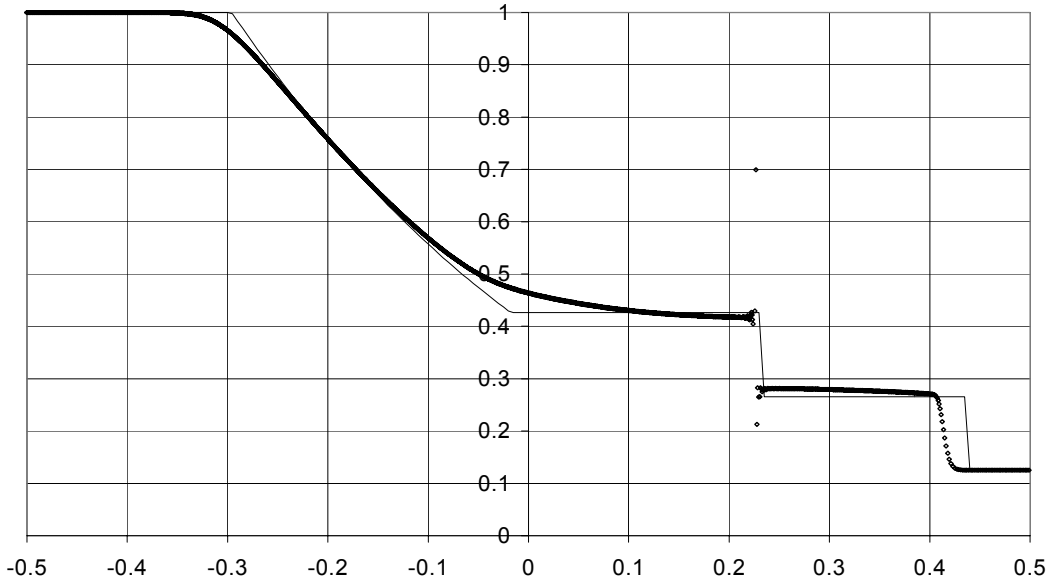

Figure 5-19: Density Profile using NSPH w. NVS

Unfortunately the results are significantly worse than the SPH ones as can be seen in Figures 5-19 to 5-20. The velocity between the expansion and compression waves is far from constant, almost like a parabolic curve. The density and pressure are slanted rather than horizontal. The reason for this behaviour is not immediately clear, but may be related to the fact that normalized SPH can only calculate linear gradients exactly. Furthermore one can notice that there is a significant lag of the shock front.

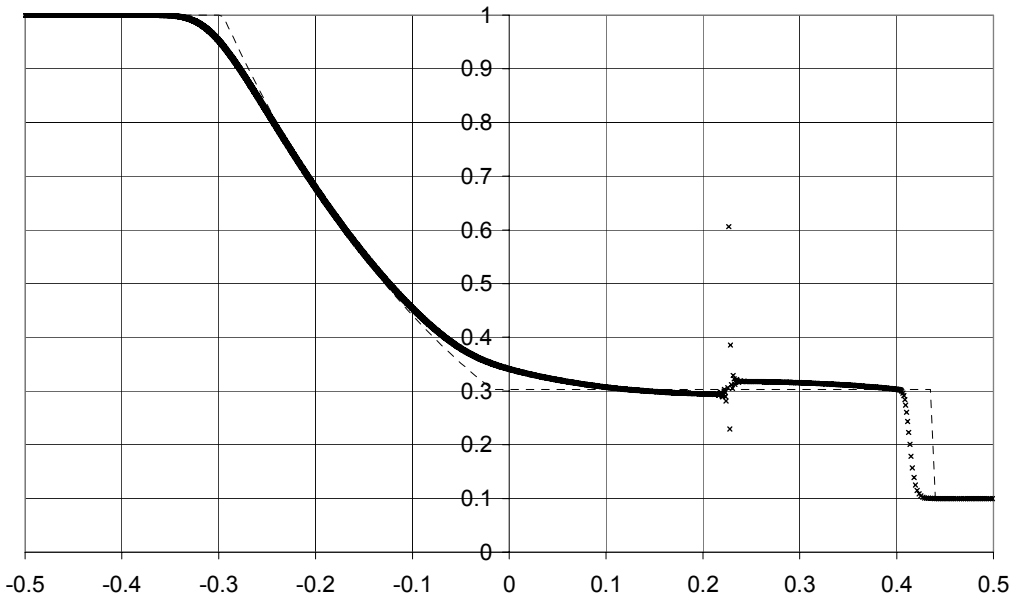

Figure 5-20: Pressure Profile using NSPH w. NVS

The results of the NSPH analysis with velocity smoothing using a reproducing kernel interpolation show similar behaviour to the normalized velocity smoothing (Figures 5-21 to 5-23). The velocity field between the shock front appears to be in this case, piecewise linear, as opposed to the curved shape in the normalized velocity smoothing (NVS).

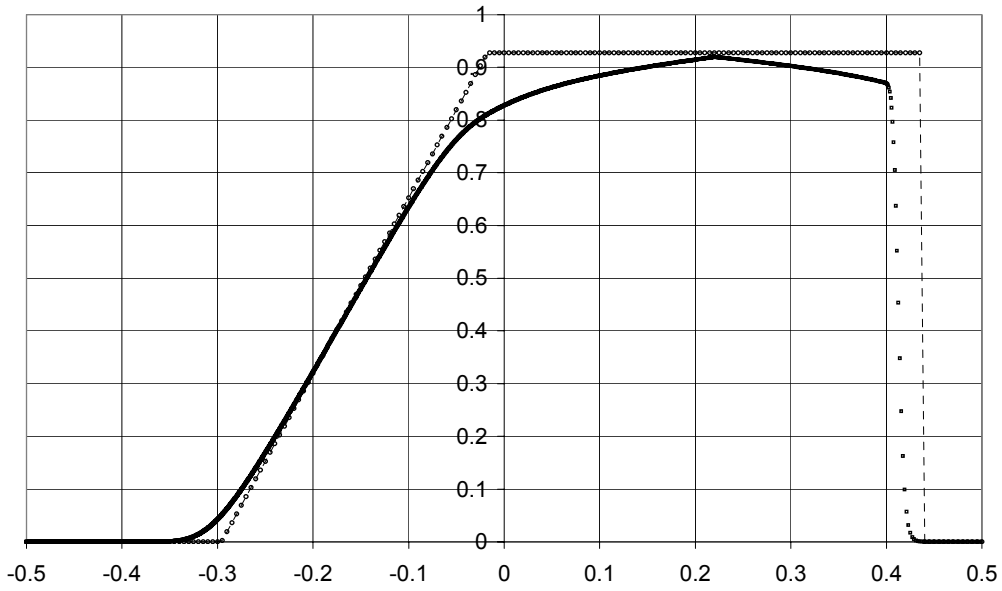

Figure 5-21: Velocity Profile using NSPH w. CVS

Other than that, similar observations can be made: the density and pressure fields are slanted, and there is a lag in the compression wave front.

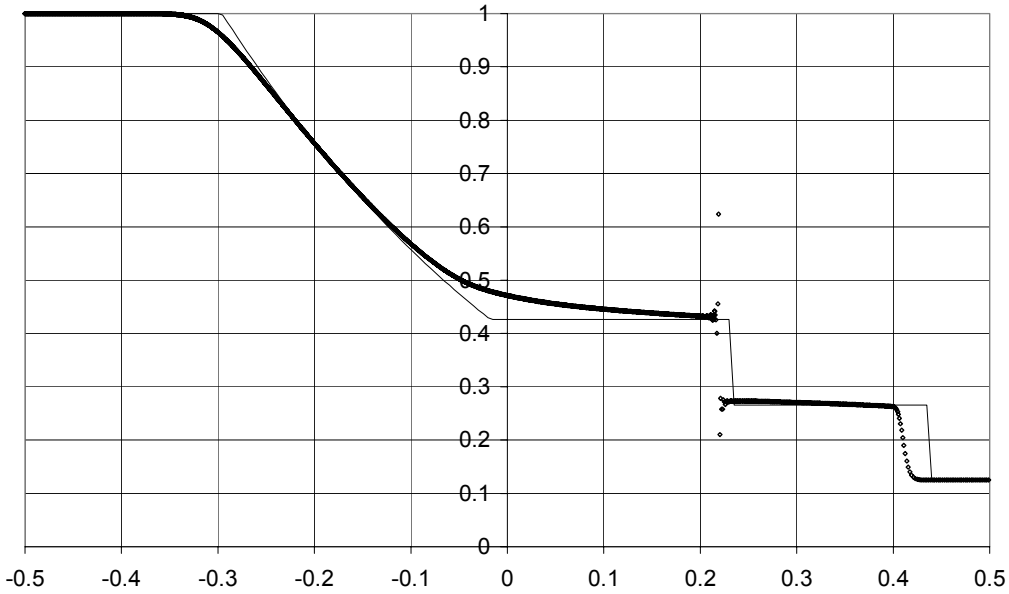

Figure 5-22: Density Profile using NSPH w. CVS

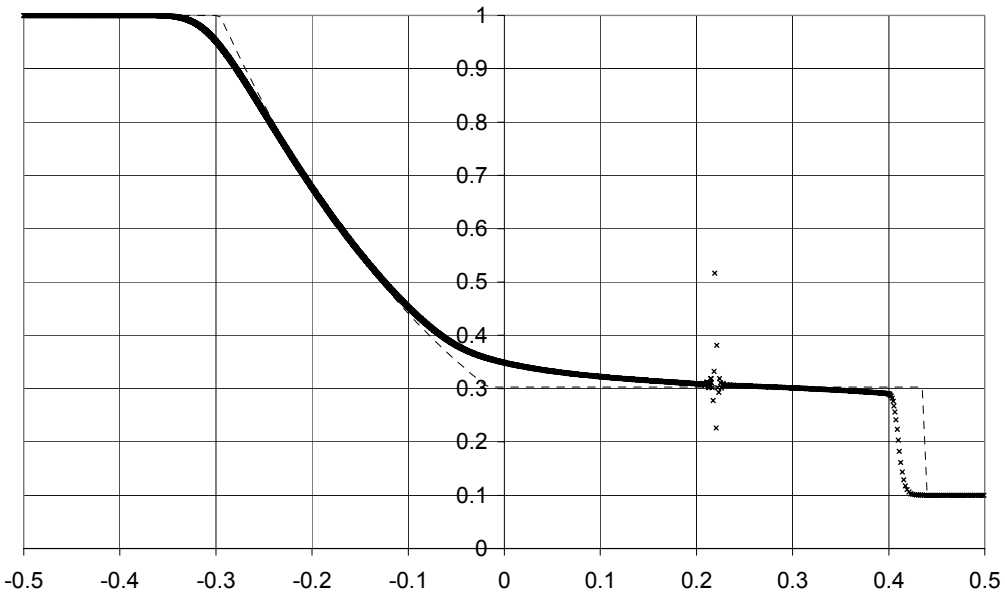

Figure 5-23: Pressure Profile using NSPH w. CVS

The simulation results of the CSPH analyses with velocity smoothing are shown in Figures 5-24 to 5-29). Again the first observation is that using the velocity smoothing the problems runs without error termination because particle mixing is prevented. Similar to the NSPH results with velocity smoothing there is an error in the propagation speed of the compression wave. On top of that the values that are obtained for the velocity, density and pressure fields between the wave fronts show a noticeable error. The effect of the fields being slanted is far less exaggerated but still present. The combination of CSPH with CVS gives marginally superior results over CSPH with NVS. Again there is a spike at the contact between the two gasses in the density and pressure fields.

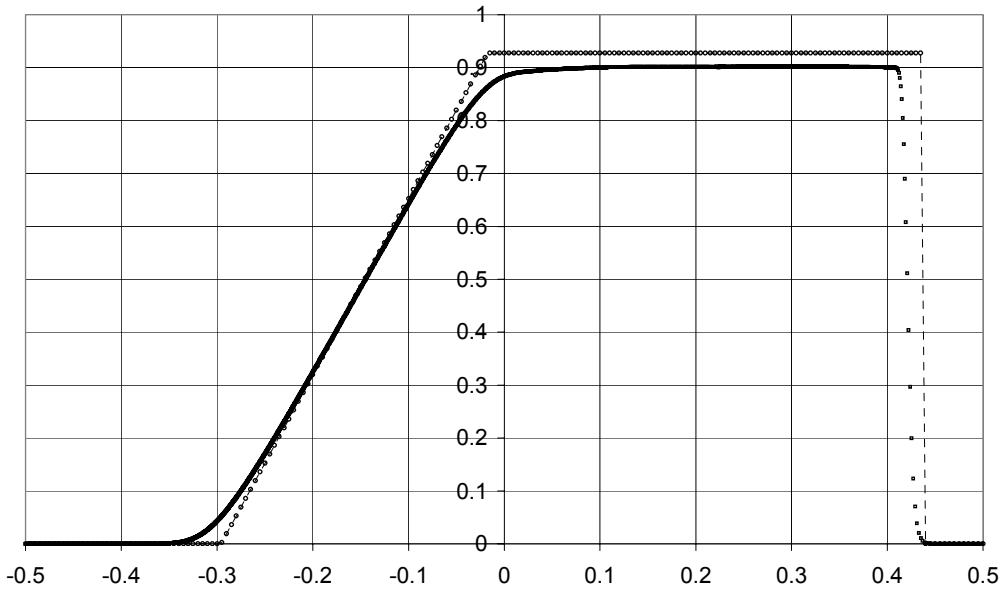

Figure 5-24: Velocity Profile after $0.25\,\mu s$ using CSPH w. NVS

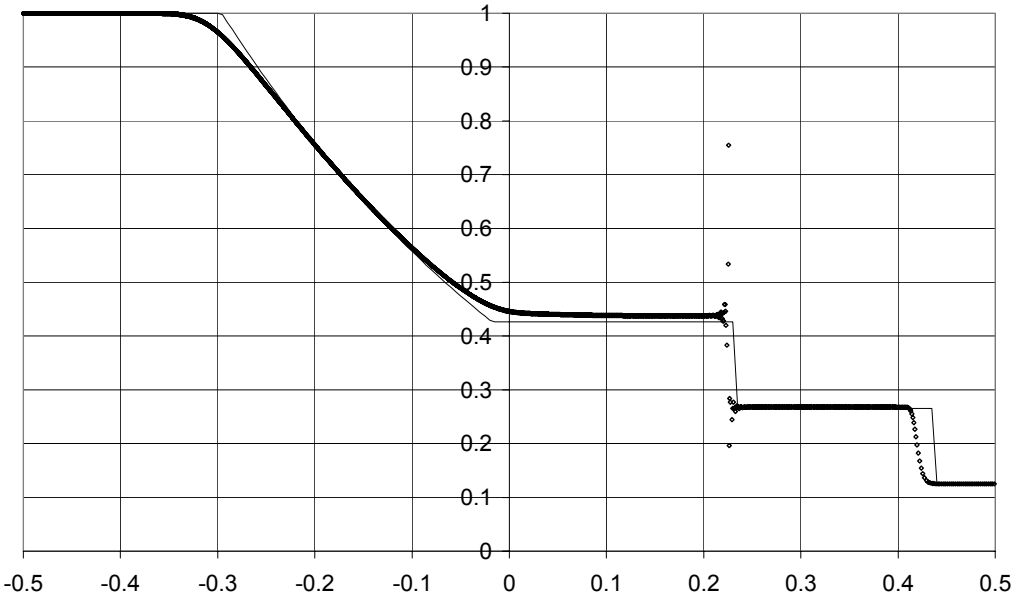

Figure 5-25: Density Profile after $0.25\,\mu s$ using CSPH w. NVS

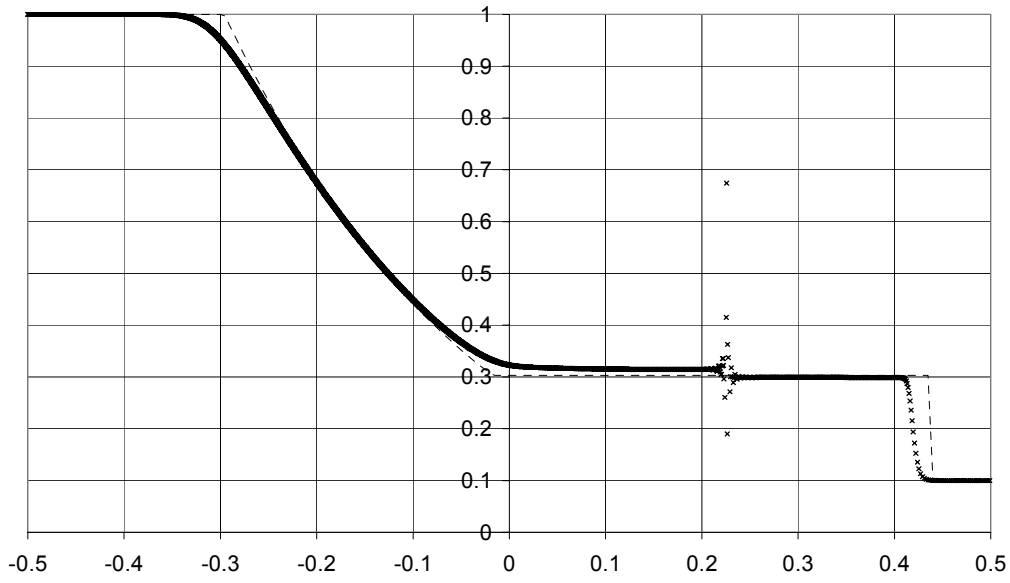

Figure 5-26: Pressure Profile after $0.25\,\mu s$ using CSPH w. NVS

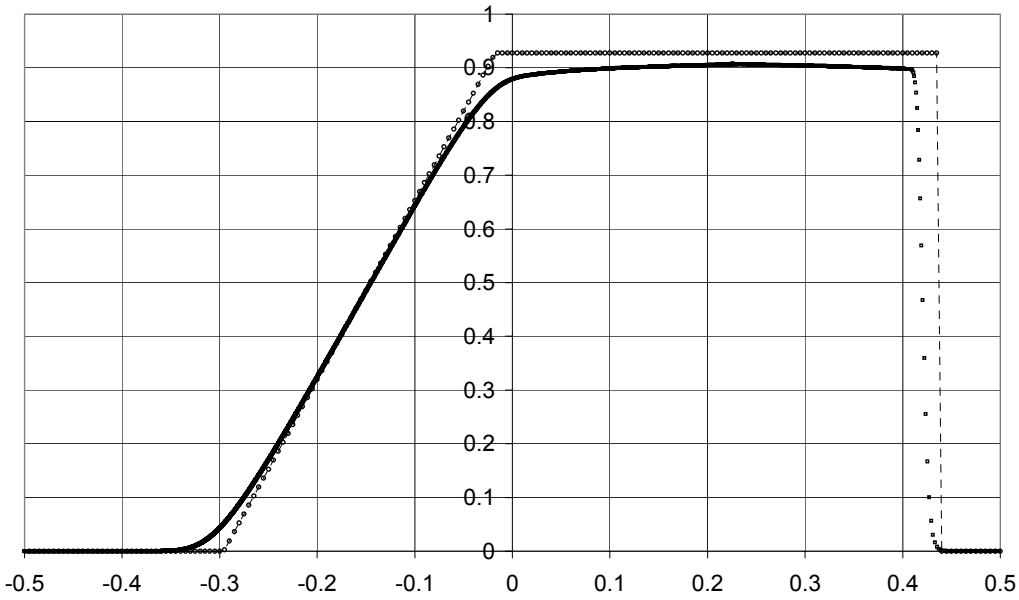

Figure 5-27: Velocity Profile after $0.25\,\mu s$ using CSPH w. CVS

The velocity, density and pressure profiles obtained by NCSPH are shown in Figures 5-30 to 5-32 and are much better than the profiles calculated using the other methods. This, first of all, shows that the improved integration due to the normalisation stops the simulation crashing. This indicates that it necessary for the correction constants to be evaluated very accurately and that a simple nodal integration is insufficient. The NCSPH results compare well with the analytical solution and those obtained by SPH method. But one can see that the oscillations behind the shock are not as

pronounced as the conventional SPH results, compare Figures 5-15 and 5-28. The density and pressure graphs show good resolution of the shocks. The spike at the contact point between the two gasses present in all the other results is not as prominent in this case.

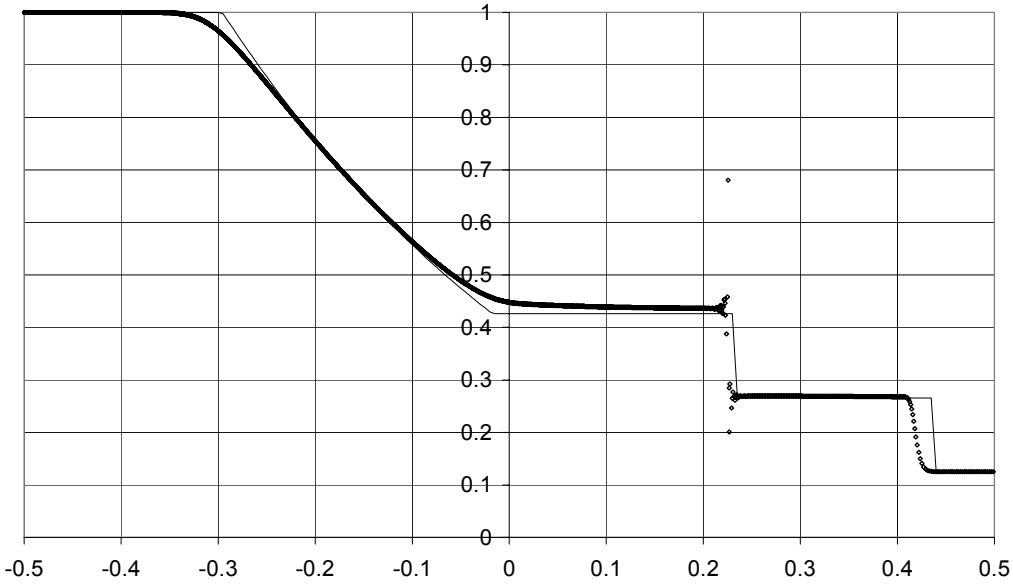

Figure 5-28: Density Profile after $0.25\,\mu s$ using CSPH w. CVS

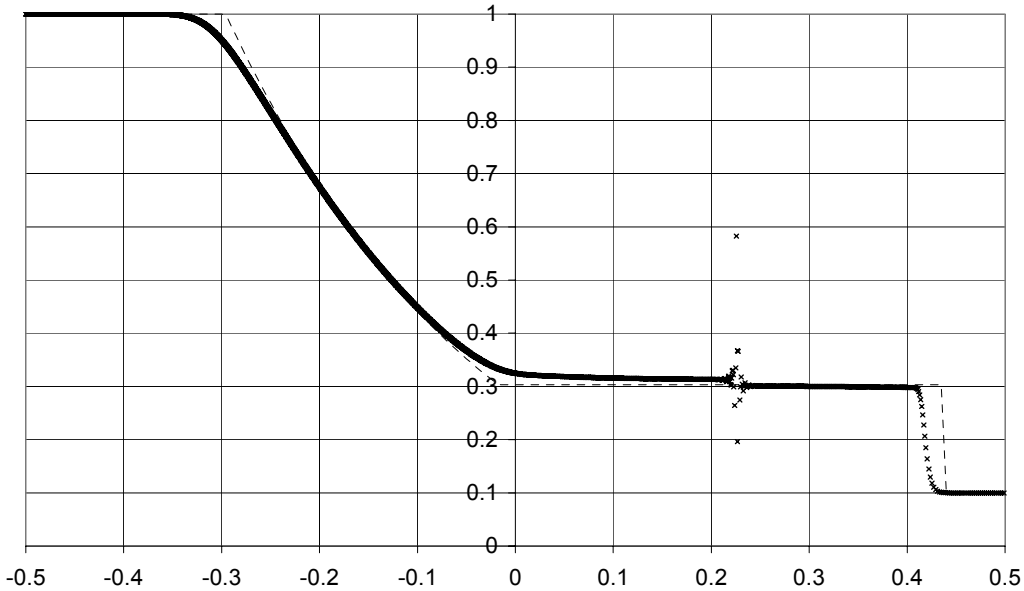

Figure 5-29: Pressure Profile after $0.25\,\mu s$ using CSPH w. CVS

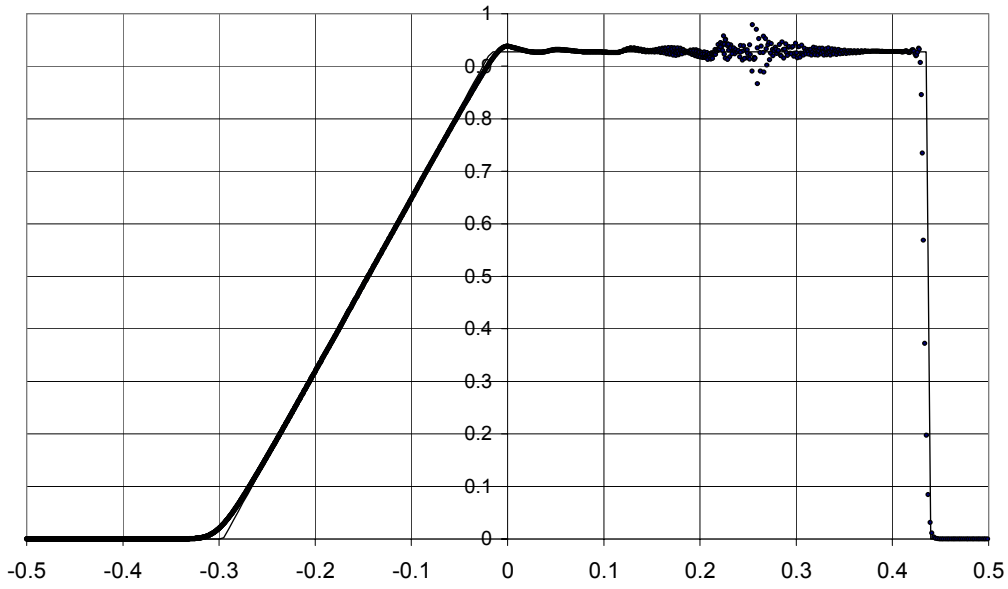

Figure 5-30: Velocity Profile after $0.25\,\mu s$ using NCPH

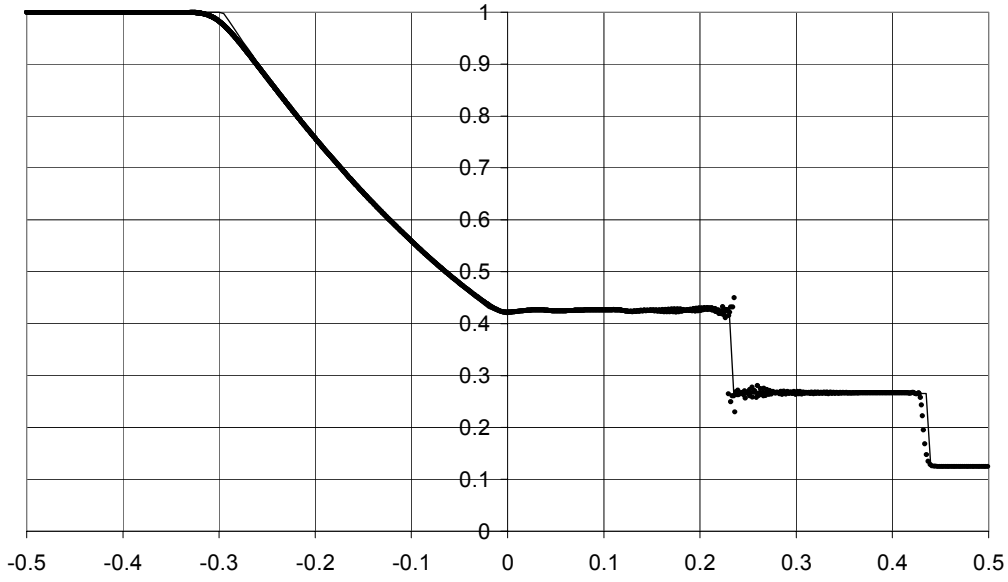

Figure 5-31: Density Profile after $0.25\,\mu s$ using NCPH

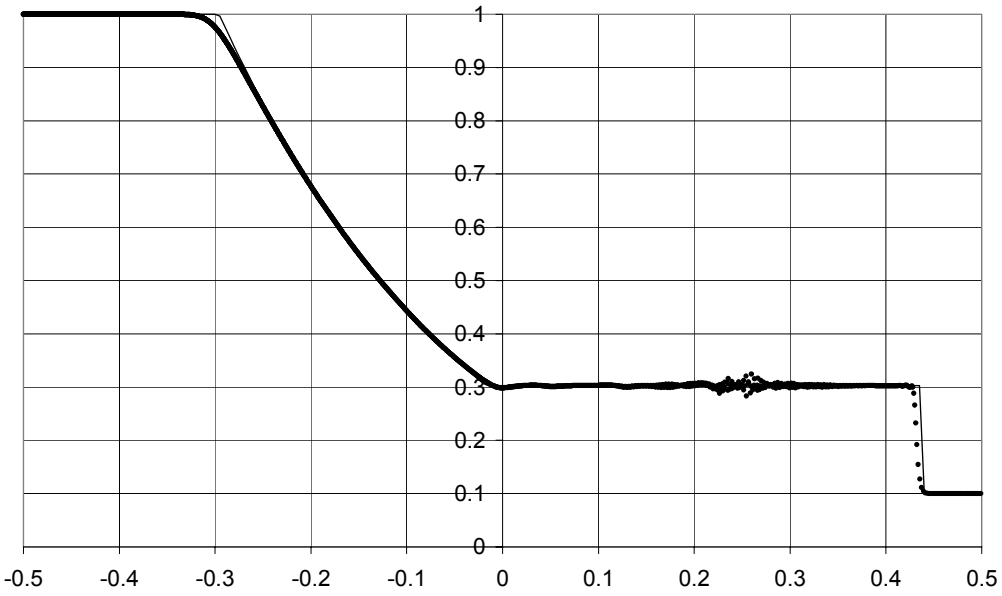

Figure 5-32: Pressure Profile after $0.25\,\mu s$ using NCSPH

Finally the combination of NCSPH with velocity smoothing was tested. The results are very good with very little oscillation, but the velocity smoothing introduces an error in wave propagation speed.

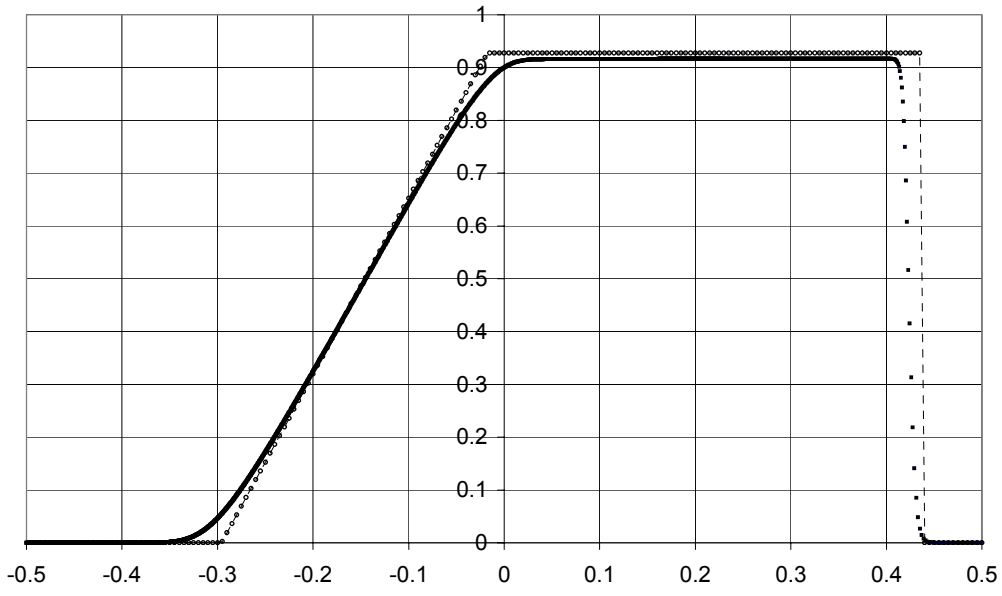

Figure 5-33: Velocity Profile after $0.25\,\mu s$ using NCSPH with VS

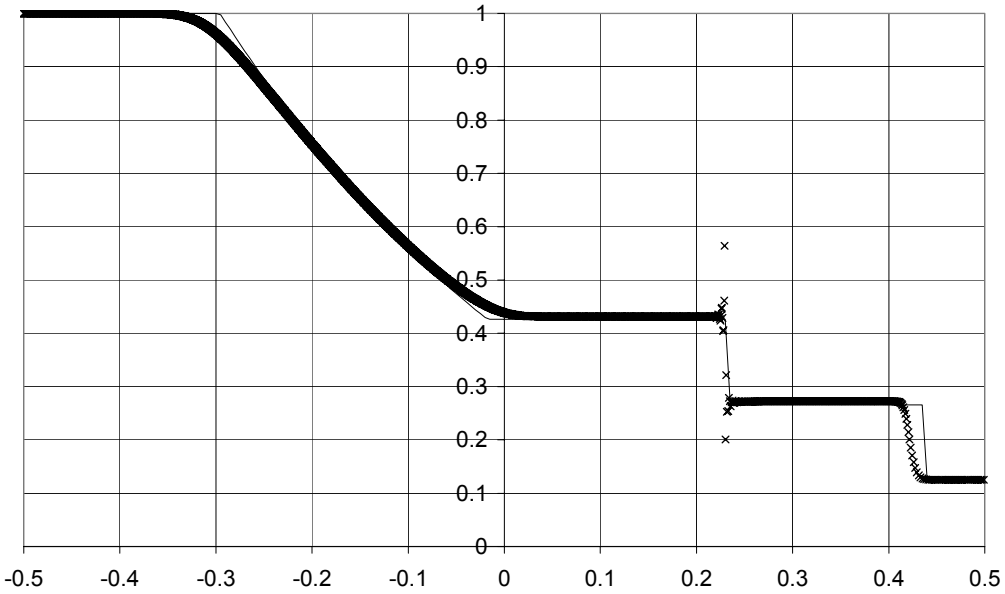

Figure 5-34: Density Profile after $0.25\,\mu s$ using NCSPH with VS

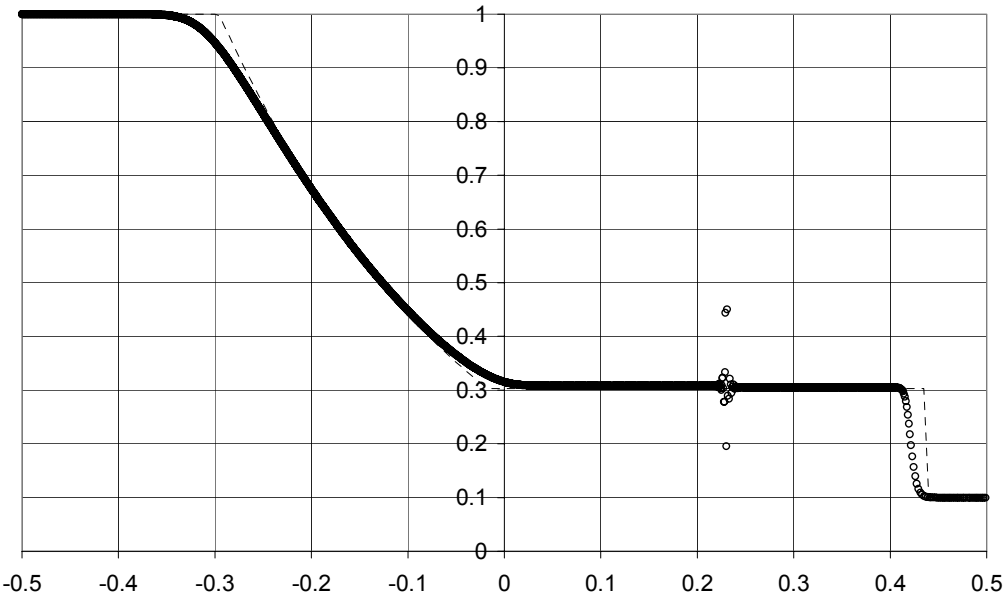

Figure 5-35: Pressure Profile after $0.25\,\mu s$ using NCSPH with VS

5.9 Discussion

From the conducted tests it can be concluded that for the reconstruction of functions and their derivatives the normalized, corrected kernel and normalized corrected kernel SPH significantly improve the results compared to those obtained with conventional SPH.

From the results of the elastic impact problem one can conclude that again the results show an improvement in that the oscillations present in the SPH solution are eliminated.

For the more severe test of a shock tube simulation the balance is slightly shifted. The conventional SPH results are accurate, but show a large amount of oscillation. These oscillations can be filtered out by applying velocity smoothing at the cost of a slightly less accurate solution because of the dispersion it causes.

The NSPH and CSPH methods can not handle the large variations and discontinuities in the field variables. So, despite improving the quality of the interpolation they perform significantly worse than conventional SPH. The combination of kernel normalization, or corrected kernels, with nodal integration is unstable if large density differences are present and the grid becomes irregular. This has been reported in several other papers such as Voth [16] and Christon [17]. It is interesting to note that SPH, despite the inaccuracy of the interpolation does not suffer from this. Using velocity smoothing solves this problem only to an extent as the solutions are stable but not very accurate. There is an error in wave propagation speed, and there are significant errors in the values obtained for the field variables between the shocks. The profiles exhibit slopes which are amplified the as simulation proceeds, hence, the method is unstable. One probable reason is the lack of a direct relation between a field and its gradients, and that the equations 5-9 and 5-10 do not satisfy Gauss/Ostrogradsky theorem. Normalized and corrected kernel velocity smoothing give similar results, the latter performing slightly better.

The best results are obtained using by the NCSPH method, the oscillations present in the SPH solution are far less pronounced in this case. Also the magnitude of the spike at the contact point between the two gasses is reduced. Adding velocity smoothing to NCSPH completely eliminates oscillations in the velocity field, and reduces those in the density and pressure fields, at the cost of an error in wave propagation speed.

5.10 Conclusion

From the conducted tests one can conclude that NCSPH performs the best. There is less oscillation in the solution than conventional SPH, and it can handle the discontinuities of a shock tube problem. This last problem is where NSPH and CSPH fail, despite showing good results for elastic impact problems.

The use of velocity smoothing provides a stabilizing factor and reduces oscillations. The disadvantage is the dispersion and error in wave propagation speed it causes.

To establish whether the improvement in results obtained using the NCSPH method is sufficient or further improvements are needed it will be necessary to conduct tests in two and three dimensions.

5.11 References

[1] W. Liu., S. Jun, Y. Zhang (1995):"Reproducing Kernel Particle Methods", *Int. J. of Num. Meth. in Fluids*, Vol. 20, 1081-1106

[2] W. Liu, S. Yun, S. Li., J. Adee, T. Belytschko T. (1995):"Reproducing Kernel Particle Methods for Structural Dynamics", Int. J. Num. Meth. Engrg., 38, 1655-1679.

[3] W. Liu., Y. Chen (1995): "Wavelet and Multiple Scale Reproducing Kernel Methods", *Int. J. of Num. Meth. in Fluids*, Vol. 21, 901-931.

[4] W. Liu, S. Jun (1993):"Reproducing Kernel Particle Methods for Elastic and Plastic Problems", *Adv. Comp. Meth. for Material Modeling*, AMD-Vol 180, 175-189.

[5] G. Johnson, S. Beissel (1996):"Normalised Smoothing Functions for SPH impact Computations", *Int. J. for Num. Meth. in Engrg*, Vol. 39, 2725-2741.

[6] L. Libersky., P. Randles, T. Carney, D. Dickinson (1997):"Recent Improvements in SPH modelling of Hypervelocity Impact", *Int. J. Impact Engng*, 20, 525-532.

[7] J. Chen (1999): "A Corrective Smoothed Particle Method for Boundary Value Problems in Heat Conduction", *Int. J. Num. Meth. Engrg*., Vol. 46, 231-252.

[8] J. Bonet, S. Kulasegaram (1998):"Correction and Stabilisation of Smoothed Particle Hydrodynamics with Applications in Metal Forming Simulations", CR/985/98, University of Wales, Swansea

[9] P. Randles and L.Libersky(1996):"Smoothed Particle Hydrodynamics: Some Recent Improvements and Applications", *Comp. Methods Appl. Mech. Engrg*., Vol. 139, 375-408.

[10] C. Guenther, D. Hicks, and J. (1994):"Conservative Smoothing versus Artificial Viscosity", Technical Report SAND94-1853, Sandia National Laboratory.

[11] D.Balsara (1995): "Von Neumann stability analysis of Smooth Particle Hydrodynamics suggestions for optimal algorithms". *J. Comp. Phys,* 121, 357-372.

[12] L. Libersky, P. Randles, T. Carney, D. Dickinson (1997): "Recent Improvements in SPH modelling of Hypervelocity Impact", *Int. J. Impact Engng*, 20, 525-532.

[13] G. Sod (1978):"A Survey of Several Finite Difference Methods for Systems of Nonlinear Hyperbolic Conservation Laws", *J. Comput. Phys*, 27, 1-31.

[14] E. Toro E.(1997): "Riemann Solvers and Numerical Methods for Fluid Dynamics", Springer, pp152-157

[15] J. Campbell, R. Vignjevic., L. Libersky (2000):"A Contact algorithm for Smooth Particle Hydrdoynamics", *Comput. Methods. Appl .Mech .Engrg*, Vol. 184,67-85.

[16] T. Voth., Christon (2001): "Discretization errors associated with reproducing kernel methods: one-dimensional domains", *Comp. Meth. Appl. Mech. Engrg*, Vol. 190, 2429-2446.

[17] M. Christon., T. Voth (2000): "Results of Von Neumann Analyses for Reproducing Kernel Semi-Discretizations, *Int. J. Num. Meth. Engrg.*, Vol. 47, 1285-1301.

6. VON NEUMANN ANALYSIS OF SPH AND NSPH

6.1 Introduction

The applications of SPH started with problems involving gas dynamics with Lucy [1] and Monaghan and Gingold [2] and later were extended to magneto-hydrodynamics by Monaghan [3]. More recently SPH has been used to simulate impact and penetration problems that include the effects of solid materials by Libersky and Petschek [4], Benz [5] Johnson *et al* [6] and Johnson [7].

During the last two decades SPH showed its ability to solve a wide range of continuum dynamic problems in open domains, many improvements have been made by Randles and Libersky [8] and G.Dilts [9] in order to increase SPH's accuracy and ability to simulate internal flows or phenomena taking into account the presence of boundary conditions.

For any good numerical method necessary requirements are stability and theoretical equations and convergence to the right solutions.

Von Neumann analysis is a perturbation method, which assumes that initial values of the perturbations are low level, and then the linearized theory may be considered as an approximation valid during some finite initial time interval.

Von Neumann analysis has been used by numerous researchers J.W. Swegle *et al* [10], J.W. Swegle *et al* [11], D.L. Hicks *et al* [12] to analyse dispersive errors associated with the SPH method when applied to elastic solids with the central difference time discretization scheme, D.S. Balsara [13] performed the analysis for barotropic material with the predictor-corrector scheme, J.P. Morris [14] investigated the dispersion error in the semi-discretized Magneto-Hydrodynamic SPH (MHDSPH) and recently J.J. Monaghan [15] analyses the dispersion relation in order to choose appropriate parameters that give accurate results for several problems.

Dispersion errors are typically characterized by the difference between physical and numerical phase velocity of a wave and by the difference between the physical group velocities of the wave train with its numerical counterpart.

The work presented here uses similar approach to that found in the references [13] and [14]. Here, the analysis is extended the analysis to a continuum media with specific constitutive equation, in

addition one uses central difference scheme. Also investigations of two formulations are made for standard SPH and for NSPH.

6.2 Governing Equations

The starting points of the analysis are the basic SPH and NSPH equations in one dimension. The mathematical theory will not be presented here; a complete derivation of the equations has been given in [2, 3, 4] for SPH and in [8, 16] for NSPH. Neglecting boundary terms, the discretized equations including artificial viscosity term becomes:

$$\begin{cases} \dfrac{dx_i(t)}{dt} = u(x_i,t) \\ \dfrac{du(x_i,t)}{dt} = -\sum_n m_n.(\dfrac{\sigma_i^{xx} - Q_i}{\rho_i^2} + \dfrac{\sigma_n^{xx} - Q_n}{\rho_n^2}).\nabla_{xi} W(x_i - x_n, h) \\ \dfrac{d\rho(x_i,t)}{dt} = \rho(x_i,t).\sum_n \dfrac{m_n}{\rho_n}.(u_i - u_n).\nabla_{x_i} W(x_i - x_n, h) \end{cases} \tag{6.1}$$

The second formulation, the weighted difference form is.

$$\begin{cases} \dfrac{dx_i(t)}{dt} = u(x_i,t) \\ \dfrac{du(x_i,t)}{dt} = -\dfrac{1}{\rho_i}\sum_n m_n.(\dfrac{\sigma_n^{xx} - Q_i - \sigma_i^{xx} + Q_n}{\rho_n}).\nabla_{xi} W(x_i - x_n, h) \\ \dfrac{d\rho(x_i,t)}{dt} = \rho(x_i,t).\sum_n \dfrac{m_n}{\rho_n}.(u_i - u_n).\nabla_{x_i} W(x_i - x_n, h) \end{cases} \tag{6.2}$$

The artificial viscosity is given by.

$$\begin{cases} Q_i = h.\rho_i.\left|\sigma_i^{xx}\right|.(\alpha.C_S + \beta.h.\left|\sigma_i^{xx}\right|) & \text{if} \quad \sigma_i^{xx} < 0 \\ Q_i = 0 & \sigma_i^{xx} \geq 0 \end{cases} \tag{6.3}$$

Where C_s stands for the speed of sound, the constants α and β are user-defined, typically, $\alpha \approx 0.9$, $\beta \approx 0.5$.

In the systems (6.1) and (6.2) above, the physical fields are the density $\rho_i = \rho(x_i, t)$, the velocity $u_i(t) = u(x_i, t)$, the scalar $\sigma_i^{xx}(t) = \sigma^{xx}(x_i, t)$ is the stress in x-direction, $m_i = m(x_i)$ is a constant mass carried by the i^{th} particle occupying the position x_i at time t. Finally $W(z, h)$ is the kernel function, where h is the spatial parameter or smoothing length and z is the relative position of particle n with respect of particle i.

The stability analysis developed here ignores the role of the artificial viscosity and the numerical experiments were performed without it.

6.3 Stability Analysis

Von Neumann analysis is based on perturbation theory combined with wave train propagation approach. Thus any physical field (scalar or vector) $\psi\left(r_i, t\right) = \psi_i\left(t\right)$ can be decomposed as follows.

$$\psi_i(t) \approx \psi_{0i} + \hat{n} \cdot \delta\psi \cdot e^{j\cdot\left(\vec{k}\cdot\vec{r}_{0i} - \omega\cdot t\right)} \tag{6.4}$$

In the expression above ψ_{0i} is the unperturbed state, $\delta\psi$ is the amplitude of the perturbation subjected to the condition $\left|\psi_i\left(t\right) - \psi_{0i}\right| << \left|\psi_{0i}\right|$ (small perturbation), $\vec{k}$ is the wave vector (direction of propagation), ω is the frequency, $\vec{r}_{0i}$ is the unperturbed space positions and $\hat{n} = \dfrac{\vec{k}}{\left|\vec{k}\right|}$ represents a unit vector. In one dimension, this expression simplifies to.

$$\psi_i(t) \approx \psi_{0i} + \delta\psi \cdot e^{j\cdot\left(k\cdot x_{0i} - \omega\cdot t\right)} \tag{6.5}$$

The perturbation defined in (6.5) is applied to following fields.

$$\psi_i(t) = \begin{pmatrix} x_i(t) \\ u_i(t) \\ \rho_i(t) \end{pmatrix}, \qquad \psi_{0i} = \begin{pmatrix} x_{0i} \\ u_{0i} \\ \rho_{0i} \end{pmatrix} \qquad \text{and} \qquad \delta\psi = \begin{pmatrix} X \\ U \\ R \end{pmatrix} \tag{6.6}$$

The unperturbed system considered consists of row of uniformly spaced particles with constant velocity $(u_{0i} = 0,\ i = -\infty,...n-1, n, n+1,..... + \infty)$ and prescribed density.

The above-mentioned assumption results in ψ_{0i} becoming:

$$\psi_{0i} = \begin{pmatrix} x_{0i} \\ 0 \\ \sum_n m_n . W(x_{0i} - x_{0n}, h) \end{pmatrix} \tag{6.7}$$

6.4 Linear Equations in SPH

To obtain the dispersion relation for $1D$ the system of equations (6.1) or (6.2) has to be linearized with respect to density. In the present work, the consideration is limited to isentropic and special cases, for which the stress and density are directly related.

$$\sigma = f(\frac{\rho}{\rho_0})$$

The case to be considered is stability analysis for elastic materials (Hooke's Law) J.W.Swegle *et al* [10]. In order to generalize the investigations the stress can be expressed as:

$$\sigma = A.\rho^{z} + B$$

Where $z \in Z$, A and B depend on the material properties in its un-deformed state and should satisfy the following requirements.

$$\begin{cases} \textit{Equilibrium Stability} & \left.\dfrac{\partial \sigma(\rho)}{\partial \rho}\right|_{S} > 0 & 6.8-a \\ \textit{Limit Condition} & \underset{\rho \to \rho_0}{Lim}\, \sigma(\rho) = \sigma_0 & 6.8-b \\ \textit{Asymptotic Limit} & \underset{\rho \to \rho_\infty}{Lim}\, \sigma(\rho) = \sigma_\infty < \infty & 6.8-c \end{cases}$$

Using Taylor expansion, the terms on the right hand side of the momentum equations in (6.1) can be linearised around ρ_0 to.

$$\begin{aligned} \left(\frac{\sigma(\rho_{0i} + \delta\rho_i)}{(\rho_{0i} + \delta\rho_i)^2}\right) &\approx \left(\frac{\sigma(\rho_{0i}) + \delta\rho_i \cdot \nabla_{\rho i}(\sigma)_{\rho_{0i}}}{\rho_{0i}^{\,2}}\right) \cdot \left(1 - 2 \cdot \frac{\delta\rho_i}{\rho_{0i}}\right) \\ &\approx \left(\frac{\sigma(\rho_{0i})}{\rho_{0i}^{\,2}}\right) + \left(\frac{\delta\rho_i}{\rho_{0i}^{\,2}}\right) \cdot \left(\nabla_{\rho i}(\sigma)_{\rho_{0i}} - 2 \cdot \frac{\sigma(\rho_{0i})}{\rho_{0i}}\right) \\ &\approx \left(\frac{\sigma}{\rho^2}\right)_{\rho_{0i}} + \delta\rho_i \cdot \left(\nabla_{\rho_i} \frac{\sigma}{\rho^2}\right)_{\rho_{0i}} \end{aligned}$$

The second order terms in $\delta\rho_i$ are neglected, and using (6.3) and (6.8-b), the equation above becomes.

$$\left(\frac{\sigma - Q}{\rho^2}\right)_{\rho_i} = \begin{cases} \dfrac{\sigma_{0i}}{\rho_{0i}^2} + \delta\rho_i \cdot \left(\nabla_\rho \dfrac{\sigma - Q}{\rho^2}\right)_{\rho_{0i}} & if \quad \sigma(\rho) < 0 \\ \dfrac{\sigma_{0i}}{\rho_{0i}^2} + \delta\rho_i \cdot \left(\nabla_\rho \dfrac{\sigma}{\rho^2}\right)_{\rho_{i0}} & if \quad \sigma(\rho) \geq 0 \end{cases} \tag{6.9}$$

Where: $\delta\rho_i = \rho_i(t) - \rho_{0i} = R \cdot e^{j\cdot(k\cdot x_{0i} - \omega\cdot t)}$.

By Taylor expansion for the kernel around unperturbed positions one gets:

$$\begin{aligned} W(x_i - x_n) &= W\left(x_{0i} - x_{0n} + X \cdot \left(e^{j\cdot k\cdot x_{0i}} - e^{j\cdot k\cdot x_{0n}}\right)\right) \\ &\approx W(x_{0i} - x_{0n}) + X \cdot e^{j\cdot(k\cdot x_{0i} - \omega\cdot t)} \cdot \left(1 - e^{-j\cdot k\cdot(x_{0i} - x_{0n})}\right) \cdot \nabla_{xi} W(x_{0i} - x_{0n}) \\ &\approx W(\delta_n) + (x - x) \cdot \left(1 - e^{j\cdot k\cdot \delta_n}\right) \cdot \nabla_{xi} W(\delta_n) \end{aligned}$$

The same approximation applied to the gradient of the kernel gives:

$$\nabla_{x_i} W(x_i - x_n) \approx \nabla_{x_{0i}} W(\delta_n) + (x_i - x_{0i}) \cdot (1 - e^{j.k.\delta_n}) \cdot \nabla_{xi}^2 W(\delta_n) \tag{6.10}$$

Where $\delta_n = (n - i).\delta_0$ represents the spacing distance between i^{th} and n^{th} particles.

6.5 Stability of the first formulation

To linearize the system (6.1), expressions (6.5) and (6.10) are substituted in the equations, by neglecting second and higher order terms one obtains the following:

$$\begin{cases} -j\cdot\omega\cdot X = U \\ j\cdot\omega\cdot U\cdot e^{j\cdot\phi_i} = R\cdot\sum_{n=-\infty}^{n=+\infty} m_n\cdot\left\{P_{oi}\cdot e^{j\cdot\phi_i} + P_{0n}\cdot e^{j\cdot\phi_n}\right\}\cdot\nabla_{xi}W(\delta_n) \\ +X\sum_{n=-\infty}^{n=+\infty} m_n.\left\{\frac{\sigma_{0i}}{\rho_{0i}^2}+\frac{\sigma_{0n}}{\rho_{0n}^2}\right\}\cdot\left(e^{j\cdot\phi_i} - e^{j\cdot\phi_n}\right)\cdot\nabla_{xi}^2 W(\delta_n) \\ -j.\omega.R\cdot e^{j\cdot\phi_i} = \rho_{0i}\cdot U\cdot\sum_{n=-\infty}^{n=\infty}\frac{m_n}{\rho_{0n}}\cdot(e^{j\cdot\phi_i} - e^{j\cdot\phi_n})\cdot\nabla_{xi}W(\delta_{i,n}) \end{cases} \tag{6.11}$$

Where $P_{0i} = (\nabla_\rho \frac{\sigma}{\rho^2})_{\rho_{0i}}$ and $P_{0n} = (\nabla_\rho \frac{\sigma}{\rho^2})_{\rho_{0n}}$. In the equations above, ϕ_i and ϕ_n denote phases of the wave at non-perturbed positions of particles i and n, thus, $\phi_i = k\cdot x_{0i} - \omega\cdot t$.

By substituting the first and the third equation from the system (6.11) in the momentum equation, one obtains:

$$D(\omega,k)\cdot U = 0 \tag{6.12}$$

The equation (6.12) gives the implicit form of dispersion relation (6.13) below.

$$D(\omega,k) = \omega^2(k) - \rho_{0i}\cdot\sum_{n'=\infty}^{\infty}\frac{m_{n'}}{\rho_{0n'}}(1-e^{j.k.\delta_{n'}})\nabla_{x_i}W(\delta_{n'})\cdot\sum_{n=-\infty}^{\infty} m_n.(P_{0i}+P_{0n}.e^{j.k.\delta_n})\cdot\nabla_{x_i}W(\delta_n)$$

$$-\sum_{n=-\infty}^{n=+\infty} m_n\cdot\left\{\frac{\sigma_{0i}}{\rho_{0i}^2}+\frac{\sigma_{0n}}{\rho_{0n}^2}\right\}\cdot\left(1-e^{j\cdot k\cdot\delta_n}\right)\cdot\nabla_{xi}^2 W(\delta_n) = 0$$

In the relation above $\omega(k) = \omega_r(k) + j\cdot\omega_i(k)$ is a complex entity $(j^2 = -1)$, with real part $\mathrm{Re}[\omega] = \omega_r$ and imaginary part $\mathrm{Im}[\omega] = \omega_i$ consequently, one has.

$$\omega^2(k) = \omega_r^2(k) - \omega_i^2(k) + 2\cdot j\cdot\omega_r(k)\cdot\omega_i(k) \tag{6.14}$$

Following the decomposition above, the real part of the dispersion relation gives (6.15):

$$\begin{cases} \omega_r^2(k)-\omega_i^2(k)=\rho_{0i}\cdot\sum_{n'}\frac{m_{n'}}{\rho_{0n'}}\cdot(1-\cos k\ \delta_{n'})\cdot\nabla W(\delta_{n'})\cdot\sum_n m_n\cdot(P_{0i}+P_{0n}.\cos k\ \delta_n)\cdot\nabla W(\delta_n) \\ \quad +\rho_{0i}\cdot\sum_{n'}\frac{m_{n'}}{\rho_{0n'}}\cdot\sin(k\ \delta_{n'})\cdot\nabla W(\delta_{n'}).\sum_n m_n\cdot P_{0n}.\sin(k\ \delta_n)\cdot\nabla W(\delta_n) \\ \quad +\sum_n m_n\cdot\left\{\frac{\sigma_{0i}}{\rho_{0i}^2}+\frac{\sigma_{0n}}{\rho_{0n}^2}\right\}\cdot(1-\cos k\ \ \delta_n)\cdot\nabla^2 W(\delta_n) \end{cases}$$

And from the imaginary part of the dispersion relation (6.16):

$$\begin{cases} 2.\omega_i(k)\cdot\omega_r(k)=\rho_{0i}\cdot\sum_{n'}\frac{m_{n'}}{\rho_{0n'}}\cdot(1-\cos k\ \delta_{n'})\cdot\nabla W(\delta_{n'})\cdot\sum_n m_n\cdot P_{0n}\cdot\sin(k\ \delta_n)\cdot\nabla W(\delta_n) \\ \quad -\rho_{0i}\cdot\sum_{n'}\frac{m_{n'}}{\rho_{0n'}}\cdot\sin(k\ \delta_{n'})\cdot\nabla W(\delta_{n'})\cdot\sum_n m_n(P_{0i}+P_{0n}\cdot\cos k\delta_n)\cdot\nabla W(\delta_n) \\ \quad -\sum_n m_n\cdot\left\{\frac{\sigma_{0i}}{\rho_{0i}^2}+\frac{\sigma_{0n}}{\rho_{0n}^2}\right\}\cdot\sin(k\ \delta_n)\cdot\nabla^2 W(\delta_n) \end{cases}$$

Each term in the expression (6.16) corresponds to a specific mechanism that occurs during the wave propagation process in the material.

The first term is a consequence of broken regularity in the distribution of particles in the neighbourhood of the particle i.

The second term corresponds to the non-uniformity of the background stress of the system in the neighbourhood of that particle. In other words for uniform background stress and regular distribution of the particles this term vanishes.

Finally, the last term corresponds to the instability due to tensile effects [Swegle, Hicks]. Implicitly, (6.16) can be expressed by:

$$\omega_i(k)\cdot\omega_r(k)=T_1(k)+T_2(k)+T_3(k) \tag{6.16a}$$

Remark:

For the purpose of the analysis presented, the following assumption is made $W \in C^2\left(D_W\right)$.

In the following, for simplicity, let us assume that the systems considered have a constant background stress, $Q_0 = \frac{\sigma_0}{\rho_0^2} = \frac{\sigma_{0n}}{\rho_{0n}^2}$ and consequently $P_0 = P_{0n}$ and, then expressions (6.15) and (6.15) reduce to (6.17) below.

$$\begin{cases} \omega_r^2(k) - \omega_i^2(k) = P_0 \cdot \left\{ \left(\sum_{n=-\infty}^{\infty} m_n \cdot \sin(k\ \delta_n) \cdot \nabla_x W(\delta_n) \right)^2 + \left(\sum_{n=-\infty}^{\infty} m_n \cdot \nabla_x W(\delta_n) \right)^2 - \left(\sum_{n=-\infty}^{\infty} m_n . \cos(k\ \delta_n) \cdot \nabla_x W(\delta_n) \right)^2 \right\} \\ \qquad + 2 \cdot Q_0 \cdot \sum_{n=-\infty}^{\infty} m_n . (1 - \cos(k\ \delta_n)) \cdot \nabla_x^2 W(\delta_n) \\ \omega_r(k) \cdot \omega_i(k) = -P_0 \cdot \sum_{n'=-\infty}^{\infty} m_{n'} \sin(k\ \delta_{n'}) \cdot \nabla_x W(\delta_{n'}) \cdot \sum_{n=-\infty}^{\infty} m_n \cos(k\ \delta_n) \cdot \nabla_x W(\delta_n) - Q_0 \cdot \sum_{n=-\infty}^{\infty} m_n \sin(k\ \delta_n) \cdot \nabla_x^2 W(\delta_n) \end{cases}$$

A trivial transformation is obtained under condition that $\omega_r(k) \neq 0$ and $\omega_i(k) \neq 0$ and those two equations can be written in the following form:

$$\begin{cases} \omega_r^4(k) - \left(P_0 \cdot A^2 + Q_0 \cdot B\right) \cdot \omega_r^2(k) - \left(P_0 \cdot A_0 \cdot D + Q_0 \cdot C\right)^2 = 0 \\ \omega_i(k) = -\dfrac{P_0 \cdot A_0 \cdot D + Q_0 \cdot C}{\omega_r(k)} \end{cases} \tag{6.18}$$

The solution of the system above is.

$$\begin{cases} \omega_r^2(k)_{\pm} = \dfrac{1}{2} \cdot \left(P_0 \cdot A^2 + Q_0 \cdot B \pm \sqrt{\left(P_0 \cdot A^2 + Q_0 \cdot B\right)^2 + 4 \cdot \left(P_0 \cdot A_0 \cdot D + Q_0 \cdot C\right)^2} \right) \\ \omega_i(k)_{\pm} = -\dfrac{P_0 \cdot A_0 \cdot D + Q_0 \cdot C}{\omega_r(k)_{\pm}} \end{cases} \tag{6.19}$$

Where the terms A, A_0, B, C and D are expressed by.

$$A^2 = \left(\sum_n m_n \cdot \sin(k\delta_n) \cdot \nabla_x W(\delta_n) \right)^2 + \left(\sum_n m_n \cdot \nabla_x W(\delta_n) \right)^2 - \left(\sum_n m_n \cdot \cos(k\,\delta_n) \cdot \nabla_x W(\delta_n) \right)^2$$

$$A_0 = \left(\sum_n m_n \cdot \sin\left(k \cdot \delta_n\right) \cdot \nabla_x W\left(\delta_n\right) \right)$$

$$B = 2 \cdot \sum_n m_n \cdot \left(1 - \cos k\delta_n\right) \cdot \nabla_x W\left(\delta_n\right)$$

$$C = \sum_n m_n \cdot \sin\left(k \cdot \delta_n\right) \cdot \nabla_x^2 W\left(\delta_n\right)$$

$$D = \sum_n m_n \cdot \cos\left(k \cdot \delta_n\right) \cdot \nabla_x W\left(\delta_n\right)$$

The first coefficient A^2 is always positive, from the second relation in (6.18) one can see that the signs of coefficients C and $A_0 \cdot D$ control the stability of the system.

The term $Q_0 \cdot C$ has been designated 'Tensile Instability term' for homogenous system by Hicks at *al.*

Finally the term $A_0 \cdot D$ expresses the instability due to the absence of the regularity in the particles distribution.

To prove that $A^2 \geq 0$ it is sufficient to observe that the inequality below is straightforward:

$$A^2 - A_0^2 = \left(\sum_n m_n \cdot \nabla_x W(\delta_n) \right)^2 - \left(\sum_n m_n \cdot \cos(k\,\delta_n) \cdot \nabla_x W(\delta_n) \right)^2 \geq 0$$

The quantity $\left(A^2 - A_0^2\right)$ has its minimal value at $\left(A^2 - A_0^2\right) = 0$ for regular distribution of particles and A^2 becomes:

$$A^2 = \left(\sum_n m_n \cdot \sin(k\ \delta_n) \cdot \nabla_x W(\delta_n) \right)^2$$

In (6.19) only waves with frequencies $\omega_r^2(k)_+ > 0$ propagate in the material, while waves with frequencies $\omega_r^2(k)_-$ have no physical meaning.

To summarize, a linear perturbation analysis using the complex-frequency (the same approach can be performed by using the complex-wave vector) reveals that the frequencies $\omega_r(k)$ and the damping coefficients $\omega_i(k)$ (instabilities) are correlated non-linearly, see relations (6.15) and (6.16), consequently the physical mechanisms outlined above involving in the control of the instabilities are also involved in the control of the frequencies of the waves.

It is then expected that some of these mechanisms will intervene on the evolution of the instabilities with more or less pronounced influence than other mechanisms.

As can be seen from the second equation in (6.19), for a given mode, say $\omega_r^0(k)$; the development of the instability of that mode, say $\omega_i^0(k)$, will depend on the sign of the quantity $P_0 \cdot A_0 \cdot D + Q_0 \cdot C$ alone while the quantity $P_0 \cdot A^2 + Q_0 \cdot D$ involves only in the frequency.

6.5.1 Numerical Example

In order to evaluate the validity of the 'constant stress background' assumption made in the previous section, an elastic model of aluminium subjected to a velocity perturbation.

The initial configuration is such that $\frac{h}{\delta_0} = 1$, where h is the smoothing length and δ_0 is the relative distance between particles. The critical wave number used in the plots is defined by: $k_{cr} = \frac{\pi}{\delta_0}$. The analytical form of the perturbation is given by:

$$\delta v(t) = V_0 \cdot \exp\left(-t^2\right) \quad with \quad 0 \le t \le 0.35\ \mu s\ . \tag{6.20}$$

Where $V_0 = 0.18\ Cm/\mu s$. In order to fulfil the linearization condition, V_0 is chosen such that $V_0 << C_s$, where C_s represents the speed of sound in aluminium at ambient conditions.

From here on, in the following graphs, thick curves correspond to a system with background stress changing with the density perturbation and thin curves correspond to a model with constant background stress.

Each colour in the plots is associated with a specific time (instant) after the disturbance was applied to the system.

For figures (6-1) to (6-5), the association between colours and time reads:

$$\begin{aligned} &red\ curves \quad \Leftrightarrow \quad t_0 = 0.205\ \mu s \\ &blue\ curves \quad \Leftrightarrow \quad t_1 = 0.568\ \mu s \\ &black\ curves \quad \Leftrightarrow \quad t_2 = 1.01\ \mu s \end{aligned}$$

First of all, $\omega_r^2(k)$ and $\omega_i(k)$ obtained from equations (6.15-6.16), and from (6.19) are represented in figures (6-1) and (6-2) respectively. These are plotted at different times to ensure that the 'constant stress background' assumption holds independently on whether particles are under tension or under compression.

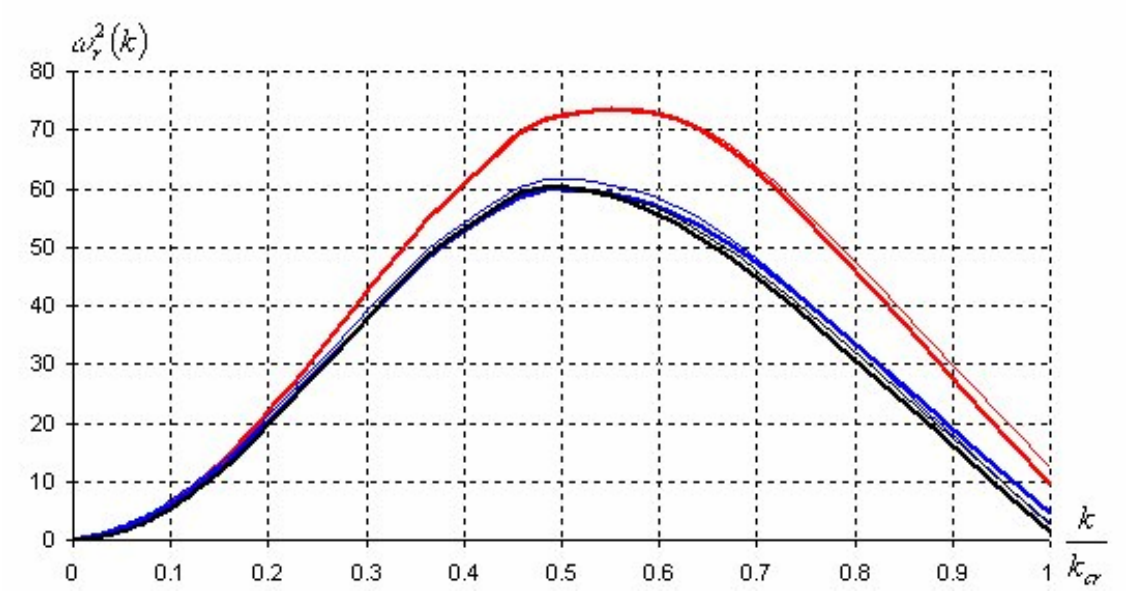

Figure 6-1: Plots of $\omega_r^2(k)$ at different instants.

From the curves in Figure 6-1, it can be seen that long modes $k \le 0.2 \cdot k_{cr}$, frequencies vary as linear function of $\frac{k}{k_{cr}}$ and the material is then non-dispersive; the phase velocity and the group velocity are equal $\left(\frac{\omega(k)}{k} = \frac{d\,\omega(k)}{d\,k}\right)$ and independent of the wavelength, in the opposite it is dispersive for intermediate modes $0.3 \le k \le 0.7 \cdot k_{cr}$ and for short modes $k \ge 0.7 \cdot k_{cr}$.

High frequencies are localized within the intermediate modes $0.3 \cdot k_{cr} \le k \le 0.7 \cdot k_{cr}$. The plot above shows also that short wave modes (local modes) have higher frequencies than long wave's modes (global modes). This result was expected, because global phenomena are slower than individual ones.

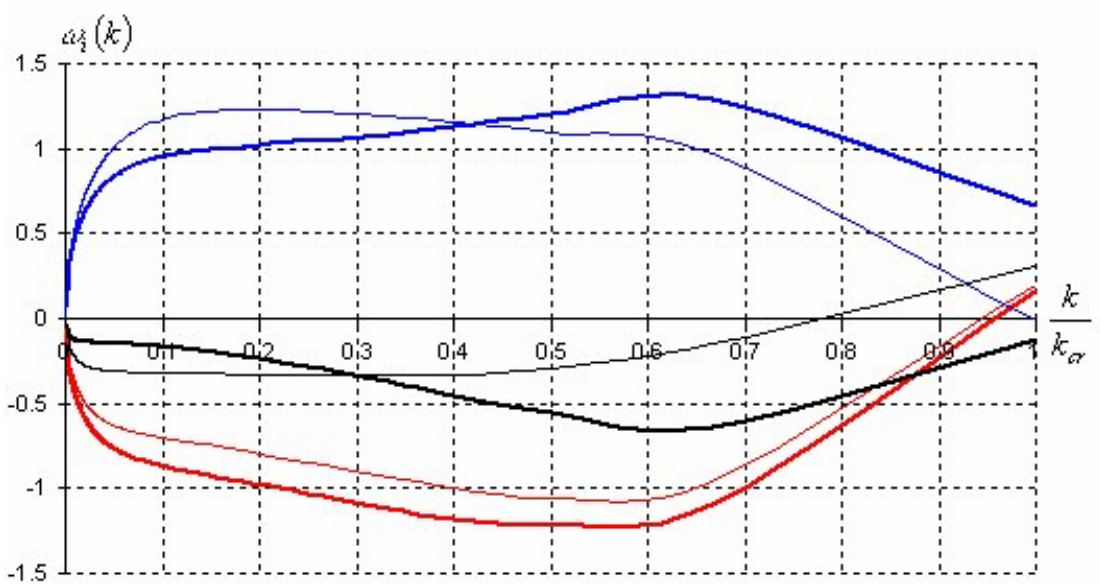

Figure 6-2: Plots of the amplification factor $\omega_i(k)$

The graph above indicates that modes are alternatively amplified $(\omega_i(k)>0 \quad blue\ curve)$ and damped $(\omega_i(k)<0 \quad red\ and\ black\ curves)$. As the simulation evolves, the amplification factor becomes smaller and the perturbation is attenuated. The constant background stress model globally predicts if modes will be amplified or attenuated (Both thick and thin curves have the same signs) but it fails to give acceptable amplitude especially at t_2. The solution of equations (6.15) and (6.16) can be written in a simplified term by introducing the following substitutions:

$$\Omega_1(k) = \frac{\rho_{0i} \cdot \sum_{n'} \frac{m_{n'}}{\rho_{0n'}} \cdot (1-\cos k\,\delta_{n'}) \cdot \nabla W(\delta_{n'}) \cdot \sum_{n} m_n \cdot P_{0n} \cdot \sin(k\,\delta_n) \cdot \nabla W(\delta_n)}{2 \cdot \omega_r(k)}$$

$$\Omega_2(k) = -\frac{\rho_{0i} \cdot \sum_{n'} \frac{m_{n'}}{\rho_{0n'}} \cdot \sin(k\,\delta_{n'}) \cdot \nabla W(\delta_{n'}) \cdot \sum_{n} m_n (P_{0i} + P_{0n} \cdot \cos k\delta_n) \cdot \nabla W(\delta_n)}{2 \cdot \omega_r(k)}$$

$$\Omega_3(k) = -\frac{\sum_{n} m_n \cdot \left\{ \frac{\sigma_{0i}}{\rho_{0i}^2} + \frac{\sigma_{0n}}{\rho_{0n}^2} \right\} \cdot \sin(k\,\delta_n) \cdot \nabla^2 W(\delta_n)}{2 \cdot \omega_r(k)}$$

Where $\Omega_1(k), \Omega_2(k)$ and $\Omega_3(k)$ correspond to the amplifications factors generated by the mechanisms $T_1(k)$ due to the irregularity in the distribution of the particles, $T_2(k)$ resulting from the non-uniformity of the background stress and $T_3(k)$ due to the tensile effect. So, for the amplification factor, one has:

$$\omega_i(k) = \Omega_1(k) + \Omega_2(k) + \Omega_3(k) \tag{6.21}$$

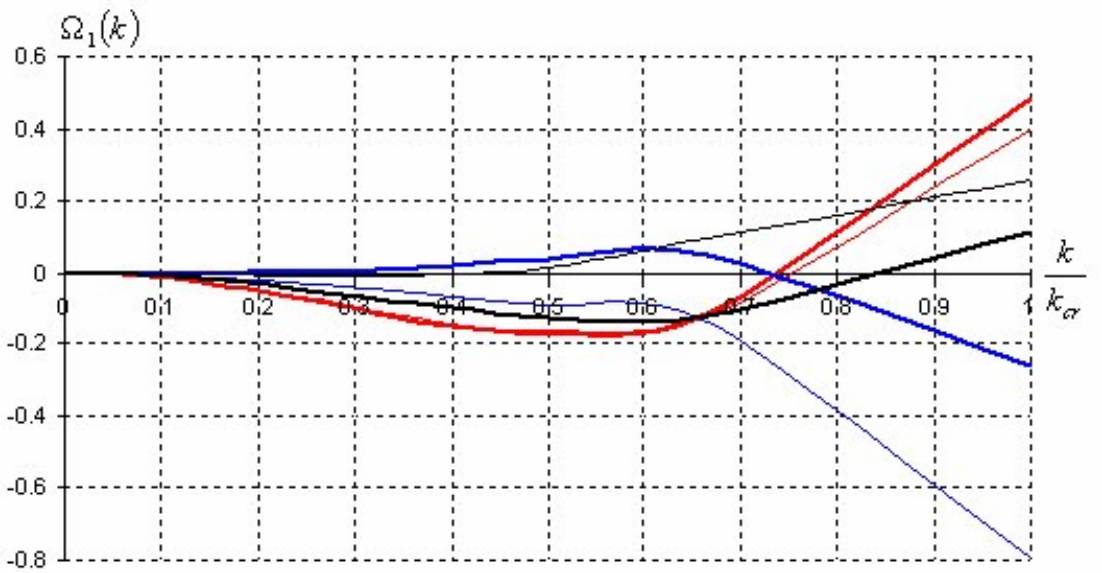

Figure 6-3: $\Omega_1(k)$, the amplification due to **the absence of a regular distribution**

As can be seen from Figure 6-3 that the distribution of particles has negligible effect on the global modes $(k \le 0.3 \cdot k_{cr})$ but its influence on the stability increases for local modes $(k \ge 0.8 \cdot k_{cr})$ where the maximum and minimum values of $\Omega_1(k)$ are reached for modes above $0.9 \cdot k_{cr}$.

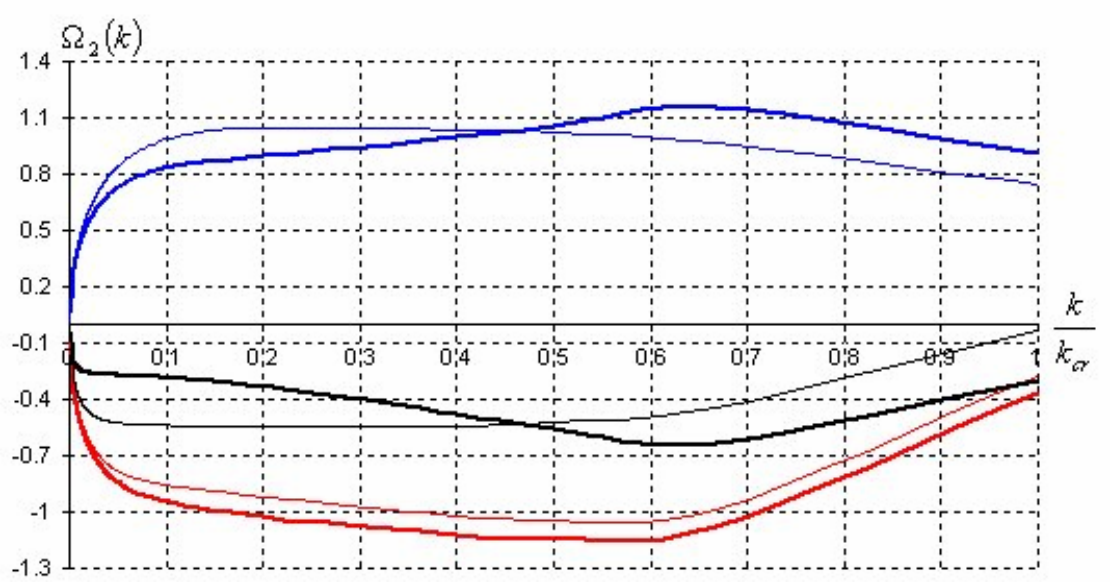

Figure 6-4: $\Omega_2(k)$, the amplification due to **the absence of a regular background stress**

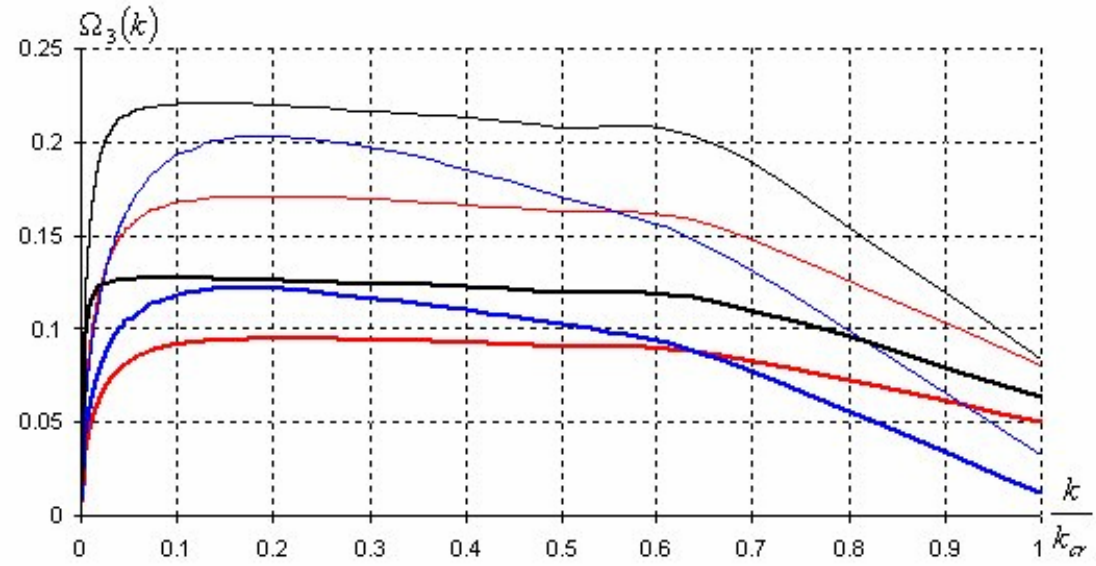

Figure 6-5: $\Omega_3(k)$,the amplification due **to the tensile term**

Figure 6-4 shows clearly that the background stress term dominates other terms. It exhibits amplitude three times higher than the amplitude of any of the other two mechanisms.

Figure 6-5 shows that the amplification due to the tensile term has a destabilizing effect for all modes. It also can be seen that the model with constant background stress over estimates the tensile term by a factor two.

6.5.2 Summary

The analysis introduced above shows the existence of three mechanisms responsible for the instability and the linearisation allows us to isolate each mechanism and its contribution to the amplification factor.

A numerical simulation was performed and results were plotted above for the frequency and for the global amplification factor.

In order to clarify the role of each identified mechanism, its corresponding amplification factor was plotted.

6.6 Stability of the second formulation

The analysis of the second SPH formulation starts by applying Taylor linearization to the momentum equation in (6.2) around ρ_{0n} and ρ_{0i} then, it follows (6.22):

$$\left(\frac{\sigma(\rho_{0n}+\delta\rho_n)-\sigma(\rho_{0i}+\delta\rho_i)}{(\rho_{0n}+\delta\rho_n)\cdot(\rho_{0i}+\delta\rho_i)}\right)\approx\left(\frac{\sigma(\rho_{0n})-\sigma(\rho_{0i})}{\rho_{0n}\cdot\rho_{0i}}\right)+\frac{\delta\rho_n}{\rho_{0i}}\cdot\left(\nabla_{\rho_n}\frac{\sigma_n}{\rho_n}\right)_{\rho_{0n}}-\frac{\delta\rho_i}{\rho_{0n}}\cdot\left(\nabla_{\rho_i}\frac{\rho_i}{\rho_i}\right)_{\rho_{0i}}$$

Where $\sigma_n=\sigma(\rho_{0n}+\delta\ \rho_n)$and $\sigma_i=\sigma(\rho_{0i}+\delta\ \rho_i)$.

By applying the same approach used in the first SPH formulation to the second formulation one obtains the dispersion relation

$$D(\omega,k)=\omega^2(k)+\left\{\rho_{0i}\sum_{n'=\infty}^{\infty}\frac{m_{n'}}{\rho_{0n'}}\cdot(1-e^{j\cdot k\cdot\delta_{n'}})\cdot\nabla_{x_i}W(\delta_{n'})\cdot\sum_{n=-\infty}^{\infty}m_n\cdot(P_{0i}-P_{0n}\cdot e^{j\cdot k\cdot\delta_n})\cdot\nabla_{x_i}W(\delta_n)\right\}$$
$$+\left\{\sum_{n=-\infty}^{\infty}m_n\cdot(\frac{\sigma_{0i}-\sigma_{0n}}{\rho_{0n}\cdot\rho_{0i}})\cdot(1-e^{j.k.\delta_n})\cdot\nabla_{x_i}^2W(\delta_n)\right\}=0$$

The real part of the equation of dispersion has the following form (6.23):

$$\begin{cases} \omega_r^2(k) - \omega_i^2(k) = -\rho_{0i} \sum_{n'} \frac{m_{n'}}{\rho_{0n'}} \cdot (1 - \cos k.\delta_{n'}) \cdot \nabla W(\delta_{n'}) \cdot \sum_n m_n (P_{0i} - P_{0n} \cdot \cos k.\delta_n) \cdot \nabla W(\delta_n) \\ \quad + \rho_{0i} \sum_{n'} \frac{m_{n'}}{\rho_{0n'}} \cdot \sin k.\delta_{n'} \cdot \nabla W(\delta_{n'}) \cdot \sum_n m_n P_{0n} \cdot \sin k.\delta_n \cdot \nabla W(\delta_n) \\ \quad - \sum_n m_n \left\{ \frac{\sigma_{0i} - \sigma_{0n}}{\rho_{0i} \cdot \rho_{0n}} \right\} \cdot (1 - \cos k.\delta_n) \cdot \nabla^2 W(\delta_n) \end{cases}$$

And the imaginary part gives (6.24):

$$\begin{cases} 2 \cdot \omega_i(k) \cdot \omega_r(k) = \rho_{0i} \sum_{n'} \frac{m_{n'}}{\rho_{0n'}} \cdot (1 - \cos k.\delta_{n'}) \cdot \nabla W(\delta_{n'}) \cdot \sum_n m_n \cdot P_{0n} \cdot \sin(k\delta_n) \cdot \nabla W(\delta_n) \\ \quad + \rho_{0i} \sum_{n'} \frac{m_{n'}}{\rho_{0n'}} \cdot \sin(k\delta_{n'}) \cdot \nabla W(\delta_{n'}) \cdot \sum_n m_n . (P_{0i} - P_{0n} \cdot \cos(k\delta_n)) \cdot \nabla W(\delta_n) \\ \quad + \sum_n m_n \cdot \left\{ \frac{\sigma_{0i} - \sigma_{0n}}{\rho_{0i} \cdot \rho_{0n}} \right\} \cdot \sin(k\ \delta_n) \cdot \nabla^2 W(\delta_n) \end{cases}$$

Where $P_{0i} = (\nabla_{\rho_i} \frac{\sigma_i}{\rho \cdot \rho_{0n}})_{\rho_{0i}}$ and $P_{0n} = (\nabla_{\rho_n} \frac{\sigma_n}{\rho \cdot \rho_{0i}})_{\rho_{0n}}$.

As in (6.16), equation (6.24) includes different mechanisms that are behind the development of the instabilities.

For models with constant background stress $\sigma_{0i} \approx \sigma_{0n}$ and where $\rho_{0i} \approx \rho_{0n}$, $P_0 = P_{0i} \approx P_{0n}$ the relations (6.23) and (6.24) above reduce to the following system (6.25):

$$\begin{cases} \omega_r^2(k) - \omega_i^2(k) = P_0 \left\{ \left(\sum_{n=-\infty}^{\infty} m_n . \sin(k\ \ \delta_n) \cdot \nabla W(\delta_n) \right)^2 - \left(\sum_{n=-\infty}^{\infty} m_n . (1 - \cos k\ \delta_n) \cdot \nabla W(\delta_n) \right)^2 \right\} \\ \omega_r(k) \cdot \omega_i(k) = P_0 \cdot \sum_{n=-\infty}^{\infty} m_n \sin(k\ \delta_n) \cdot \nabla W(\delta_n) \cdot \sum_{n=-\infty}^{\infty} m_n . (1 - \cos k\ \delta_n) \cdot \nabla W(\delta_n) \end{cases}$$

The solution of the system above is given by:

$$\begin{cases} \omega_r^{\,2}(k)_{\pm} = P_0 \cdot A_0^{\,2} \\ \omega_i(k)_{\pm} = \sqrt{P_0} \cdot A_c \end{cases} \tag{6.26}$$

Where $A_0^{\,2} = \left(\sum_n m_n \cdot \sin(k\,\delta_n) \cdot \nabla W(\delta_n) \right)^2$ and $A_c^2 = \left(\sum_n m_n \cdot (1 - \cos k\,\delta_n) \cdot \nabla W(\delta_n) \right)^2$.

Here again, one ignores 'evanescent waves' $\omega_-^2(k)$ and considers only propagating waves $\omega_+^2(k)$ such that $P_0 > 0$.

In symmetric distribution and for long waves propagation, when $A_c \to 0$, the second formulation 'Weighted difference formalism' in these limit is marginally stable (perturbations are neither amplified nor attenuated) $(\omega_i(k) \to 0)$.

Recently, Belytschko et *al* [18] derived the same relation by using Lagrangian kernel (Lagrangian integral) combined with the first formulation 'SPH formalism'.

6.7 Numerical Example

The same numerical test is performed with the second formulation, figures (6-6) and (6-7) represent the frequency and the amplification factor at instants.

The colours of the plots indicate time history as follow.

$$\begin{aligned} &\textit{red curves} \quad \Leftrightarrow \quad t_0 = 0.204\ \mu s \\ &\textit{blue curves} \quad \Leftrightarrow \quad t_1 = 0.485\ \mu s \\ &\textit{black curves} \quad \Leftrightarrow \quad t_2 = 1.01\ \mu s \end{aligned}$$

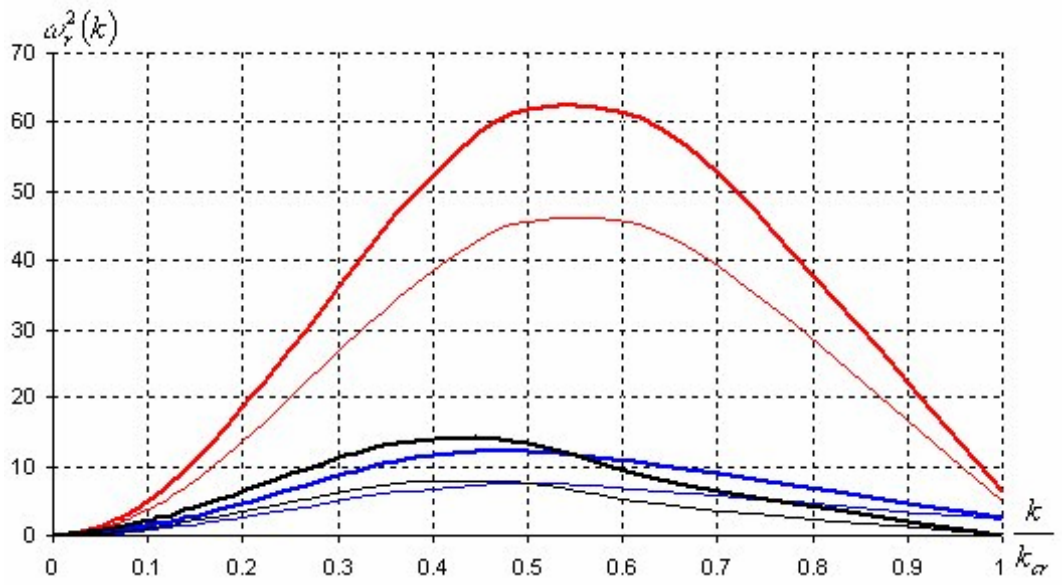

Figure 6-6: Plots of $\omega_r^2(k)$ at times different instants

The graph above shows an abnormal change in the frequencies. These reduce six times for all modes over the time period considered. This drop indicates that the phase velocities of waves are smaller and that the waves propagate slowly in the material.

The formulation shows also that the non-dispersive zone is located for long waves $k \leq 0.2 \cdot k_{cr}$. The model with constant background stress gives inaccurate frequencies, and lower than their counterpart obtained by the first SPH formulation.

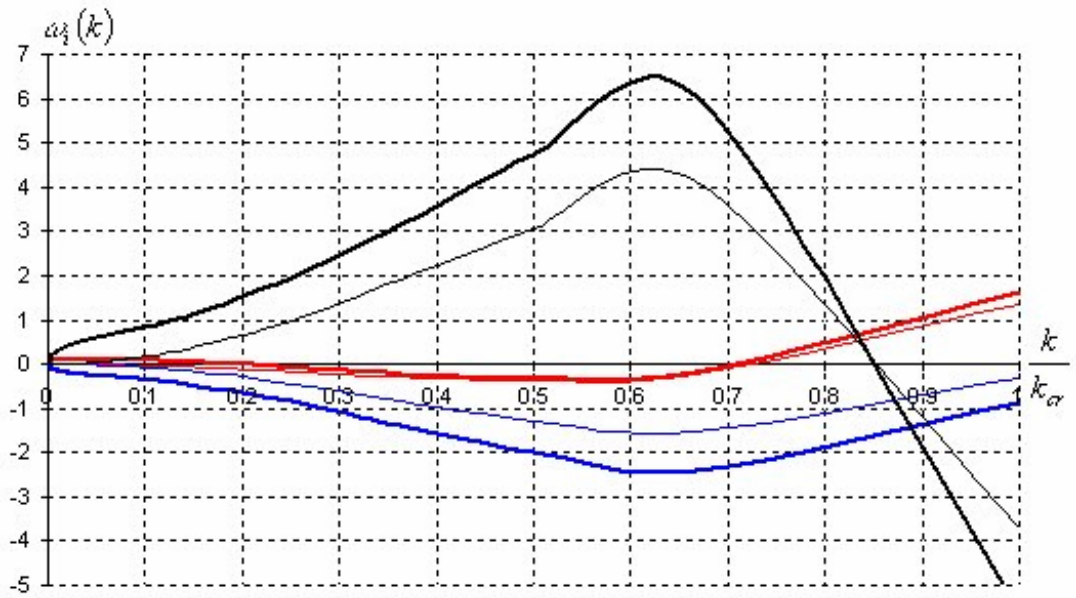

Figure 6-7: Plots of the amplification factor $\omega_i(k)$ at different instants

The amplification factor in Figure 6-7 changes its sign as time evolves, in comparison to Figure 6-2, the amplitude of the amplification factor is much higher. Here again, constant background stress model shows its limitation concerning its capacity to predict accurate results.

The amplification factor can be decomposed as:

$$\omega_i(k) = \Omega_1(k) + \Omega_2(k) + \Omega_3(k) \tag{6.27}$$

With:

$$\Omega_1(k) = \frac{\rho_{0i} \cdot \sum_{n'} \frac{m_{n'}}{\rho_{0n'}} \cdot (1 - \cos k\,\delta_{n'}) \cdot \nabla W(\delta_{n'}) \cdot \sum_{n} m_n \cdot P_{0n} \cdot \sin(k\,\delta_n) \cdot \nabla W(\delta_n)}{2 \cdot \omega_r(k)}$$

$$\Omega_2(k) = \frac{\rho_{0i} \cdot \sum_{n'} \frac{m_{n'}}{\rho_{0n'}} \cdot \sin(k\,\delta_{n'}) \cdot \nabla W(\delta_{n'}) \cdot \sum_{n} m_n (P_{0i} - P_{0n} \cdot \cos k\delta_n) \cdot \nabla W(\delta_n)}{2 \cdot \omega_r(k)}$$

$$\Omega_3(k) = \frac{\sum_{n} m_n \cdot \left\{ \frac{\sigma_{0i} - \sigma_{0n}}{\rho_{0i} \cdot \rho_{0n}} \right\} \cdot \sin(k\,\delta_n) \cdot \nabla^2 W(\delta_n)}{2 \cdot \omega_r(k)}$$

One can see that $\Omega_3(k) = 0$ for systems with constant background stress and graphical representations of $\Omega_1(k)$, $\Omega_2(k)$ and $\Omega_3(k)$ are given below.

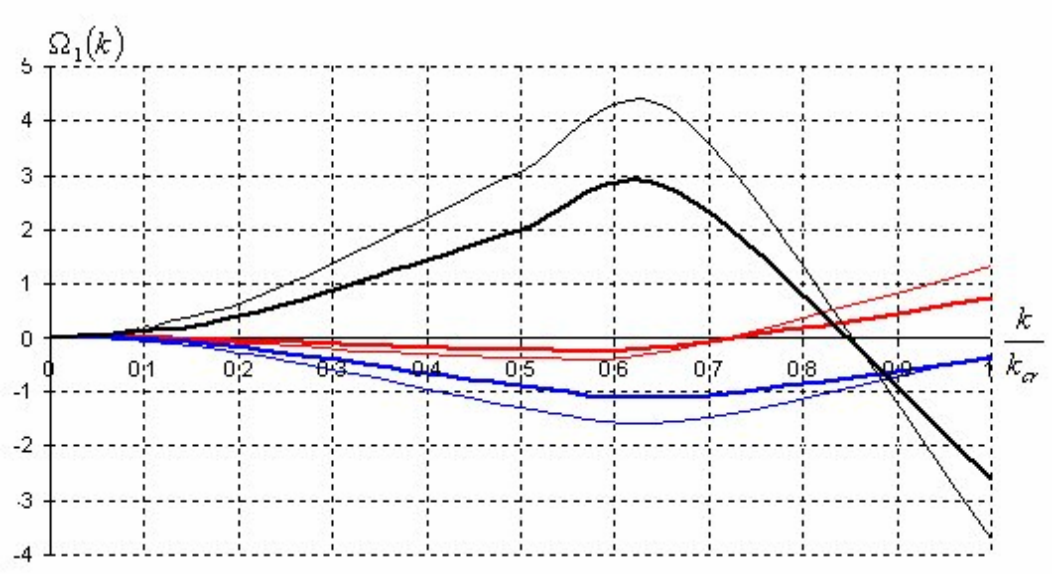

Figure6-8: $\Omega_1(k)$, the amplification due **to the absence of a regular distribution**

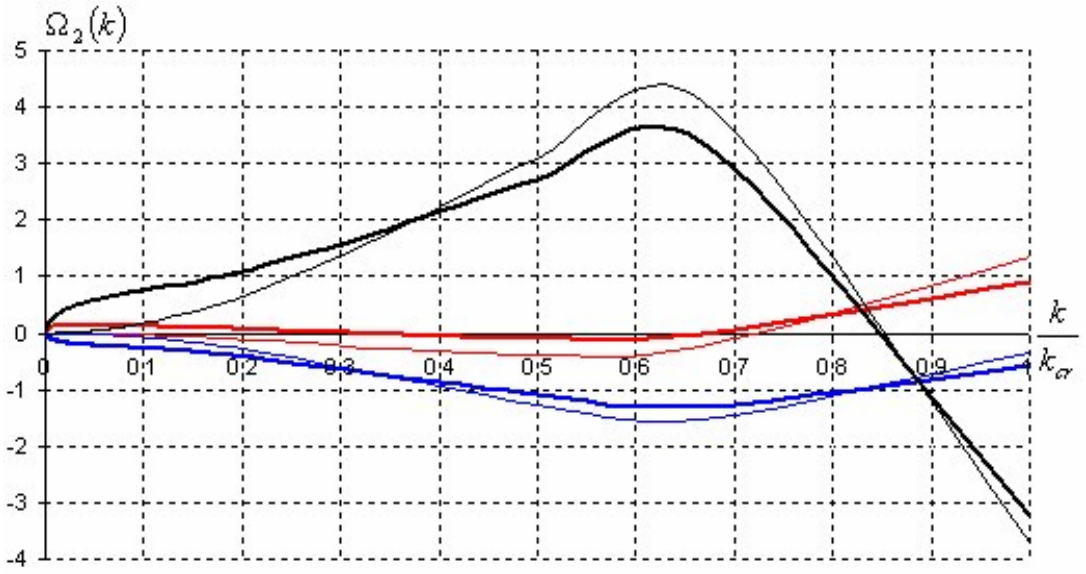

Figure 6-9: $\Omega_2(k)$, the amplification due **to the absence of a regular background stress**

As in figure 6-3, figure 6-8 shows that the distribution of particles has negligible effect on the global modes $(k \le 0.2 \cdot k_{cr})$.

In contrast with the first formulation, where the background stress term control the stability, in the case here, the comparison of figures 6-8 and 6-9 show that except for global modes $(k \le 0.2 \cdot k_{cr})$

both the background stress term and the distribution of particles play almost an equivalent role in the development of the instability..

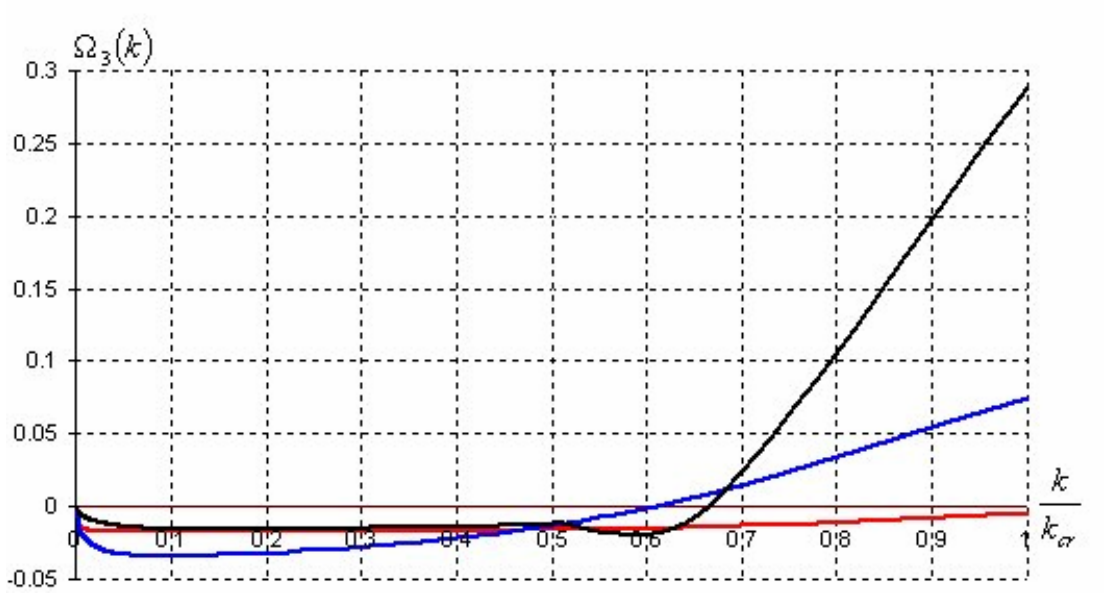

Figure 6-10: $\Omega_3(k)$, the amplification due **to the tensile term**

The graph 6-10 shows that tensile term changes its sign again around $0.6 \cdot k_{cr}$. This term has stabilizing effect for modes $(k \leq 0.6 \cdot k_{cr})$ and becomes destabilizing term for modes $(k \geq 0.7 \cdot k_{cr})$. This term increases and the simulation diverges at approximately $t \approx 1.2\,\mu s$. The comparison of the curve above to the curve in figure 6-5 shows a nearly perfect opposition (symmetry) in the behaviour of the tensile term.

6.7.1 Summary

The linear analysis for the second formulation shows again the existence of three mechanisms responsible for the instability except for the cases where constant background stress assumption was made (in this case tensile term vanishes).

Frequencies, amplification factors and their corresponding components were plotted at approximately the same instants as for the first SPH formulation. The second formulation is unstable and diverges after a period of time of $t \approx 1.2\,\mu s$.

In this second SPH formulation, our numerical test shows that the mechanism due to the absence of the regular distribution of the particles and the non-uniform background stress term are responsible of the development of the instability for both short modes $\left(k \le 0.3 \cdot k_{cr}\right)$ and intermediate modes $\left(0.3 \le k \le 0.8 \cdot k_{cr}\right)$, in the same time the tensile term develops the instability for modes such that $\left(k \ge 0.8 \cdot k_{cr}\right)$.

6.8 Linear Equations in NSPH

To achieve linear consistency, SPH method has been reformulated in [8]. The aims of these corrections are, to guarantee the normalization condition and to improve SPH derivative estimates for the gradient of the stress and the divergence of the velocity field. Detailed derivations of these corrections can be found in [8, 16 and 17]. Here, one gives a brief description.

Any field $\psi(x,t)$ is smoothed by normalized kernel, then

$$\left\langle \psi(x_i,t) \right\rangle_N \approx \frac{\sum_n \frac{m_n}{\rho_n} \cdot \psi_n(t) \cdot W(x_i - x_n, h)}{\sum_n \frac{m_n}{\rho_n} \cdot W(x_i - x_n, h)} = \frac{\left\langle \psi(x_i,t) \right\rangle}{M(x_i)} \tag{6.28}$$

And its derivative in $1D$ is estimated by:

$$\left\langle \nabla_{x_i} \psi(x_i,t) \right\rangle_N \approx \frac{\sum_n \frac{m_n}{\rho_n} \cdot (\psi_i - \psi_n(t)) \cdot \nabla_{x_i} W(x_i - x_n, h)}{\sum_n \frac{m_n}{\rho_n} (x_i - x_n(t)) \cdot \nabla_{x_i} W(x_i - x_n, h)} = \frac{\left\langle \nabla_{xi} \psi(x_i,t) \right\rangle}{N(x_i)} \tag{6.29}$$

Where $M(x)$ and $N(x)$ are the first and the second function of normalization and are expressed by:

$$M(x) = \sum_n \frac{m_n}{\rho_n} \cdot W(x - x_n, h) \qquad (6.30-a)$$

$$N(x) = \sum_n \frac{m_n}{\rho_n} \cdot \nabla_{x_n} W(x - x_n, h) \qquad (6.30-b)$$

It follows then, the normalized SPH formalism:

$$\begin{cases} \dfrac{dx_i(t)}{dt} = u(x_i, t) \\ \dfrac{du(x_i,t)}{dt} = -N(x_i)^{-1} \cdot \sum_n m_n . (\dfrac{\sigma_n^{xx} - Q_n - \sigma_i^{xx} + Q_i}{\rho_i \cdot \rho_n}) . \nabla_{xi} W(x_i - x_n, h) \\ \dfrac{d\rho(x_i,t)}{dt} = \rho(x_i,t) \cdot N(x_i)^{-1} . \sum_n \dfrac{m_n}{\rho_n} . (u_i - u_n) . \nabla_{x_i} W(x_i - x_n, h) \end{cases} \qquad (6.31)$$

6.8.1 Stability of the Normalized formulation

The analysis of the normalized formulation takes $N(x_i)$ in consideration, then, following the strategy of linearization based on Taylor expansion as before around ρ_{0n}, ρ_{0i} and x_{0i} one obtains:

$$\begin{aligned} N(x_i)^{-1} \cdot \left(\frac{\sigma_i - \sigma_n}{\rho_i \cdot \rho_n} \right) \approx N(x_{0i})^{-1} \cdot \left(\frac{\sigma_i - \sigma_n}{\rho_i \cdot \rho_n} \right)_{\rho_{0i} \cdot \rho_{0n}} + \delta\rho_i \cdot N(x_{0i})^{-1} \cdot \left(\nabla_{\rho_i} \frac{\sigma_i}{\rho_i \cdot \rho_{0n}} \right)_{\rho_{0i}} \\ - \delta\rho_n \cdot N(x_{0i})^{-1} \cdot \left(\nabla_{\rho_n} \frac{\sigma_n}{\rho_{0i} \cdot \rho_n} \right)_{\rho_{0n}} - \delta\, x_i \cdot \left(\frac{\sigma_i - \sigma_n}{\rho_i \cdot \rho_n} \right)_{\rho_{0i}, \rho_{0n}} \cdot \left(N^{-2}(x_i) \cdot \nabla_{xi} N(x_i) \right)_{x_{0i}} \end{aligned} \qquad (6.32)$$

Where, $\sigma_i = \sigma(\rho_{0i} + \delta\ \rho_i)$, $\sigma_n = \sigma(\rho_{0n} + \delta\ _n\ )$ and $N(x_i) = N(x_{0i} + \delta\ x_i)$

The linearization procedure applied to the expression $N(x_i)$ gives (6.33):

$$
\begin{aligned}
N(x_i) &= \sum_n \frac{m_n}{\rho_n} \cdot (x_i - x_n) \cdot \nabla W(x_i - x_n) \\
&= \sum_n m_n \cdot \frac{\left\{x_{0i} - x_{0n} + X \cdot \left(e^{j\cdot\phi_i} - e^{j\cdot\phi_n}\right)\right\}}{\rho_{0n} + R \cdot e^{j\cdot\phi_n}} \cdot \nabla W(x_{0i} - x_{0n} + X \cdot \left(e^{j\cdot\phi_i} - e^{j\cdot\phi_n}\right)) \\
&\approx \sum_n \frac{m_n}{\rho_{0n}} \cdot \left\{x_{0i} - x_{0n} + X \cdot \left(e^{j\cdot\phi_i} - e^{j\cdot\phi_n}\right)\right\} \cdot \nabla W(x_{0i} - x_{0n} + X \cdot \left(e^{j\cdot\phi_i} - e^{j\cdot\phi_n}\right)) \cdot \left\{1 - \frac{R}{\rho_{0n}} \cdot e^{j\cdot\phi_n}\right\} \\
&\approx N(x_{0i}) + X \cdot e^{j\cdot\phi_i} \cdot \sum_n \frac{m_n}{\rho_{0n}} \cdot \left(1 - e^{j\cdot\delta_n}\right) \cdot \left(\nabla W(\delta_n) + (x_{0i} - x_{0n}) \cdot \nabla^2 W(\delta_n)\right)
\end{aligned}
$$

In the equation above, terms with $\frac{R}{\rho_{0n}} \cdot e^{j\cdot\phi_n}$ were omitted because $\frac{m_n}{\rho_{0n}} \frac{R}{\rho_{0n}} <<< 1$ and the higher order terms in X were omitted. The first term in the right hand side of (6.33) expresses the second normalization coefficient for unperturbed system.

$$
N(x_{0i}) = \sum_n \frac{m_n}{\rho_{0n}} \cdot \left(x_{0i} - x_{0n}\right) \cdot \nabla W(\delta_n) \tag{6.34}
$$

In one hand, the first order term in the right hand side of (6.33) can be expressed as a perturbation of $N(x_i)$ via the perturbation of the particles positions, in the second hand, this term can be identified as the gradient of $N(x_i)$, then:

$$
\left(\nabla N(x_i)\right)_{x_{0i}} \approx \sum_n \frac{m_n}{\rho_{0n}} \cdot \left(1 - e^{j\cdot k\cdot\delta_n}\right) \cdot \left(\nabla W(\delta_n) + (x_{0i} - x_{0n}) \cdot \nabla^2 W(\delta_n)\right) \tag{6.35}
$$

For symmetric kernels and regular distribution, the relation above reduces to:

$$\left(\nabla N(x_i)\right)_{x_{0i}} = -\sum_n \frac{m_n}{\rho_{0n}} \cdot e^{j\cdot k\cdot \delta_n} \cdot \left(\nabla W(\delta_n) + (x_{0i} - x_{0n}) \cdot \nabla^2 W(\delta_n)\right) \qquad (6.36)$$

The system considered here has a spatial periodicity of δ_0 then the Fourier transform $\hat{W}(k)$ of the kernel $W(z)$ has a wave number periodicity of $k_{cr} = \frac{2\cdot\pi}{\delta_0}$. It follows that:

$$W(\delta_n) = \int_{-\frac{\pi}{\delta_0}}^{\frac{\pi}{\delta_0}} \frac{dk}{2\cdot\pi} \cdot e^{-j\cdot k\cdot \delta_n} \cdot \hat{W}\left(k\right)$$

And

$$\hat{W}(k) = \delta_0 \cdot \sum_{n=-\infty}^{+\infty} e^{j\cdot k\cdot \delta_n} \cdot W(\delta_n) = \sum_{n=-\infty}^{+\infty} \frac{m_n}{\rho_{0n}} \cdot e^{j\cdot k\cdot \delta_n} \cdot W(\delta_n) \qquad (6.37)$$

In the same way, one has:

$$\left(-j\cdot k\right)^m \cdot \hat{W}(k) = \sum_{n=-\infty}^{+\infty} \frac{m_n}{\rho_{0n}} \cdot e^{j\cdot k\cdot \delta_n} \cdot \left(\nabla^m W(\delta_n)\right) \quad for\ \ m = 1,2,3\cdots \qquad (6.38)$$

Note that $x_{0i} - x_{0n} = -\delta_n$ and by using the property above for $m = 2$, one obtains:

$$\begin{aligned}\sum_{n=-\infty}^{+\infty} \frac{m_n}{\rho_{0n}} \cdot \left(x_{0i} - x_{0n}\right) \cdot e^{j\cdot k\cdot \delta_n} \cdot \nabla^2 W(\delta_n) &= -\sum_{n=-\infty}^{+\infty} \frac{m_n}{\rho_{0n}} \cdot \delta_n \cdot e^{j\cdot k\cdot \delta_n} \cdot \nabla^2 W(\delta_n) \\ &= \frac{-1}{j} \cdot \frac{\partial}{\partial k}\left(\sum_{n=-\infty}^{+\infty} \frac{m_n}{\rho_{0n}} \cdot e^{j\cdot k\cdot \delta_n} \cdot \nabla^2 W(\delta_n)\right) \\ &= -j \cdot \frac{\partial\left(k^2 \cdot \hat{W}(k)\right)}{\partial k}\end{aligned} \qquad (6.39)$$

Finally by using the expression (6.37) and (6.38), (6.36) becomes:

$$\begin{aligned}\left(\nabla N(x_i)\right)_{x_{0i}} &= j\cdot\left(k\cdot\hat{W}(k)+\frac{\partial\left(k^2\cdot\hat{W}(k)\right)}{\partial k}\right)\\ &= j\cdot k\cdot\left(3\cdot\hat{W}(k)+k\cdot\frac{\partial\hat{W}(k)}{\partial k}\right)\end{aligned} \tag{6.40}$$

Useful results that one can extract from the form (6.40) is that in the long waves limit $(k\to 0)$ or for formulations using kernels such that $\hat{W}(k)=\hat{W}(k_{cr})\cdot\left(\frac{k_{cr}}{k}\right)^3$, the expression above vanishes and the expression in (6.32) differs from the expression in (6.22) only by a factor $\frac{1}{N(x_i)}$.

Applying linearization procedure to the Normalized SPH system gives:

$$\begin{cases} -j\cdot\omega\cdot X = U \\ j\cdot\omega\cdot U\cdot e^{j\cdot\phi_i} = -R\cdot N_{0i}^{-1}\sum_{n=-\infty}^{n=+\infty} m_n\cdot\left\{P_{oi}\cdot e^{j\cdot\phi_i}-P_{0n}\cdot e^{j\cdot\phi_n}\right\}\cdot\nabla_{xi}W(\delta_n) \\ \quad -X\cdot N_{0i}^{-1}\cdot\sum_{n=-\infty}^{n=+\infty} m_n\cdot\left\{\frac{\sigma_{0i}-\sigma_{0n}}{\rho_{0i}\cdot\rho_{0n}}\right\}\cdot\left(e^{j\cdot\phi_i}-e^{j\cdot\phi_n}\right)\cdot\nabla_{xi}^2W(\delta_n) \\ \quad +X\cdot N_{0i}^{-2}\cdot e^{j\cdot\phi_i}\cdot\left(\nabla_{xi}N\right)_{0i}\cdot\sum_{n=-\infty}^{n=+\infty} m_n\cdot\left\{\frac{\sigma_{0i}-\sigma_{0n}}{\rho_{0i}\cdot\rho_{0n}}\right\}\cdot\nabla_{xi}W(\delta_n) \\ -j.\omega.R\cdot e^{j\cdot\phi_i} = \rho_{0i}\cdot U\cdot N_{0i}^{-1}\cdot\sum_{n=-\infty}^{n=\infty}\frac{m_n}{\rho_{0n}}\cdot(e^{j\cdot\phi_i}-e^{j\cdot\phi_n})\cdot\nabla_{xi}W(\delta_{i,n}) \end{cases} \tag{6.41}$$

In the above system $N_{0i}=N(x_{0i})$, $P_{0i}=\left(\nabla_{\rho_i}\frac{\sigma_i}{\rho_i\cdot\rho_{0n}}\right)_{\rho_{0i}}$ and $P_{0n}=\left(\nabla_{\rho_n}\frac{\sigma_n}{\rho_{0i}\cdot\rho_n}\right)_{\rho_{0n}}$.

By using the expressions of X and R in the momentum equation, one obtains the dispersion relation (6.42).

$$D(\omega,k)=\omega^2(k)+\rho_{0i}\cdot N_{0i}^{-2}\cdot\sum_n\frac{m_n}{\rho_{0n}}\cdot(1-e^{j\cdot k\cdot\delta_n})\cdot\nabla W(\delta_n)\cdot\sum_{n'}m_{n'}\cdot(P_{0i}-P_{0n'}\cdot e^{j\cdot k\cdot\delta_{n'}})\cdot\nabla W(\delta_{n'})$$
$$+N_{0i}^{-1}\cdot\sum_n m_n\cdot\left\{\frac{\sigma_{0i}-\sigma_{0n}}{\rho_{0i}\cdot\rho_{0n}}\right\}\cdot(1-e^{j\cdot k\cdot\delta_n})\cdot\nabla^2W(\delta_n)$$
$$-N_{0i}^{-2}\cdot\nabla N_{0i}\cdot\sum_n m_n\cdot\left\{\frac{\sigma_{0i}-\sigma_{0n}}{\rho_{0i}\cdot\rho_{0n}}\right\}\cdot\nabla W(\delta_n)=0$$

Taking into account the expression of $\nabla_x N_{0i}$ given in (6.35) for general distribution of particles, the real part of the relation above gives (6.43).

$$\begin{cases}\omega_r^2(k)-\omega_i^2(k)=-\rho_{0i}\cdot N_{0i}^{-2}\cdot\sum_n\frac{m_n}{\rho_{0n}}\cdot(1-\cos k\delta_n)\cdot\nabla W(\delta_n)\cdot\sum_{n'}m_{n'}\cdot(P_{0i}-P_{0n'}\cdot\cos k\delta_{n'})\cdot\nabla W(\delta_{n'})\\ \quad+\rho_{0i}\cdot N_{0i}^{-2}\cdot\sum_n\frac{m_n}{\rho_{0n}}\cdot\sin k\delta_n\cdot\nabla W(\delta_n)\cdot\sum_{n'}m_{n'}\cdot P_{0n'}\cdot\sin k\delta_{n'}\cdot\nabla W(\delta_{n'})\\ \quad-N_{0i}{}^{-1}\cdot\sum_n m_n\cdot\left\{\frac{\sigma_{0i}-\sigma_{0n}}{\rho_{0i}\cdot\rho_{0n}}\right\}\cdot(1-\cos k\delta_n)\cdot\nabla^2W(\delta_n)\\ \quad+N_{0i}^{-2}\cdot\sum_{n'}\frac{m_{n'}}{\rho_{0n'}}\cdot\left[(1-\cos k\delta_{n'})\cdot\left\{\nabla W(\delta_{n'})+\delta_{n'}\cdot\nabla^2W(\delta_{n'})\right\}\right]\cdot\sum_n m_n\cdot\left\{\frac{\sigma_{0i}-\sigma_{0n}}{\rho_{0i}\cdot\rho_{0n}}\right\}\cdot\nabla W(\delta_n)\end{cases}$$

And the imaginary part is given by (6.44) below.

$$\begin{cases}2.\cdot\omega_r(k)\cdot\omega_i(k)=\rho_{0i}\cdot N_{0i}{}^{-2}\cdot\sum_n\frac{m_n}{\rho_{0n}}\cdot(1-\cos k\delta_n)\cdot\nabla W(\delta_n)\cdot\sum_{n'}m_{n'}\cdot P_{0n'}\cdot\sin k\delta_{n'}\cdot\nabla W(\delta_{n'})\\ \quad+\rho_{0i}\cdot N_{0i}{}^{-2}\cdot\sum_n\frac{m_n}{\rho_{0n}}\cdot\sin k\delta_n\cdot\nabla W(\delta_n)\cdot\sum_{n'}m_{n'}\cdot(P_{0i}-P_{0n'}\cdot\cos k\delta_{n'})\cdot\nabla W(\delta_{n'})\\ \quad+N_{0i}{}^{-1}\cdot\sum_n m_n\cdot\left\{\frac{\sigma_{0i}-\sigma_{0n}}{\rho_{0i}\cdot\rho_{0n}}\right\}\cdot\sin k\delta_n\cdot\nabla^2W(\delta_n)\\ \quad-N_{0i}{}^{-2}\cdot\sum_{n'}\frac{m_{n'}}{\rho_{0n'}}\cdot\left[\sin k\delta_{n'}\cdot\left\{\nabla W(\delta_{n'})+\delta_{n'}\cdot\nabla^2W(\delta_{n'})\right\}\right]\cdot\sum_n m_n\cdot\left\{\frac{\sigma_{0i}-\sigma_{0n}}{\rho_{0i}\cdot\rho_{0n}}\right\}\cdot\nabla W(\delta_n)\end{cases}$$

The system (6.43-6.44) exhibits a fundamental difference to those obtained from other formulations by the presence of an extra-term. By splitting the last term, the equation (6.44) can be rearranged in order to identify the three mechanisms mentioned in the first and in the second formulation, then (6.45)

$$\begin{cases} 2.\cdot\omega_r(k)\cdot\omega_i(k) = \rho_{0i}\cdot N_{0i}^{-2}\cdot\sum_n \dfrac{m_n}{\rho_{0n}}\cdot(1-\cos k\delta_n)\cdot\nabla W(\delta_n)\cdot\sum_{n'} m_{n'}\cdot P_{0n'}\cdot\sin k\delta_{n'}\cdot\nabla W(\delta_{n'}) \\ + N_{0i}^{-2}\cdot\sum_n \dfrac{m_n}{\rho_{0n}}\sin k\delta_n\cdot\nabla W(\delta_n)\left\{\rho_{0i}\sum_{n'} m_{n'}\cdot(P_{0i}-P_{0n'}\cdot\cos k\delta_{n'})\cdot\nabla W(\delta_{n'}) - \sum_{n'} m_{n'}\cdot\left\{\dfrac{\sigma_{0i}-\sigma_{0n'}}{\rho_{0i}\cdot\rho_{0n'}}\right\}\nabla W(\delta_{n'})\right\} \\ + N_{0i}^{-1}\cdot\sum_n m_n\cdot\left\{\dfrac{\sigma_{0i}-\sigma_{0n}}{\rho_{0i}\cdot\rho_{0n}} - \dfrac{\delta_n}{N_{0i}}\cdot\sum_{n'} m_{n'}\cdot\left\{\dfrac{\sigma_{0i}-\sigma_{0n'}}{\rho_{0i}\cdot\rho_{0n'}}\right\}\cdot\nabla W(\delta_{n'})\right\}\cdot\sin k\delta_n\cdot\nabla^2 W(\delta_n) \end{cases}$$

For systems with constant background stress, where, $\rho_{0i}\approx\rho_{0n}$, and $\sigma_{0i}\approx\sigma_{0n}$ the equations (6.43) and (6.45) above simplify to (6.46).

$$\begin{cases} \omega_r^2(k)-\omega_i^2(k) = P_0\cdot N_{0i}^{-2}\left\{\left(\sum_{n=-\infty}^{\infty} m_n.\sin(k.\delta_n)\cdot\nabla W(\delta_n)\right)^2 - \left(\sum_{n=-\infty}^{\infty} m_n.(1-\cos k.\delta_n)\cdot\nabla W(\delta_n)\right)^2\right\} \\ \omega_r(k)\cdot\omega_i(k) = P_0\cdot N_{0i}^{-2}\cdot\sum_{n=-\infty}^{\infty} m_n\sin(k.\delta_n)\cdot\nabla W(\delta_n)\cdot\sum_{n=-\infty}^{\infty} m_n.(1-\cos k.\delta_n)\cdot\nabla W(\delta_n) \end{cases}$$

The system above differs from (6.25) by a factor N_0^2 and its solution is given by:

$$\begin{cases} \omega_r^2(k) = P_0\cdot N_0^{-2}\cdot A_0^2 \\ \omega_i(k) = \sqrt{P_0}\cdot N_0^{-1}\cdot A_c \end{cases} \qquad (6.47)$$

Where $A_0^2 = \left(\sum_n m_n \cdot \sin(k\ \delta_n) \cdot \nabla W(\delta_n) \right)^2$ and $A_c^2 = \left(\sum_n m_n \cdot (1 - \cos k\ \delta_n) \cdot \nabla W(\delta_n) \right)^2$

Same as in the second formulation, the amplification factor in NSPH is dominated by the term by $\frac{A_c}{N_0}$.

6.8.2 Numerical Example

In the plots below, time history is indicated by coloured curves as earlier. In the present formulation, this reads.

$$\begin{aligned} &\textit{red curves} \quad \Leftrightarrow \quad t_0 = 0.204\ \mu\, s \\ &\textit{blue curves} \quad \Leftrightarrow \quad t_1 = 0.491\ \mu\, s \\ &\textit{black curves} \quad \Leftrightarrow \quad t_2 = 0.767\ \mu\, s \end{aligned}$$

For the normalized SPH formulation, the plots frequencies and amplifications factors are reported in figure (6-11) and figure (6-12) at indicated instants.

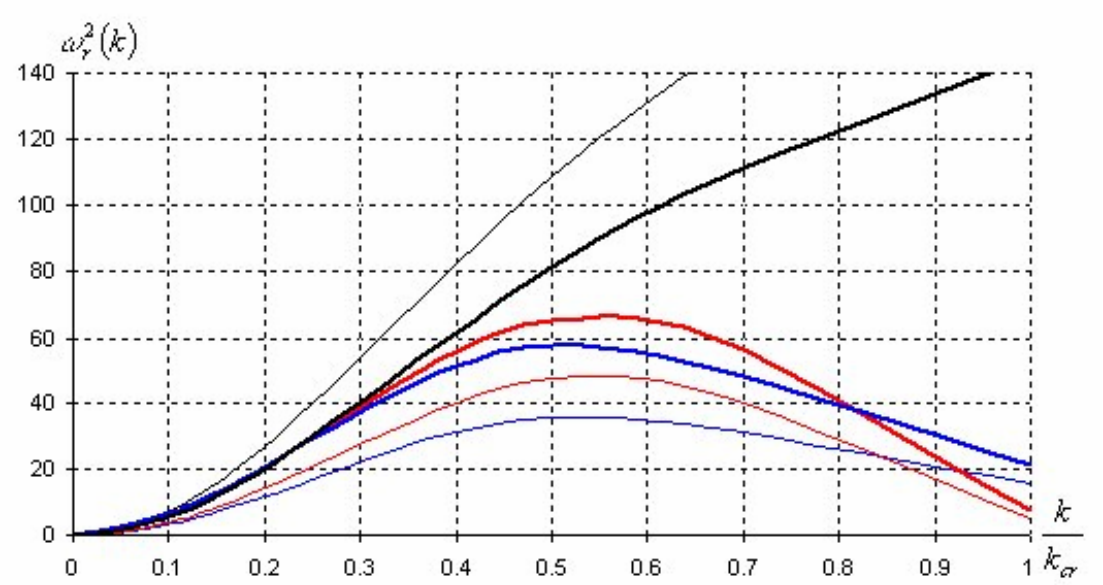

Figure 6-11: Plots of $\omega_r^2(k)$ at different times

The frequencies above have similar evolution as in the first formulation at least during a period of time, but as simulation evolves all modes see their frequencies increasing rapidly and reaching the saturation after a hundred cycles at time $t \approx 0.953\,\mu s$. The model with constant background stress produces inaccurate results concerning frequencies.

This formulation shows that the material is non-dispersion for long modes $k \le 0.2 \cdot k_{cr}$.

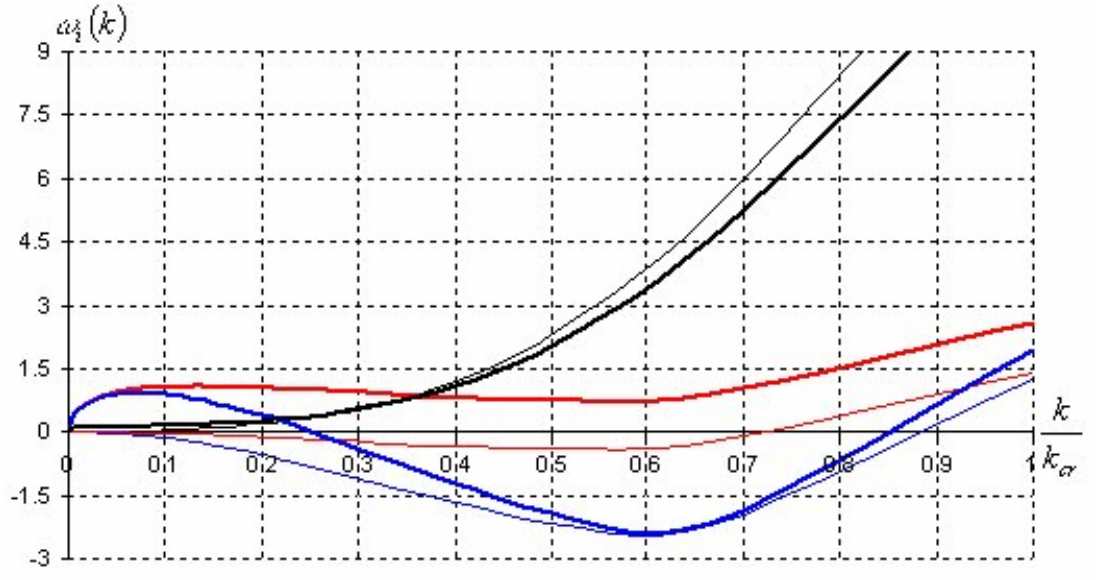

Figure 6-12: Plots of the amplification factor $\omega_i(k)$ at different times

The figure 6-12 shows some similarities with figure 6-7 for initial time steps. The amplification factor exhibits high variations at time t_1 and shows that short modes $\left(k \geq 0.8 \cdot k_{cr}\right)$ and long modes $\left(k \leq 0.2 \cdot k_{cr}\right)$ are instable while intermediates modes $\left(0.3 \cdot k_{cr} \leq k \leq 0.29 \cdot k_{cr}\right)$ are stable. Few cycles later, the amplification factor increased and reached higher values especially for short modes. This suggests that these modes are more sensitive to develop instability. The numerical experiment aborts after a period of $\approx 0.953\,\mu s$.

The figure 6-12 shows also that the constant background stress model is not able to predict reasonably neither the sign of the amplification factor nor its amplitude.

In the expression (6.46) the amplification factor can be decomposed into:

$$\omega_i(k) = \Omega_1(k) + \Omega_2(k) + \Omega_3(k) \tag{6.48}$$

With:

$$\Omega_1(k) = N_0^{-2} \cdot \frac{\rho_{0i} \cdot \sum_{n'} \frac{m_{n'}}{\rho_{0n'}} \cdot (1 - \cos k\,\delta_{n'}) \cdot \nabla W(\delta_{n'}) \cdot \sum_{n} m_n \cdot P_{0n} \cdot \sin(k\,\delta_n) \cdot \nabla W(\delta_n)}{2 \cdot \omega_r(k)}$$

$$\Omega_2(k) = N_0^{-2} \frac{\sum_{n'} \frac{m_{n'}}{\rho_{0n'}} \sin(k\,\delta_{n'}) \nabla W(\delta_{n'}) \left\{ \rho_{0i} \cdot \sum_{n} m_n (P_{0i} - P_{0n} \cdot \cos k\delta_n) \nabla W(\delta_n) - \sum_{n} m_n \frac{\sigma_{0i} - \sigma_{0n}}{\rho_{0i} \cdot \rho_{0n}} \nabla W(\delta_n) \right\}}{2 \cdot \omega_r(k)}$$

$$\Omega_3(k) = \frac{N_0^{-1}}{2 \cdot \omega_r(k)} \cdot \sum_{n} m_n \cdot \left\{ \frac{\sigma_{0i} - \sigma_{0n}}{\rho_{0i} \cdot \rho_{0n}} - \frac{\delta_n}{N_{0i}} \cdot \sum_{n'} m_{n'} \cdot \left\{ \frac{\sigma_{0i} - \sigma_{0n'}}{\rho_{0i} \cdot \rho_{0n'}} \right\} \cdot \nabla W(\delta_{n'}) \right\} \cdot \sin k\delta_n \cdot \nabla^2 W(\delta_n)$$

Below, figures 6-13, 6-14 and 6-15 represent the expressions above for a given times.

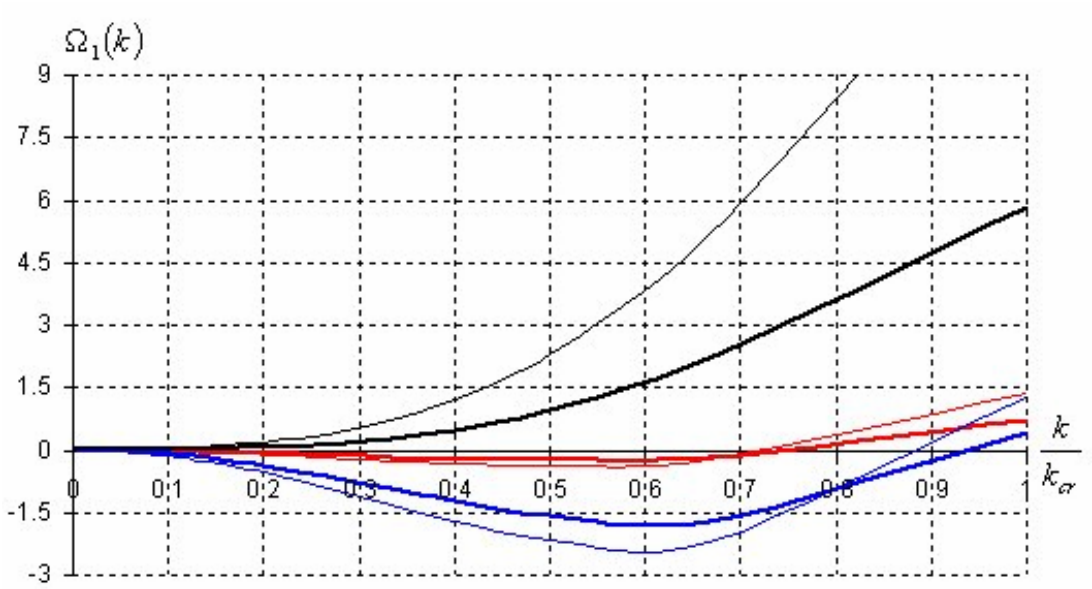

Figure 6-13: $\Omega_1(k)$, the amplification due **to the absence of a regular distribution**

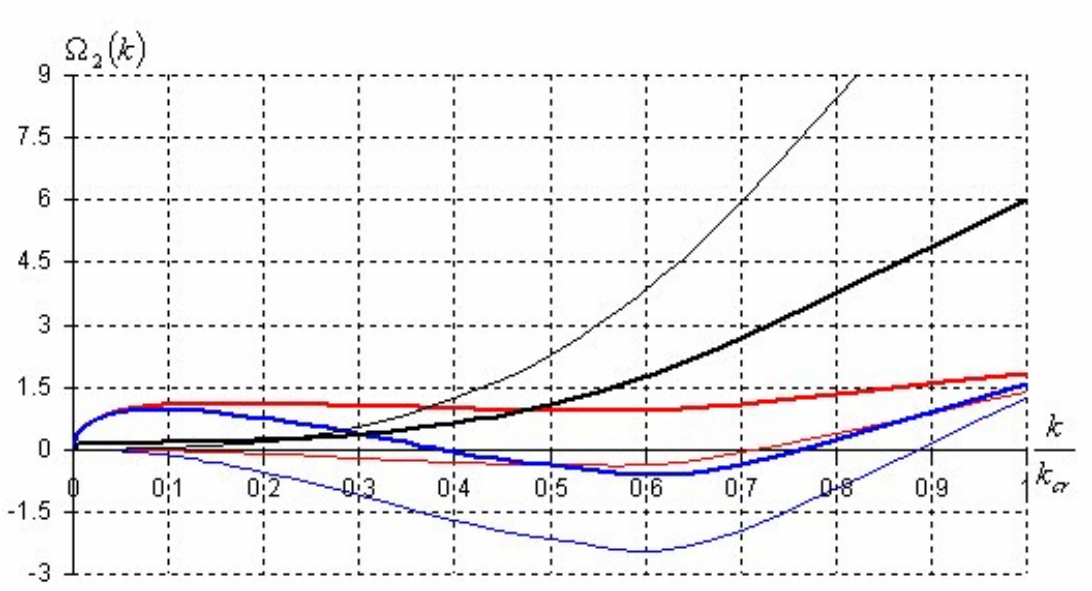

Figure 6-14: $\Omega_2(k)$, the amplification due **to the absence of a regular background stress**

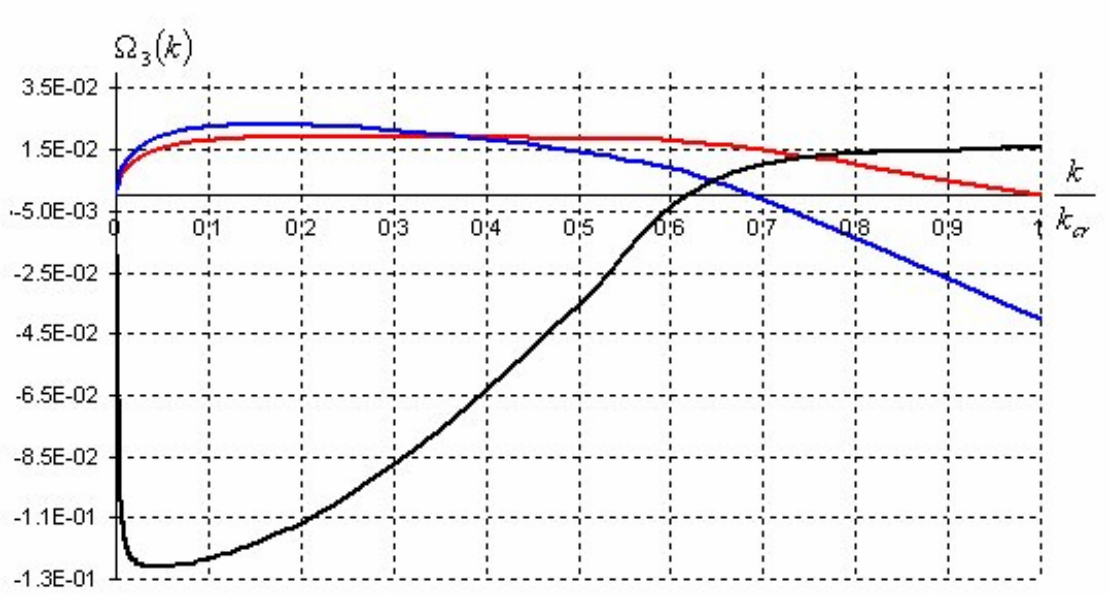

Figure 6-15: $\Omega_3(k)$ the amplification due **to the tensile term**

As in the second formulation, the roles of the particle distribution and the background stress are almost comparable and are dominant in the development of the instability. The tensile term has a destabilizing effect for intermediate and short modes, while it is stabilizing for the local modes. The curve above exihibts identical evolution to the curve in Figure 6-5 for initial time steps.

6.8.3 Summary

The linear analysis for the normalized SPH was presented. The expression of the amplification factor was modified in order to show the presence of three mechanisms responsible for the instability.

The numerical test allows us to plot frequencies, amplification factors and their corresponding components during a period of time before that the formulation diverges at $t = 0.953\,\mu s$.

In this formulation, two mechanisms; the non-regular distribution of the particles and the non-uniform background stress effect were identified as responsible of the instability. This instability seems to take place first for short modes.

The tensile term effect, due to the presence of the normalisation coefficient was kept negligible and even play a stabilising role for those modes such that $\left(k \le 0.6 \cdot k_{cr} \right)$.

6.9 Conclusion

This work has attempted to take full advantage from Von Neumann analysis by using a complex dispersion relation in order to identify different mechanism responsible of instability and the following mechanisms have identified:

- The mechanism due to the effect of non-regular distribution of the particles (Symmetry / non-Symmetry effect).
- The mechanism due to the effect of non-uniform background stress of the particles.
- The mechanism due to the tensile term.

Numerical test performed above fulfills the linearization conditions; the evaluation of these mechanisms indicates that their amplitudes are subjected to variation depending on the modes as well as on the formulation used.

The first SPH formulation and the normalized SPH formulation show globally comparable frequencies (before divergence of the NSPH) while the second formulation gives a very low frequencies. However, the first formulation produces higher frequencies than the second formulation and than the normalized form.

In the same time tensile term presents identical evolution in the first and in the last formulation.

The analysis shows that for the three formulations the particle distribution plays a minor role for global modes and becomes dominant for local modes.

Meanwhile, the background stress mechanism seems to be more important than the tensile mechanism.

Even if tensile instability subsists during the propagation, the system still is stable and the initial perturbation is damped.

In the first formulation and in the normalized formulation, the experiment shows that the tensile mechanisms are nearly identical and opposite to the tensile term in the second formulation.

The constant background stress simplification was acceptable for evaluating the frequencies but not the mechanisms of instability.

6.10 References

[1] L. Lucy. (1977): "A Numerical Approach to the Testing of the Fission Hypothesis", *The Astronomical J.*, 82, 1013-1024.

[2] R. A. Gingold and J. J. Monaghan (1977): *Mon. Not. R. Astr. Soc.*, 181, 375-389

[3] J. J. Monaghan (1982): "On the Problem of Penetration in Particle Methods", *J. of Comp. Phys*., 82, 1-15.

[4] L. Libersky, A. Petcshek., T. Carney, J. Hipp and F. Allahdadi (1993): "High Strain Lagrangian Hydrodynamics", *J. Comput. Phys*., 109, 67-75.

[5] W. Benz. (1995): "Simulation of Brittle Solids using Smoothed Particle Hydrodynamics", *Comput. Phys. Comm*., Vol. 87, 253-265.

[6] S. Johnson, R. Stryck and S. Beissel (1996): "SPH for High Velocity Impact Computations", *Comp. Meth. Appl. Mech. Engrg.*, Vol 139, 347-373.

[7] G. R. Johnson (1998):'Artificial Viscosity Effects for SPH Impact Computation', *Int. J. Impact Engng* Vol 18, No5, pp,477-488).

[8] P. Randles, L. Libersky (1996): "Smoothed Particle Hydrodynamics: Some Recent Improvements and Applications", *Comp. Methods Appl. Mech. Engrg*., Vol. 139, 375-408.

[9] G. Dilts and A. I. Haque (2000): Three-Dimensional Boundary Detection for Smoothed Particle Hydrodynamics. LA-UR-00-4419. Los Alamos National Laboratory.

[10] J. Swegle, D. Hicks, S. Attaway (1994): "An Analysis of Smoothed Particle Hydrodynamics"*, SAND93-2513*, Sandia National Laboratories, Albuquerque.

[11] J. Swegle, D. Hicks, S. Attaway (1994): "Smoothed Particle Hydrodynamics Stability Analysis"*, J. Compu. Phys.* 116,123-134

[12] D. L. Hicks, J. W. Swegle, S. W. Attaway: 'Conservative Smoothing Stabilizes Discrete-Numerical Instabilities in SPH Material Dynamics Computations' Appl. Math. Comp 85:209-226 (1997)

[13] D. Balsara (1995): "Von Neumann stability analysis of Smooth Particle Hydrodynamics suggestions for optimal algorithms". *J. Comp. Phys,* 121, 357-372.#

[14] J. P. Morris (1995): An overview of the method of Smoothed Particle Hydrodynamics. Fachbereich Mathematik. Kaiserslautern Universitat. Bericht 95-152.

[15] J. J. Monaghan(1999): 'SPH without a Tensile Instability'. *J. Compu. Phys* 159,290-311

[16] P. Randles, L. Libersky (2000): "Normalised SPH with stress Points", *Int. J. Numer. Meth. Engng*, Vol. 48,1445-1462

[17] J. Campbell, R. Vignjevic, L Libersky (2000):' A Contact algorith for Smooth Particle Hydro-Dynamics', *Comput. Methods. Appl. Mech. Engng*. Vol 184, 67-85.

[18] T. Belytschko, Y. Guo, W.K. Liu and S. P. Xiao (2000): 'A Unified Stability Analysis of Meshless Particle Methods', *Int. J. Num. Meth. Engng*, 48.1359

7. ERROR PROPAGATION AND THE AMPLIFICATIONS MATRIX IN SPH AND NSPH

7.1 Introduction

Accuracy and stability of numerical schemes are related to the requirement that the difference between the computed fields and the fields' solutions of the exact continuum equations (dynamical system) goes to zero as calculations proceed and time evolves.

These numerical errors have different origins. The first origin is round off errors due to the capacity of the computer (single, double precisions. etc), The second origin is from the truncation errors due to replacing continuous fields by sets of discrete values.

Round off errors are generally ignored because they are much smaller than truncation errors.

Even if initially both round off errors and truncation errors are small, truncation errors can grow and affect the stability of the scheme and result in non-physical solutions.

The stability of any numerical scheme resides in its ability to control the rate of growing cumulative truncation errors also the time step is restricted to a small value in comparison to the period of the system.

The measure of stability necessitates the description of the behaviour of errors by considering the space-time discretization of the equations of evolutions. Explicit numerical schemes are widely used because of they are relatively simple to implement but are conditionally stable while implicit schemes are more stable but expensive in time consuming.

The objective of the work presented here is the calculation of the amplification matrix when a central difference scheme in time is used with particles approximations. The criterion of the spectral radius to identify the domain of stability is the point of reference to identify the domains of stability.

Here, for clarity a $1D$ model only is considered and only isentropic deformation processes are investigated also, two cases are investigated and systems with regular distribution of particles and the same system with non-regular distributions and quasi-incompressible material.

The extension of the present analysis to a high space dimension systems of particles with a more complete and specific constitutive relations would not be difficult. The main problem is the exploitation of information that can be extracted from such models. The need of objective equations of evolution (Jaumann rate, Truesdell rate or Green Naghdi rate) for the deviatoric stress, Benson [1] and the equations of displacements and accelerations for each space dimensions increases the number of the eigenvalues to be considered and a clear representation of the domain of stability becomes out of reach.

Randles *et al* [2] in their investigation on the stability of the Dual Particle Dynamic DPD and SPH in 2D used an elasticity tensor combined to an incremental scheme to update the constitutive relation.

7.2 Amplification Matrix

To integrate numerically the equations of motion in time, a central difference scheme is used. One starts by assuming that initial conditions are known. The system to integrate is expressed by.

$$\begin{cases} \rho_i^{\,n} = \rho_i^{\,n-1} + \left(\dfrac{d\rho_i}{dt} \right)^{n-\frac{1}{2}} \cdot dt^{\,n-\frac{1}{2}} \\ u_i^{\,n+\frac{1}{2}} = u_i^{\,n-\frac{1}{2}} + \left(\dfrac{du_i}{dt} \right)^{n} \cdot dt^{\,n} \\ x_i^{\,n+1} = x_i^{\,n} + u_i^{\,n+\frac{1}{2}} \cdot dt^{\,n+\frac{1}{2}} \end{cases} \tag{7.1}$$

with $$x_i^{\,n-\frac{1}{2}} = x_i^{\,n} - u_i^{\,n-\frac{1}{2}} \cdot dt^{\,n-\frac{1}{2}} / 2 \tag{7.1.a}$$

and $$dt^n = (dt^{\,n-\frac{1}{2}} + dt^{\,n+\frac{1}{2}}) / 2$$

The indices n and i in (7.1) refer to the time step and to the particle i respectively while ρ, u *and* x refer to the density, velocity and position.

In order to solve the previous system one needs to close (7.1) with a relation linking the stress to one or more variable of the system. Implicitly, if σ represents the stress, then $\sigma = f(\rho, u, \nabla u, \cdots)$.

The model used is an isentropic model; where the scalar stress depends only on the density.

For the sake of clarity and for simplicity one assumes constant time step, $dt^{n-\frac{1}{2}} = dt^{n+\frac{1}{2}}$, then, the system above can be expressed in a compact form by.

$$\overrightarrow{U_i^{n+1}} = \overrightarrow{U_i^n} + dt^n \cdot \overrightarrow{F_i^n(U_i)} \tag{7.2}$$

Where the state vector is given by: $\overrightarrow{U_i}^n = \begin{pmatrix} \rho_i^{n-1} \\ u_i^{n-\frac{1}{2}} \\ x_i^n \end{pmatrix}$ and $\overrightarrow{F_i^n(U)} = \begin{pmatrix} f_{1i}^{n-\frac{1}{2}} \\ f_{2i}^n \\ f_{3i}^{n+\frac{1}{2}} \end{pmatrix} = \begin{pmatrix} \left(\frac{d\rho_i}{dt}\right)^{n-\frac{1}{2}} \\ \left(\frac{du_i}{dt}\right)^n \\ u_i^{n+\frac{1}{2}} \\ \end{pmatrix}$.

The error propagation equations are derived by letting $\vec{\varepsilon}_i^{\,n} = \begin{pmatrix} \varepsilon_\rho^{n-1} \\ \varepsilon_u^{n-\frac{1}{2}} \\ \varepsilon_x^n \end{pmatrix}_i$ be the error vector and by letting the approximate solution be $\overrightarrow{U_i^n} = \overrightarrow{\widetilde{U}_i^n} + \overrightarrow{\varepsilon_i^n}$ at time $n.dt^n$. The linearization of (7.2) around the exact solution $\overrightarrow{\widetilde{U}_i^n}$ and by equating terms of the same order one gets an expression for the error vector evolution.

$$\overrightarrow{\varepsilon_i^{n+1}} = \overrightarrow{\varepsilon_i^n} + dt^n \cdot \overline{\overline{\nabla_U F_i^{n+\frac{1}{2}}(U)}}\Big|_{\vec{\varepsilon}_i = \vec{0}} \cdot \overrightarrow{\varepsilon_i} \tag{7.3}$$

Where $\vec{\varepsilon}_i = \vec{\varepsilon}_i(n, n \pm \frac{1}{2})$ should be identified by using (8.1) and where $\overline{\overline{\nabla_U F_i^n(U)}}\Big|_{\vec{\varepsilon}_i = \vec{0}}$ should be build by a combination of the sub- Jacobean matrices with respect to the vector $\vec{U}_i$.

Because of the central difference scheme used, the errors components are evaluated at different times; the expression in (7.3) is considered in detail in order to extract the amplification matrix of the scheme.

$$\begin{pmatrix} \varepsilon_\rho^{\,n} \\ \varepsilon_u^{\,n+\frac{1}{2}} \\ \varepsilon_x^{\,n+1} \end{pmatrix}_i = \begin{pmatrix} \varepsilon_\rho^{\,n-1} \\ \varepsilon_u^{\,n-\frac{1}{2}} \\ \varepsilon_x^{\,n} \end{pmatrix}_i + dt^n \cdot \begin{pmatrix} \frac{\partial f_{1i}^{\,n-\frac{1}{2}}}{\partial \rho_i} & \frac{\partial f_{1i}^{\,n-\frac{1}{2}}}{\partial u_i} & \frac{\partial f_{1i}^{\,n-\frac{1}{2}}}{\partial x_i} \\ 0 & 0 & 0 \\ 0 & 0 & 0 \end{pmatrix} \cdot \begin{pmatrix} \varepsilon_\rho^{\,n-\frac{1}{2}} \\ \varepsilon_u^{\,n-\frac{1}{2}} \\ \varepsilon_x^{\,n-\frac{1}{2}} \end{pmatrix}_i$$

$$+ dt^n \cdot \begin{pmatrix} 0 & 0 & 0 \\ \frac{\partial f_{2i}^{\,n}}{\partial \rho_i} & \frac{\partial f_{2i}^{\,n}}{\partial u_i} & \frac{\partial f_{2i}^{\,n}}{\partial x_i} \\ 0 & 0 & 0 \end{pmatrix} \cdot \begin{pmatrix} \varepsilon_\rho^{\,n} \\ \varepsilon_u^{\,n} \\ \varepsilon_x^{\,n} \end{pmatrix}_i \qquad (7.4)$$

$$+ dt^n \cdot \begin{pmatrix} 0 & 0 & 0 \\ 0 & 0 & 0 \\ \frac{\partial f_{3i}^{\,n+\frac{1}{2}}}{\partial \rho_i} & \frac{\partial f_{3i}^{\,n+\frac{1}{2}}}{\partial u_i} & \frac{\partial f_{3i}^{\,n+\frac{1}{2}}}{\partial x_i} \end{pmatrix} \cdot \begin{pmatrix} \varepsilon_\rho^{\,n+\frac{1}{2}} \\ \varepsilon_u^{\,n+\frac{1}{2}} \\ \varepsilon_x^{\,n+\frac{1}{2}} \end{pmatrix}_i$$

The system above is non-homogenous. A variety of approximations schemes can be constructed in order to make it homogenous and then a closed system. Some of these are based on the following interpolations along with the relation (7.1-a):

$$\varepsilon_{\rho}^{n-\frac{1}{2}} = a \cdot \varepsilon_{\rho}^{n} + (1-a) \cdot \varepsilon_{\rho}^{n-1} \qquad (7.4-a)$$

$$\varepsilon_{x}^{n+\frac{1}{2}} = (1-b) \cdot \varepsilon_{x}^{n} + b \cdot \varepsilon_{x}^{n+1} \qquad (7.4-b)$$

$$\varepsilon_{u}^{n} = c \cdot \varepsilon_{u}^{n+\frac{1}{2}} + (1-c) \cdot \varepsilon_{u}^{n-\frac{1}{2}} \qquad (7.4-c)$$

$$\varepsilon_{x}^{n-\frac{1}{2}} = \varepsilon_{x}^{n} - h.o.t\left(dt^{n-\frac{1}{2}} \right) \qquad (7.4-d)$$

Where $0 \le a, b, c \le 1.$ are real constants of interpolations. Fortunately in the system (7.4), $\frac{\partial f_{3i}^{n+\frac{1}{2}}}{\partial \rho_i} = 0$, consequently no extrapolation 'implicit interpolation' is needed concerning the density error. Similarly, $\frac{\partial f_{2i}^{n}}{\partial u_i} = 0$, the error interpolation given by the relation(7.4-c) becomes irrelevant.

The choice of the closure relation is not unique and is of interest because it affects the diagonal entries of the system (7.4). Then one might be inclined to expect that mathematical expressions of the eigenvalues of the amplification matrix are dependant on the chosen closure relation; in the same time, one expects that the dominant mechanisms behind the dynamics of the error vector and the behaviour of the model are not blurred.

In this work, a 'full explicit closure' is adopted $a = b = 0$. Among other closure approximations, 'full implicit closure', $a = b = 1$ or 'implicit-explicit closure', $a = b = \frac{1}{2}$ can be used. The closure approximation chosen here provides unconditional existence of the amplification matrix, thus, the system (7.4) can be transformed into (7.5):

$$\begin{pmatrix} \varepsilon_{\rho}^{n} \\ \varepsilon_{u}^{n+\frac{1}{2}} \\ \varepsilon_{x}^{n+1} \end{pmatrix}_i = \begin{pmatrix} \varepsilon_{\rho}^{n-1} \\ \varepsilon_{u}^{n-\frac{1}{2}} \\ \varepsilon_{x}^{n} \end{pmatrix}_i + dt^n \cdot \begin{pmatrix} \frac{\partial f_{1i}^{n-\frac{1}{2}}}{\partial \rho_i} & \frac{\partial f_{1i}^{n-\frac{1}{2}}}{\partial u_i} & \frac{\partial f_{1i}^{n-\frac{1}{2}}}{\partial x_i} \\ 0 & \frac{\partial f_{2i}^{n}}{\partial u_i} & \frac{\partial f_{2i}^{n}}{\partial x_i} \\ 0 & 0 & \frac{\partial f_{3i}^{n+\frac{1}{2}}}{\partial x_i} \end{pmatrix} \cdot \begin{pmatrix} \varepsilon_{\rho}^{n-1} \\ \varepsilon_{u}^{n-\frac{1}{2}} \\ \varepsilon_{x}^{n} \end{pmatrix}_i$$

$$+ dt^n \cdot \begin{pmatrix} 0 & 0 & 0 \\ \frac{\partial f_{2i}^{n}}{\partial \rho_i} & 0 & 0 \\ \frac{\partial f_{3i}^{n+\frac{1}{2}}}{\partial \rho_i} & \frac{\partial f_{3i}^{n+\frac{1}{2}}}{\partial u_i} & 0 \end{pmatrix} \cdot \begin{pmatrix} \varepsilon_{\rho}^{n} \\ \varepsilon_{u}^{n+\frac{1}{2}} \\ \varepsilon_{x}^{n+1} \end{pmatrix}_i \qquad (7.5)$$

Where $\frac{\partial f_{\alpha i}^{m}}{\partial \chi} = \left.\frac{\partial f_{\alpha i}^{m}}{\partial \chi_i}\right|_{\varepsilon_\chi = 0}$, in this expression $\alpha = 1,2,3$, $m = n, n \pm \frac{1}{2}$ and $\chi = u, x, \rho$.

The system above in (7.5) can be rearranged by collecting terms to:

$$\left(I_d - dt^n \cdot \overline{\overline{G_i^n(U)}} \right) \cdot \vec{\varepsilon}_i^{\,n+1} = \cdot \left(I_d + dt^n \cdot \overline{\overline{H_i^n(U)}} \right) \cdot \vec{\varepsilon}_i^{\,n} \qquad (7.6)$$

Expressing, the amplification matrix $\overline{\overline{A_i^n(U)}}$ by the quantity below:

$$\overline{\overline{A_i^n(U)}} = \left(I_d - dt^n \cdot \overline{\overline{G_i^n(U)}} \right)^{-1} \cdot \left(I_d + dt^n \cdot \overline{\overline{H_i^n(U)}} \right) \qquad (7.7)$$

The error propagation equation in (7.6) takes the form:

$$\vec{\varepsilon}_i^{\,n+1} = \overline{\overline{A_i^{\,n}(U)}} \cdot \vec{\varepsilon}_i^{\,n} = \left(\overline{\overline{A_i^{\,n}(U)}}\right) \cdot \left(\overline{\overline{A_i^{\,n-1}(U)}}\right) \cdot \vec{\varepsilon}_i^{\,n-1}$$

$$= \ldots\ldots = \left(\overline{\overline{A_i^{\,n}(U)}}\right)\left(\overline{\overline{A_i^{\,n-1}(U)}}\right)\ldots\left(\overline{\overline{A_i^{\,1}(U)}}\right) \cdot \vec{\varepsilon}_i^{\,1} \tag{7.8}$$

In (7.7), I_d represents unity Matrix. The matrices $\overline{\overline{G_i^n(U)}}$ and $\overline{\overline{H_i^n(U)}}$ are given by:

$$\overline{\overline{G_i^n(U)}} = \begin{pmatrix} 0 & 0 & 0 \\ \dfrac{\partial f_{2i}^{\,n}}{\partial \rho_i} & 0 & 0 \\ \dfrac{\partial f_{3i}^{\,n+\frac{1}{2}}}{\partial \rho_i} & \dfrac{\partial f_{3i}^{\,n+\frac{1}{2}}}{\partial u_i} & 0 \end{pmatrix} \text{(7.9-a) and} \quad \overline{\overline{H_i^n(U)}} = \begin{pmatrix} \dfrac{\partial f_{1i}^{\,n-\frac{1}{2}}}{\partial \rho_i} & \dfrac{\partial f_{1i}^{\,n-\frac{1}{2}}}{\partial u_i} & \dfrac{\partial f_{1i}^{\,n-\frac{1}{2}}}{\partial x_i} \\ 0 & \dfrac{\partial f_{2i}^{\,n}}{\partial u_i} & \dfrac{\partial f_{2i}^{\,n}}{\partial x_i} \\ 0 & 0 & \dfrac{\partial f_{3i}^{\,n+\frac{1}{2}}}{\partial x_i} \end{pmatrix} \tag{7.9-b}$$

As consequence of the choice for the closure of the system (7.4), the matrix $\overline{\overline{A_i^n(U)}}$ is always defined since $\det\left|I_d - dt \cdot \overline{\overline{G(U)}}\right| = 1 \neq 0 \quad \forall (i,n) \in N^2$. From the linear combination of the expressions (7.9-a) and (7.9-b) above, one obtains the Jacobean matrix of the system considered:

$$\overline{\overline{\nabla_U F_i^n(U)}} = \overline{\overline{\nabla_U G_i^n(U)}} + \overline{\overline{\nabla_U H_i^n(U)}} \tag{7.10}$$

The explicit forms (7.10) for different SPH formulations discussed in the previous chapter are given below. For first formulation, (equations 2.1 section 2. chapter 6) is given by (7.11):

$$\overline{\overline{\nabla_U F_i^n(U)}} = \begin{pmatrix} -divu_i & \rho_i \cdot \sum_k \frac{m_k}{\rho_k} \cdot \nabla_{xi} W & \rho_i \cdot \sum_k \frac{m_k}{\rho_k} \cdot (u_i - u_k) \cdot \nabla_{xi}^2 W \\ -\nabla_{\rho i}\left(\frac{\sigma_i}{\rho_i^2}\right) \cdot \sum_k m_k \cdot \nabla_{xi} W & 0 & -\sum_k m_k \cdot (\frac{\sigma_i}{\rho_i^2} + \frac{\sigma_k}{\rho_k^2}) \cdot \nabla_{xi}^2 W \\ 0 & 1 & divu_i \end{pmatrix}$$

Its counter-part for the weighted difference form (equations 2.2 section 2. chapter 6) is (7.12):

$$\overline{\overline{\nabla_U F_i^n(U)}} = \begin{pmatrix} -divu_i & \rho_i \cdot \sum_k \frac{m_k}{\rho_k} \cdot \nabla_{xi} W & \rho_i \cdot \sum_k \frac{m_k}{\rho_k} \cdot (u_i - u_k) \cdot \nabla_{xi}^2 W \\ \frac{-1}{\rho_i} \cdot \left(\frac{du_i}{dt}\right) + \frac{\nabla_{\rho_i} \sigma_i}{\rho_i} \cdot \sum_k \frac{m_k}{\rho_k} \cdot \nabla_{xi} W & 0 & -\sum_k m_k \cdot \left(\frac{\sigma_k - \sigma_i}{\rho_k \cdot \rho_i}\right) \cdot \nabla_{xi}^2 W \\ 0 & 1 & divu_i \end{pmatrix}$$

For Normalized SPH (equations 5.5 section 5. chapter 6) the Jacobean has the form (7.13):

$$\overline{\overline{\nabla_U F_i^n(U)}} = \frac{1}{N(x_i^n)} \begin{pmatrix} -divu_i & \rho_i \cdot \sum_k \frac{m_k}{\rho_k} \cdot \nabla_{xi} W & \rho_i \cdot \sum_k \frac{m_k}{\rho_k} \cdot (u_i - u_k) \cdot \nabla_{xi}^2 W - L_i^n \cdot \left(\frac{d\rho_i}{dt}\right) \\ \frac{-1}{\rho_i} \cdot \left(\frac{du_i}{dt}\right) + \frac{\nabla_{\rho_i} \sigma_i}{\rho_i} \cdot \sum_k \frac{m_k}{\rho_k} \cdot \nabla_{xi} W & 0 & -\sum_k m_k \cdot \left(\frac{\sigma_k - \sigma_i}{\rho_k \cdot \rho_i}\right) \cdot \nabla_{xi}^2 W - L_i^n \cdot \left(\frac{du_i}{dt}\right) \\ 0 & N(x_i^n) & divu_i \end{pmatrix}$$

Where $N(x_i^n)$ is the coefficient of normalization and $L_i^n = L(x_i^n)$ are expressed respectively by.

$$N(x_i) = \sum_k \frac{m_k}{\rho_k} \cdot (x_i - x_k) \cdot \nabla_{x_i} W(x_i - x_k, h)$$

$$L(x_i) = \frac{\nabla_{xi} N(x_i)}{N(x_i)} = \frac{1}{N(x_i)} \cdot \left(\sum_k \frac{m_k}{\rho_k} \cdot \nabla_{xi} W + \sum_k \frac{m_k}{\rho_k} \cdot (x_i - x_k) \cdot \nabla_{xi}^2 W \right)$$

Where $\left(\frac{d\rho_i}{dt}\right)$ and $\left(\frac{du_i}{dt}\right)$ are given using the weighted difference formulation.

For systems with regular distributions of particles; then $\left(\sum_k \frac{m_k}{\rho_k}\cdot\nabla_{xi}W\right)\approx 0$. Obviously, for these distributions, Jacobeans and the expressions above simplify significantly. For incompressible media, the Jacobeans $\overline{\overline{\nabla_U F_i^n(U)}}$ have zero entries in its diagonal; in this case the equation of continuity in the system (7.1) is redundant and should be omitted or replaced by a trivial relation, for example $\rho_i^n = \rho_i^n$.

7.3 Stability Criteria

If any of the eigenvalues of $\overline{\overline{A^n(U)}}$ has its module larger than unity, then the original error will be eventually amplified exponentially as $\lambda_{\max}^n$. A stability criterion for time integration scheme is fulfilled when the spectral radius $\lambda_{\max} = \max\left[\left|\lambda_1\right|,\left|\lambda_2\right|,\left|\lambda_3\right|\right] \le 1$

Where $\left|\lambda_k\right|$ is the module of the k^{th} eigenvalues of the amplification matrix. These eigenvalues are found by solving for λ the equation bellow:

$$\det\left[\overline{\overline{A(U)}} - \lambda\cdot I_d\right] = 0 \tag{7.14}$$

As a result of a product of a lower diagonal matrix $\left(I_d - dt^n\cdot\overline{\overline{G(U)}}\right)^{-1}$ with an upper diagonal matrix, $\left(I_d + dt^n\cdot\overline{\overline{H(U)}}\right)$, the matrix $\overline{\overline{A^n(U)}}$ is a full matrix (no zero entries) and the following steps allow us to avoid the calculation of the matrix $\left(I_d - dt^n\cdot\overline{\overline{G(U)}}\right)^{-1}$ in the relation (7.7). For clarity, dt is used instead of dt^n and the index i is omitted.

$$\det\left[\overline{\overline{A(U)}}-\lambda\cdot I_d\right]=0 \Leftrightarrow \det\left[\left(I_d-dt\cdot\overline{\overline{G(U)}}\right)^{-1}\cdot\left(I_d+dt\cdot\overline{\overline{H(U)}}\right)-\lambda\cdot I_d\right]=0$$

$$\Leftrightarrow \det\left[\left(I_d-dt\cdot\overline{\overline{G(U)}}\right)^{-1}\cdot\left(\left(I_d+dt\cdot\overline{\overline{H(U)}}\right)-\lambda\cdot\left(I_d-dt\cdot\overline{\overline{G(U)}}\right)\right)\right]=0$$

$$\Leftrightarrow \det\left[\left(I_d-dt\cdot\overline{\overline{G(U)}}\right)^{-1}\right]\cdot\det\left[\left(I_d+dt\cdot\overline{\overline{H(U)}}\right)-\lambda\cdot\left(I_d-dt\cdot\overline{\overline{G(U)}}\right)\right]=0$$

$$\Leftrightarrow \frac{1}{\det\left[I_d-dt\cdot\overline{\overline{G(U)}}\right]}\cdot\det\left[\left(I_d+dt\cdot\overline{\overline{H(U)}}\right)-\lambda\cdot\left(I_d-dt\cdot\overline{\overline{G(U)}}\right)\right]=0$$

$$\Leftrightarrow \det\left[(1-\lambda)\cdot I_d+dt\cdot\left(\overline{\overline{H(U)}}+\lambda\cdot\overline{\overline{G(U)}}\right)\right]=0$$

7.4 Systems with regular distribution

Let $h_{i\le j}$ denotes the elements of the matrix $\overline{\overline{H(U)}}$ and $g_{i>j}$ denotes the elements of the matrix $\overline{\overline{G(U)}}$ with $i,\ j=1,2,3$.

Since here only systems with regular distributions of particles are considered, then $h_{12}=0$, also one has $g_{31}=h_{22}=0,\ g_{32}=1$ and finally $Trace\left[\overline{\overline{H(U)}}\right]=0$ which leads to $h_{33}=-h_{11}$.

With these simplifications, the determinant in (7.14) can be expressed by:

$$\det\left[\overline{\overline{A(U)}}-\lambda\cdot I_d\right]=\det\begin{pmatrix}1-\lambda-dt\cdot h_{11} & 0 & dt\cdot h_{13}\\ \lambda\cdot dt\cdot g_{21} & 1-\lambda & dt\cdot h_{23}\\ 0 & \lambda\cdot dt & 1-\lambda+dt\cdot h_{11}\end{pmatrix} \qquad (7.15)$$

It follows then:

$$\det\left[\overline{\overline{A(U)}}-\lambda\cdot I_d\right]=\lambda^2\cdot dt\cdot\widetilde{g}_{21}\cdot\widetilde{h}_{13}-\lambda\cdot\widetilde{h}_{23}\cdot dt\cdot\left(1-\lambda-\widetilde{h}_{11}\right)+\left(1-\lambda+\widetilde{h}_{11}\right)\cdot(1-\lambda)\cdot\left(1-\lambda-\widetilde{h}_{11}\right)=0$$

In the expression above, $\widetilde{h}_{ij}=dt\cdot h_{ij}$ and $\widetilde{g}_{ij}=dt\cdot g_{ij}$, after some manipulations, one gets:

$$\eta^{3} + \eta^{2} \cdot \Phi(dt) - \eta \cdot \left\{ \Phi(dt) + \Omega(dt) + \Gamma(dt)^{2} \right\} + \Omega(dt) = 0 \quad (7.16)$$

Where $\eta = 1 - \lambda$, $\Phi(dt), \Omega(dt)$ *and* $\Gamma(dt)^2$ are third and second order function in time step dt, given by:

$$\begin{aligned}
\Phi(dt) &= dt \cdot \left(\tilde{h}_{13} \cdot \tilde{g}_{21} + \tilde{h}_{23} \right) \\
&= dt^{3} \cdot h_{13} \cdot g_{21} + dt^{2} \cdot h_{23} \\
&= dt^{3} \cdot \alpha + dt^{2} \cdot \beta \\
\\
\Omega(dt) &= dt \cdot \left(\tilde{h}_{13} \cdot \tilde{g}_{21} + \tilde{h}_{11} \cdot \tilde{h}_{23} \right) \\
&= dt^{3} \cdot \left(\tilde{h}_{13} \cdot \tilde{g}_{21} + \tilde{h}_{11} \cdot \tilde{h}_{23} \right) \\
&= dt^{3} \cdot \omega \\
\\
\Gamma(dt) &= dt \cdot h_{11} = -dt \cdot \gamma
\end{aligned} \quad (7.16\text{-a})$$

In the relations above, α, ω denote combinations of fields characterising the state of the particles, terms like α, β, γ contain all physical fields and mechanisms outlined in the previous chapter.

7.4.1 Physical Meaning of α, β and ω

Before continuing the above investigations further, it may be essential to give a physical meaning of each term involved in the relations (7.16-a) within the context of the analysis.

$$\begin{aligned}
h_{11} = \gamma = \frac{\delta\rho}{\rho} &\equiv \langle \textit{Compression / Dilation Term} \rangle \\
h_{13} = \nabla^{2} u &\equiv \langle \textit{Diffusion Term} \rangle \\
h_{23} = \beta &\equiv \langle \textit{Tensile Term} \rangle
\end{aligned}$$

Concerning g_{21}, recall first that the quantity $\rho_i \cdot \nabla_{\rho_i} \sigma_i = K_i$ represents the elastic bulk modulus of the isentropic material. From now on, one refers to the term $\rho_i \cdot g_{21}$ by a **'Residual Acceleration due to the error in Density'.**

The residual acceleration is expressed by $\rho_i \cdot g_{21} = \sum_k m_k \cdot \left(\frac{\sigma_i - K_i}{\rho_i^2} - \frac{\sigma_k}{\rho_k^2} \right) \cdot \nabla W - \frac{du_i}{dt}$, for the first SPH formulation while the second and the third formulations lead to $\rho_i \cdot g_{21} = \frac{K_i}{\rho_i} \cdot \sum_k \frac{m_k}{\rho_k} \cdot \nabla W - \frac{du_i}{dt}$ and to $\rho_i \cdot g_{21} = \frac{1}{N_i} \cdot \left(\frac{K_i}{\rho_i} \cdot \sum_k \frac{m_k}{\rho_k} \cdot \nabla W - \frac{du_i}{dt} \right)$ respectively. The factors α and ω are combinations of the following:

$$\alpha \equiv \langle Diffusion * \mathrm{Re}sidual\ Acceleration \rangle / Density$$
$$\omega \equiv \langle \alpha + Compression * Tensile\,Term \rangle$$

From (7.16), it is obvious that a trivial solution is $\lambda \to 1$ when $dt \to 0$, and then the scheme is unconditionally stable. The eigenvalues solutions of (7.16) are found by using Derive 5.0 [3], and are:

$$\lambda_1 = \frac{3+\Phi}{3} - \frac{2 \cdot \Theta}{3} \cdot \sin\left[\frac{1}{3} \left(\arccos\left(-\frac{3 \cdot \Phi \cdot \Theta^2 - \Phi^3 + 27 \cdot \Omega}{2 \cdot \Theta^3} \right) + \frac{3 \cdot \pi}{2} \right) \right]$$

$$\lambda_2 = \frac{3+\Phi}{3} + \frac{2 \cdot \Theta}{3} \cdot \sin\left[\frac{1}{3} \left(\arcsin\left(\frac{3 \cdot \Phi \cdot \Theta^2 - \Phi^3 + 27 \cdot \Omega}{2 \cdot \Theta^3} \right) + \pi \right) \right]$$

$$\lambda_3 = \frac{3+\Phi}{3} - \frac{2 \cdot \Theta}{3} \cdot \sin\left[\frac{1}{3} \arcsin\left(\frac{3 \cdot \Phi \cdot \Theta^2 - \Phi^3 + 27 \cdot \Omega}{2 \cdot \Theta^3} \right) \right]$$

Where $\Theta = \sqrt{\Phi^2 + 3 \cdot (\Phi + \Omega + \Gamma^2)}$ and $\Theta \in \Re^{*+}$, the condition on the spectral radius is obtained by letting χ be the argument of the eigenvalue λ_{max}, then:

$$\lambda_{max} = \frac{3+\Phi}{3} \pm \frac{2 \cdot \Theta}{3} \cdot \sin\chi \quad \Leftrightarrow \quad -1 \le \sin\chi = \mp \frac{3 \cdot \lambda_{max} - 3 - \Phi}{2 \cdot \Theta} \le +1$$

$$\Leftrightarrow \quad -1 \le \frac{\Phi - 2 \cdot \Theta}{3} + 1 \le \lambda_{max} \le \frac{\Phi + 2 \cdot \Theta}{3} + 1 \le +1$$

This leads to conditions:

$$\begin{cases} 2 \cdot \Theta + \Phi \le 0 \\ 2 \cdot \Theta - \Phi - 6 \le 0 \end{cases} \Rightarrow \begin{cases} -2 \cdot \Theta \ge \Phi \\ 2 \cdot \Theta \le \Phi + 6 \end{cases}$$

$$\Rightarrow \begin{cases} (\Phi + 2)^2 + 4 \cdot \Gamma^2 + 4 \cdot \Omega \ge 4 \\ \Phi^2 + 4 \cdot \Gamma^2 + 4 \cdot \Omega \le 9 \end{cases} \tag{7.17}$$

The graphical representation of (7.17) in the space (Φ, Γ, Ω) is the intersection of inner and outer disks with radiuses depending on Ω.

In order to solve (7.17) for the time step dt, Randles [4] suggested that the terms containing time steps of high order (third order and higher) remain bounded, this suggest that (α, β, γ) have a finite upper and lower limits. One can then omit terms of order higher than the third order in dt in the expression of $\Phi^2(dt)$. The inequalities in (7.17) reduce to:

$$\begin{cases} 4 \cdot dt^2 \cdot \{(\omega + \alpha) \cdot dt + \beta + \gamma^2\} \ge 0 \\ 4 \cdot dt^2 \cdot \{\omega \cdot dt + \gamma^2\} \le 9 \end{cases} \Leftrightarrow \begin{cases} dt \ge \frac{-(\beta + \gamma^2)}{\omega + \alpha} = -\frac{\beta + \gamma^2}{2 \cdot \omega + \beta \cdot \gamma} \\ \omega \cdot dt^3 + \gamma^2 \cdot dt^2 - \frac{3}{2} \le 0 \end{cases} \tag{7.18}$$

Let D be the domain of solutions dt for the second inequality in (7.18), recalling that $dt=0$ is solution $(dt=0\in D)$ and since only time steps such that $dt\geq 0$ are of an interest then D takes the form below:

$$\begin{cases} D=[0.\,,T_{\min}]\cup[T_{\text{int}}\,,T_{\max}] \\ with\quad T_{\min}=Min\,\{dt_1,dt_2,dt_3\},T_{\max}=Max\,\{dt_1,dt_2,dt_3\} \\ and\quad dT_{\min}\leq dT_{\text{int}}\leq dT_{\max} \end{cases} \tag{7.19}$$

The solutions dt_1, dt_2 and dt_3 are the boundary solutions and are obtained via Derive5.0 [3] and are expressed by:

$$dt_1=-\frac{\gamma^2}{3\cdot\omega}+\frac{2\cdot\gamma^2}{3\cdot|\omega|}\cdot\cos\left[\frac{1}{3}\left(\arccos\left(\frac{81\cdot\omega^2-4\cdot\gamma^6}{4\cdot\gamma^6}\cdot sign(\omega)\right)\right)\right]$$

$$dt_2=-\frac{\gamma^2}{3\cdot\omega}+\frac{2\cdot\gamma^2}{3\cdot|\omega|}\cdot\sin\left[\frac{1}{3}\left(\arcsin\left(\frac{4\cdot\gamma^6-81\cdot\omega^2}{4\cdot\gamma^6}\cdot sign(\omega)\right)+\pi\right)\right] \tag{7.20}$$

$$dt_3=-\frac{\gamma^2}{3\cdot\omega}+\frac{2\cdot\gamma^2}{3\cdot|\omega|}\cdot\sin\left[\frac{1}{3}\left(\arcsin\left(\frac{4\cdot\gamma^6-81\cdot\omega^2}{4\cdot\gamma^6}\cdot sign(\omega)\right)\right)\right]$$

It is obvious that the domain D depends on the values $(\gamma,\omega)=(\gamma,\alpha-\gamma\cdot\beta)$. If D_S denotes the domain of stability (Domain of Solutions of the system (7.18), a necessary condition for the

existence of the stability of the space-time discretization scheme is that $D_S \subseteq D \cap \left[-\frac{\beta + \gamma^2}{2 \cdot \omega + \gamma \cdot \beta}, \infty \right[\subseteq \Re^{*+}$.

For clarity, one needs to introduce sets of surfaces in the space (γ, ω) that correspond to different boundaries of the domains D and D_S as well sets of volumes expressed by the distances between these surfaces.

A - $S^i(\gamma, \omega), i = \{1, 2, 3\}$ are surfaces representing the eigenvalues solutions $dt_i, i = \{1, 2, 3\}$ given in the graphs 7-1 to 7-3.

B - $S^\beta(\gamma, \omega) = -\frac{\beta + \gamma^2}{2 \cdot \omega + \gamma \cdot \beta}$, $\beta \in \Re$ is parametric surfaces given by the first inequality in (7.18).

C- $S^{i,j}(\gamma, \omega) = \left(S^i(\gamma, \omega) - S^j(\gamma, \omega) \right)$, i *and* $j = \{1, 2, 3\}$ That represents the gap between the surfaces $S^i(\gamma, \omega)$ *and* $S^j(\gamma, \omega)$

D- $S^{i,\beta}(\gamma, \omega) = \left(S^i(\gamma, \omega) - S^\beta(\gamma, \omega) \right)$, $i = \{1, 2, 3\}$ *and* $\beta \in \Re$ is the graph that represents the volume delimited by the surfaces $S^i(\gamma, \omega)$ *and* $S^\beta(\gamma, \omega)$.

All surfaces are represented by using Mathematica 3.0 [4], graph 7.1 and graph 7.2 represent the surfaces $S^1(\gamma, \omega < 0)$ *and* $S^1(\gamma, \omega > 0)$ respectively, the separation into cases $\omega > 0$ and $\omega < 0$ is justified later on. .

The graph 7.2 represents the shape of $S^2(\gamma, \omega)$ while the graph 7.3 shows the shape of the surface $S^3(\gamma, \omega)$, the domain of the plots is limited to $(\gamma, \omega) \in [-1000., +1000.] \times [-500., +500.]$.

Red arrows in the graphs 7-1, 7-3 and in 7-4 indicate regions within the surfaces (the eigenvalues) are either non-defined or where they exhibit non-real amplitudes (the eigenvalues are then complex numbers).

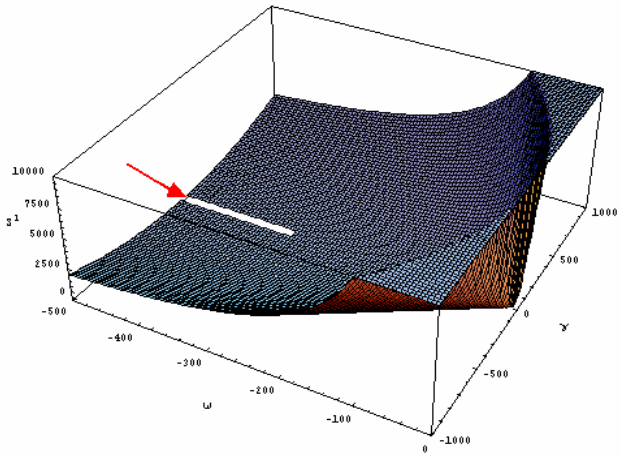

Figure 7-1: Surface $S^1(\gamma\ ,\omega\ <0)$

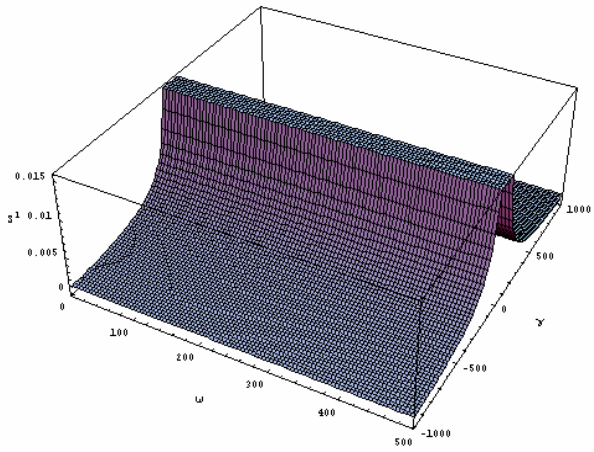

Figure 7-2: Surface $S^1(\gamma\ ,\omega\ >0)$

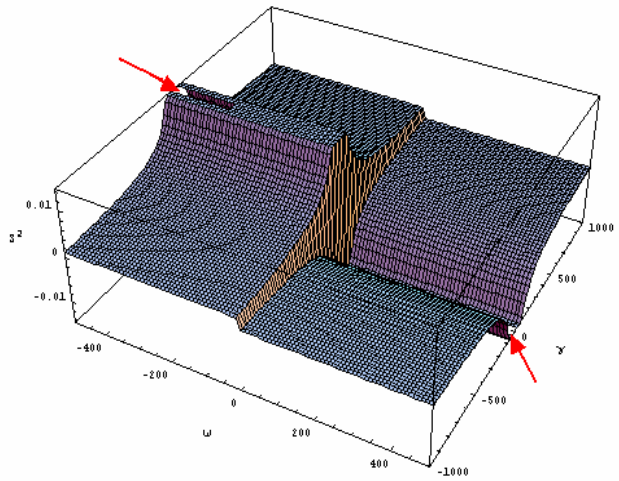

Figure 7-3: Surface $S^2(\gamma\ ,\omega\ )$

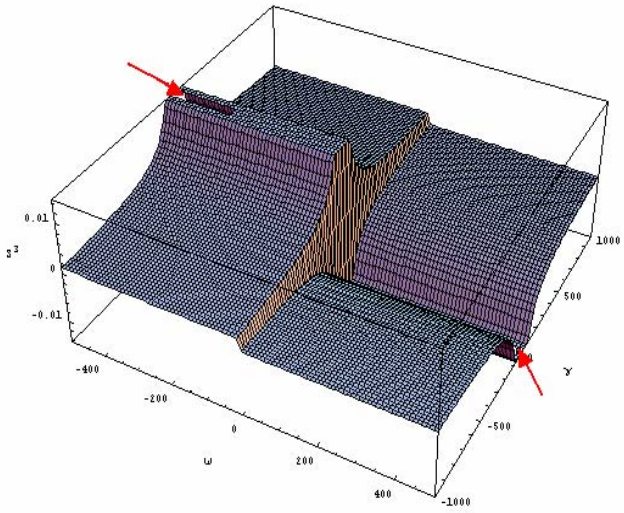

Figure 7-4: Surface $S^3(\gamma\ ,\omega\ )$

The eigenvalues $S^2(\gamma,\omega)$ and $S^3(\gamma,\omega)$ have similar shapes and comparable amplitudes for γ and ω, the difference between their amplitudes exist but is insignificant for a wide range of γ and of ω. This difference is illustrated by the shape of $S^{3,2}(\gamma\ ,\omega)$ in the figure 7-5.

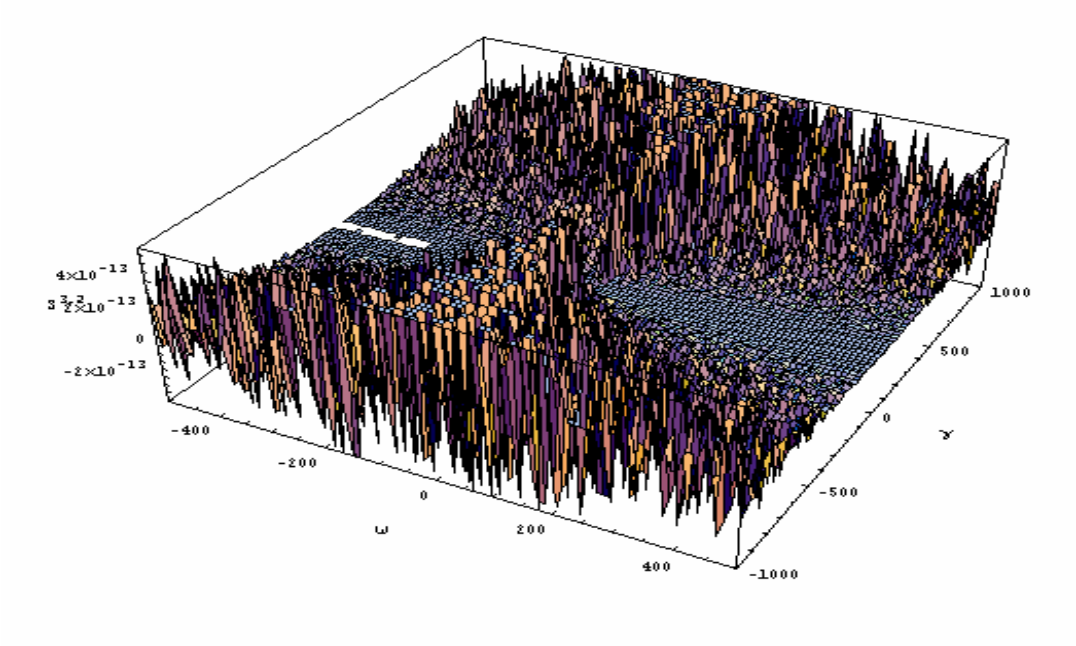

Figure 7-5: Difference $S^3(\gamma\ ,\omega\ )-S^2(\gamma\ ,\omega\ )$

As a consequence of the expressions of the eigenvalues as it can be observed from the figures 7-1 and 7-2 the gap between amplitudes of $S^1(\gamma,\omega<0)$ *and* $S^1(\gamma,\omega>0)$ is significant, the delimitation of the domains of stability requires the consideration of the case $\omega>0$ and the case $\omega<0$.

7.4.2 Case $\omega \succ 0$

One should notice that from figures 7-1, 7-2, 7-3 and 7-4 the domain D is determined only by the first eigenvalue dt_1, this leads to $D=\left[0.\,,S^1(\gamma\ ,\omega)\right]$.

The completion of the determination of the domain of stability $D_S=D\cap\left[S^{\beta}\,,\infty\right[$ requires the delimitation of its lower bound with surfaces $S^{\beta}(\gamma\ ,\omega)$, to achieve this, a series of plots where produced below, figures 7-6 to 7-13 represent the shape of surfaces $S^{\beta}(\gamma\ ,\omega)$ for some representative parameters $\beta=-20.0\,,-5.0\,,-0.5\,,\ 0.1\,,\ 0.5\,,\ 1.5\,,\ 5.0\,,20.0$.

Except for $S^{0.}(\gamma\ ,\omega)$ which is always negative, it can be seen from these figures that not only the shapes change their signs but also the heights of their amplitudes. The zones with higher amplitudes

play a major role in the delimitation of the domain of stability in the sense that they control the extension and the restriction of the domain of stability.

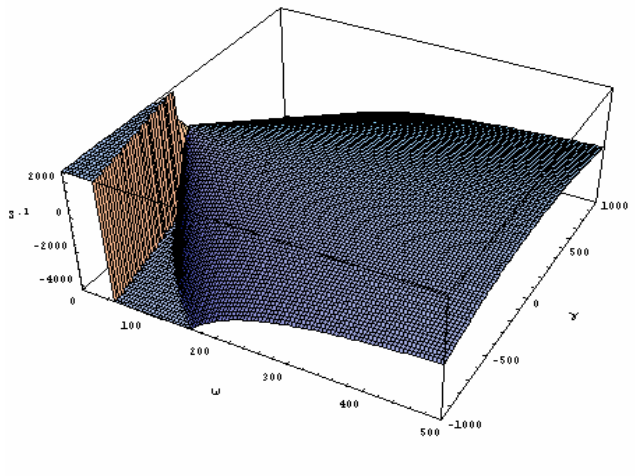

Figure 7-6: Surface $S^{0.1}(\gamma,\omega)$

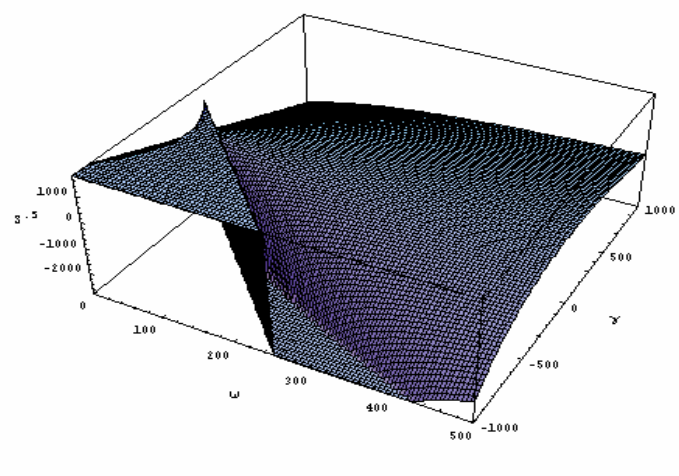

Figure 7-7: Surface $S^{0.1}(\gamma,\omega)$

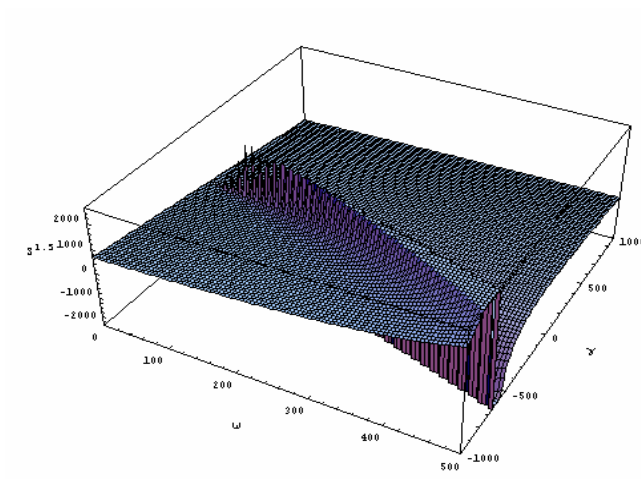

Figure 7-8: Surface $S^{1.5}(\gamma,\omega)$

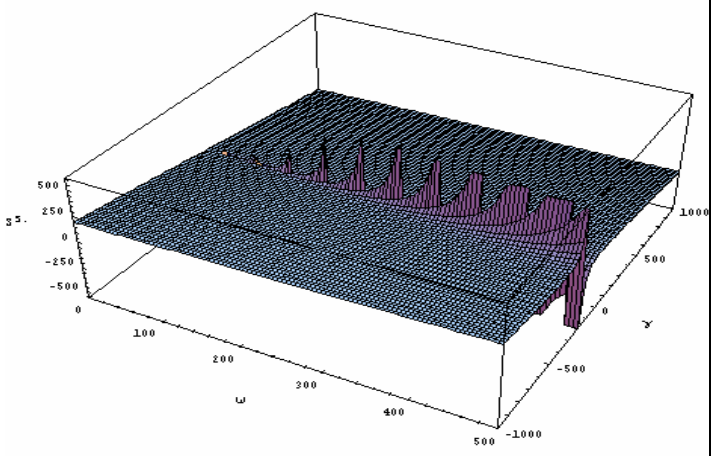

Figure 7-9: Surface $S^{5.0}(\gamma,\omega)$

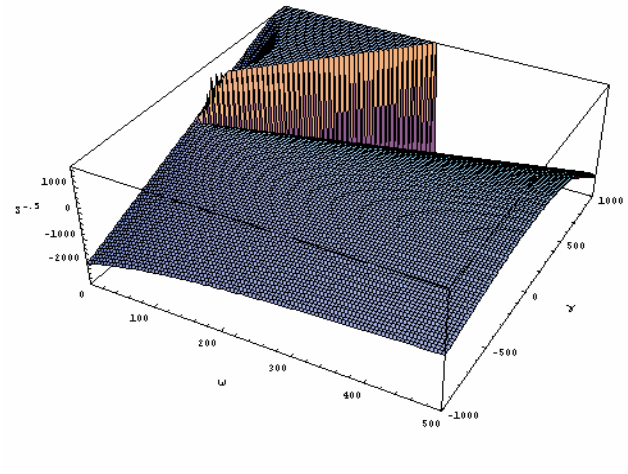

Figure 7-10: Surface $S^{-0.50}(\gamma\,,\omega)$

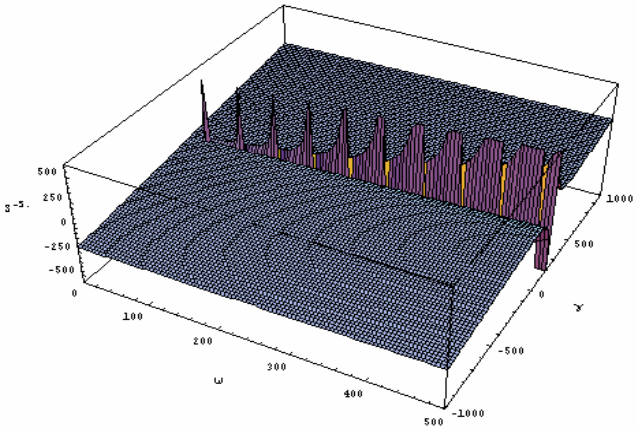

Figure 7-11: Surface $S^{-5.0}(\gamma\,,\omega)$

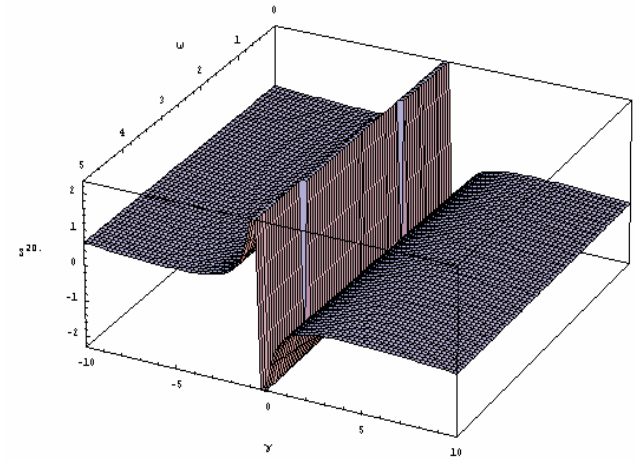

Figure 7-12: Surface $S^{+20.}(\gamma\,,\omega)$

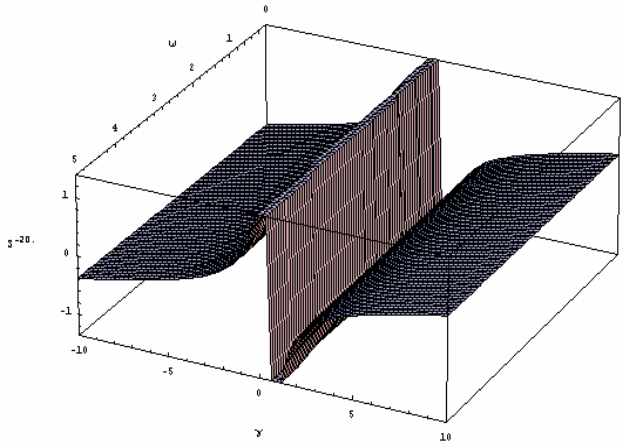

Figure 7-13: Surface $S^{-20.}(\gamma\,,\omega)$

Consider now the figures 7-14 to 7-17 which are the shapes $S^{i,\beta}$ that give an ideas of the domain of stability D_S (half- upper volume) and how it evolves with the β – *parameter*. In the following, coarse grids represent the eigenvalues, in this case $S^{1}(\gamma\,,\omega)$ while the fine grids represent surfaces $S^{\beta}(\gamma\,,\omega)$.

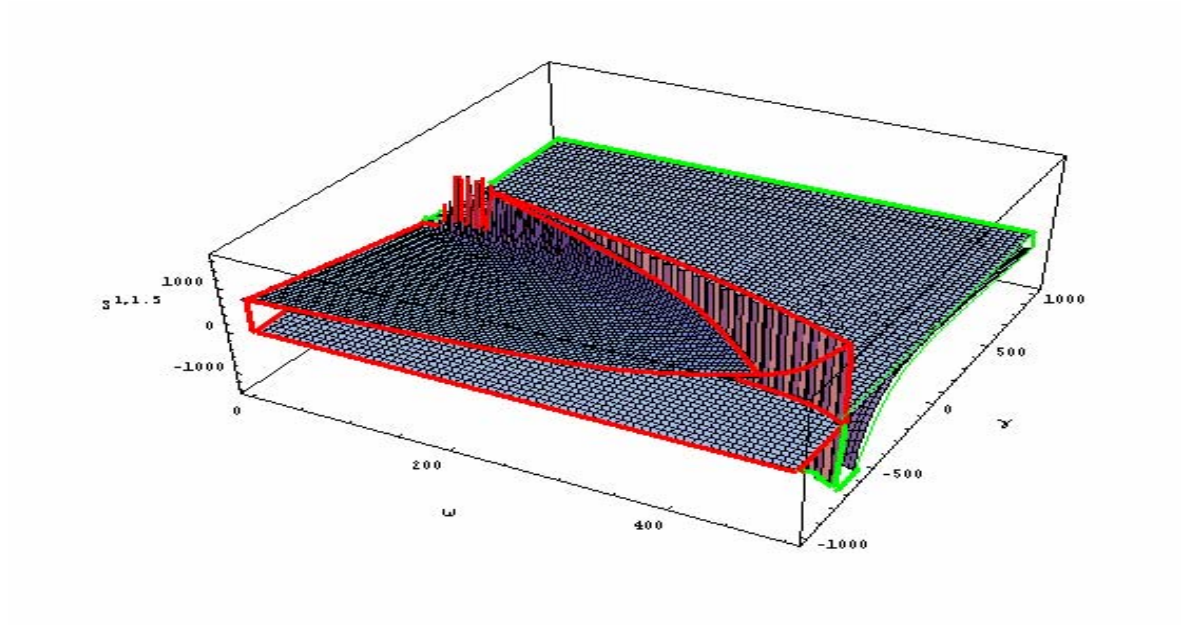

Figure 7-14: Profile of the domain $S^{1,1.5}(\gamma, \omega)$

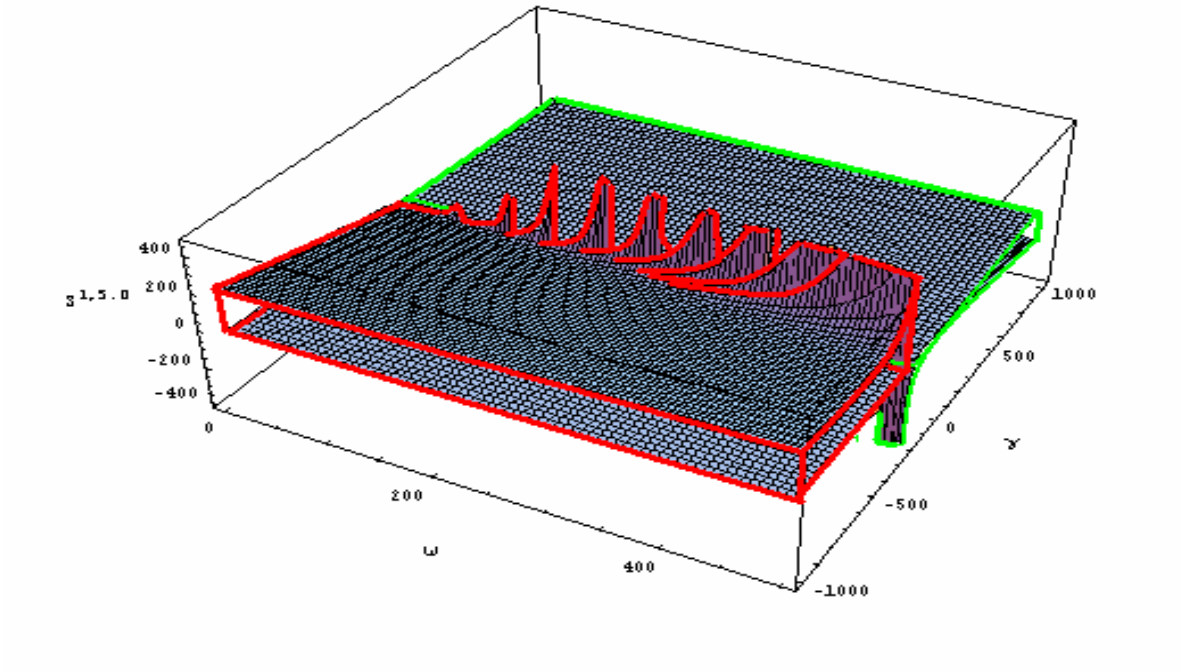

Figure 7-15: Profile of the domain $S^{1,5.0}(\gamma, \omega)$

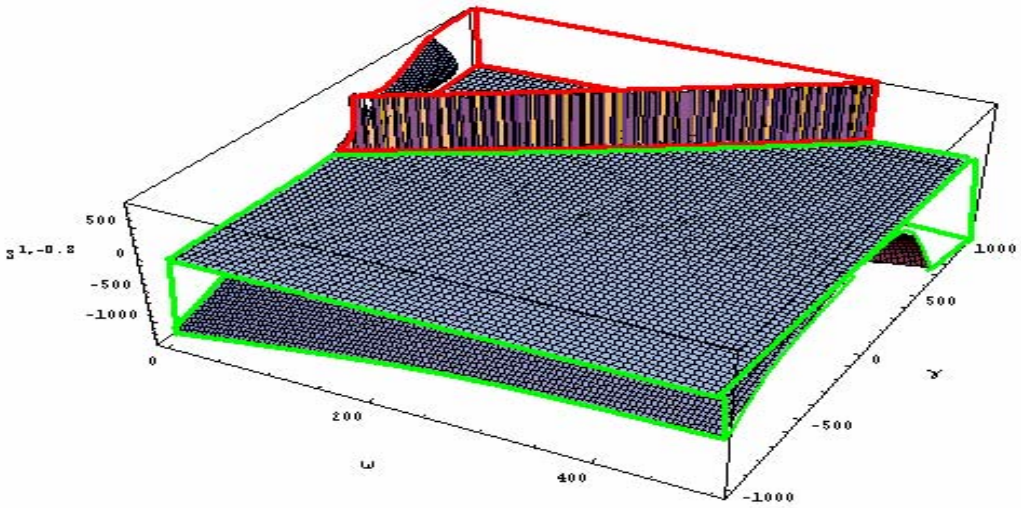

Figure 7-16: Profile of the domain $S^{1,-0.8}(\gamma, \omega)$

In the light of the figures 7-14 to 7-17 a representative picture of the domain of stability D_S can be build; these are situated at the positive amplitude within the volumes between 'Fine grids' and 'Coarse grids' in this order and are delimited by 'Green Segments'.

The zones of instability, where the stability could not be reached, were clearly shown where 'Fine grids' locates above 'Coarse grids'; these volumes are delimited by 'Red Segments'.

7.4.3 Case $\omega \prec 0$

As in the previous case, one begins by illustrating the shapes of the eigenvalues, recall that the figures 7.1, 7.2 and 7.4 represent the three eigenvalues.

A first observation of the figures above shows that the shapes of the eigenvalues are similar, that the first eigenvalue $S^1(\gamma\ ,\omega)$ has higher amplitude than those of $S^2(\gamma\ ,\omega)$ and of $S^3(\gamma\ ,\omega)$.

The amplitudes of the surfaces $S^2(\gamma\ ,\omega)\ and\ S^3(\gamma\ ,\omega)$ exhibit almost identical values. The figure 7.5 represents the difference between these surfaces and it shows the change of its sign when ω or γ approaches small values.

The fundamental difference with the previous case is that all the three eigenvalues have positive amplitudes; and the expression of the domain D is expressed by $D=[0.\ ,S_{mi}]\cup[S_{ma}\ ,S^1]$.

Where at this stage, two other entities $S_{mi}\ and\ S_{ma}$ were introduced and are given by, $S_{mi}=Min\left[S^2(\gamma\ ,\omega)\ ,S^3(\gamma\ ,\omega)\right]$, $S_{ma}=Max\left[S^2(\gamma\ ,\omega)\ ,S^3(\gamma\ ,\omega)\right]$, S_{mi} is illustrated in the figure 7-18 and the figure 7-19 show the shapes $S^1(\gamma\ ,\omega)\ and\ S_{ma}$, the space between these two surfaces represents the second part of the domain D.

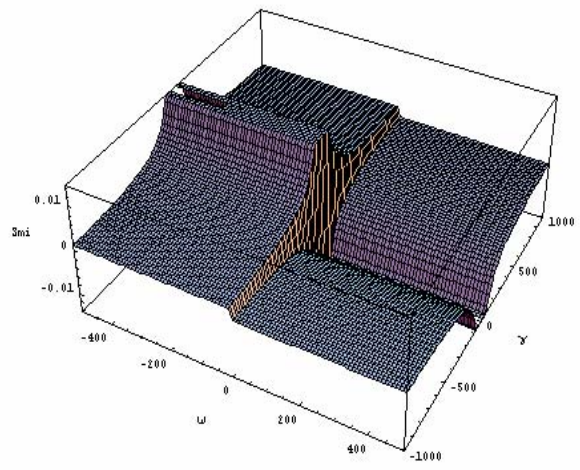

Figure 7-18: Profile of the domain $[0.\ ,S_{mi}]$

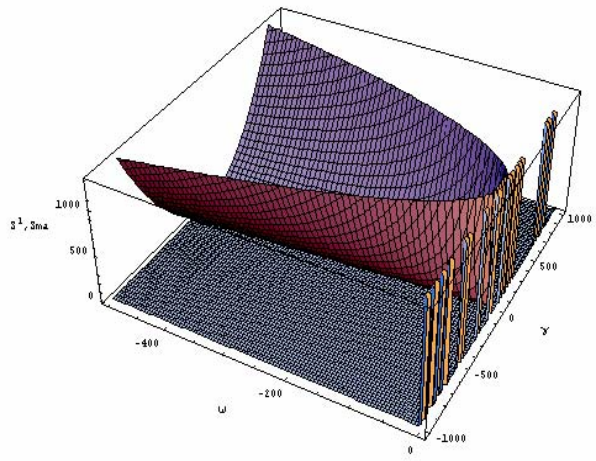

Figure 7-19: Profile of the domain $[S_{ma}\ ,S^1(\gamma\ ,\omega)]$

Below, parametric surfaces $S^{\beta}(\gamma, \omega)$ were represented for $\beta = -5.0, -1.0, -0.5, 0.5, 1.5, 5.0$ in the figures 7-20 to 7-25. as in the previous graphs, figures 7-6 to 7-13, the variation of β produces a peak of the amplitude, this peak propagates on clock-wise or anti clock-wise orientation depending on the sign of β *and* ω.

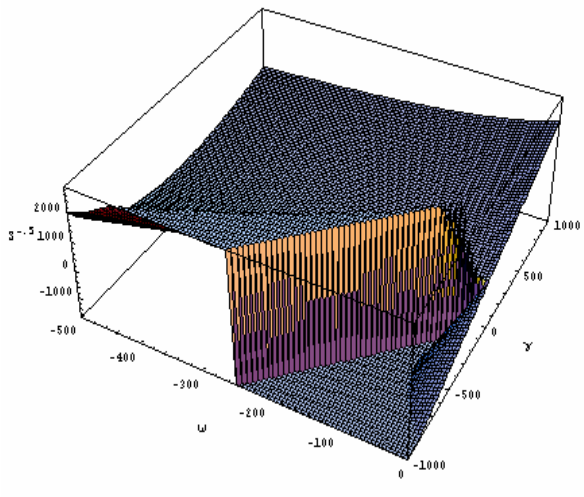

Figure 7-20: Surface $S^{-0.5}(\gamma, \omega)$

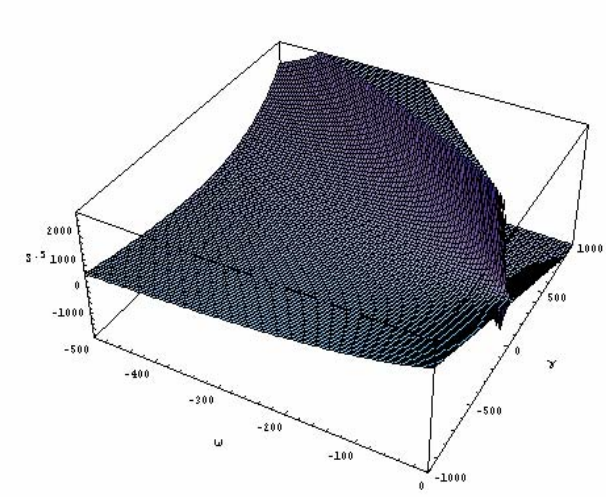

Figure 7-21: Surface $S^{0.5}(\gamma, \omega)$

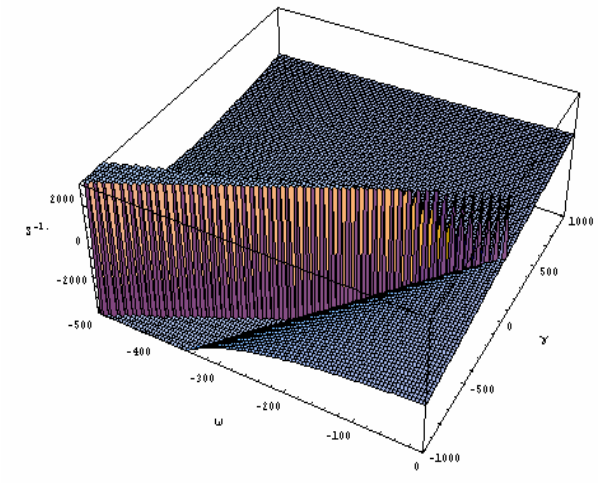

Figure 7-22: Surface $S^{-1.0}(\gamma, \omega)$

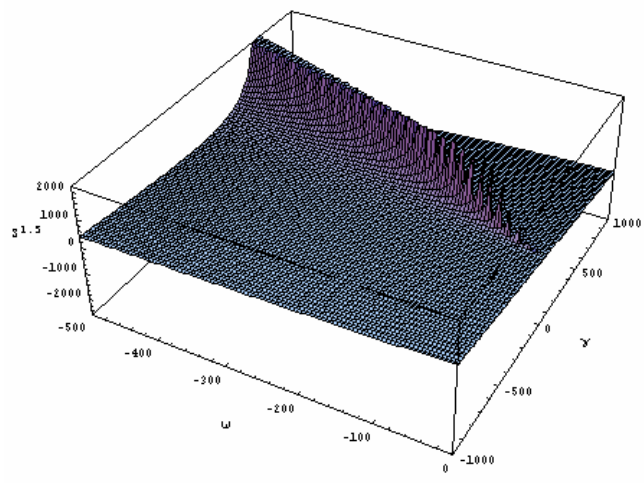

Figure 7-23: Surface $S^{1.5}(\gamma, \omega)$

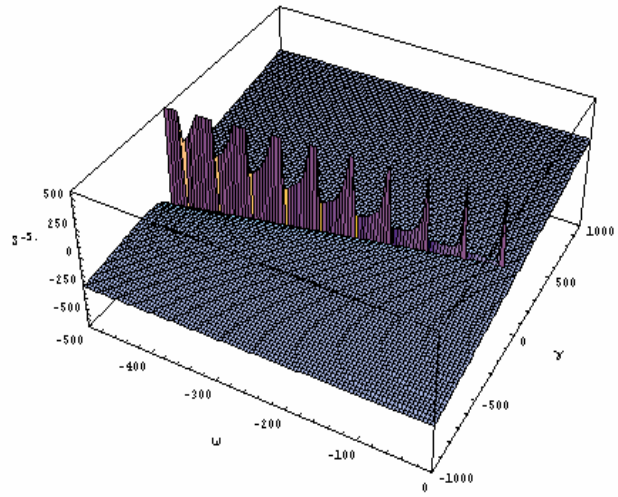

Figure 7-24: Surface $S^{-5.0}(\gamma\,,\omega)$

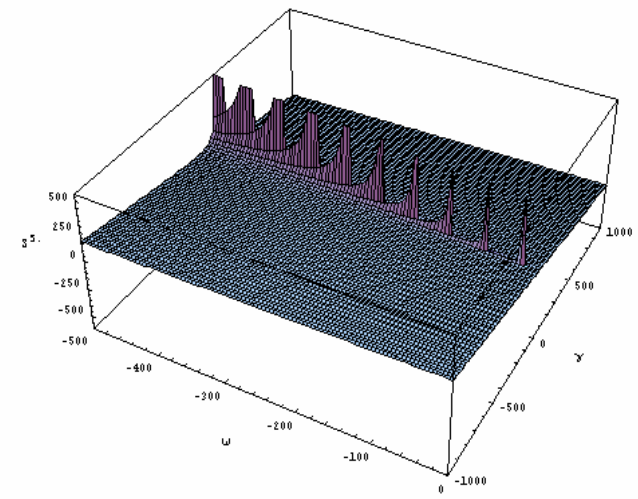

Figure 7-25: Surface $S^{-5.0}(\gamma\,,\omega)$

In order to illustrate images of the domain of stability D_S, the graphs below figures 7-26 to 7-27 are plotted for $\beta = 0.5\,,1.5\,,5.0$, and the graphs 7-28 to 7-30 indicate the profile of D_S for $\beta = -1.0$.

For the need of clarity in the graphic representations of D_S, different sizes of grids were used:

The coarsest grids represent the surface $S^1(\gamma\,,\omega)$.Coarse grid describes the surfaces of S_{ma}.

The finest grid represents the parametric surface $S^{\beta}(\gamma\,,\omega)$.

The main part of the domain of stability is contained in the interval $\left[S_{ma}\,,S^1(\gamma\,,\omega)\right]$. The other part given by $[0.\,,S_{\min}]$ exists but its contribution to D_S is tiny and its graphical representation becomes difficult, that is why only the first part of D_S retains attention.

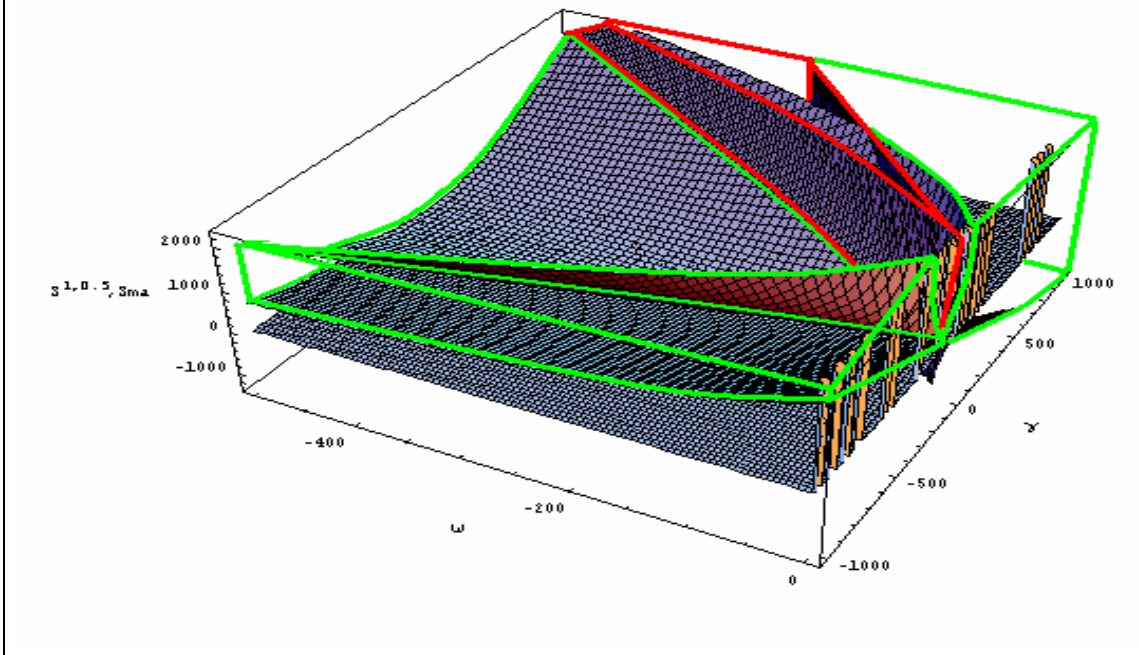

Figure 7-26: Profile of the domain $\left[S_{ma}\ , S^{\,1,\,0.5}(\gamma,\omega)\right]$

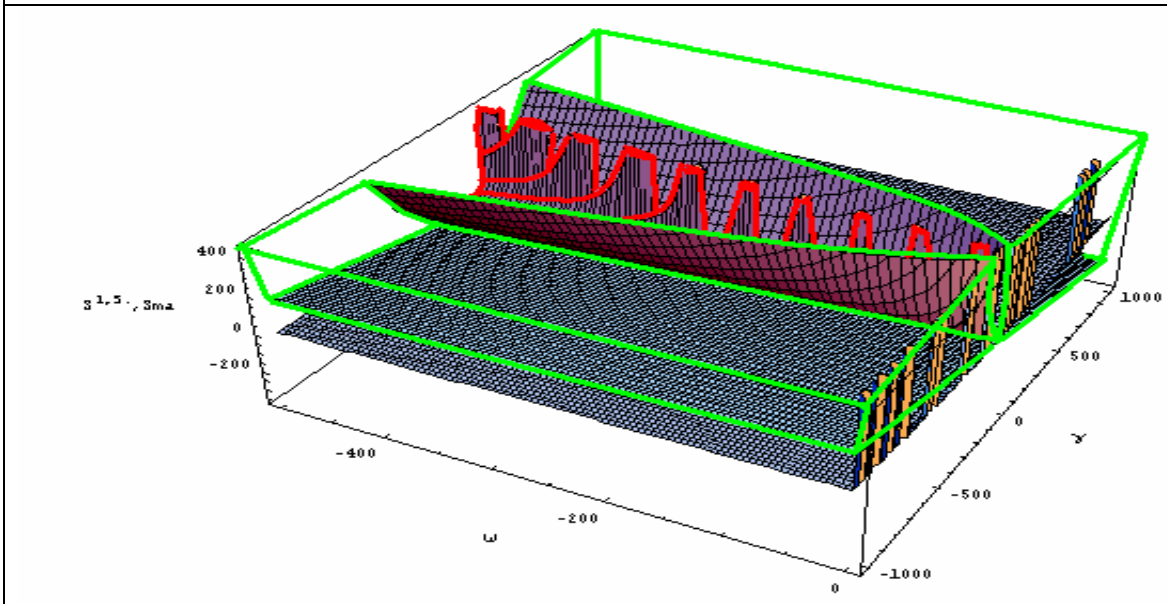

Figure 7-27: Profile of the domain $\left[S_{ma}\ , S^{\,1,\,5\cdot 0}(\gamma,\omega)\ \right]$

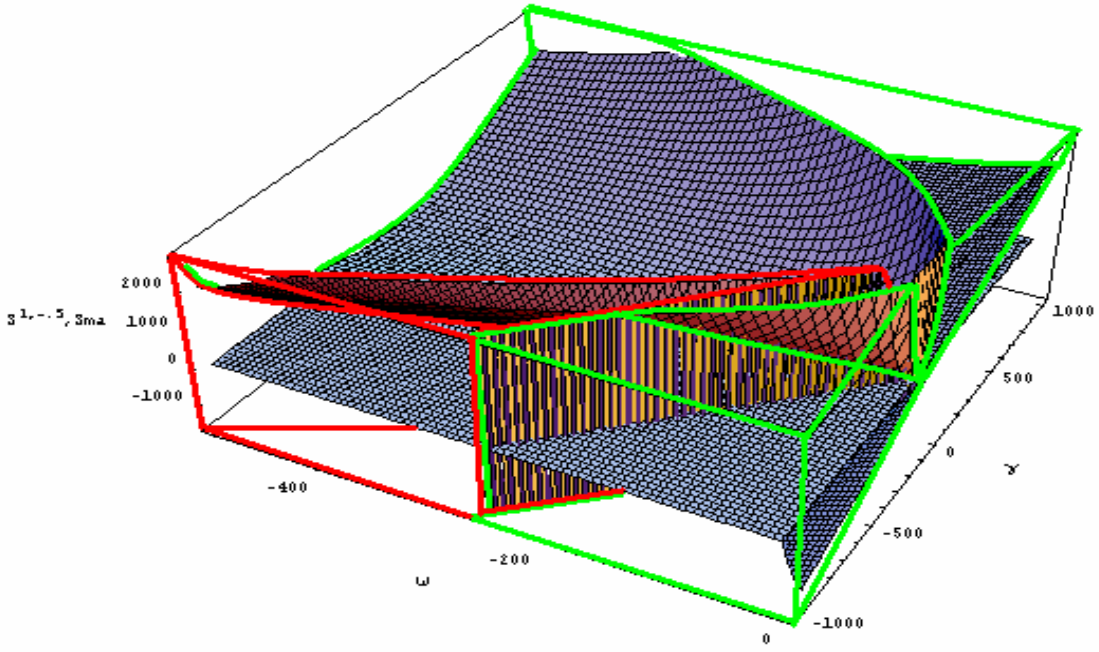

Figure 7-28: Profile of the domain $\left[S_{ma}\ , S^{\,1,\,-0.5}(\gamma,\omega)\ \right]$

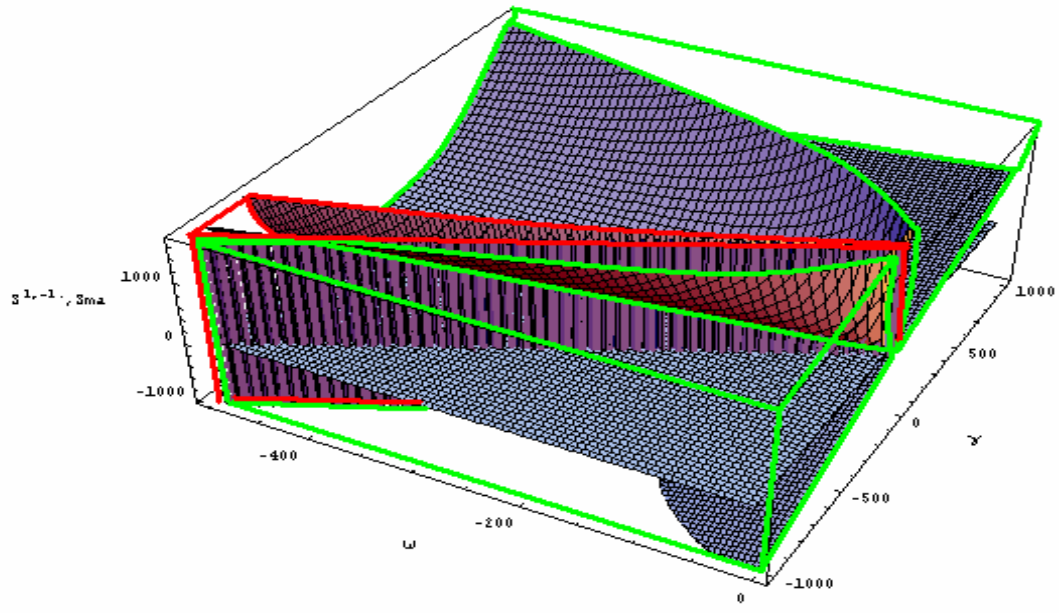

Figure 7-29: Profile of the domain $\left[S_{ma}\ , S^{\,1,\,-1.0}(\gamma,\omega)\ \right]$

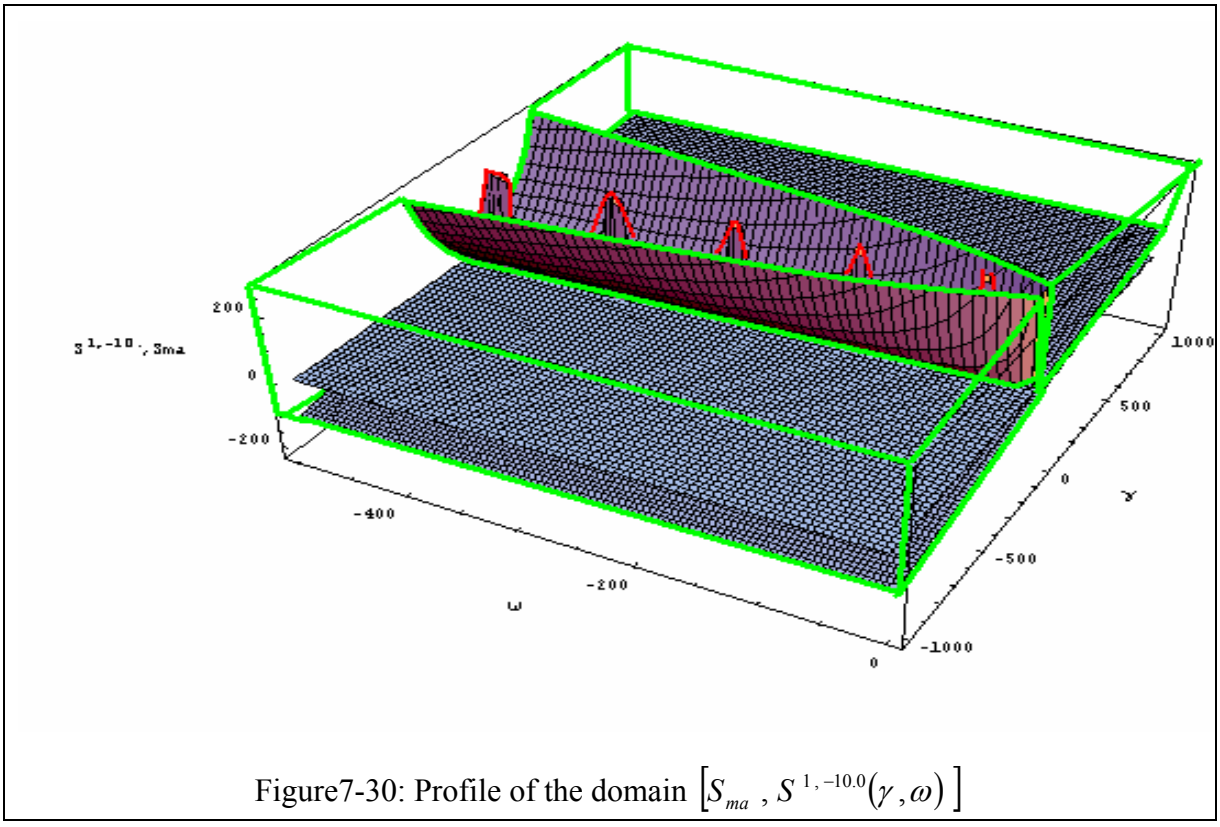

Figure7-30: Profile of the domain $\left[S_{ma}\ ,\ S^{\,1,\,-10.0}(\gamma,\omega)\ \right]$

From graphs 7-26 to 7-30 it is now possible to show volumes delimited by surfaces and to identify the domain of interest (stability), which is explicitly given by $D_{\,S}=\left[0.\ ,\ S_{mi}\ \right]\cup\left[S_{ma}\ ,\ S^{1}\right]\cap\left[S^{\,\beta}\ ,\ \infty\right[$.

This domain exists within regions where $S^{\,\beta}\leq S_{ma}$, volumes located between 'Finest grids' and 'Coarsest grids' in this order. The stability also exists where $0\leq\ S^{\,\beta}<S^{\,1}$, these volumes are identified by 'Green Borders' in the figures.

Finally, within regions where $S^{\,\beta}$ and $S^{\,1}$ swap $\left(S^{\,\beta}\geq S^{\,1}\right)$, $D_{\,S}=\emptyset$ and the stability could not be expected. The zones of instability were represented by a kind of **'Truncated Dams'** in figures 7-26 to 7-27 and in figures 7-28 to 7-29.

As β increases or decreases far from zero these zones reduce to a series of **'Truncated Peaks'** see figure 7-27 and figure 7-30. The volumes identified with 'Red Contours' indicate the instable zones while the 'Green Contours' indicate borders of stability.

7.5 Systems with non-regular distribution

For complexity reason, in this section, one is only intended to give brief theoretical implications on the stability domain when a non-spatially homogenous system is considered. One keeps the same notations as in the previous section; consequently instead of the determinant in (7.15) one has the relation below:

$$\det\left[\overline{\overline{A(U)}}-\lambda\cdot I_d\right]=\det\begin{pmatrix}1-\lambda-dt\cdot h_{11} & dt\cdot h_{12} & dt\cdot h_{13}\\ \lambda\cdot dt\cdot g_{21} & 1-\lambda & dt\cdot h_{23}\\ 0 & \lambda\cdot dt & 1-\lambda+dt\cdot h_{11}\end{pmatrix} \quad (7.21)$$

This leads to:

$$\eta^3+\eta^2\cdot\Phi_N(dt)-\eta\cdot\left\{\Phi_N(dt)+\Omega_N(dt)+\Gamma_N(dt)^2\right\}+\Omega_N(dt)=0 \quad (7.22)$$

Where $\Phi_N(dt)$, $\Omega_N(dt)$ and $\Gamma_N(dt)$ are functions expressing the non-regular distributions effects and are related to their counter part for the regular distributions $\Phi(dt)$, $\Omega(dt)$ and $\Gamma(dt)$ respectively by:

$$\begin{aligned}\Phi_N(dt)&=\Phi(dt)+\xi(dt)\\ \Omega_N(dt)&=\Omega(dt)-\xi(dt)\cdot\Gamma(dt)\\ \Gamma_N(dt)&=\Gamma(dt)\\ \xi(dt)&=\tilde{h}_{12}\cdot\tilde{g}_{21}=dt^2\cdot h_{12}\cdot g_{21}\end{aligned} \quad (7.23)$$

It has to be noticed that $\xi(dt)$ is of second order in dt while the compression-dilation effect expressed by $\Gamma(dt)$ is of first order.

The same approach and with the same approximation as previously leads to a system below:

$$\begin{cases}(\Phi+\xi\ +2)^2+4\cdot\Gamma^2+4\cdot(\Omega-\xi\cdot\Gamma)\geq 4\\ (\Phi+\xi\ )^2\quad\ +4\cdot\Gamma^2+4\cdot(\Omega-\xi\cdot\Gamma)\leq 9\end{cases} \tag{7.24}$$

And to (7.25) below:

$$\begin{cases}4\cdot dt^2\cdot\{(\omega+\alpha-\gamma\cdot\mu)\cdot dt+\beta+\gamma^2+\mu\}\geq 0\\ 4\cdot dt^2\cdot\{(\omega-\gamma\cdot\mu)\cdot dt+\gamma^2\}\leq 9\end{cases}\Leftrightarrow\begin{cases}dt\geq\dfrac{-(\beta+\gamma^2+\mu)}{\omega+\alpha-\gamma\cdot\mu}=-\dfrac{\beta+\mu+\gamma^2}{2\cdot\alpha-(\beta+\mu)\cdot\gamma}\\ (\alpha-(\beta+\gamma)\cdot\mu)\cdot dt^3+\gamma^2\cdot dt^2-\dfrac{3}{2}\leq 0\end{cases}$$

It is interesting to see from the inequalities above that in one hand, the order-disorder effect contained in the $\mu-term$ appears as an additive effect to the tensile factor described by the $\beta-term$ and in the other hand it is present in the formulas as multiplicative term with the compression-dilation factor expressed by the $\gamma-term$, this expresses a correlation between the two phenomena.

This simply expresses what one was intuitively expecting:

The additive relation means that the presence of the order-disorder distribution in any system can be seen as a generator of tensile instability when $\beta\cdot\mu>0$ or as an attenuator of it when $\beta\cdot\mu<0$.

The multiplicative relation says that for incompressible systems of particles, when $\gamma\to 0.$, the order-disorder aspect play negligible role and can be omitted while for compressible media it has to be considered.

Due to the approximation made before (neglecting terms with order higher than the third), the analysis performed in the previous section can be adapted to systems with non-regular distributions, but a satisfactory representation of the profiles of the instability domains is complicated by the presence of the extra-term μ.

7.6 Conclusions

In this chapter the error propagation analysis has been presented. From the definition of the amplification matrix one was able to give an idea of how errors propagated and to produce a view of the evolution of the domain of stability (Stability of the numerical scheme) as function of different mechanisms mentioned above and outlined in the previous chapter.

However, caution should be taken because of some assumptions made above to reach these results. A First approximation deals with the time step; one supposes that $dt^{n-\frac{1}{2}} = dt^{n+\frac{1}{2}}$, the second approximation lies on the neglect of high order terms in time step, Randles [4]. The first of these simplifications have a direct effect on the skeleton of the amplification matrix and the second one affects the delimitations of the domain D_S. Finally the non-uniqueness of the closure relation appears to be a source of speculations concerning the correct and a rigorous choice that has to be adopted and its impact on the prediction of stability.

A major consequence is that the tensile factor $\beta - term$ becomes a dummy term by variable changing, $\omega = (\alpha - \gamma \cdot \beta)$ which is why one can represent the domain of stability D_S as function of (γ, ω).

Because of the presence of the absolute value of $|\omega|$ in the expressions of the eigenvalues (equations (7.20)) and because there is no direct relation between α, γ *and* β it is not possible to represent surfaces and entities in dimensions higher than two, the approach used consists on reducing the dimension of the stability domain to (γ, ω) it also offers the flexibility that as one can see from the expressions of the domain D *and* D_S any single mechanisms of the $triplet - (\alpha, \beta, \gamma)$ can be isolated from the others, and by controlling its amplitudes as parameter it is possible to predict its influence.

The results presented show the predominance of the first eigenvalues to delimit the stability domain also how the tensile term acts on the determination of the boundaries of the domain of stability .The tensile term was used here as a parameter because its importance was widely mentioned in many investigations, J. W. Swegle *al* [5] and more recently by T.Belytschko *et al* [6].

For systems with non-regular distribution of particles, *the quartet* $-(\alpha, \beta, \gamma, \eta)$ has to be considered instead of *the triplet* $-(\alpha, \beta, \gamma)$. It is rather information that has to be considered and any reduction to a lower dimension will make the analysis of the domain D_S less accurate and cloudy.

7.7 References

[1] D. J. Benson: Computational methods in Lagrangian and Eulerian hydrocodes. Comp. Meth. Appl. Mech. Eng. September 1992, Vol 99, Issue 2-3, Pages 235-394.

[2] Ph. Randles, A. Petschek,L. Libersky and C. Dyka: ”Stability of DPD and SPH”. Springer Series Special Issue, Lecture Notes in Computational Science and Engineering, Proceedings of International Workshop on Mesh free Methods for Partial Differential Equations, Sept. 11-14, 2001, Bonn, Germany.

[3] B. Kutzler and V. Kokol-Voljc(2000), The Mathematical Assistant. *Derive*^{TM} 5.0 , version 5.07. Texas Instruments Incorporated Software, Dallas, Texas, USA.

[4] Ph. Randles, Private communications.

[5] S. Wolfram (1996), The Mathematica book version 3.0. Third edition. Wolfram edition. Cambridge University Press.

[6] J. W. Swegle, D. L. Hicks and S. W. Attaway S. W. (1995) Smoothed Particle Hydrodynamic Stability Analysis, J. Comp. Phy. 116:123.

[7] T. Belytschko, Y. Guo, W. K. Liu and S. P. Xiao (2002): A Unified Stability Analysis of Meshless Particle Methods, International Journal for Numerical Methods in Engineering, Vol 19/7, pp1129-1157

8. MATERIAL CHARACTERISATION: MATERIAL MODEL AND EQUATION OF STATE

8.1 Introduction

In all media a change in external environment elicits a response from a material, and physical properties express the relation between response and applied forces.

In solid mechanics Cauchy expressed that principle by generalizing Hooke's law and introduced a fourth rank tensor C relating the strain ε (intensive parameter) to the stress σ (extensive parameter) by $\sigma = C \cdot \varepsilon$. The tensor C constitutes an equilibrium property of the material and is subjected to certain thermodynamic and symmetry restrictions.

However, H. Tresca is in his experiments found that solids when subjected to very great pressure ultimately flow. This ability of solids to flow under stress is called *plasticity*. The *plasticity* of materials is shown as the ultimate limit of their *elasticity.*

Beyond the elastic limit, the behaviour of solids is rather complicated and Hooke's law is no longer valid, some ingredient and criteria have to be considered to describe the plasticity.

An exhaustive description of the theory of elasticity and plasticity was widely detailed by many authors, R. Hill [1], W. Prager [2], Love [3], L.E. Malvern [4], P. Karasudhi [5] and is not given in this work.

The theory of elasto- plasticity is a patchwork theory that involves different constitutive relations that are applied in the various stages of deformations. Elasticity is assumed to prevail about some reference configuration as long as yield condition is not reached. This yield condition is a relation among the components of the stress deviator. Once it is reached during loading, the elastic equations are replaced by another set of relations that comprise: the persistence of the yield condition and flow rule, such as the Prandtl-Reuss equations.

'*Unified Theories'* of elasto-plasticity intend to represent all aspects of elasticity and plasticity through a single set of constitutive relations. Among these theories, the Bodner and Partom unified-theory [6] is the most popular. B. Bernstein in his formulation [7] considered a class of strain

energy functions and concluded that elastic behaviour corresponds to uniqueness of solutions while the plastic regime results from the failure of the equations to meet the *Lipschitz condition* [8].

Concerning numerical methods, first developments and implementations of material models for impacted materials in particle methods in particularly in SPH were pioneered by Libersky *et al* [9] by using an elastic-plastic material model. Later on P. Randles *et al* [10] and P. Randles and L. Libersky [11] extended the work of the former authors by using the well known Johnson-Cook material model.

The aim of the work presented here is intended to give an example of how the equations of dynamic can be completed or closed by a choice of material model combined with equations of states. Hydrodynamic ram example is used and numerical results obtained with standard SPH. The present simulation results used two equation of state for water were first compared to numerical data obtained by L. Libersky [12] and to experimental data supplied by R. Vignjevic [13].

8.2 Material Characterizations

With the symmetry properties of isotropic, homogenous and visco-plastic materials, Hooke's law (in elastic-range) may be reduced to:

$$\sigma_{\alpha\beta} = \lambda \cdot \varepsilon_{\lambda\lambda} \cdot \delta_{\alpha\beta} + 2 \cdot G \cdot \varepsilon_{\alpha\beta} \quad with \quad 1 \le \alpha, \beta \le 3 \tag{8.1}$$

Where $\sigma_{\alpha\beta}$ represent the components of *the stress tensor* $\overline{\overline{\sigma}}$ while λ and G are Lame constants.

$\varepsilon_{\alpha\beta} = \frac{1}{2} \cdot \left(\frac{\partial d_\alpha}{\partial x_\beta} + \frac{\partial d_\beta}{\partial x_\alpha} + \frac{\partial d_\lambda}{\partial x_\alpha} \cdot \frac{\partial d_\lambda}{\partial x_\beta} \right)$ expresses the entries of *the strain tensor* $\overline{\overline{\varepsilon}}$ in rectangular Cartesian coordinates (x_1, x_2, x_3) and d_α stands for the components of the particles displacements (points or elements of solid) and is function of space and time.

For infinitesimal strains only the linear part of $\varepsilon_{\alpha\beta}$ is considered. The diagonal part in (8.1) is referred to as spherical part and reflects the change of the volume of the material under compression

while the non-diagonal part referred to as the strain deviator part $S_{\alpha\beta}$ (traceless part) reflects the deformation of materials without change of the volume, so instead of (8.1), one uses:

$$\sigma_{\alpha\beta} = -P \cdot \delta_{\alpha\beta} + S_{\alpha\beta} \tag{8.2}$$

Above $P = \frac{Trace\overline{\overline{\sigma}}}{3}$ is the mean stress and is expressed by an adequate functional equation of state *EOS*.

The equation (8.2) shows that the applied load to the body is borne by the pressure in the material and in part by its resistance to shear; these components will be discussed separately later on. A combination of (8.1) and (8.2) leads to:

$$S_{\alpha\beta} = 2 \cdot G \cdot \overline{\varepsilon}_{\alpha\beta} \quad \Leftrightarrow \quad \overline{\overline{S}} = 2 \cdot G \cdot \left(\overline{\overline{\varepsilon}} - \frac{Trace\,\overline{\overline{\varepsilon}}}{3} \cdot I_d \right) \tag{8.3}$$

Where I_d is the identity matrix.

8.2.1 Linear Elastic and Plastic behaviour of Materials

The figure below shows a schematic relation between the applied tensile loads σ to a slab of metal with the elongation ε occurring in the material, Y. C. Fung [14].

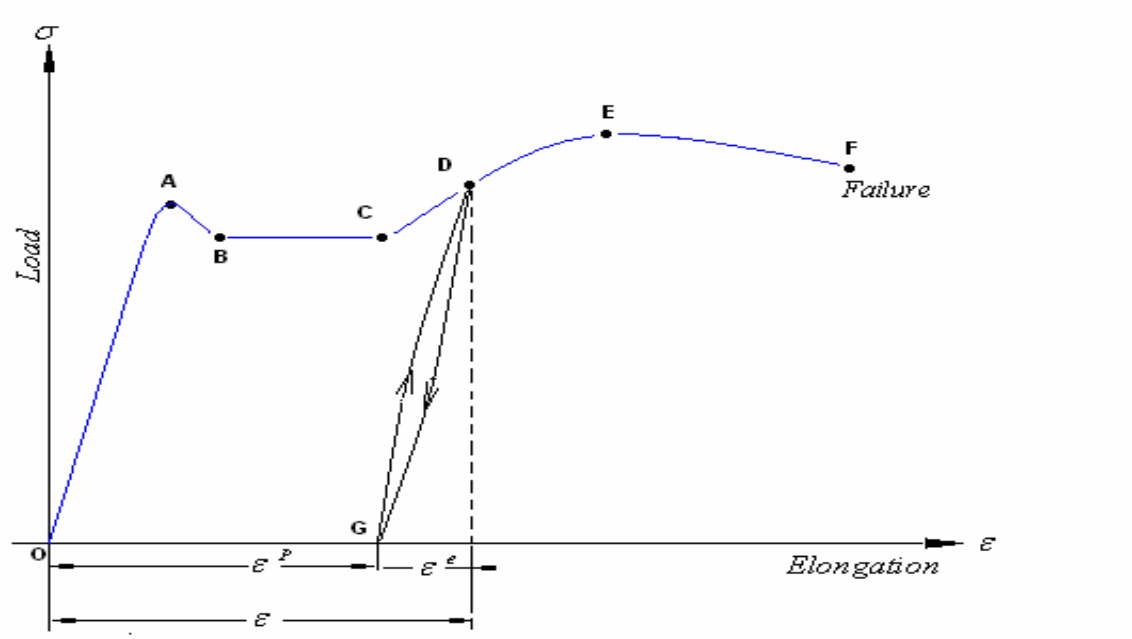

Figure 8-1: Example of stress-strain (load-elongation) curve in simple tension test

The linear part OA corresponds to the elastic region where load and strain are proportional, at the point A, the material yields; the transitional elastic to plastic part AB I s unstable and is not considered here. The ideal plastic range is represented by the plateau part BC; it shows that elongations increase while the tensile loads remain unchanged. The concave curve CF contains the point E where the maximum load is reached. In the neighbouring of E, the necking can take place under continued elongation and beyond where the material flows and finally to break at point F.

In this section, one provides a brief outline of the equations in classical theory of plasticity that will be used in the subsequent numerical examples.

Various theories of plasticity exist, but they proceed commonly by a basic assumption that the strain tensor $\overline{\overline{\varepsilon}}$ can be additively decomposed into an elastic strain tensor $\overline{\overline{\varepsilon}}^{e}$ (reversible) that can be computed from the deviatoric stress by Hooke's law and to the plastic strain tensor $\overline{\overline{\varepsilon}}^{P}$, which is dissipative and non-recoverable (irreversible). The possibility of any nonlinear interaction between $\overline{\overline{\varepsilon}}^{e}$ and $\overline{\overline{\varepsilon}}^{P}$ is not considered.

This linear decomposition holds whether the solid is isotropic or anisotropic, homogenous or heterogeneous. Nemat-Nasser in [15] discussed mathematical justifications of the decomposition approach for infinitesimal deformations, it follows then.

$$\overline{\overline{\varepsilon}} = \overline{\overline{\varepsilon^{e}}} + \overline{\overline{\varepsilon^{P}}} \tag{8.4}$$

In classical plasticity it is assumed that the hydrostatic pressure has no influence on the way with witch solid elements distort (on the material plastic deformations); the plastic deformations are considered to be incompressible. This assumption holds mainly for dense metals (which is the case considered here). Rocks, soils and porous media, polymers and ceramics exhibit plastic volumetric deformations, F. Z. Li [16]. It follows then.

$$\varepsilon^{P}_{\alpha\alpha} = 0 \tag{8.5}$$

In some applications of plasticity, one is interested only in the total amount of plastic flow, and the rate of increment $\frac{d\overline{\overline{\varepsilon^{P}}}}{dt} = \overline{\overline{\dot{\varepsilon}^{P}}}$, the plastic strain occurs in the direction of the applied stress and that the Prandtl-Reuss flow rule holds.

$$\frac{d\overline{\overline{\varepsilon^{P}}}}{dt} = \lambda_{P} \cdot \overline{\overline{S}} \tag{8.6}$$

Where $\lambda_{P} \geq 0$ is a load history factor of proportionality that is obtained by squaring equation (8.6).

$$\lambda_{P} = \sqrt{\frac{Trace\left(\overline{\overline{\dot{\varepsilon}^{P}}} \cdot \overline{\overline{\dot{\varepsilon}^{P}}}\right)}{Trace\left(\overline{\overline{S}} \cdot \overline{\overline{S}}\right)}} \tag{8.7}$$

Note that λ_{P}^{2} is a ratio of the second invariant of the plastic strain rate to the stress deviator tensor.

The objective incremental equation for the deviator strain is not unique, C.Truesdell [17], G. C. Johnson and D. J. Bammann [18], D.Benson [19]. The Jaumann-Zaremba rate is mainly used in hydro-codes like MAGI and MCM, which leads to.

$$\frac{d\overline{\overline{S}}}{dt}+\lambda_{P}\cdot\overline{\overline{S}}=2\cdot G\cdot\left(\overline{\overline{\dot{\varepsilon}}}-\frac{Trace\,\overline{\overline{\dot{\varepsilon}}}}{3}\cdot I_{d}\right)+\overline{\overline{\Omega}}\cdot\overline{\overline{S}}+\left(\overline{\overline{\Omega}}\cdot\overline{\overline{S}}\right)^{T} \tag{8.8}$$

With $\left(\overline{\overline{\Omega}}\cdot\overline{\overline{S}}\right)^{T}$ is the transpose tensor of $\left(\overline{\overline{\Omega}}\cdot\overline{\overline{S}}\right)$, $\overline{\overline{\dot{\varepsilon}}}$ and $\overline{\overline{\Omega}}$ represent the linear strain rate and the spin tensor, the latter is given by:

$$\dot{\varepsilon}_{\alpha\beta}=\frac{1}{2}\cdot\left(\frac{\partial u_{\alpha}}{\partial x_{\beta}}+\frac{\partial u_{\beta}}{\partial x_{\alpha}}\right)\quad\text{and}\quad\Omega_{\alpha\beta}=\frac{1}{2}\cdot\left(\frac{\partial u_{\alpha}}{\partial x_{\beta}}-\frac{\partial u_{\beta}}{\partial x_{\alpha}}\right) \tag{8.9}$$

Where u_{α} stands for the cartesian velocity of the particle or element of the substance.

The material is elastic $\left(\lambda_{P}=0\right)$ obeys Hooke's law as long as Von Mises yield criterion is fulfilled:

$$Trace\left(\overline{\overline{S}}\cdot\overline{\overline{S}}\right)\leq\frac{2}{3}\cdot Y^{2}\left(\varepsilon^{P}\right) \tag{8.10}$$

With $Y\left(\varepsilon^{P}\right)$ stands for the yield strength in tension, $\varepsilon^{P}=\sqrt{\frac{2}{3}\cdot Trace\left(\overline{\overline{\varepsilon^{P}}}\cdot\overline{\overline{\varepsilon^{P}}}\right)}$ represents the effective plastic strain.

Currently, many numerical codes model Von Mises tensile flow stress as functions of temperature, strain rate and of the equivalent plastic strain.

Various approaches were adopted to define the function $Y\left(\varepsilon^{P}\right)$ in (8.10). Johnson-Cook model [20], Zerilli-Armstrong model [21] and Steinberg-Cochran-Guinan model [22] are among of them and are widely adopted and used by the engineers' community.

The Johnson-Cook visco-plastic model allows us to express the yield stress.

$$Y\left(\varepsilon^{P}\right)=\left(A+B\cdot\left(\varepsilon^{P}\right)^{n}\right)\cdot\left(1+C\cdot Ln\left(\frac{\dot{\varepsilon}^{P}}{\dot{\varepsilon}_{0}}\right)\right)\cdot\left(1-T_{*}^{m}\right) \tag{8.11}$$

Where A, B, C, n and m are material constants, the homologous temperature is given by $T_{*}=\frac{T-T_{room}}{T_{melt}-T_{room}}$ while $\dot{\varepsilon}_{0}=1.0\,s^{-1}$ is a normalization constant. In the relation (8.11), $\dot{\varepsilon}^{P}=\frac{d\varepsilon^{P}}{dt}=\sqrt{\frac{2}{3}\cdot Trace\left(\overline{\overline{\dot{\varepsilon}^{P}}}\cdot\overline{\overline{\dot{\varepsilon}^{P}}}\right)}$ denotes the rate of effective plastic strain with respect to time.

In numerical tests, the stress deviators $\overline{\overline{S}}_{num}$ are calculated on the basis of elastic flow, in cases where (8.10) is not respected, a parameter γ_{P} is introduced and one has.

$$Trace\left(\gamma_{P}\cdot\overline{\overline{S}}_{num}\cdot\gamma_{P}\cdot\overline{\overline{S}}_{num}\right)=\frac{2}{3}\cdot Y^{2}\left(\varepsilon^{P}\right) \tag{8.12}$$

Where γ_{P} is a corrector factor that can be extracted from (8.12) in the same way as λ_{P}. The plastic flow part is then estimated through:

$$\overline{\overline{S}}=\sqrt{\frac{2\cdot Y^{2}\left(\varepsilon^{P}\right)}{3\cdot Trace\left(\overline{\overline{S}}_{num}\cdot\overline{\overline{S}}_{num}\right)}}\cdot\overline{\overline{S}}_{num} \tag{8.13}$$

The plastic strain rate is then given by:

$$\frac{d\overline{\overline{\varepsilon^{P}}}}{dt}=\left(\frac{1-\sqrt{\frac{2\cdot Y^{2}\left(\varepsilon^{P}\right)}{3\cdot Trace\left(\overline{\overline{S}}_{num}\cdot\overline{\overline{S}}_{num}\right)}}}{2\cdot G}\right)\cdot\overline{\overline{S}} \tag{8.14}$$

The relation above gives an explicit expression of λ_{P}.

8.3 Equation of state EOS

The equation of state formally is a functional relationship among the thermo dynamical variables for systems in equilibrium. The thermodynamic parameters for our purpose are pressure P, volume V or (the specific volume $\rho = \frac{1}{V}$, the density) and temperature T or (the internal energy E) for which the EOS can be written as.

$$f(P, V, T) = 0 \tag{8.15}$$

Equation (8.15) represents a surface in (P, V, T)space. The isotherm (T=Constant), the isentrop (The entropy S= Constant) and shock Hugoniot are particular curves on this surface.

For crystalline solids, to obtain the form of f, physicists developed two approaches that were used; the thermodynamic approach and the 'lattice dynamic' approach see I. Jackson and S. M. Rigden [23] for the development and connection between these two approaches.

The latest approach, based on the statistical mechanics which represents one of the cornerstones of the modern physics that provides concepts upon which one builds the analyses and the understanding of the thermo-dynamic of systems in equilibrium and in non-equilibrium. Often, the harmonic oscillator 'lattice dynamic' serves as the basis for the construction of the thermal equation of state, M. Born and K. Huang [24].

To obtain the form of f, it is convenient to introduce the Helmoltz free energy of the solid.

$$F(T, V) = F_0(V) + F_{vib}(T, V) \tag{8.16}$$

In the relation above $F_0(V)$ represents the cohesive energy at absolute zero temperature and $F_{vib}(T, V)$ is the classical vibrational free energy of the crystalline solid (vibrations of atoms about

their mean positions). Ionizations, molecular dissociations, electronic excitations and other effects were omitted from the additive relation above.

Expressions for the internal energy and other thermodynamic functions are similar to equation (8.15) and the pressure is obtained as the volume derivative.

$$P(T,V) = -\left(\frac{\partial F}{\partial V}\right)_T = -\frac{dF_0(V)}{dV} - \left(\frac{\partial F_{vib}(T,V)}{\partial V}\right)_T \tag{8.17}$$

8.3.1 Mie- Gruneisen-Debye model

The derivation of the Mie-Grüneisen equation of state assumes the existence of a characteristic temperature $\theta(V)$ to represent the volume dependence of the vibrational free energy such that $\left(\frac{\partial F_{vib}}{\partial V}\right)_T = -\frac{\gamma(V)}{V}\cdot E_{vib}(T,V)$, then the equation (8.17) becomes.

$$P(T,V) = -\frac{dF_0(V)}{dV} + \frac{\gamma(V)}{V}\cdot E_{vib}(T,V) = P_0(V) + \frac{\gamma(V)}{V}\cdot[E(T,V) - E_0(V)] \tag{8.18}$$

Where, the total energy is composed into a cold part and into a vibrational or thermal energy as follow.

$$E(T,V) = E_0(V) + E_{vib}(T,V)$$

The Gruneisen parameter in Debye's model is obtained by assuming the persistence of the harmonic oscillations dependant on the volume alone with isotropic compressions of the solids. I. Jackson and S. M. Rigden [23]:

$$\begin{aligned}\gamma\left(V\right) &= -\frac{d\ln\theta\left(V\right)}{d\ln V} \\ &= \gamma_0 \cdot \left(\frac{V}{V_0}\right)^q\end{aligned} \tag{8.19}$$

Where q is a constant that is usually in the range $(0,1)$.

The Gruneisen parameter is also related to the ratio of thermal pressure to the thermal energy of the lattice, as it can be seen by the differentiation of (8.18) with respect to the energy.

$$\frac{\gamma\left(V\right)}{V} = \left(\frac{\partial P}{\partial E}\right)_V = \frac{1}{C_V} \cdot \left(\frac{\partial P}{\partial T}\right)_V \tag{8.20}$$

In practice, the pressure is needed around Hugoniot curves $P_H(V)$, the equation (8.18) becomes.

$$P(T,V) = P_H\left(V\right) + \frac{\gamma\left(V\right)}{V} \cdot \left[E(T,V) - E_H\left(V\right)\right] \tag{8.21}$$

Where $P_H(V) = \dfrac{C_0^2 \cdot \left(1 - \dfrac{V}{V_0}\right)}{V_0 \cdot \left(1 - S_0 \cdot \left(1 - \dfrac{V}{V_0}\right)\right)^2}$ and $E_H(V) = E_0(V) + \dfrac{P_H(V) + P_0(V)}{2} \cdot (V_0 - V)$ (5.21-a)

The constant S_0 depends on the material considered and C_0 is the speed of sound in the material at standard condition.

8.3.2 Murnaghan relationship model

The most pressure-volume isotherms can be fitted by Murnaghan relationship, O.L. Anderson [25]. This relationship holds remarkably well for a great number of substances. Although it has no theoretical grounds, it is useful simple equation of state.

$$P(T,V)=\frac{B^*(P_0)}{\Gamma}\cdot\left[\left(\frac{V_0}{V}\right)^{\Gamma}-1\right] \tag{8.22}$$

Mathematical assumption behind the derivation of the relationship above is that the isothermal bulk modulus $B_T(T,V)=-V\cdot\left(\frac{\partial P}{\partial V}\right)_T$ and the isentropic bulk modulus $B_S(T,V)=-V\cdot\left(\frac{\partial P}{\partial V}\right)_S$ are linear with pressure (first order in Taylor series).

$$\begin{aligned} B_S(T,V) &= -V\cdot\left(\frac{\partial P}{\partial V}\right)_S \\ &= B(P_0)+\left(P(T,V)-P_0\right)\cdot\left(\left(\frac{\partial B}{\partial P}\right)_S\right)_{P_0} \\ &= B(P_0)-P_0\cdot\left(\left(\frac{\partial B}{\partial P}\right)_S\right)_{P_0}+P(T,V)\cdot\left(\left(\frac{\partial B}{\partial P}\right)_S\right)_{P_0} \\ &= B^*(P_0)+P(T,V)\cdot\left(\left(\frac{\partial B}{\partial P}\right)_S\right)_{P_0} \end{aligned} \tag{8.23}$$

By integration, the empirical relationship in (8.22) is recovered with $\Gamma = \left(\left(\frac{\partial B}{\partial P} \right)_S \right)_{P_0}$ and

$B^*(P_0) = \frac{C_0^2}{V_0}$ where C_0 represents the speed of sound in the material at standard state is recovered.

It is understood that under certain conditions (Debye's Theory), the classical solid state theory permitted to build Mie-Grüneisen-Debye equation of state, however the extension of the equation of state to solid materials subjected to chocks where temperatures approach or exceed melting temperatures can leads to non-reliable and non-physical results.

In the other hand, in many simulations, Mie-Grüneisen-Debye equation of state is used to describe the thermo-dynamic properties of liquids, although liquids are characterized by a different kind of interactions and disorder.

Murnaghan relationship is used for isentropic flows independently from the nature of the substance, Ya.B.Zel'dovich and Yu. P. Raiser [26]. When modelling compressible liquids, it is assumed to be barotropic and Murnaghan relationship is an adequate alternative. In C. Hunter [27], G.J. Ball *et al* [28] it was used to describe the collapse of cavities in water.

8.4 Numerical Tests

Hydrodynamic ram phenomenon consists on the collision of solid flyer with a liquid-filled container; the impact gives birth to a complicated sequence of energy and momentum transfer from a projectile to fluid- filled container. Complexity and additional difficulties appear when materials considered are thermodynamically different.

The geometry of the model is identical to the one used in R.Vignjevic *et al* [29] and a schematic description of the problem is given in figure 3.1. Johnson-Cook material model and Mie-Grüneisen equation of state were used for both the steel projectile and for the tank walls aluminium. Concerning water, two simulations were performed, the first test used Mie-Grüneisen equation and the second one used Murnaghan relationship.

Eulerian pressure sensores are located as shown in the figure 3.1, only the three closest sensors to the projectile were considered in simulations. These are termed first, second and third sensors.

Symmetry considerations allow us to reduce the number of particles used to $n_P = 378150$.

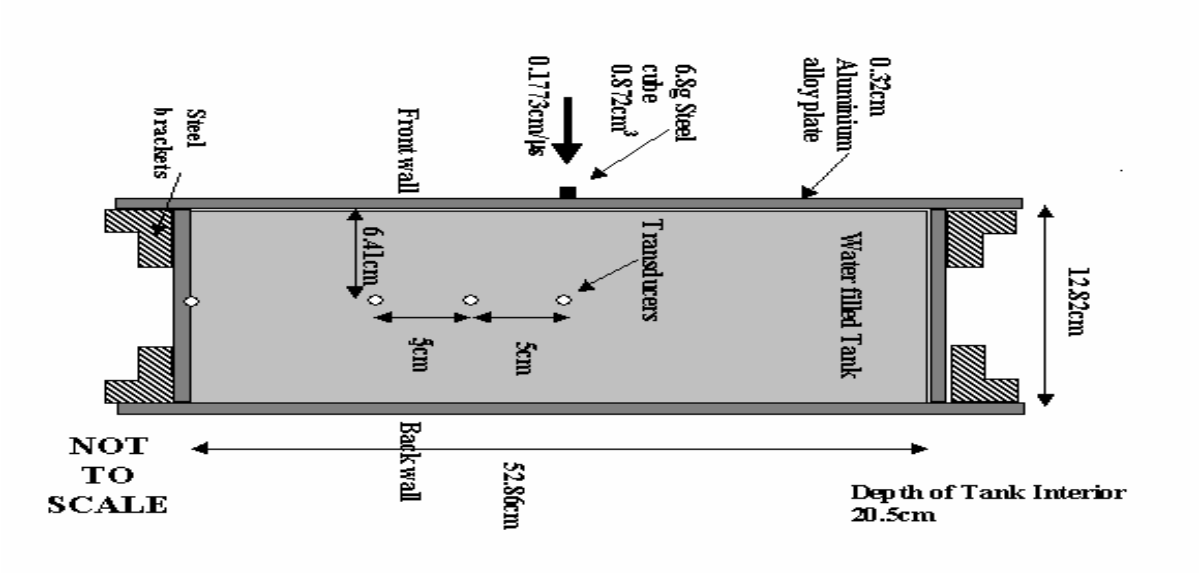

Figure 8-2: Presentation of fuel tank cross section, the projectile and pressure transducers

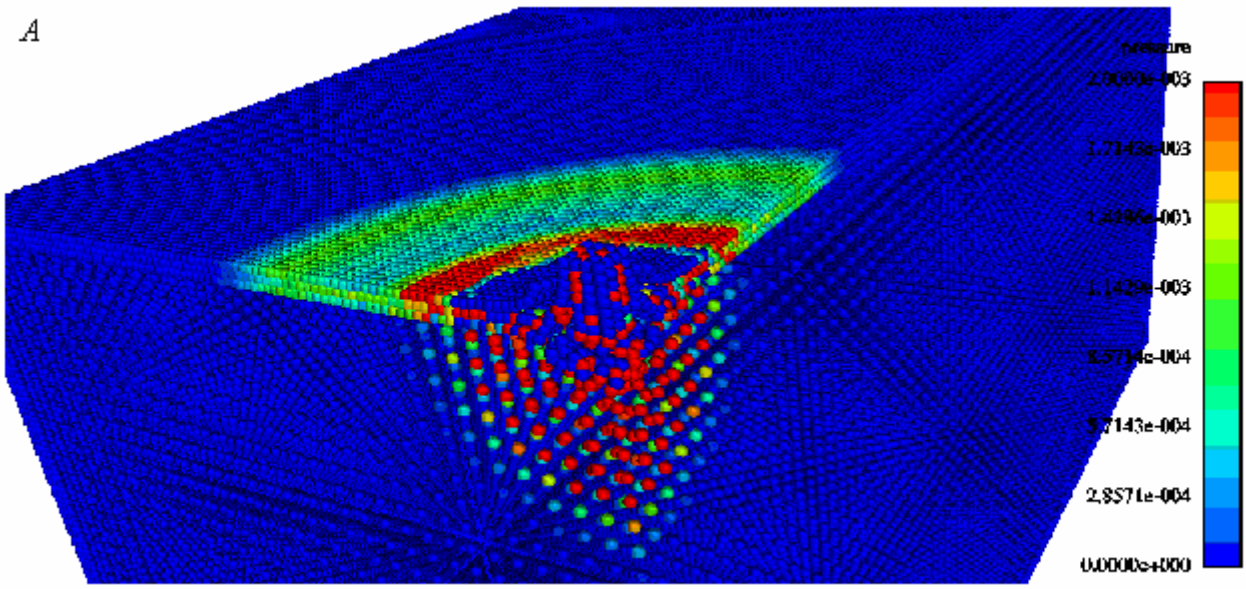

Figure 8-3:Pressure distribution at time $t = 10\,\mu s$ after impact

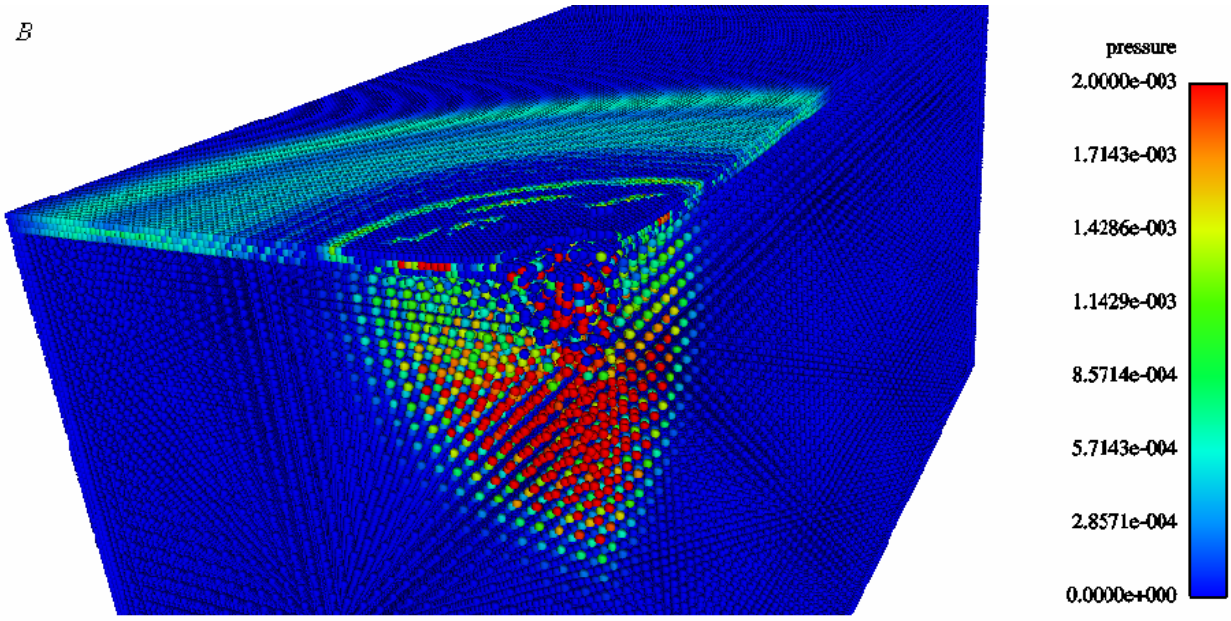

Figure 8-4:Pressure distribution at time $t = 20\,\mu s$ after impact

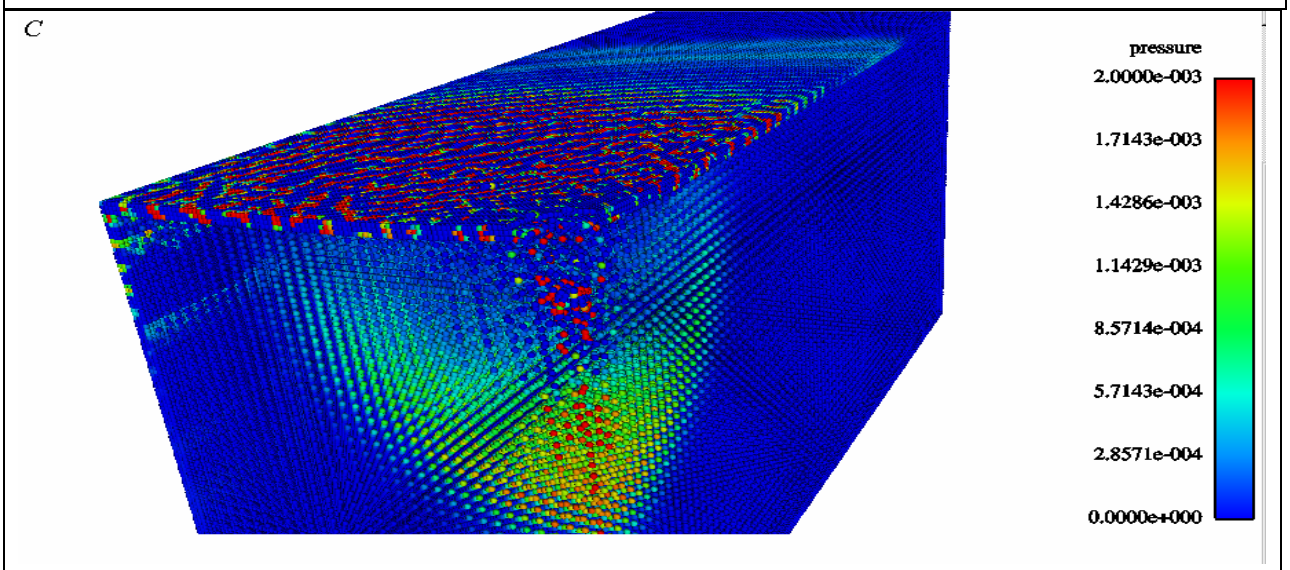

Figure 8-5:Pressure distribution at time $t = 40\,\mu s$ after impact

As it was expected, the impact induces a stress wave in the aluminium wall with speed of propagation higher than the speed of pressure wave in the water. The profiles of pressure on aluminium plate in figures 8-3 and 8-4 show the existence of circular, distinctive front of

propagations. When the wave reaches the side walls of the container, the direction of propagation changes and is propagating down the wall see Figure 8-5.

In the water a spherical shock is formed in front of the flyer. As the projectile progresses through the water, the shock expands radially away from the impact axis and by imparting radial impulses to the fluid creates cavitations behind the projectile.

The figure 8-6 above shows the transient pressure detected by the transducers; this figure is adapted from simulations performed by L. Libersky *et al.*

The axial transducer pressure time history profile (red curve) shows the existence of two peaks separated by a 'plateau' followed by step at time $t = 52\,\mu s$ and a sharp jump up in the pressure around $t = 62\,\mu s$. The first peak represents the main shock front while the second peak represents the pressure carried by the flyer. The step in front of the second peak at time $t = 52\,\mu s$ corresponds to the contact of the flyer with the transducer.

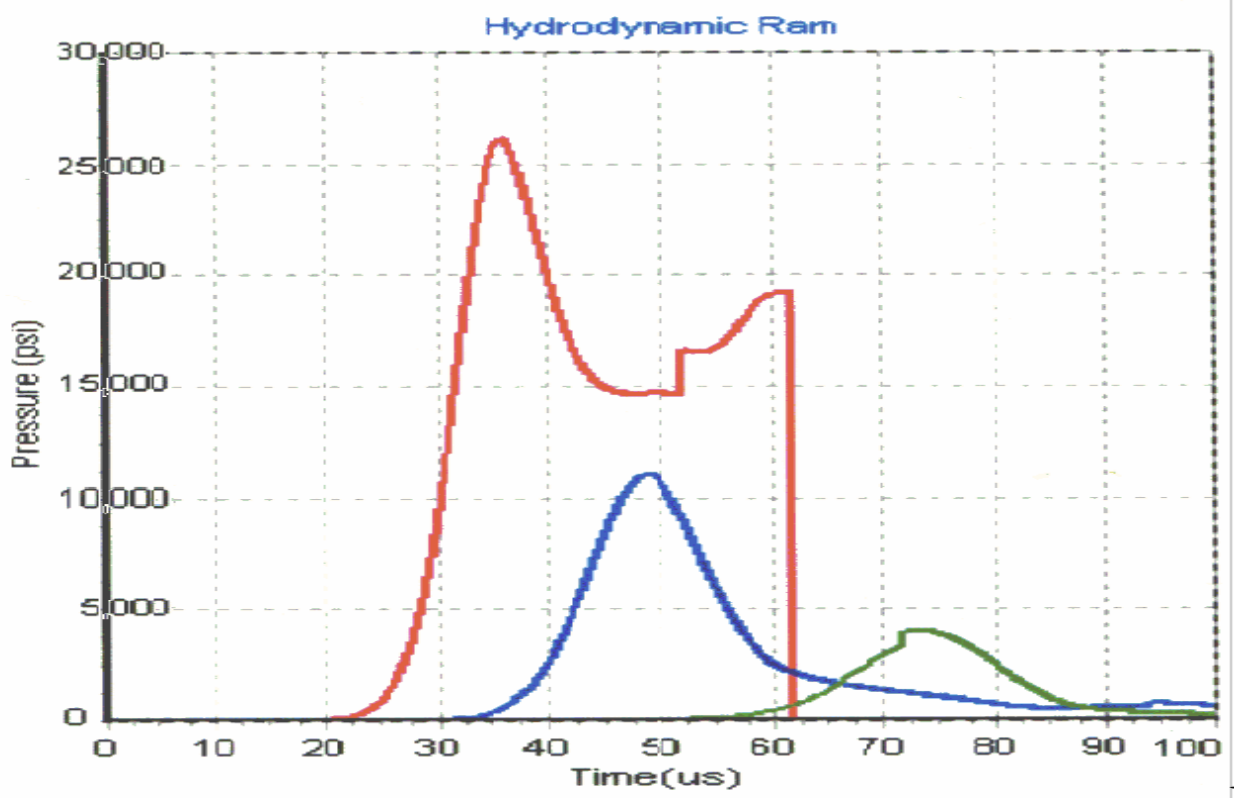

Figure 8-6:Profile of pressure semsors time history (Adapted from L.Libesky et al)

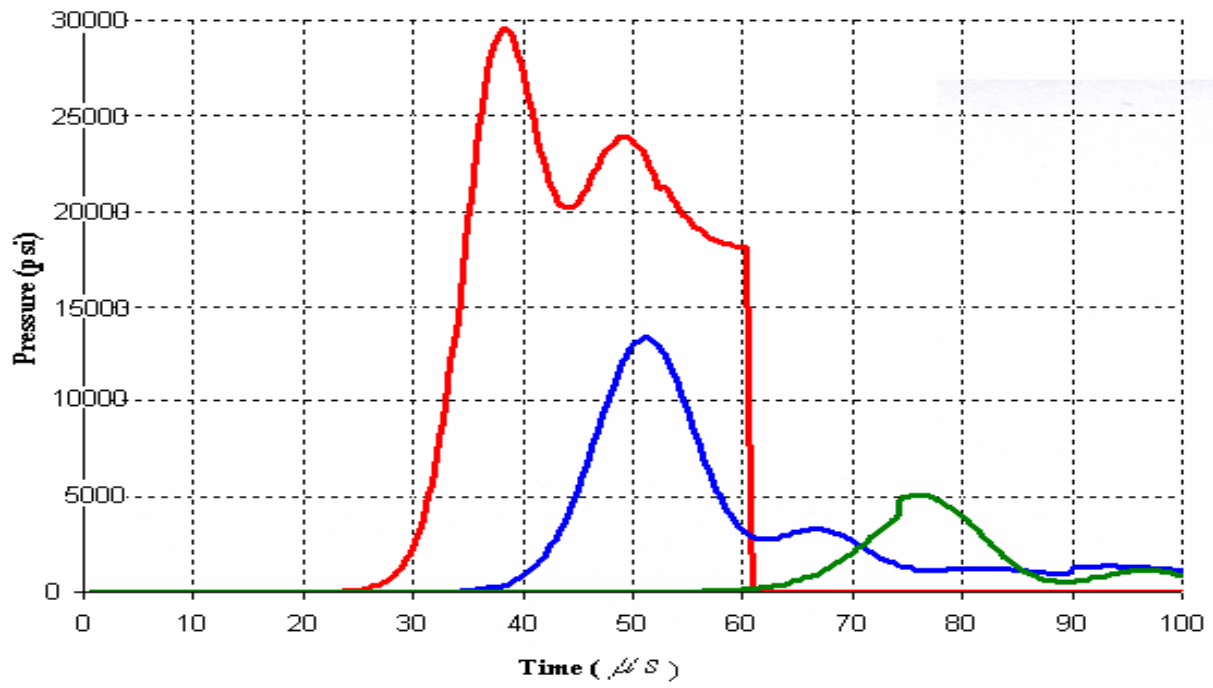

Figure 8-7: Profile of pressure sensor time history using Mie-Grüneisen EOS for water

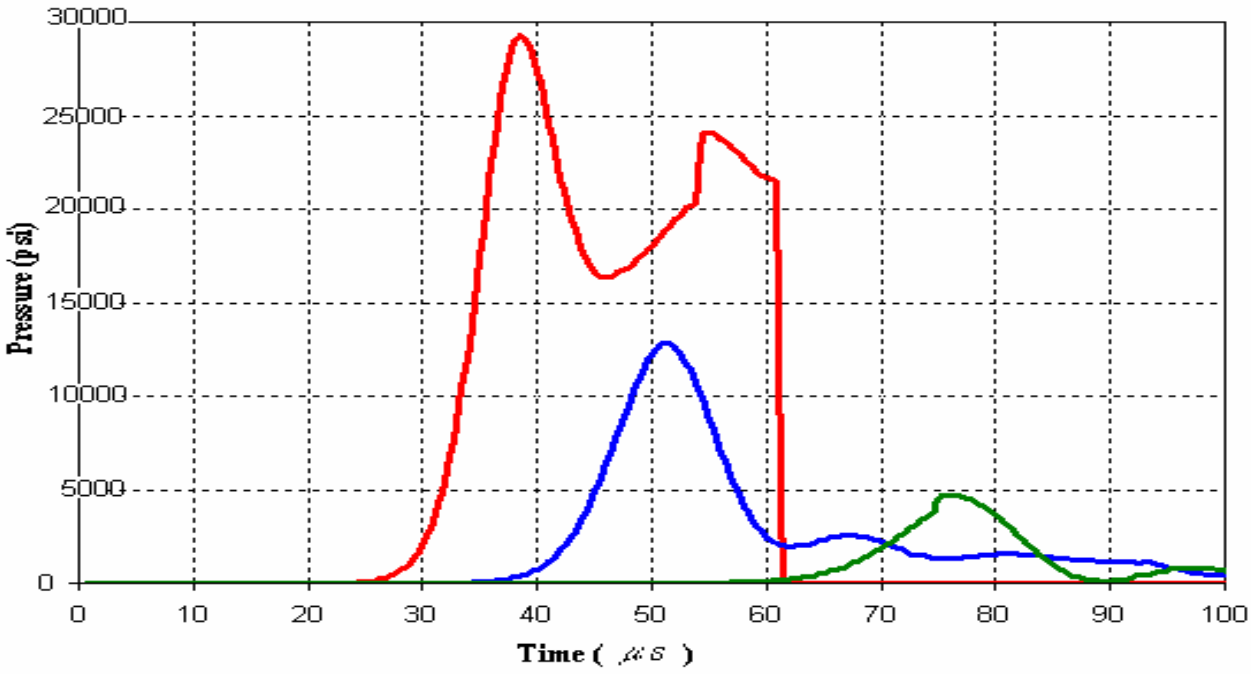

Figure 8-8:Profile of pressure sensor time history using Murnaghan relationship for water

Curves in figures 8-7 and 8-8 correspond to the data obtained in the present simulations. These results over-estimate the transient pressure in comparison to the result in the figure 8-6 by about $(8\% \sim 10\%)$. The profiles of the pressure detected by the second (blue curves) and the third sensors (green curves) are very similar.

All three plots show that the transient pressure detected by the second (blue curve) and the third transducers (green curve) exhibit a Voigt profiles, and the peak pressure has decayed in intensity.

Concerning, the axial transducer (first sensor-red curve), the figure 8-7 shows a poor agreement with the curve in 8-6 characterized by the absence a step-pressure. The absence of a step-pressure means that the transient pressure in the nearest neighbours of the flyer is as higher than the pressure carried by the core flyer itself, so the step-pressure is invisible to the transducer.

The figure 8-8 shows acceptable agreement with 8-6; again, it is characterized by the absence of a 'plateau' but detects the step-pressure (jump) that indicates the contact between the flyer and the sensor.

The figure 8-9 below compares experimental transient pressure profiles with the present results using Murnaghan relationship for water. An overestimation of the pressure $(\sim 28\%)$ can be seen for the axial transducer mainly concerning the front peak. In part, this difference results from the fact that in experiments, the first sensor is not located at the axe of impact but away from it. It detects an attenuated peak and delayed signal by about $(\sim 8\ \mu s)$. The second and the third sensors detections show an acceptable agreement. The other part of the difference comes from imperfections inherent to any experimental test (power of resolution of the transducers, vibrations, positioning, etc …).

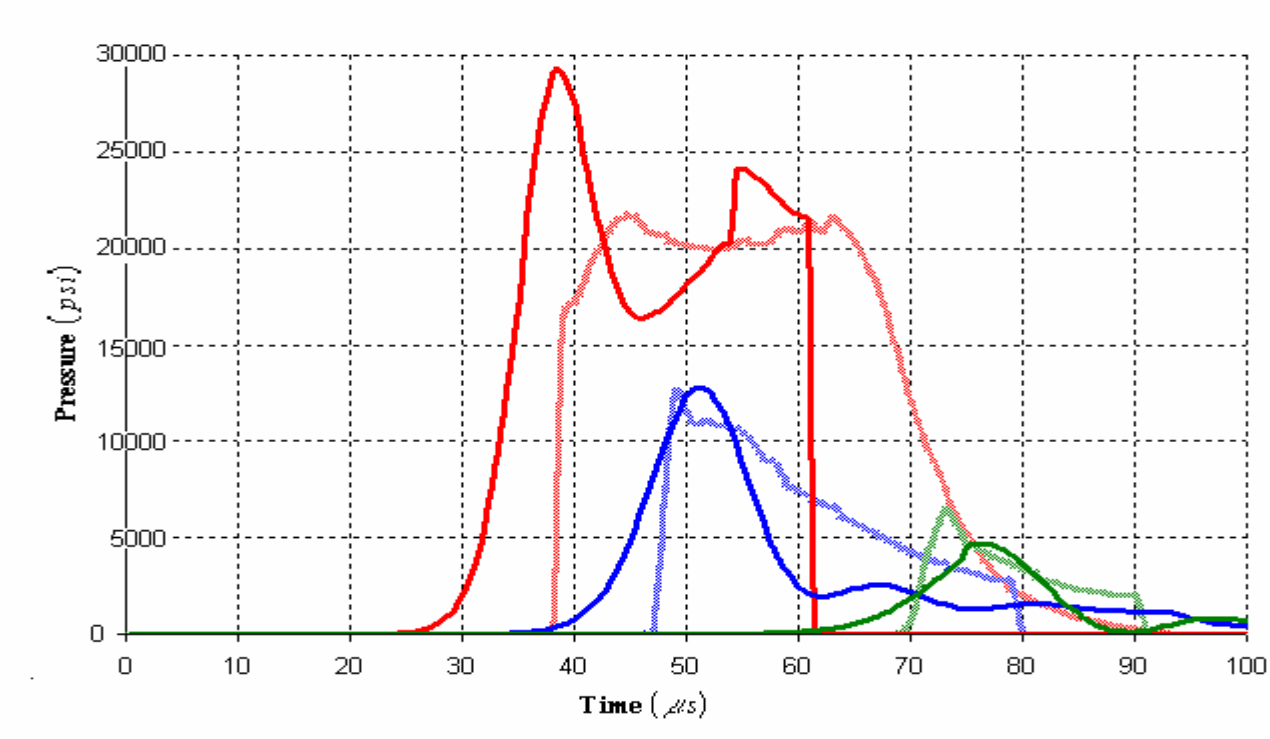

Figure 8-9:Comparison of transient experimental pressure (Faded curves) with actual simulation (Bold curves)

8.5 Conclusion

In this work, it is attended to give a succinct and brief overview of material characterization in order to close the equations of dynamic in SPH formalism.

A hydro-dynamic ram problem test is performed. Results presented in this work show an acceptable agreement with those obtained in [12]. Using Murnaghan relationship for water gives more acceptable results in comparison to Mie-Grüneisen-Debye *EOS* and to experimental data.

8.6 References

[1] R. Hill, *The Mathematical Theory Of Plasticity*, Oxford At The Clarendon Press, 1950

[2] W. Prager and P. Hodgs, *Theory Of Perfectly Plastic Solids*, Dover Publications, Inc. New York 1968.

[3] A. E. H. Love, *A Treatise On The Mathematical Theory Of Elasticity*. Fourth edition, Dover Publication 1944.

[4] L. E. Malvern, *Introduction to the Mechanics of Continuous Medium*, Prentic-Hall, Englwood Cliffs, N. J.1969

[5] P. Karasudhi,' Foundation Of Solid Mechanics'

[6] K. S. Chan, S. R. Bodner, U. S. Lindholm, Phenomenological Modeling of Hardening and Thermal Recovery in Metals. *Journal of Engineering Material and Technology*. Jan 1988, Vol. 110/ 1.

[7] B. Bernstein,'Unified Theory of Elasticity and Plasticity'. *International Journal of Engineering Sciences*. 1977, Vol 15, pp-645-660.

[8] R. A. Struble, *Non-Linear Differential Equations*, McGraw-Hill Book Company, Inc. 1962

[9] L. Libersky, A. G. Petschek, in Proceedings, *The next Free Lagrange Conf*., Jackson Hole, WY 1990, edited by H. E, Trease, J. W. Fritts and W. P. Cowley (Springer-Verlag, New York,1991).

[10] P. Randles, T. C. Carney, L. D. Libersky, J. D. Renick, A. G. Petschek, 'Calculation Of Oblic Impact and Fracture Of Tungsten Cubes Using Smoothed Particle Hydrodynamics'. *Int. J. Impact Engng,* Vol. 17, pp. 661-672, 1995.

[11] P.W. Randles, L.D. Libersky,'Smoothed Particle Hydrodynamics: Some recent improvements and applications'. *Comput. Methods Appl. Mech. Engng*. 139 (1996) 375-408

[12] L. Libersky. Private Communication.

[13] R. Vignjevic. Private Communication.

[14] Y. C. Fung, *Foundations of solid Mechanics*, Prentic-Hall, Englwood Cliffs, N. J., 1965.

[15] S. Nemat-Nasser, 'On finite Deformation Elasto-Plasticity'. *International Journal of Solides and Structures.* Vol. 18, No. 10, pp. 857-872; 1982.

[16] Z. Li, 'The analytic solution of near-tip stress fields for perfectly plastic pressure-sensitive material under plan stress condition'. *International Journal of fracture* 53:325-336, 1992

[17] C. A. Truesdell,'The simplest rate theory of pure elasticity', Communications on pure and applied Mathematics, Vol. VIII, 123-132 (1955).

[18] G. C. Johnson and D. J. Bammann, 'A Discussion of Stress Rates in Finite Deformation Problems'. *International Journal Solides and Structures.* Vol. 20, No. 8, pp. 725-737; 1984.

[19] D. J. Benson,'Computational methods in Lagrangian and Eulerian hydrocodes', *Comput. Methods Appl. Mech. Engng*. 99(1992) 235-394.

[20] G. R. Johnson, W. H. Cook,' Fracture characteristics of three metals subjected to various strains, strain rates, temperatures and pressures', Engineering Fracture Mechanics Vol. 21 No. 1 pp. 31-48 (1985).

[21] F. J. Zerilli, R. W. Armstrong,' Dislocation-mechanics-based constitutive relations for material dynamics calculations', J. Appl. Phys. 61(5), 1 March 1987.

[22] D. J. Steinberg, S. G. Cochran, M. W. Guinan, ' A constitutive model for metals applicable at high-strain rate', J. Appl. Phys. 51(3), March 1980.

[23] I. Jackson, S. M. Rigden, 'Analysis of P-V-T data: constraints on the thermoelastic properties of high-pressure minerals'. Physics of the earth and planetary interiors 96 (1996) 85-112.

[24] M. Born, K. Huang, Dynamical Theory of Crystal Lattices. Oxford University Press. Oxford 1954.

[25] O. L. Anderson, The use of Ultrasonic Measurements Under Modest Pressure to Estimate Compression At High Pressure. J. Phys. Chem. Solids. 1966. Vol. 27, pp. 547-565.

[26] Ya. B. Zel'dovich and Yu. P. Raizer, *'Physics Of Shock Waves And High-Temperature Hydrodynamic Phenomena'*. Vol II. Academic Press 1967.

[27] C. Hunter, 'On the collapse of an empty cavity in water', *Journal of Fluid Mechanics*. Vol 8 (1960).

[28] G. J. Ball, B. P. Howell, T. G. Leighton, M. J. Schofield, Shock-induced collapse of cylindrical air cavity in water: a Free-Lagrange simulation. *22nd International Symposium on Sock Waves, Imperial College, London, UK, July 18-23, 1999*.

[29] R. Vignjevic, T. de Vyust, J. Campbell, L. Libersky,' Modeling of Hydrodynamic Ram using Smoothed Particle Hydrodynamics'. Internal Communication.

9. CONCLUSIONS AND FUTURE WORK SUGGESTIONS

The current research work offered a detailed investigation of some problems inherent to a family of meshless methods, especially the Smoothed Particle Hydrodynamics (SPH) and the Normalised Smoothed Particles Hydrodynamics (NSPH) methods.

The first focal point was the derivation of SPH formalism through a number of conventional methods which offered a valuable contribution to the understanding of the SPH approach from different point of view.

The use of the *'Hamilton's variational principle'* to derive the equations of motion in the SPH form is a novelty that offers a powerful theoretical apparatus to corroborate the authority and the ability of this method to be considered as a mature numerical method.

The examination of the interpolant convolution technique spotlighted the difficulty of obtaining the consistency of the method due to the deficiency in the control of the gradient of smoothing length

The evaluation of the effect of the ratio of the smoothing length to the particles distance remains an unsolved problem concerning the stability of the SPH method.

The second focal point was stability analysis of the SPH method and its progeny. This included:

The Von Neumann analysis based on a complex dispersion relation which is innovative of use in the particle methods. It proved for the first time the existence of three mechanisms accountable for the development of the instabilities.

These mechanisms are:

Tensile instability

Irregular distribution of particles

Non-homogenous background stress

The results and the mechanisms derived in this work envelop those obtained by Swegle, Hattaway and recently by Belytschko.

The procedure showed also that these mechanisms are non-linearly correlated to each other. The use of normalised kernels is recommended and kernels of class C^2 are necessary in order to suppress in part the discontinuity in the tensile term.

The error propagation investigation based on the amplification matrix showed that the three mechanisms listed above contribute in a complex way to the definition of the stability domain of the numerical scheme.

Until recently, it was considered in SPH method that only the tensile term is the major source of instability. In this respect, this work highlighted the importance of the tensile term on the delimitation of the domain of stability. Our approach, based on the amplification matrix concept, can be used to highlight the consequence of some other physical mechanisms on the numerical stability and it can be extended without difficulty to a range of numerical schemes.

The expressions for amplification factors obtained from a simplified model illustrate the difficulties related to modification of the SPH and NSPH methods in order to make them stable. The easiest mechanism to modify is the second mechanism outlined above (Redistribution of particles), this requires the introduction of the remeshing concept in the particle methods.

In concluding, our approach to the understanding of the SPH method and its progeny consisted in accommodating the complex Von Neumann analysis and the error propagation via the amplification matrix (and via the Jacobean) in the stability investigations. By doing so, we were able to erect a link between the physics and the numerics that govern our model.

Finally, an example application, the hydrodynamic ram problem, illustrates the capability of the SPH method with all its short comings to give good results when analysing a complex problem.

Recommendation for further computational work should include the implementation of a constitutive equation of evolution for the smoothing length in order to capture anisotropic deformations.

From a theoretical point of view, supplementary investigations concerning *'Hamilton's principle'* in its smoothed version (in sense of the SPH formulation) will probably lead to a superior correction of the governing equations of motion in the SPH form via *'Euler-Lagrange'* equations.

In the long term, more analyses concerning the amplification factors are essential to emphasize the precise function of each term within each formulation. Then it may be possible to build a code that can switch automatically between different formulations depending on the regions and on the minimization of the destabilising terms.